2016

Hadron Physics in Tests of Fundamental Symmetries

Chien Yeah Seng
University of Massachusetts Amherst, cseng@physics.umass.edu

HADRON PHYSICS IN TESTS OF FUNDAMENTAL SYMMETRIES

A Dissertation Presented

by

CHIEN YEAH SENG

Submitted to the Graduate School of the
University of Massachusetts Amherst in partial fulfillment
of the requirements for the degree of

DOCTOR OF PHILOSOPHY

May 2016

Department of Physics

HADRON PHYSICS IN TESTS OF FUNDAMENTAL SYMMETRIES

A Dissertation Presented

by

CHIEN YEAH SENG

Approved as to style and content by:

Michael J. Ramsey-Musolf, Chair

Barry Holstein, Member

Lorenzo Sorbo, Member

Hongkun Zhang, Member

Rory Miskimen, Department Chair
Department of Physics

DEDICATION

To my family

ACKNOWLEDGMENTS

The completion of this thesis as well as my PhD study would be impossible without the help from many people whom I wish to take this opportunity to express my deepest gratitude to.

First of all I wish to thank Prof. Michael Ramsey-Musolf, my PhD advisor and thesis committee chair. He is the person who raised my entire interest and guided me into the area of QCD and hadron physics. He is also a great teacher who teaches me how to live and work like a true researcher. Next, I would like to also express my gratitude to all the other members in my thesis committee: Prof. Barry Holstein, Prof. Lorenzo Sorbo and Prof. Hongkun Zhang. The whole procedure would be impossible without their active participation. Also, I want to pay special thanks to Carlo Dallapiccola and Jane Knapp, the graduate program director and manager. They provided me countless helps during my PhD life in Amherst.

I am also extremely grateful to all the previous and current colleagues in my research group, both in Wisconsin and in UMass. In particular, I wish to give very special thanks to Hiren Patel, Mario Pitschmann and Huaike Guo as I have learned a lot from them through formal and informal discussions. Of course, all my collaborators in various projects will never be forgotten as well. I wish to express my gratitude to Jordy de Vries, Emanuele Mereghetti and Craig Roberts. They are no mere collaborators of mine but are also extremely helpful in shaping my research career in general.

Next, I am indebted to all the professors whom I learned physics from, in particular to Prof. Daniel Chung from University of Wisconsin-Madison for everything he taught

me about Quantum Field Theory. His lectures notes are so clear and detailed that I am always benefited from them during my research.

Last but not least, I want to thank my dad Ah Loke Seng, my mom Suk Hen Kok, my elder brother Chien Wei Seng and my girlfriend Fang Ye. I simply wouldn't be myself without them playing their roles in my life.

ABSTRACT

HADRON PHYSICS IN TESTS OF FUNDAMENTAL SYMMETRIES

MAY 2016

CHIEN YEAH SENG

B.Sc., TSINGHUA UNIVERSITY

M.P.H., HONG KONG UNIVERSITY OF SCIENCE AND TECHNOLOGY

Ph.D., UNIVERSITY OF MASSACHUSETTS AMHERST

Directed by: Professor Michael J. Ramsey-Musolf

Low energy precision tests of fundamental symmetries provide excellent probes for the Beyond Standard Model Physics. Theoretical interpretations of these experiments often involve the application of non-perturbative Quantum Chromodynamics in the study of hadronic matrix elements that may either serve as signals of new physics or Standard Model backgrounds. In this work I present a series of studies on different hadronic matrix elements using various low-energy effective approaches to Quantum Chromodynamics, and discuss the impact of these studies on our knowledge of Standard Model and Beyond Standard Model physics.

TABLE OF CONTENTS

LIST OF TABLES

LIST OF FIGURES

Figure **Page**

INTRODUCTION

Searches for Beyond Standard Model (BSM) physics are usually classified into three categories, namely the energy frontier, the precision frontier and the cosmic frontier. The energy frontier generally involves collision of particle beams which are energetic enough to create new states of matter. Countless achievements have been made at this frontier and are impossible to be summarized in a few pages. Among them are the discovery of the W and Z boson [1, 2], the charm [3, 4], bottom [5] and top quark [6, 7] and most recently the Higgs-like scalar [8, 9]. On the other hand, researches at the cosmic frontier involve studies of large scale structures of the universe. In fact it is fair to say that most of the evidences that point towards the existence of a BSM theory come from observations at this frontier. Examples include the discovery of the solar neutrino deficit that gave the first hint for neutrino oscillation [10, 11], the study of galaxy rotation curves [12, 13] and the gravitational lensing of Bullet Clusters that provide proofs for the existence of dark matter [14] and the study of the Cosmic Microwave Background (CMB) together with large scale structure measurements which reconfirms the matter-antimatter asymmetry in cosmic scale [15, 16] in addition to our daily experience.

In this work, we will however concentrate on the third frontier, namely the precision frontier. Complementary to the two frontiers above, researches carried out at the precision frontier involve measuring physical quantities to a very high precision and comparing theoretical predictions with experimental measurements. A typical example is the measurement of the anomalous magnetic dipole moment (AMDM) of the electron to one part in a trillion [17] which agrees with the prediction of Quantum

Electrodynamics (QED) [18], showing that the theory works with high accuracy. Beside that, the study of the left-right asymmetry in the electron-deuteron deep inelastic scattering (DIS) provided the value of the weak mixing angle θ_w in Standard Model (SM)[19]. The measurement of Z-mass and width gave a range of possible Higgs mass even before the direct measurement from LHC [20]. Recently, the anomaly in the muon $g-2$ experiment provides interesting but not yet definite signal for the possible existence of BSM physics [21].

Among all experiments at the precision frontier, tests for fundamental symmetries are of particular interest for us. Symmetry is one of the basic ingredients of the quantum field theory (QFT) which is believed to be the correct language to describe the microscopic world. There are discrete symmetries such as charge conjugation (C), parity (P), time reversal (T) and also continuous symmetries such as the invariance of the theory under global and local phase transformations which lead to conservation laws such as the charge conservation. The study of how fundamental symmetries are conserved or broken in basic laws of nature is a persistent theme in modern physics. The first definite sign for the violation of a particular discrete symmetry, namely parity, was observed by Wu and her company in the β-decay of ^{60}Co[22]. This observation was an essential input in the formulation of the charged weak interaction theory in terms of left-handed fermions. It was found later through neutral kaon decays that even CP is violated in the weak interaction [23] due to the existence of the complex phase in the Cabibbo-Kobayashi-Maskawa (CKM) matrix [24]. Tests of conservation laws also play crucial roles in the search of BSM physics. As an example, the experimental confirmation of neutrino oscillation proved that lepton flavors are not conserved and unavoidably pointed us to the need of a BSM explanation [25, 26, 27]. Besides, many BSM scenarios predict large violation of discrete symmetries such as C and CP-violation which could be tested in low energy precision experiments.

Since there are many possible candidates for the BSM theory, it may sound complicated if we have to study each of them separately. One could therefore take another approach (namely the "bottom-up approach") following the language of Effective Field Theory (EFT) [28]. In this approach the only assumption is that the new degrees of freedom (DOFs) in the BSM physics are heavy and can be integrated out to produce higher-dimensional effective operators consist of SM DOFs. As a result, one just need to write down the most general Lagrangian consists of all SM DOFs and respects the SM gauge invariance. There is an infinite tower of operators satisfying these two criteria, but operators with higher dimensions are more suppressed by inverse powers of the energy scale of the unknown BSM physics. Therefore, to achieve a level of finite precision one only needs to retain a finite number of operators. To such extent the effective theory is still predictive despite the fact that it is non-renormalizable in the conventional sense. There is only one dimension-5 operator that respects SM gauge symmetry and it gives the Majorana mass term for neutrinos. In dimension 6 there are 59 operators (barring flavor structures and Hermitian conjugations) that respect SM gauge symmetry and conserve baryon number [29].

Currently we do not find any significant deviation from SM so precision tests of fundamental symmetries are placing bounds on the Wilson coefficients of the effective operators. However, once our experiment is precise enough to discover a finite deviation from the SM prediction, then we immediately face the problem of which linear combination of operators is responsible for the observed result. It is therefore necessary to perform symmetry tests in different particle systems to disentangle contributions from different operators. Note that apart for elementary particles such as electron, systems at which precision experiments are performed are usually low-energy bound states of the strong interaction. We must be able to accurately evaluate matrix elements of the effective operators with respect to these bound states in order to draw accurate bounds on the Wilson Coefficients of these operators from our

results of precision experiments. However, when we try to proceed in this direction we immediately run into the difficulty in performing analytic calculations involving bound states of the strong interaction from first principle.

Quantum Chromodynamics (QCD) is a gauge theory that describes the strong interaction between quarks through the exchange of gluons which are $\mathrm{SU}(3)_C$ gauge bosons. Even though there are many evidences that it is indeed the correct theory of the strong interaction, only very limited analytical results using perturbation theory at high energy can be derived from first principle, thank to its asymptotically-free behavior at high energy [30, 31]. On the other hand, the theory becomes non-perturbative at energy < 1 GeV so the conventional perturbation theory based on the expansion in powers of the strong coupling constant α_s fails. Some very interesting emergent features of theory in this energy regime such as confinement and dynamical chiral symmetry breaking (DCSB) are still not well understood. Although lattice QCD [32] provides a promising way to extract numerical results from first principle calculations, but it is subject to numerous technical difficulties and therefore has a limited range of application. Furthermore, not just satisfied by just obtaining numerical answers, we need a more intuitive understanding of how low-energy QCD behaves. For the latter purpose and also practical reasons, many effective approaches to low energy QCD are formulated that allow studies of hadronic or nuclear properties, and each of them tries to capture some known behaviors of the original theory such as confinement and chiral symmetry breaking. Among them are the Chiral Perturbation Theory (ChPT), constituent quark model, Regge Theory, Dyson-Schwinger Equation (DSE), QCD sum rules and others.

We have two main tasks in this work. On the one hand, we will introduce a number of effective approaches to QCD which allow us to perform analytical and numerical studies of both static and dynamical properties of hadrons. On the other hand, we will apply these effective approaches in the calculation of hadronic matrix elements and the

determination of specific SM backgrounds that enter various precision experiments in tests of fundamental symmetries. In particular, we will concentrate on EDM searches in hadrons, precision experiments involving the neutron β-decay and the study of P-violation in the electron-deuteron parity-violating deep inelastic scattering (e-D PVDIS).

EDMs And Hadronic Matrix Elements

Ever since the discovery of P-violation in the weak interaction, people are puzzled by the fact that discrete symmetries such as P and CP are violated only in the weak interaction and not in other interactions. Various experiments have been carried out to test the conservation of these discrete symmetries in strong and electromagnetic sector. Back in the 50s, Smith, Purcell and Ramsey had suggested the test of P-invariance in the strong interaction by searching for intrinsic electric dipole moment (EDM) of the neutron [33]. Since then, experimental techniques have improved much and searches of permanent EDMs in different particle systems have been carried out but so far all of them have returned null results. This raised another interesting question known as the strong CP-problem, namely: due to the non-trivial vacuum structure of QCD, one can write down a term in the Lagrangian which is P and CP-violating and is characterized by the parameter $\bar{\theta}$. In general there is no constraint on the value of $\bar{\theta}$ by the theory itself so it could be of order one by naturalness. However, the (so-far) vanishing of EDMs in all hadronic systems indicates that the value of $\bar{\theta}$ has to be fine-tuned to an extremely small number, which makes the whole theory seems unnatural. There have been several proposed solution to this problem. Among them are the massless up quark solution [34], the Peccei-Quinn symmetry [35] and the Nelson-Barr mechanism [36, 37] but so far none of them seems completely satisfactory.

Particle	Current upper bound on EDM (e cm)
e	8.7×10^{-29}
Hg	3.1×10^{-29}
p	7.9×10^{-25}
n	2.9×10^{-26}

Table I.1. Examples of current upper bounds on EDM of particles

Apart from mere curiosity, searches of permanent EDMs are also essential in the understanding of the baryon asymmetry of the universe (BAU). According to the three Sakharov criteria, a necessary condition for the BAU to occur is the existence of C and CP-violating interactions [38]. It is well-known that the amount of CP-violation provided by the CKM matrix in SM is too small to explain the amount of asymmetry we observed [39, 40], so BSM theories with extra sources of CP-violation are very much desired. These theories are usually subject to constraints from low energy precision measurements such as EDM searches. In this sense, EDM searches provide very sensitive probes to BSM theories which are relevant to the understanding of baryogenesis, namely the mechanism which is responsible for the generation of the current BAU.

Table I.1 gives examples of current upper bounds on EDMs for some representative particles (more about the current and future experimental status of EDM searches will be described in the following chapters). In terms of EFT, if we restrict ourselves to the first generation of quarks and leptons, then there are altogether 13 operators which are CP-odd and with dimension less than or equal to 6. They could induce CP-violating observables such as EDMs at low energy systems therefore the search of EDMs in hadronic and nuclear systems is a very efficient way to constrain the Wilson coefficients of these operators. However, in order to construct a precise formula which links the Wilson coefficients of the 13 operators to the EDMs we probe at hadronic

systems we must be able to reduce the theoretical uncertainty in the calculation of relevant hadronic matrix elements.

In this work we will present several case studies on EDMs induced by BSM physics in different hadronic systems. First we will work with the ρ-meson which is the simplest possible hadron that could possess an EDM. The aim of this work is to find a single framework that can deal with the hadronic matrix elements of different sources of CP-violation in a unified and coherent manner. We will show that the Dyson-Schwinger Equation is good choice for this purpose. Within the framework of DSE we will compute the ρ-EDM induced by the quark EDM, the quark chromo-EDM, the QCD θ-term and the four quark operator (which covers most operators of P and CP-violation up to dimension 6). This work shall serve as a prototype for future studies of more realistic systems such as nucleon within the same theoretical framework.

On the other hand, it is known that a significant amount of BSM-induced nucleon EDM enters in the form of long-distance contribution, namely the contribution via effective P and CP-odd pion-nucleon couplings. Chiral Perturbation Theory provides a model-independent description of the properties of QCD in this regime as it is simply the most general theory at low energy which is consistent with the exact and approximate symmetries of QCD. With the aid of ChPT we will perform an investigation on the pion loop correction to the nucleon EDM induced by the P and T-odd pion-nucleon coupling $\bar{g}_\pi^{(i)}$.

Finally, we would like to mention that although it is commonly understood that SM-induced EDMs are too small to be observed with the current experimental precision, it is still worth a detailed study since the complex phase in the CKM matrix is currently the only experimentally-confirmed source of CP-violation in nature. For this purpose we will also present an updated work on the SM-induced nucleon EDM. We will show that previous studies on this topic were based on a flawed effective theory

of hadrons that does not posses a valid expansion scheme at low energy. Also, their results face large uncertainties due to poorly known physical constants in the weak sector at that time. Our updated study will try to fix these two problems and obtain a better determination of the nucleon EDM with a smaller theoretical uncertainty.

Scalar And Tensor Charges In The Neutron β-Decay

The β-decay of nuclei became an excellent playground for the test of fundamental symmetries since the discovery of parity violation in the β-decay of ^{60}Co which led eventually to the V-A structure of the charged weak interaction. Recently nuclear β-decays have been studied extensively for the purpose of BSM searches [41]. In the language of EFT, the most general effective Lagrangian without derivatives that triggers the nuclear β-decay can be parameterized as [42]

$$\mathcal{L}_\beta = -\frac{4G_F V_{ud}}{\sqrt{2}} \sum_{\alpha,\beta,\gamma} a^\gamma_{\alpha\beta} \bar{e}_\alpha \Gamma^\gamma \nu_e \bar{u} \Gamma_\gamma d_\beta + h.c. \tag{1}$$

Here $\alpha, \beta = L, R$ denote the chirality of fermions while $\gamma = S, V, T$ labels the Dirac structure of Γ which can be either scalar, vector or tensor.

If we concentrate on the β-decay of neutron, then the differential width of this process can be parameterized as [43]

$$\frac{d\Gamma}{dE_e d\Omega_e d\Omega_\nu} \propto |\vec{p}_e| E_e E_\nu^2 (1 + \frac{\vec{p}_e \cdot \vec{p}_\nu}{E_e E_\nu} + \hat{s} \cdot (A\frac{\vec{p}_e}{E_e} + B\frac{\vec{p}_\nu}{E_\nu} + D\frac{\vec{p}_e \times \vec{p}_\nu}{E_e E_\nu})). \tag{2}$$

In particular, any non-zero value of the coefficient D will be a signature of T-violation (which implies CP-violation assuming that CPT is a good symmetry) in the neutron β-decay. The current best experimental determination of the neutron D-coefficient is given by $D = (-0.96 \pm 1.89 \pm 1.01) \times 10^{-4}$ which is consistent with zero [44]. Effects of T-violation in many BSM scenarios can therefore be tested by more precise experimental determination of the D-coefficient.

In terms of the parametrization in Eq. (1), the value of D is related to the imaginary part of $a^{\gamma}_{\alpha\beta}$ which depends on the specific BSM realization. However the application of Eq. (1) in the computation of the neutron D-coefficient given in Eq. (2) requires the evaluation of the hadronic matrix element $\langle p|\, \bar{u}_\alpha \Gamma^\gamma d_\beta \,|n\rangle$ at small momentum transfer. When $\gamma = V$, the relevant matrix elements are called the vector (g_V) and axial (g_A) charges. They can be determined quite precisely by experiment. On the other hand, when $\gamma = S$ or T the corresponding hadronic matrix elements are called scalar (g_S) and tensor (g_T) charges respectively. The current experimental values of these charges suffer from very large uncertainty [45] so theoretical modelings are needed.

We will present a calculation of the nucleon scalar and tensor charges using the Dyson-Schwinger Equation formalism with a simplified vector-like interaction between quarks. This simplified model has been shown to give identical results with more sophisticated truncation schemes of DSE when dealing with static behaviors of hadrons. The application of this formalism allows us to compute hadronic matrix elements using the conventional Feynman diagram approach with dressed propagators and vertices while only very little amount of numerical calculation is required. In particular, we will show that the inclusion of an axial-like diquark correlation in the nucleon is essential to reproduce a nucleon tensor charge that falls within current range of uncertainty of the current experiment. This work therefore contributes to both the search of BSM physics and also the understanding of quark correlations in the nucleon.

Higher-Twist Correction And The Study of Nucleon Spin In Parity-Violating Deep Inelastic Scattering

A good way to study the parity violation in the weak interaction is to perform deep inelastic scattering between on the deuteron target with longitudinally-polarized

electrons. The left-right symmetry A_{RL} of this process is defined as:

$$A_{RL} \equiv \frac{d\sigma_R - d\sigma_L}{d\sigma_R + d\sigma_L} \tag{3}$$

where $d\sigma_{R(L)}$ is the differential cross section of the process with right (left)-handed electron. If one neglects sea quark effects and assume charge symmetry, then it turns out that the leading-order SM prediction to A_{RL} is completely free from any influence from the low energy QCD. It thus provides an accurate measure to the weak mixing angle θ_W of the electroweak theory.

The 12GeV upgrade of the Jefferson Lab and the usage of the SoLID spectrometer enable a 0.5% precision measurement of A_{RL} in the e-D PVDIS over a broad range of kinematics [46]. A precise measurement of A_{RL} and the search of its deviation from the SM-prediction provide sensitive probes or constraints for many BSM scenarios. However, at this level of precision many SM background effects have to be appropriately taken into account in order to disentangle them from BSM signals. Among them is the "higher-twist" effect which originated from QCD interactions between partons. It will add corrections that scale as inverse powers of q^2 on top of the free parton picture where q is the momentum change of the electron.

Previous studies of the higher-twist effects made use of effective quark models that assume isotropic (polar-)angular distribution of quarks in the nucleon. Examples of them are the QCD bag model [47] and the isotropic light-cone wavefunctions [48]. In our work, we would like to find out how things may change if a particular component of the parton angular momentum which, with a specific choice of gauge, can be interpreted as the orbital angular momentum of the quarks in the nucleon, is taken into account. This is motivated by the yet unsolved problem about how one could decompose the spin of a nucleon in terms of different components of angular momentum of quarks and gluons. We will show in this work that, apart from resolving one of the many SM backgrounds to the search of BSM physics in e-D PVDIS, the study of the

higher-twist matrix element is interesting by itself as it sheds new lights on the study of the rule of angular momentum in the structure of the nucleon.

The Arrangement Of The Contents

The contents of this thesis are arranged as follows: in Chapter 1 I will provide a brief introduction to the Dyson-Schwinger Equation and describe the "contact-interaction" approximation and apply the DSE formalism to compute the EDM of the ρ-meson induced by various CP-violating effective operators. In Chapter 2 I apply the same formalism in the calculation of the scalar and tensor charges of the nucleon. In Chapter 3 I will introduce some essential concepts of the Chiral Perturbation Theory and its heavy baryon reduction. In Chapter 4 I apply the two-flavor ChPT to compute the nucleon EDM induced by the P,T-odd pion-nucleon coupling. In Chapter 5 I will apply the three-flavor ChPT to study the SM-induced nucleon EDMs. In Chapter 6 I study the higher-twist correction to the e-D PVDIS and draw connections with the nucleon spin problem. In the last chapter I will present some general discussions and draw my conclusions.

CHAPTER 1

ELECTRIC DIPOLE MOMENT OF THE ρ-MESON

1.1 Introduction

The action for any local quantum field theory is invariant under the transformation generated by the antiunitary operator CPT, which is the product of the inversions: C, charge conjugation; P, parity transformation; and T, time reversal. The combined CPT transformation provides a rigorous correspondence between particles and antiparticles, and it relates the S matrix for any given process to its inverse, where all spins are flipped and the particles replaced by their antiparticles. Lorentz and CPT symmetry together have many consequences, amongst them, that the mass and total width of any particle are identical to those of its antiparticle.

It is within this context that the search for the intrinsic electric dipole moment (EDM) of an elementary or composite but fundamental particle has held the fascination of physicists for over sixty years [49]. Its existence indicates the simultaneous violation of parity- and time-reversal-invariance in the theory that describes the particle's structure and interactions; and the violation of P- and T-invariance entails that CP symmetry is also broken. This last is critical for our existence because we represent a macroscopic excess of matter over antimatter. As first observed by Sakharov [38], in order for a theory to explain an excess of baryon matter, it must include processes that change baryon number, and break C- and CP-symmetries;

---

[0]Reprinted article with permission from M. Pitschmann, C. Y. Seng, M. J. Ramsey-Musolf, C. D. Roberts, S. M. Schmidt and D. J. Wilson, Phys. Rev. C **87** (2013) no.1, 015205, Copyright (2013) by the American Physical Society. DOI: http://dx.doi.org/10.1103/PhysRevC.87.015205

and the relevant processes must have taken place out of equilibrium, otherwise they would merely have balanced matter and antimatter. (Alternately, the presence of CPT violation can circumvent the out-of-equilibrium environment.)

The electroweak component of the Standard Model (SM) is capable of satisfying Sakharov's conditions, owing to the existence of a complex phase in the 3×3-CKM matrix which enables processes that mix all three quark generations. However, this high-order process is too weak to explain the observed matter-antimatter asymmetry [50, 51, 52]. Hence, it is widely expected that any description of baryogenesis will require new sources of CP violation beyond the SM. This presents little difficulty, however, because extensions of the SM typically possess CP-violating interactions, whose parameters must, in fact, be tuned to small values in order to avoid conflict with known bounds on the size of such EDMs [52, 53, 54, 55, 56]. (For recent analyses, see, e.g., Refs. [57, 58, 59] and references therein.)

The question here is how such bounds should be imposed. That is not a problem for elementary particles, like the electron. However, it is a challenge when the SM extension produces an operator involving current-quarks and/or gluons. In that case the CP violation is expressed as an hadronic property and one must have at hand a nonperturbative method with which to compute the impact of CP-violating features of partonic quarks and gluons on the hadronic composite.

To elucidate, extensions of the SM are typically active at some large but unspecified energy-scale, Λ, and their effect at an hadronic scale is expressed in a low-energy effective Lagrangian:

$$\mathcal{L}_{\rm eff} \sim \sum_{j,k} K_j \, \mathcal{O}_j^{(k)} \Lambda^{4-k}, \tag{1.1}$$

where $\mathcal{O}_j^{(k)}$ are composite CP-odd local operators of dimension $k \geq 4$ and $\{K_j\}$ are dimensionless strength parameters, which monitor the size of the model's CP-violating phases and commonly evolve logarithmically with the energy scale. The calculation of an hadronic EDM therefore proceeds in two steps. The first, easier,

part requires calculation of the coefficients $\{K_i\}$ in a given model. This involves the systematic elimination of degrees-of-freedom that are irrelevant at energy-scales less than Λ. The second, far more challenging exercise, is the nonperturbative problem of translating the current-quark-level interaction in Eq. (1.1) into observable properties of hadrons.

We illustrate the procedure in the case of the ρ-meson. Not that there is any hope of measuring a ρ-meson EDM but because the nonperturbative methods necessary can most readily be illustrated in the case of systems defined by two valence-quark degrees-of-freedom. In taking this path, we follow other authors [60, 61, 62] but will nonetheless expose novel insights, especially because we consider more operator structures than have previously been considered within a single unifying framework. It is worth remarking here that particles with spin also possess a magnetic dipole moment. That moment is aligned with the particle's spin because it is the only vector available. The same is true of the expectation value of any electric dipole moment.

Herein we shall estimate the contribution of some dimension four, five and six operators to the EDM of the ρ^+-meson; viz., the impact on the ρ of the local Lagrangian density

$$\begin{aligned}\mathcal{L}_{\rm eff} &= -i\bar{\theta}\frac{g_s^2}{32\pi^2}\,G^a_{\mu\nu}\tilde{G}^a_{\mu\nu} - \frac{i}{2}\sum_{q=u,d} d_q\,\bar{q}\,\gamma_5\sigma_{\mu\nu}q\,F_{\mu\nu} \\ &\quad -\frac{i}{2}\sum_{q=u,d}\tilde{d}_q\,\bar{q}\,\tfrac{1}{2}\lambda^a\gamma_5\sigma_{\mu\nu}q\,g_s G^a_{\mu\nu} + \frac{\mathcal{K}}{\Lambda^2}\,i\varepsilon_{jk}\left[\bar{Q}_j d\,\bar{Q}_k\gamma_5 u + \text{h.c.}\right], \qquad (1.2)\end{aligned}$$

where: latin superscripts represent colour; g_s is the strong coupling constant; $F_{\mu\nu}$ and $G^a_{\mu\nu}$ are photon and gluon field-strength tensors, respectively, and $\tilde{G}^a_{\mu\nu} = (1/2)\epsilon_{\mu\nu\lambda\rho}G^a_{\lambda\rho}$; $\{\bar{Q}_i|i=1,2\} = \{\bar{u}_L, \bar{d}_L\}$, with the subscript indicating left-handed; $\bar{\theta}$ is QCD's effective θ-parameter, which combines $\theta_{\rm QCD}$ and the unknown phase of the current-quark-mass matrix; and $\{d_q\}$, $\{\tilde{d}_q\}$ are quark EDMs and chromo-EDMs, respectively.

We note that Eq. (1.2) is expressed at a renormalisation scale $\zeta \sim 2\,\mathrm{GeV}$, which is far below that of electroweak symmetry breaking but still within the domain upon which perturbative QCD is applicable. Moreover, we have chosen to include just one dimension-six operator in the Lagrangian; i.e., a particular type of four-fermion interaction. There is a host of dimension-six operators, Weinberg's CP-odd three-gluon vertex amongst them [63]. However, for our illustrative purpose, nothing is lost by omitting them because the potency of the one operator we do consider can serve as an indication of the strength with which each might contribute.

One merit of our analysis of the contribution from Eq. (1.2) to the EDM of the ρ^+-meson is the connection of these EDM responses with values of a vast array of hadron observables that are all computed within precisely the same framework using exactly the same parameters [64, 65, 66, 67, 68, 69]. We explain this framework in Sec. 1.2. In addition to providing the first such comprehensive treatment, our study is novel in considering the impact of a dimension-six operator on the ρ^+-meson's EDM.

We introduce the ρ-meson electromagnetic form factors in Sec. 1.3. The effects of Eq. (1.2) on the ρ-meson bound-state are analysed in Sec. 1.4. Each interaction term is considered separately, so that we present a raft of algebraic formulae that are readily combined, evaluated and interpreted. Numerical results are provided in Sec. 1.5 and placed in context with previous studies. Section 1.6 is an epilogue.

1.2 ρ-meson as a Bound State

1.2.1 ρ-γ Vertex

The ρ^+-meson is a composite particle and thus its EDM appears in the dressed vertex that describes its coupling with the photon; viz.,

$$\mathcal{P}^T_{\alpha\alpha'}(p)\Gamma_{\alpha'\mu\beta'}(p,p')\mathcal{P}^T_{\beta'\beta}(p') = \mathcal{P}^T_{\alpha\alpha'}(p)\Big\{(p+p')_\mu[-\delta_{\alpha'\beta'}\mathcal{E}(q^2)+q_{\alpha'}q_{\beta'}\mathcal{Q}(q^2)] - (\delta_{\mu\alpha'}q_{\beta'}-\delta_{\mu\beta'}q_{\alpha'})\mathcal{M}(q^2) - i\varepsilon_{\alpha'\beta'\mu\sigma}q_\sigma\mathcal{D}(q^2)\Big\}\mathcal{P}^T_{\beta'\beta}(p')\,, \quad (1.3)$$

where: p_α is the momentum of the incoming ρ-meson; p'_β, that of the outgoing ρ; $q_\mu = p'_\mu - p_\mu$; and

$$\mathcal{P}^T_{\alpha\beta}(p) = \delta_{\alpha\beta} - \frac{p_\alpha p_\beta}{p^2}\,. \quad (1.4)$$

The vertex involves four scalar form factors whose $q^2 = 0$ values are understood as follows: $\mathcal{E}(0)$, electric charge, which is "1" in this case; $\mathcal{M}(0)$, magnetic moment, μ_ρ, in units of $e/[2m_\rho]$, where e is the magnitude of the electron charge; $\mathcal{Q}(0) = (2/m_\rho^2)(Q_\rho + \mu_\rho - 1)$, with Q_ρ the meson's electric quadrupole moment; and $\mathcal{D}(0)$ is the meson's electric dipole moment, in units of $e/[2m_\rho]$.

1.2.2 Contact Interaction

Our goal is calculation of the last of these, $\mathcal{D}(0)$, and for this we choose to work within the continuum framework provided by QCD's Dyson-Schwinger equations (DSEs) [70, 71, 72]. To be specific, we perform the computation using a global-symmetry-preserving treatment of a vector×vector contact-interaction because that has proven to be a reliable explanatory and predictive tool for hadron properties measured with probe momenta less-than the dressed-quark mass, $M \sim 0.4\,\mathrm{GeV}$ [64, 65, 67, 66, 68, 69].

To expand upon the reasons for this choice of interaction we note that DSE kernels with a closer connection to perturbative QCD; namely, which preserve QCD's one-loop renormalisation group behaviour, have long been employed in studies of the spectrum and interactions of mesons [73, 74, 75]. Such kernels are developed in the rainbow-ladder approximation, which is the leading-order in a systematic and global-symmetry-preserving truncation scheme [76, 77]; and their model input is expressed

via a statement about the nature of the gap equation's kernel at infrared momenta. With a single parameter that expresses a confinement length-scale or strength [78, 79], they have successfully described and predicted numerous properties of vector [79, 80, 81, 82, 83] and pseudoscalar mesons [79, 82, 83, 84, 85, 86, 87] with masses less than 1 GeV, and ground-state baryons [88, 89, 90, 91]. Such kernels are also reliable for ground-state heavy-heavy mesons [92]. Given that contact-interaction results for low-energy observables are indistinguishable from those produced by the most sophisticated interactions, it is sensible to capitalise on the simplicity of the contact-interaction herein.

The starting point for our study is the dressed-quark propagator, which is obtained from the gap equation:

$$S(p)^{-1} = i\gamma\cdot p + m + \int \frac{d^4q}{(2\pi)^4} g^2 D_{\mu\nu}(p-q)\frac{\lambda^a}{2}\gamma_\mu S(q)\frac{\lambda^a}{2}\Gamma_\nu(q,p), \tag{1.5}$$

wherein m is the Lagrangian current-quark mass, $D_{\mu\nu}$ is the vector-boson propagator and Γ_ν is the quark–vector-boson vertex. We use

$$g^2 D_{\mu\nu}(p-q) = \delta_{\mu\nu}\frac{4\pi\alpha_{\rm IR}}{m_G^2}\,, \tag{1.6}$$

where $m_G = 0.8\,$GeV is a gluon mass-scale typical of the one-loop renormalisation-group-improved interaction introduced in Ref. [83], and the fitted parameter $\alpha_{\rm IR}/\pi = 0.93$ is commensurate with contemporary estimates of the zero-momentum value of a running-coupling in QCD [93, 94]. Equation (1.6) is embedded in a rainbow-ladder truncation of the DSEs, which is the leading-order in the most widely used, symmetry-preserving truncation scheme [77]. This means

$$\Gamma_\nu(p,q) = \gamma_\nu \tag{1.7}$$

in Eq. (1.5) and in the subsequent construction of the Bethe-Salpeter kernels. One may view the interaction in Eq. (1.6) as being inspired by models of the Nambu–Jona-Lasinio (NJL) type [95]. However, in implementing the interaction as an element in a rainbow-ladder truncation of the DSEs, our treatment is atypical; e.g., we have a single, unique coupling parameter, whereas common applications of the NJL model have different, tunable strength parameters for each collection of operators that mix under symmetry transformations.

Using Eqs. (1.6), (1.7), the gap equation becomes

$$S^{-1}(p) = i\gamma\cdot p + m + \frac{16\pi}{3}\frac{\alpha_{\rm IR}}{m_G^2}\int\frac{d^4q}{(2\pi)^4}\,\gamma_\mu\,S(q)\,\gamma_\mu\,, \tag{1.8}$$

an equation in which the integral possesses a quadratic divergence, even in the chiral limit. When the divergence is regularised in a Poincaré covariant manner, the solution is

$$S(p)^{-1} = i\gamma\cdot p + M\,, \tag{1.9}$$

where M is momentum-independent and determined by

$$M = m + M\frac{4\alpha_{\rm IR}}{3\pi m_G^2}\int_0^\infty ds\,s\,\frac{1}{s+M^2}\,. \tag{1.10}$$

Our regularisation procedure follows Ref. [96]; i.e., we write

$$\begin{aligned}\frac{1}{s+M^2} &= \int_0^\infty d\tau\,{\rm e}^{-\tau(s+M^2)} \\ &\to \int_{\tau_{\rm uv}^2}^{\tau_{\rm ir}^2} d\tau\,{\rm e}^{-\tau(s+M^2)} &(1.11)\\ &= \frac{{\rm e}^{-(s+M^2)\tau_{\rm uv}^2} - e^{-(s+M^2)\tau_{\rm ir}^2}}{s+M^2}\,, &(1.12)\end{aligned}$$

where $\tau_{\rm ir,uv}$ are, respectively, infrared and ultraviolet regulators. It is apparent from Eq. (1.12) that $\tau_{\rm ir} =: 1/\Lambda_{\rm ir}$ finite implements confinement by ensuring the absence of

quark production thresholds [70, 97]. Since Eq. (1.6) does not define a renormalisable theory, then $\Lambda_{\rm uv} := 1/\tau_{\rm uv}$ cannot be removed but instead plays a dynamical role, setting the scale of all dimensioned quantities.

Using Eq. (1.11), the gap equation becomes

$$M = m + M\frac{4\alpha_{\rm IR}}{3\pi m_G^2}\ \mathcal{C}^{\rm iu}(M^2)\,, \tag{1.13}$$

where

$$\begin{aligned}\mathcal{C}^{\rm iu}(M^2) &= M^2\overline{\mathcal{C}}^{\rm iu}(M^2) &(1.14)\\ &= M^2\big[\Gamma(-1,M^2\tau_{\rm uv}^2) - \Gamma(-1,M^2\tau_{\rm ir}^2)\big]\,, &(1.15)\end{aligned}$$

with $\Gamma(\alpha,y)$ the incomplete gamma-function, and, for later use, we define

$$\mathcal{C}_1^{\rm iu}(z) = -z(d/dz)\mathcal{C}^{\rm iu}(z). \tag{1.16}$$

In rainbow-ladder truncation, with the interaction in Eq. (1.6), the homogeneous Bethe-Salpeter equation for the colour-singlet ρ-meson is

$$\Gamma^\rho_\mu(k;P) = -\frac{16\pi}{3}\frac{\alpha_{\rm IR}}{m_G^2}\int\frac{d^4q}{(2\pi)^4}\,\gamma_\sigma\chi^\rho_\mu(q;P)\gamma_\sigma\,, \tag{1.17}$$

where $\chi^\rho_\mu(q;P) = S(q+P)\Gamma^\rho_\mu(q;P)S(q)$ and $\Gamma_\mu(q;P)$ is the meson's Bethe-Salpeter amplitude. Since the integrand does not depend on the external relative-momentum, k, then a global-symmetry-preserving regularisation of Eq. (1.17) yields solutions that are independent of k. With a dependence on the relative momentum forbidden by

E_π	F_π	E_ρ	M	$\kappa_\pi^{1/3}$	m_π	m_ρ	f_π	f_ρ
3.639	0.481	1.531	0.368	0.243	0.140	0.929	0.101	0.129

Table 1.1. Results obtained with $\alpha_{\rm IR}/\pi = 0.93$ and (in GeV): $m = 0.007$, $\Lambda_{\rm ir} = 0.24$, $\Lambda_{\rm uv} = 0.905$ [66]. The Bethe-Salpeter amplitudes are canonically normalised; κ_π is the in-pion condensate [98, 99, 100]; and $f_{\pi,\rho}$ are the mesons' leptonic decay constants. Empirical values are $\kappa_\pi \approx (0.22\,{\rm GeV})^3$ and [101] $f_\pi = 0.092\,{\rm GeV}$, $f_\rho = 0.153\,{\rm GeV}$. All dimensioned quantities are listed in GeV.

the interaction, then the rainbow-ladder vector-meson Bethe-Salpeter amplitude takes the form

$$\Gamma^\rho_\mu(P) = \gamma^T_\mu E_\rho(P), \tag{1.18}$$

where $P_\mu \gamma^T_\mu = 0$, $\gamma^T_\mu + \gamma^L_\mu = \gamma_\mu$. We assume isospin symmetry throughout and hence do not explicitly include the Pauli isospin matrices.[1]

Values of some meson-related quantities, of relevance herein and computed using the contact-interaction, are reported in Table 1.1. We quote pion properties in order to provide a broader picture: the pion's Bethe-Salpeter amplitude is

$$\Gamma^\pi(P) = \gamma_5 \left[i E_\pi(P) + \frac{1}{M} \gamma \cdot P F_\pi(P) \right]. \tag{1.19}$$

1.3 ρ-meson Form Factors

At this point we can proceed to computation of the form factors. In order to ensure a symmetry-preserving treatment, one must calculate the vertex in Eq. (1.3) at the same level of approximation as used for the dressed-quark propagator and meson Bethe-Salpeter amplitude; i.e., the generalised impulse approximation:

$$\Gamma_{\alpha\mu\beta}(p,p') \;=\; \Gamma^u_{\alpha\mu\beta}(p,p') + \Gamma^d_{\alpha\mu\beta}(p,p')\,, \tag{1.20}$$

[1]Note, too, that we use a Euclidean metric: $\{\gamma_\mu, \gamma_\nu\} = 2\delta_{\mu\nu}$; $\gamma_\mu^\dagger = \gamma_\mu$; $\gamma_5 = \gamma_4\gamma_1\gamma_2\gamma_3$, ${\rm tr}[\gamma_5\gamma_\mu\gamma_\nu\gamma_\rho\gamma_\sigma] = -4\epsilon_{\mu\nu\rho\sigma}$; $\sigma_{\mu\nu} = (i/2)[\gamma_\mu, \gamma_\nu]$; $a \cdot b = \sum_{i=1}^4 a_i b_i$; and P_μ timelike $\Rightarrow P^2 < 0$.

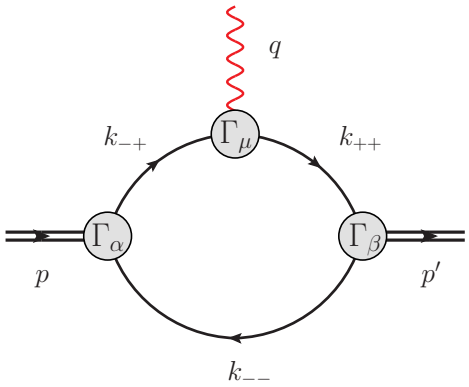

Figure 1.1. Impulse approximation to the ρ-γ vertex, Eq. (1.21): solid lines – dressed-quark propagators; and shaded circles, clockwise from top – Bethe-Salpeter vertex for quark-photon coupling, and Bethe-Salpeter amplitudes for the ρ^+-meson.

$$\Gamma^f_{\alpha\mu\beta}(p,p') = 2\int \frac{d^4k}{(2\pi)^4}\,\mathrm{Tr}_{CD}\Big\{ i\Gamma^{\rho_j}_\beta(k;-p')S(k_{++}) \times i\Gamma^f_\mu(k_{-+},k_{++})S(k_{-+})i\Gamma^{\rho_j}_\alpha(k-q/2;p)S(k_{--})\Big\}, \tag{1.21}$$

wherein the trace is over colour and spinor indices and $k_{\alpha\beta} = k + \alpha q/2 + \beta p/2$. We illustrate Eq. (1.21) in Fig. 1.1.

In evaluating Eq. (1.20) we write:

$$S_f = S + \delta_{\not CP}\, S_f\,, f = u, d, \tag{1.22}$$

where S is given in Eq. (1.9), with the dressed-mass obtained from Eq. (1.10), and the broken-CP corrections $\delta_{\not CP}\, S_f$ are detailed below; and the ρ-amplitude

$$\Gamma^{\rho_j}_\alpha = \gamma^T_\alpha E_\rho(P) + \Gamma^{\rho_j \not CP}_\alpha\,, \tag{1.23}$$

with $E_\rho(P)$ explained in connection with Eq. (1.18) and the broken-CP corrections $\Gamma^{\rho_j \not CP}_\alpha$ explained below. Our computed values for the dressed-quark mass, M, and E_ρ are listed in Table 1.1.

The remaining element in Eq. (1.20) is the dressed-quark–photon vertex. We are only interested in the $q^2 = 0$ values of the form factors and hence may use

$$
\begin{aligned}
e\Gamma_\mu(p_1,p_2) &= e\tilde{\mathcal{Q}}\,\gamma_\mu + i\tilde{\mathcal{D}}\gamma_5\sigma_{\mu\nu}(p_2-p_1)_\nu && (1.24)\\
&=: e\,\mathrm{diag}[e_u\Gamma^u_\mu(p_1,p_2), -e_d\Gamma^d_\mu(p_1,p_2)], && (1.25)
\end{aligned}
$$

where e is the positron charge, $\tilde{\mathcal{Q}} = \mathrm{diag}[e_u = 2/3, -e_d = 1/3]$ and $\tilde{\mathcal{D}} = \mathrm{diag}[d_u, -d_d]$, with d_f the EDM of a current quark with flavour f. N.B. The second term in Eq. (1.24) describes the explicit current-quark EDM interaction in Eq. (1.2). In Sec. 1.4 we show that the other terms in Eq. (1.2) generate additional contributions that interfere with this explicit term.

Note that both structures in the vertex, Eq. (1.24), are in general multiplied by momentum-dependent scalar functions. Naturally, the vector Ward-Takahashi identity ensures that the coefficient of the $\tilde{\mathcal{Q}}\gamma_\mu$ term is "1" at $q^2 = 0$. In connection with the tensor term, one knows from Ref. [66] that a tensor vertex is not dressed in the rainbow-ladder treatment of the contact interaction. However, with a more sophisticated interaction, strong interaction dressing of the $\gamma_5\sigma_{\mu\nu}$ part of the quark-photon vertex might be significant, given that the dressed-quark-photon vertex certainly possesses a large dressed-quark anomalous magnetic moment term owing to dynamical chiral symmetry breaking [102]. At $q^2 = 0$, this could enhance the strength of the $\tilde{\mathcal{D}}$ term by as much as a factor of ten. If so, then sensitivity to current-quark EDMs is greatly magnified. It is worth bearing this in mind.

Working with Eq. (1.3), it is sufficient herein to employ three projection operators:

$$
\begin{aligned}
P^1_{\alpha\mu\beta} &= \mathcal{P}^T_{\alpha\sigma}(p) P_\mu \mathcal{P}^T_{\sigma\beta}(p')\,, && (1.26a)\\
P^2_{\alpha\mu\beta} &= \mathcal{P}^T_{\alpha\alpha'}(p)\,\mathcal{P}^T_{\beta'\beta}(p')\left(\frac{\delta_{\mu\beta'}q_{\alpha'} - \delta_{\mu\alpha'}q_{\beta'}}{q^2} + \frac{P_\mu\delta_{\alpha'\beta'}}{6p^2}\right), && (1.26b)\\
P^3_{\alpha\mu\beta} &= \frac{1}{2iq^2}\,\mathcal{P}^T_{\alpha\alpha'}(p)\varepsilon_{\alpha'\beta'\mu\sigma}q_\sigma\mathcal{P}^T_{\beta'\beta}(p')\,, && (1.26c)
\end{aligned}
$$

with $p' = p + q$, $P = p + p'$, for then

$$\mathcal{E}(0) = \lim_{q^2 \to 0} \frac{1}{12 m_\rho^2} P^1_{\alpha\mu\beta} \Gamma_{\alpha\mu\beta} \,, \tag{1.27a}$$

$$\mathcal{M}(0) = \lim_{q^2 \to 0} \frac{1}{4} P^2_{\alpha\mu\beta} \Gamma_{\alpha\mu\beta} \,, \tag{1.27b}$$

$$\mathcal{D}(0) = \lim_{q^2 \to 0} P^3_{\alpha\mu\beta} \Gamma_{\alpha\mu\beta} \,, \tag{1.27c}$$

and $\mu_\rho = \mathcal{M}(0)\, e/[2m_\rho]$, $d_\rho = \mathcal{D}(0)\, e/[2m_\rho]$. So long as a global-symmetry-preserving regularisation scheme is implemented, $\mathcal{E}(0) = 1$; the value of $\mathcal{M}(0)$ is then a prediction, which can both be compared with that produced by other authors and serve as a benchmark for our prediction of $\mathcal{D}(0)$.

At this point one has sufficient information to calculate the ρ-meson's magnetic moment. We simplify the denominator in Eq. (1.20) via a Feynman parametrisation:

$$\begin{aligned} & \left(k_{++}^2 + M^2\right)^{-1} \left(k_{-+}^2 + M^2\right)^{-1} \left(k_{--}^2 + M^2\right)^{-1} \\ = \; & 2 \int_0^1 \int_0^{1-x} dx\, dy \Big[k^2 + M^2 + \frac{1}{4} \left[p^2 - 2\,(1 - 2x - 2y)\, p \cdot q + q^2 \right] \\ & - (1 - 2y)\, q \cdot k + (1 - 2x)\, p \cdot k \Big]^{-3} . \end{aligned} \tag{1.28}$$

This appears as part of an expression that is integrated over four-dimensional k-space. The expression is simplified by a shift in integration variables, which exposes a denominator of the form $1/[k^2 + \tilde{M}^2]^3$, with

$$\tilde{M}^2 = M^2 + x(x-1)\, m_\rho^2 + y(1 - x - y)\, Q^2 \,. \tag{1.29}$$

One thereby arrives at a compound expression that involves one-dimensional integrals of the form in Eq. (1.10), which we regularise via Eq. (1.11) and generalisations thereof; viz.,

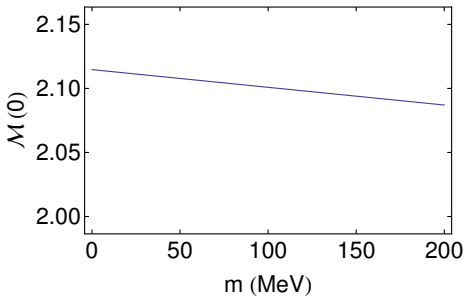

Figure 1.2. Evolution of ρ-meson magnetic moment with current-quark mass. $m = 170\,\mathrm{MeV}$ corresponds to the mass of the s-quark in our treatment of the contact interaction [69], so the difference between $\mathcal{M}_\rho(0)$ and $\mathcal{M}_\phi(0)$ is just 1%.

$$\int ds\, \frac{s}{[s+\omega]^2} = -\frac{d}{d\omega}\, \mathcal{C}^{\rm iu}(\omega) =: \overline{\mathcal{C}}_1^{\rm iu}(\omega)\,, \tag{1.30a}$$

$$\int ds\, \frac{s}{[s+\omega]^3} = \frac{1}{2}\frac{d^2}{d\omega^2}\, \mathcal{C}^{\rm iu}(\omega) =: \overline{\mathcal{C}}_2^{\rm iu}(\omega)\,, \tag{1.30b}$$

$$\int ds\, \frac{s^2}{[s+\omega]^3} = \overline{\mathcal{C}}_1^{\rm iu}(\omega) - \omega \overline{\mathcal{C}}_2^{\rm iu}(\omega)\,, \tag{1.30c}$$

etc. Details for this component of our computation may be found in Ref. [66] and pursuing it to completion one obtains the magnetic moment listed in Table 1.2.

We depict the evolution of $\mathcal{M}(0)$ with current-quark mass in Fig. 1.2: $\mathcal{M}(0)$ is almost independent of m. This outcome matches that obtained in Ref. [81] using a renormalisation-group-improved one-gluon exchange kernel and hence a momentum-dependent dressed-quark mass-function of the type possessed by QCD [103, 104, 105, 106]. The behaviour in Fig. 1.2 will serve to benchmark that of the ρ-meson's EDM.

1.4 ρ-meson EDM: Formulae

We now turn to computation of the effect of the interaction terms in Eq. (1.2) on the ρ-meson. There are three types of contribution, which arise separately through modification of: (1) the quark-photon vertex, Eq. (1.24); (2) the ρ-meson Bethe-Salpeter amplitude, Eq. (1.23); and (3) the dressed-quark propagator, Eq. (1.22).

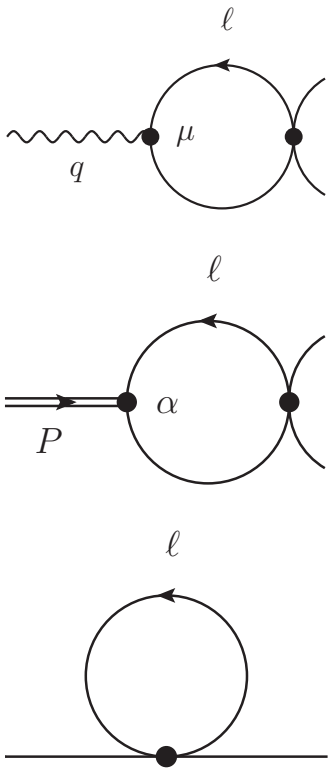

Figure 1.3. *Top* – Correction to the quark-photon vertex generated by the four-fermion operator in Eq. (1.31). The unmodified quark-photon vertex is the left dot, whereas the right dot locates insertion of $\mathcal{L}_6$. If the internal line represents a circulating d-quark then, owing to the $\mathcal{L}_6$ insertion, the external lines are u-quarks, and vice versa. *Middle* – Analogous correction to the ρ-meson Bethe-Salpeter amplitude. The unmodified amplitude is the left dot, whereas the right dot locates insertion of $\mathcal{L}_6$. The lower internal line is an incoming d-quark and the upper external line is an outgoing u-quark. *Bottom* – $\mathcal{L}_6$-correction to the dressed-quark propagator, with the dot locating the operator insertion. If the outer line is a u-quark, then the internal line is a d-quark; and vice versa.

1.4.1 Four-fermion interaction

We begin with the dimension-six operator, which can be written explicitly as

$$\mathcal{L}_6 = i\frac{\mathcal{K}}{2\Lambda^2}\left[\bar{u}^a d^a \bar{d}^b \gamma_5 u^b + \bar{u}^a \gamma_5 d^a \bar{d}^b u^b - \bar{d}^a d^a \bar{u}^b \gamma_5 u^b - \bar{d}^a \gamma_5 d^a \bar{u}^b u^b\right], \tag{1.31}$$

with summation over the repeated colour indices. This operator generates all three types of modification.

1.4.1.1 $\mathcal{L}_6$ – quark-photon vertex

This contribution is depicted in the top panel of Fig. 1.3. Consider first the case of d-quarks circulating in the loop, then straightforward but careful analysis of the induced Wick contractions produces the following result:

$$\Gamma_\mu^{\gamma_{\mathcal{L}_6^d}} = -i\frac{\mathcal{K}}{\Lambda^2}\frac{e_d}{e_u}\int\frac{d^4\ell}{(2\pi)^4}\left[I_\mu^{12}+N_c I_\mu^3\right], \tag{1.32a}$$

$$I_\mu^{12} = -P_R S(\ell+q)\gamma_\mu S(\ell)P_R + P_L S(\ell+q)\gamma_\mu S(\ell)P_L\,, \tag{1.32b}$$

$$I_\mu^{3} = P_L\,\mathrm{tr}\{S(\ell+q)\gamma_\mu S(\ell)P_L\} - P_R\,\mathrm{tr}\{S(\ell+q)\gamma_\mu S(\ell)P_R\}\,, \tag{1.32c}$$

where $P_{R,L}=(1/2)(1\pm\gamma_5)$. These right- and left-handed projection operators satisfy $P_R+P_L=I_{\rm D}$.

Further simplification of the integrand reveals

$$\begin{aligned} I_\mu^{12} &= I_\mu^1 + I_\mu^2 \\ &= \frac{i\gamma\cdot q}{(\ell+q)^2+M^2}\gamma_\mu\frac{M}{\ell^2+M^2}\gamma_5 + 2i\frac{\ell_\mu}{(\ell+q)^2+M^2}\frac{M}{\ell^2+M^2}\gamma_5\,, \end{aligned} \tag{1.33a}$$

$$I_\mu^3 = \frac{2i(2\ell_\mu+q_\mu)}{(\ell+q)^2+M^2}\frac{M}{\ell^2+M^2}\gamma_5\,, \tag{1.33b}$$

so that one may subsequently obtain

$$\int\frac{d^4\ell}{(2\pi)^4}I_\mu^1 = (q_\mu+i\sigma_{\mu\nu}q_\nu)\gamma_5\frac{iM}{16\pi^2}\int_0^1 dx\,\overline{\mathcal{C}}_1^{\rm iu}(\omega_q)\,, \tag{1.34a}$$

$$\int\frac{d^4\ell}{(2\pi)^4}I_\mu^2 = -q_\mu\gamma_5\frac{iM}{8\pi^2}\int_0^1 dx\,x\,\overline{\mathcal{C}}_1^{\rm iu}(\omega_q)\,, \tag{1.34b}$$

$$\int\frac{d^4\ell}{(2\pi)^4}I_\mu^3 = q_\mu\gamma_5\frac{iM}{8\pi^2}\int_0^1 dx\,(1-2x)\,\overline{\mathcal{C}}_1^{\rm iu}(\omega_q)\,, \tag{1.34c}$$

where $\omega_q=x(1-x)q^2+M^2$. Combining the terms, Eq. (1.32a) becomes

$$\Gamma_\mu^{\gamma_{\mathcal{L}_6^d}} = \frac{\mathcal{K}}{\Lambda^2}\frac{e_d}{e_u}\frac{M}{16\pi^2}\int_0^1 dx\,\overline{\mathcal{C}}_1^{\rm iu}(\omega_q)[(1+2N_c)(1-2x)q_\mu+i\sigma_{\mu\nu}q_\nu]\gamma_5 \tag{1.35}$$

$$\stackrel{q^2=0}{=} \frac{\mathcal{K}}{\Lambda^2}\frac{e_d}{e_u}\frac{M}{16\pi^2}\overline{\mathcal{C}}_1^{\rm iu}(M^2)i\sigma_{\mu\nu}q_\nu\gamma_5\,. \tag{1.36}$$

In the other case, with a u-quark circulating in the loop, one obtains

$$\Gamma_\mu^{\gamma_{\mathcal{L}_6^u}} \stackrel{q^2=0}{=} \frac{\mathcal{K}}{\Lambda^2}\frac{e_u}{e_d}\frac{M}{16\pi^2}\overline{\mathcal{C}}_1^{\rm iu}(M^2) i\sigma_{\mu\nu}q_\nu\gamma_5\,. \tag{1.37}$$

Plainly, the net correction to the quark-photon vertex can now be cast in the form of the second term in Eq. (1.24) and hence is readily expressed in $\mathcal{D}(0)$.

1.4.1.2 $\mathcal{L}_6$ – Bethe-Salpeter amplitude

This correction is depicted in the middle panel of Fig. 1.3. Each of the four terms in Eq. (1.31) generates a distinct contribution. That from the first and second are:

$$\begin{aligned}
\Gamma_\alpha^{\rho\mathcal{L}_6^1} &= -i\frac{\mathcal{K}}{\Lambda^2}N_c E_\rho\, P_R \\
&\quad \times{\rm tr}\int\frac{d^4\ell}{(2\pi)^4}S(\ell)P_R S(\ell+P)\gamma_\alpha^T\,, \qquad (1.38a)\\
\Gamma_\alpha^{\rho\mathcal{L}_6^2} &= -i\frac{\mathcal{K}}{\Lambda^2}E_\rho\, P_R \\
&\quad \times\int\frac{d^4\ell}{(2\pi)^4}S(\ell+P)\gamma_\alpha^T S(\ell)P_R\,. \qquad (1.38b)
\end{aligned}$$

The third and fourth terms are identical, up to sign-change and the replacement $P_R \to P_L$; and hence

$$\Gamma_\alpha^{\rho\mathcal{L}_6} = i\frac{\mathcal{K}}{\Lambda^2}E_\rho\int\frac{d^4\ell}{(2\pi)^4}\big[I_\alpha^{12{\rm T}} + N_c I_\alpha^{3{\rm T}}\big], \tag{1.39}$$

where the superscript "T" indicates that $\gamma_\alpha^{\rm T}$ is here used in the expressions for I^{12}, I^3.

Now, using the formulae of Sec. 1.4.1.1, one arrives at

$$\Gamma_\alpha^{\rho\mathcal{L}_6} = -i\frac{\mathcal{K}}{\Lambda^2}\frac{ME_\rho}{16\pi^2}\gamma_5\sigma_{\alpha\nu}P_\nu\int_0^1 dx\,\overline{\mathcal{C}}_1^{\rm iu}(\omega_P)\,, \tag{1.40}$$

where $\omega_P = x(1-x)P^2 + M^2$, $P^2 = -m_\rho^2$. This is one of the additive corrections to the Bethe-Salpeter amplitude anticipated in Eq. (1.23).

1.4.1.3 $\mathcal{L}_6$ – quark propagator

The final modification arising from the dimension-six operator is that depicted in the bottom panel of Fig. 1.3. So long as the correction is small, it modifies the dressed-quark propagator as follows:

$$S(k) \to S(k) + \delta_{\mathcal{L}_6} S(k) = S(k) + S(k) i\Gamma^{S\mathcal{L}_6} S(k)\,, \tag{1.41}$$

where, once again, each of the four terms in Eq. (1.31) contributes. Their sum is

$$\begin{aligned}\Gamma^{S\mathcal{L}_6} = \frac{\mathcal{K}}{\Lambda^2}\int \frac{d^4\ell}{(2\pi)^4}\big[&P_R S(\ell) P_R - P_L S(\ell) P_L \\ &+ N_c P_R \,\mathrm{tr}\{S(\ell) P_R\} - N_c P_L \,\mathrm{tr}\{S(\ell) P_L\}\big]\,.\end{aligned} \tag{1.42}$$

Now

$$\begin{aligned}P_R S(\ell) P_R - P_L S(\ell) P_L &= \frac{M}{\ell^2 + M^2}\gamma_5 \\ &= \frac{1}{2}\big[P_R \,\mathrm{tr}\{S(\ell) P_R\} - P_L \,\mathrm{tr}\{S(\ell) P_L\}\big],\end{aligned} \tag{1.43}$$

so that with little additional algebra one arrives at

$$\delta_{\mathcal{L}_6} S(k) = \frac{i}{k^2 + M^2}(1 + 2N_c)\frac{\mathcal{K}}{\Lambda^2}\frac{M}{16\pi^2}\mathcal{C}^{\mathrm{iu}}(M^2)\gamma_5\,. \tag{1.44}$$

1.4.2 Quark chromo-EDM

The term in the middle line of Eq. (1.2) also generates all three types of modification described in the opening lines of this Section. Notably, owing to dynamical chiral symmetry breaking, the dressed-quark-gluon coupling possesses a chromomagnetic moment term that, at infrared momenta, is two orders-of-magnitude larger than the perturbative estimate [102]. One may reasonably expect similar strong-interaction dressing of a light-quark's chromo-EDM interaction with a gluon, in which case sensitivity to the current-quark's chromo-EDM is very much enhanced.

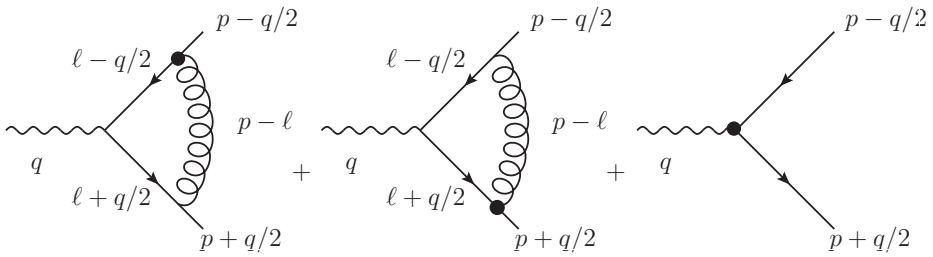

Figure 1.4. Correction to the quark-photon vertex generated by the quark chromo-EDM operator in Eq. (1.2): the incoming and outgoing quark lines have the same flavour, f. The dot in the left two diagrams locates insertion of $\mathcal{L}_{CEDM}$, whilst that in the rightmost diagram indicates the second term in Eq. (1.24); i.e., the explicit quark EDM.

1.4.2.1 $\mathcal{L}_{CEDM}$ – quark-photon vertex

This contribution is depicted in Fig. 1.4. After a lengthy analysis, in which we represent the exchanged gluon via Eq. (1.6), the sum of the two leftmost diagrams produces

$$\begin{aligned}
\Gamma^{\gamma(g)}_{\mu} &= \frac{1}{6i\pi}\frac{\tilde{d}_f\alpha_{\rm IR}}{m_G^2}\int_0^1 dx\,\big[\mathcal{C}^{\rm iu}(\omega_q)-\mathcal{C}_1^{\rm iu}(\omega_q)\big]\,\Big\{2q_\alpha\,\sigma_{\mu\alpha}\gamma_5 \\
&\quad -6i\big[3(x-1/2)q_\mu-p_\mu\big]\,\gamma_5\Big\}-\frac{1}{3\pi}\frac{\tilde{d}_f\alpha_{\rm IR}}{m_G^2}\int_0^1 dx\,\overline{\mathcal{C}}_1^{\rm iu}(\omega_q)\,\times \\
&\quad \Big\{6\big[\omega_q-2M^2\big]\,p_\mu\gamma_5-6\big[(x-1/2)\omega_q+2x(1-x)q\cdot p\big]\,q_\mu\gamma_5 \\
&\quad +M\big[((x-1/2)q+p)\cdot\gamma\big]q_\alpha\sigma_{\alpha\mu}\gamma_5 \\
&\quad +Mq_\alpha\sigma_{\alpha\mu}\gamma_5\big[((x-1/2)q+p)\cdot\gamma\big]\Big\}\,, \qquad (1.45)
\end{aligned}$$

where, again, $\tilde{d}_f$ is the chromo-EDM of a quark with flavour f.

As we are interested solely in the EDM, we may consider $q^2=0$, at which value the result simplifies greatly:

$$\begin{aligned}
\Gamma^{\gamma(g)}_{\mu} &= \frac{1}{3i\pi}\frac{\tilde{d}_f\alpha_{\rm IR}}{m_G^2}\big[\mathcal{C}^{\rm iu}(M^2)-\mathcal{C}_1^{\rm iu}(M^2)\big]\big[\gamma_5\sigma_{\mu\alpha}q_\alpha+3ip_\mu\,\gamma_5\big] \\
&\quad +\frac{1}{3\pi}\frac{\tilde{d}_f\alpha_{\rm IR}}{m_G^2}\,\overline{\mathcal{C}}_1^{\rm iu}(M^2)\,\Big[M\{\gamma\cdot p,\gamma_5\sigma_{\mu\alpha}\}q_\alpha+2p\cdot q q_\mu\gamma_5 \\
&\quad +6M^2p_\mu\gamma_5\Big]. \qquad (1.46)
\end{aligned}$$

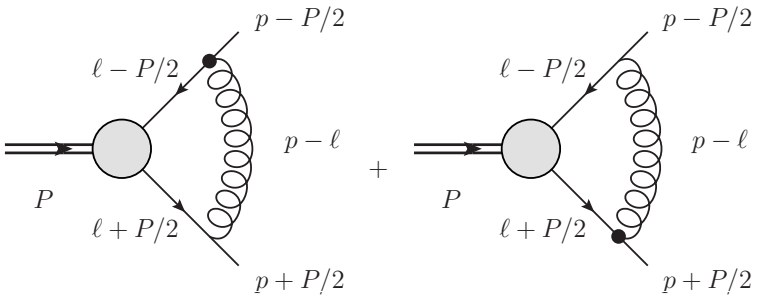

Figure 1.5. Correction to the ρ-meson Bethe-Salpeter amplitude generated by the quark chromo-EDM operator in Eq. (1.2): the incoming line is a d-quark and the outgoing line is a u-quark. In each case the dot locates insertion of $\mathcal{L}_{CEDM}$.

Plainly, the net correction to the quark-photon vertex from these two diagrams can now be cast in the form of the second term in Eq. (1.24), which, in fact, is precisely the rightmost diagram in Fig. 1.4 because $q = p_2 - p_1$.

1.4.2.2 $\mathcal{L}_{CEDM}$ – Bethe-Salpeter amplitude

This correction is expressed in Fig. 1.5. Owing to similarity between the $\mathcal{L}_{\rm eff}$-uncorrected ρ-meson amplitude and quark-photon vertex, the results can be read from those in Sec. 1.4.2.1; viz., with $\tilde{d}_\pm = \tilde{d}_u \pm \tilde{d}_d$,

$$
\begin{aligned}
\Gamma^{\rho(g)}_\alpha \;=\; & \frac{1}{6i\pi}\frac{\alpha_{\rm IR}}{m_G^2}E_\rho \int_0^1 dx\,\left[\mathcal{C}^{\rm iu}(\omega_P) - \mathcal{C}_1^{\rm iu}(\omega_P)\right] \\
& \times\Big\{\left[(\tilde{d}_+ - 3(x-1/2)\tilde{d}_-)P_\beta - \tilde{d}_- p_\beta\right]\sigma_{\mu\beta}\gamma_5\mathcal{P}^T_{\mu\alpha} \\
& \quad +3i\tilde{d}_+ p_\mu\gamma_5\mathcal{P}^T_{\mu\alpha} - 3\tilde{d}_- M\gamma_\mu\gamma_5\mathcal{P}^T_{\mu\alpha}\Big\} \\
& -\frac{1}{3\pi}\frac{\alpha_{\rm IR}}{m_G^2}E_\rho\int_0^1 dx\,\bar{\mathcal{C}}_1^{\rm iu}(\omega_P)\Big\{3\tilde{d}_+\left[\omega_P - 2M^2\right]p_\mu\gamma_5\mathcal{P}^T_{\mu\alpha} \\
& -\tilde{d}_-\left([\omega_P - 2M^2][(x-1/2)P_\beta + p_\beta]\right) i\gamma_5\sigma_{\beta\mu}\mathcal{P}^T_{\mu\alpha} \\
& +M\tilde{d}_d\left[((x-1/2)P+p)\cdot\gamma\right]P_\beta\sigma_{\beta\mu}\gamma_5\mathcal{P}^T_{\mu\alpha} \\
& +M\tilde{d}_u P_\beta\sigma_{\beta\mu}\gamma_5\mathcal{P}^T_{\mu\alpha}\left[((x-1/2)P+p)\cdot\gamma\right]\Big\}. \qquad (1.47)
\end{aligned}
$$

Figure 1.6. Correction to the dressed-quark propagator generated by the quark chromo-EDM operator in Eq. (1.2). In each image the dot locates insertion of $\mathcal{L}_{CEDM}$.

In computing the vertex in Eq. (1.20) one must employ Fig. 1.5 and also its charge conjugate, the form of which is obtained from Eq. (1.47) via the interchange $\tilde{d}_u \leftrightarrow \tilde{d}_d$, and $p \to -p$, $P \to -P$.

1.4.2.3 $\mathcal{L}_{CEDM}$ – quark propagator

The last modification generated by the chromo-EDM term in Eq. (1.2) is that to the quark propagator, Fig. 1.6. The self-energy insertion is readily evaluated:

$$\Gamma^{S(g)} = \tilde{d}_f \, \frac{8}{\pi} \, \frac{\alpha_{\rm IR}}{m_G^2} \, \mathcal{D}^{\rm iu}(M^2) \gamma_5 \,, \tag{1.48}$$

where

$$\mathcal{D}^{\rm iu}(\omega) = \int ds \frac{s^2}{s+\omega} \to \int_{\tau_{\rm uv}^2}^{\tau_{\rm ir}^2} d\tau \, \frac{2}{\tau^3} \, \exp(-\tau\omega), \tag{1.49}$$

so that, with $f = u, d$,

$$\delta_{(g)} S_f(k) = \frac{i}{k^2 + M^2} \, \tilde{d}_f \, \frac{8}{\pi} \, \frac{\alpha_{\rm IR}}{m_G^2} \, \mathcal{D}^{\rm iu}(M^2) \gamma_5 \,. \tag{1.50}$$

1.4.3 θ-term

Owing to a connection between the Higgs mechanism for generating current-quark masses in the SM and CP violation in the weak interaction, the effect of the θ-term can completely be expressed through a $U_A(1)$ rotation of the current-quark mass-matrix. We consider the s-quark to be massive and $m_u = m_d$, in which case the effect

of the first term in Eq. (1.2) is expressed simply in a modification of the dressed-quark propagator:

$$S(k) \quad \to \quad \frac{1}{i\gamma\cdot k + M + \frac{i}{2} m\,\bar\theta\,\gamma_5} \tag{1.51}$$

$$\overset{m\bar\theta\,\text{small}}{\approx} \quad S(k) - \frac{1}{k^2+M^2}\frac{i}{2} m\,\bar\theta\,\gamma_5\,. \tag{1.52}$$

1.4.3.1 Dressed-quark anomalous chromomagnetic moment

In our global-symmetry-preserving rainbow-ladder treatment of the contact interaction, the general form of the ρ-meson's Bethe-Salpeter amplitude is given in Eq. (1.18). The absence of a term $\sigma_{\mu\nu}P_\nu F_\rho(P)$ is an artefact of the rainbow-ladder truncation: even using Eq. (1.6), a Bethe-Salpeter amplitude with $F_\rho(P) \neq 0$ is obtained in any symmetry-preserving truncation that goes beyond this leading order [77]. One material consequence of this omission is complete cancellation of all terms at leading-order in $\bar\theta$, so that the θ-term's contribution to the ρ-meson's EDM is anomalously suppressed in rainbow-ladder truncation. This defect may be ameliorated by acknowledging that the dressed-quark-gluon vertex possesses an anomalous chromomagnetic moment coupling which is enhanced by dynamical chiral symmetry breaking [102]. We therefore include an effect generated by

$$\Gamma^{\rm acm}_\mu(p_i,p_f) = \frac{\mu^{\rm acm}}{2M}\sigma_{\mu\nu}(p_f-p_i)_\nu\,, \tag{1.53}$$

where [107] $\mu^{\rm acm} \sim (-1/4)$.

In order to explicate the effect we find it convenient to first express collectively the corrections to the dressed-quark propagator computed above; viz., from Eqs. (1.44), (1.50), (1.52),

$$
\begin{aligned}
S(k) &\to S(k) - i\gamma_5 \frac{\lambda}{k^2+M^2}\,, && (1.54)\\
\lambda_{\mathcal{L}_6} &= -(1+2N_c)\frac{\mathcal{K}}{\Lambda^2}\frac{M}{16\pi^2}\mathcal{C}^{\rm iu}(M^2)\,, && (1.55)\\
\lambda_{(g)} &= -\tilde{d}_f\,\frac{8}{\pi}\,\frac{\alpha_{\rm IR}}{m_G^2}\,\mathcal{D}^{\rm iu}(M^2)\,, && (1.56)\\
\lambda_{\bar\theta} &= \frac{1}{2} m\bar\theta\,. && (1.57)
\end{aligned}
$$

Our corrections are now obtained via the diagrams in Fig. 1.5, except that here the dots represent Eq. (1.53), and one simultaneously adds the correction to one and then the other propagator. In this way, careful but straightforward computation yields

$$
\begin{aligned}
\Gamma^{\lambda,{\rm acm}}_\mu &= \frac{\alpha_{\rm IR}}{2i\pi m_G^2}\frac{\lambda^1\mu_2^{\rm acm}-\lambda^2\mu_1^{\rm acm}}{2M}\int_0^1 dx\,\left[\mathcal{C}^{\rm iu}(\omega_P)-\mathcal{C}_1^{\rm iu}(\omega_P)\right]\gamma_\mu\gamma_5\\
&+\frac{\alpha_{\rm IR}}{6i\pi m_G^2}\frac{1}{M}\int_0^1 dx\,\bar{\mathcal{C}}_1^{\rm iu}(\omega_P)\Big\{3\mu_-^{\rm acm}\gamma\cdot(p+(x-1/2)P)\\
&\times[(1-x)\lambda^1-x\lambda^2]P_\mu + i\big[(1-x)\lambda^1+x\lambda^2\big)\big]\big[\mu_1^{\rm acm}\gamma_\nu P_\alpha\sigma_{\alpha\mu}\\
&-\mu_2^{\rm acm}P_\alpha\sigma_{\alpha\mu}\gamma_\nu\big](p+(x-1/2)P)_\nu - \lambda^- M\big[\mu_+^{\rm acm}(p+(x-1/2)P)_\beta\sigma_{\mu\beta}\\
&+3i\mu_-^{\rm acm}(p+(x-1/2)P)_\mu\big]\Big\}\gamma_5\,, \qquad (1.58)
\end{aligned}
$$

where $\mu_\pm^{\rm acm}=\mu_1^{\rm acm}\pm\mu_2^{\rm acm}$, and $\{\lambda^i,\,i=1,2\}$ represents the quark propagator correction on each leg with $\lambda^\pm=\lambda^1\pm\lambda^2$.

One can now adapt the general expression in Eq. (1.58) to the particular cases of relevance herein. The first is the ρ-meson Bethe-Salpeter amplitude. Capitalising on isospin symmetry, which entails $\mu_u^{\rm acm}=\mu_d^{\rm acm}=:\mu^{\rm acm}$, one finds

$$
\begin{aligned}
\Gamma^{\rho\,{\rm acm}}_\alpha &= \frac{\alpha_{\rm IR}}{2i\pi m_G^2}\frac{\mu^{\rm acm}\lambda^-}{2M}E_\rho\int_0^1 dx\,\left[\mathcal{C}^{\rm iu}(\omega_P)-\mathcal{C}_1^{\rm iu}(\omega_P)\right]\gamma_\mu\mathcal{P}_{\mu\alpha}\gamma_5\\
&+\frac{\alpha_{\rm IR}}{3i\pi m_G^2}\frac{\mu^{\rm acm}}{2M}E_\rho\int_0^1 dx\,\bar{\mathcal{C}}_1^{\rm iu}(\omega_P)\Big\{i\big[(1-x)\lambda^1\\
&+x\lambda^2\big]\big(\gamma_\beta P_\nu\sigma_{\nu\alpha}-P_\nu\sigma_{\nu\alpha}\gamma_\beta\big)(p+(x-1/2)P)_\beta\\
&-2\lambda^- M\mathcal{P}_{\mu\alpha}(p+(x-1/2)P)_\nu\sigma_{\mu\nu}\Big\}\gamma_5\,, \qquad (1.59)
\end{aligned}
$$

where "λ" is constructed from the correction specified in one of Eqs. (1.55) – (1.57).

The other case is the quark-photon vertex, for which the correction is found with $\lambda^1 = \lambda^2 = \lambda$, since the quark flavours are identical, and we need only consider $q^2 = 0$:

$$\Gamma_\mu^{\gamma\,\mathrm{acm}} = \frac{\alpha_{\mathrm{IR}}}{3\pi m_G^2}\frac{\mu^{\mathrm{acm}}\lambda}{2M}\bar{\mathcal{C}}_1^{\mathrm{iu}}(M^2)\gamma_5\big[\gamma\cdot p\,,\,\sigma_{\mu\alpha}q_\alpha\big]\,. \tag{1.60}$$

1.5 ρ-meson EDM: Results

1.5.1 Analysis without Peccei-Quinn symmetry

In order to obtain a result for the ρ-meson's EDM, d_ρ, it remains only to sum the various contributions derived in Sec. 1.4 as they contribute to Eq. (1.20), evaluated with the parameter values in Table 1.1:

$$\begin{aligned} d_\rho &= -2.88\times 10^{-3}\,\mu^{\mathrm{acm}}\,e\bar{\theta}/\mathit{s} \\ &\quad +0.785\,(d_u - d_d) \\ &\quad +(1.352 + 0.775\,\mu^{\mathrm{acm}})e(\tilde{d}_u - \tilde{d}_d) \\ &\quad -(0.091 - 2.396\,\mu^{\mathrm{acm}})e(\tilde{d}_u + \tilde{d}_d) \\ &\quad -e\frac{\mathit{s}\mathcal{K}}{\Lambda^2}\,(2.696 - 6.798\,\mu^{\mathrm{acm}})\times 10^{-3}\,. \end{aligned} \tag{1.61}$$

In this formula, d_f, $\tilde{d}_f$ carry a dimension of inverse-mass and $\mathit{s} = 1\,\mathrm{GeV}$.

A nugatory transformation allows one to rewrite Eq. (1.61) in terms of dimensionless electric and chromoelectric quark dipole moments; viz.,

$$\begin{aligned} d_\rho &= -2.88\times 10^{-3}\,\mu^{\mathrm{acm}}\,e\bar{\theta}/\mathit{s} \\ &\quad +\frac{v_H}{\Lambda^2}\Big[0.785\,(D_u - D_d) \\ &\quad +(1.352 + 0.775\,\mu^{\mathrm{acm}})e(\tilde{D}_u - \tilde{D}_d) \\ &\quad -(0.091 - 2.396\,\mu^{\mathrm{acm}})e(\tilde{D}_u + \tilde{D}_d) \\ &\quad -(1.096 - 2.763\,\mu^{\mathrm{acm}})\times 10^{-5}\,e\mathcal{K}\Big]\,, \end{aligned} \tag{1.62}$$

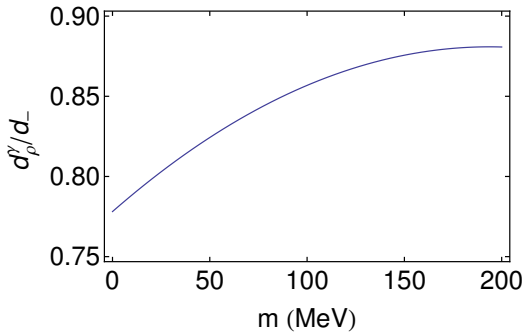

Figure 1.7. Evolution of the quark-EDM component of the ρ-meson's EDM with current-quark mass, assuming d_- is independent of m. $m = 170\,\mathrm{MeV}$ corresponds to the mass of the s-quark in our treatment of the contact interaction [69], so the difference between d_ρ^γ and d_ϕ^γ is 10%.

where $v_H = 246\,\mathrm{GeV}$ is the cube-root of the phenomenological Higgs vacuum expectation value. In a class of models that includes, e.g., Ref. [108], one finds

$$D_f \sim \frac{m_f}{v_H} \sim 2 \times 10^{-5}, \tag{1.63}$$

a result which may be used to inform expectations about the "natural" magnitude of the terms in Eqs. (1.61), (1.62).

There are four distinct types of contribution to d_ρ in Eq. (1.61). The first is associated with the θ-term; and it is notable that this contribution vanishes in the absence of a dressed-quark anomalous magnetic moment, a feature which emphasises the connection between topology and dynamical chiral symmetry breaking that is highlighted, e.g., in Eq. (21) of Ref. [87]. Our result may directly be compared with that obtained in a sum rules analysis; viz.,

$$\begin{aligned} \text{herein}: &\quad -2.9 \times 10^{-3}\, \mu^{\mathrm{acm}}\, e\bar{\theta} \sim 0.7 \times 10^{-3}\, e\bar{\theta} \\ \text{Ref. [62]}: &\quad 4.4 \times 10^{-3}\, e\bar{\theta}\,. \end{aligned} \tag{1.64}$$

The second contribution owes to an explicit dressed-quark EDM. It has been computed via a number of methods, so that a comparison with our results is readily

compiled:

$$\begin{array}{ccccc} \text{herein} & \text{DSE}\,[60] & \text{BM}\,[60] & \text{nrQM}\,[60] & \text{sum rules}\,[62] \\ 0.79 & 0.72 & 0.83 & 1.00 & 0.51\,, \end{array} \tag{1.65}$$

where each entry is multiplied by $d_- = (d_u - d_d)$; and DSE [60] summarises results obtained from momentum-dependent DSE input, BM [60] reports a bag-model result, and nrQM [60] is the non-relativistic constituent-quark value. We depict the current-quark mass dependence of this contribution in Fig. 1.7. It is notable that the magnitude of these results matches an existing DSE estimate of the analogous contribution to the neutron's EDM [109]. Moreover, based on Ref. [110], a perturbative analysis would yield $2m_\rho d_\rho^{\rm pert} = 2m\, d_-$, where m is the current-quark mass. With the parameter values employed herein, this is $d_\rho^{\rm pert} = 0.014\, d_-$, which is just $\sim 2\%$ of the order-of-magnitude specified by the values in Eq. (1.65).

The third contribution to d_ρ is generated by the quark's chromoelectric dipole moment. Its subcomponents are detailed in Table 1.3. The net result is comparable in magnitude and sign with that produced by the quark EDM, Eq. (1.65). In comparison with a sum rules computation [62], however, our result is an order of magnitude larger, has the opposite sign and contains a sizeable $\tilde{d}_+$-term. At least the first two of these marked discrepancies are insensitive to reasonable variations in $\mu^{\rm acm}$. It is worth emphasising here that our calculation has no other variable parameters: the two specifying our model, listed in Table 1.1, were fixed in prior studies of an array of meson and baryon observables [64, 65, 67, 66, 68, 69]. This mismatch will receive further attention in future work.

The four-fermion interaction is responsible for the final contribution in Eq. (1.61). Its subcomponents are detailed in Table 1.4. As ours is the first estimate of the contribution from a dimension-six operator to the ρ-meson's EDM, there is no ready substantial comparison. On the other hand, the result in Table 1.4 is quickly seen to be "natural" in size. The dimension-six operator is associated with a coupling $\mathcal{K}/\Lambda^2$,

which has mass-dimension "−2". In order to obtain a quantity with mass-dimension "−1", this coupling must be multiplied by another energy scale. We are interested in an hadronic EDM, so that scale should be typical of hadron physics; e.g., the dressed-quark mass "M". Finally, a loop correction is required for the generation of an EDM, and loops are characterised by a factor $1/(16\pi^2)$. Putting these quantities together yields an expectation based on naive dimensional analysis; viz.,

$$d_\rho^{D=6} \sim e \frac{1}{16\pi^2} \frac{M}{v_H} \frac{v_H \mathcal{K}}{\Lambda^2} \sim 1 \times 10^{-5} \frac{e v_H \mathcal{K}}{\Lambda^2}\,, \tag{1.66}$$

in agreement with the magnitude of the final row in Table 1.4. Comparison with Eq. (1.63), furthermore, indicates that in our computation the quark-EDM and dimension-six contributions are naturally related via

$$d_\rho^{q\mathrm{EDM}}\, \mathcal{K} \sim d_\rho^{D=6}. \tag{1.67}$$

1.5.2 Peccei Quinn Symmetry

The leading term in Eq. (1.62) is that associated with $\bar{\theta}$. Arising from a dimension-four operator, this contribution is not suppressed by a large beyond-SM mass-scale. One may furthermore expect that, absent any symmetry to prevent it, a typical non-SM for CP-violation will produce large corrections to $\bar{\theta}$. In order to reconcile this with the remarkably small upper-bound on $\bar{\theta}$ placed by the neutron's EDM, one must accept that the initial value of $\bar{\theta}$ is very finely tuned. There is nothing to prevent this from being simply an accident of Nature. However, some view that possibility as aesthetically displeasing and prefer to introduce a new dynamical degree of freedom, the axion, a pseudo-Goldstone boson, whose role is to cancel the effect of $\bar{\theta}$ [35]. It is notable that there is currently no empirical evidence in favour of the axion's existence and the remaining domain of parameter space is small [115].

Notwithstanding this, in the context of EDM estimates it is customary to expose the possible effect of axion physics on the results in Eq. (1.61) or (1.62). Here there is a complication. If one considers an extension of the SM with a collection of CP-odd operators that may mix with the $\bar{\theta}$-term, then the effective potential describing axion physics at the hadronic scale can plausibly acquire terms that shift its minimum to a nonzero value of the effective $\bar{\theta}$-parameter, $\bar{\theta}_{\text{induced}}$ [55]. The quark chromoelectric dipole moment interaction is one such operator. In its case, within a sum rules calculation [62], the net effect of this mixing is elimination of $\bar{\theta}$ in favour of a modest enhancement in magnitude of the coefficients of $\tilde{d}_{\pm}$ in Eq. (1.61), with no change in sign.

The implications for our study are plain. Allowing an axion-like mechanism to play a role, then $\bar{\theta}$ disappears from Eqs. (1.61) and (1.62), and any measurement of an hadron EDM, here that of the ρ-meson, places a little more stringent constraint on $\tilde{d}_{\pm}$ in particular but also on $d_{\pm}$ and $\mathcal{K}$.

This is, perhaps, particularly relevant to $\mathcal{K}$, since the high-scale physics that generates this operator will typically also produce a complex phase for the quark masses. Within the low-energy effective theory of Eq. (1.2), this phase will arise from one-loop contributions to the quark propagator containing one insertion of the CP-violating four-quark operator and the quark Yukawa interaction. Consequently, constraints on $\bar{\theta}$ imply a bound on $\mathcal{K}$. On the other hand, with the elimination of $\bar{\theta}$ via an axion effective potential, the term modulated by $\mathcal{K}$ is exposed to independent constraint [56]. Computing the contribution of the four-quark CP-violating operator to the axion potential, determining the resulting dependence of $\bar{\theta}_{\text{induced}}$ on $\mathcal{K}$, and deriving the expression corresponding to Eq. (1.62) will be the subject of future work.

1.6 Epilogue

Using the leading-order in a global-symmetry-preserving truncation of QCD's Dyson-Schwinger equations, we computed the electric dipole moment of the ρ-meson, d_ρ, that is generated by the leading dimension-four and -five CP-violating operators and an example of a dimension-six operator. We employed a momentum-independent form for the leading-order kernel in the gap- and Bethe-Salpeter equations. This is known to produce results for low-energy pseudoscalar- and vector-meson observables that are indistinguishable from those obtained with the most sophisticated interactions available when they are analysed using the same truncation. Since the dipole moment is a low-energy observable, our predictions should be similarly reliable, in which case the framework we employ and elucidate can usefully be adapted to the more challenging task of computing the neutron's EDM, d_n.

We find that the two dimension-five operators; namely, quark-EDM and -chromo-EDM, characterised by d_q and $\tilde{d}_q$, respectively, produce contributions to d_ρ whose coefficients are of the same sign and within a factor of two in magnitude. This contrasts with an extant sum rules evaluation, in which the coefficients of the contributions have the opposite sign and differ by a factor of four in magnitude. Since all studies agree within a factor of two on the quark-EDM coefficient, the discrepancy resides with the chromo-EDM contribution. These differences invite further analysis and guarantee relevance to a DSE evaluation of the impact of $\tilde{d}_q$ on the neutron's EDM.

Absent a mechanism that suppresses a θ-term in any beyond-Standard-Model action, the tight constraints on the magnitude of a contribution from this term to the neutron's EDM also apply to contributions from a dimension-six four-fermion operator to this or another hadron's EDM. Should such a mechanism exist, however, we find that a dimension-six operator can match the quark-EDM and chromo-EDM in importance.

Using the techniques described herein, calculation of the neutron's EDM is underway.

This work and Ref. [66]	2.11
DSE: RL RGI-improved [81]	2.01
DSE: EF parametrisation [111]	2.69
LF CQM [112]	2.14
LF CQM [113]	1.92
Sum Rules [114]	1.8 ± 0.3
point particle	2

Table 1.2. Magnetic moment of the ρ-meson calculated using our framework; and a comparison with other computations. Legend: *RL RGI-improved*, treatment of a renormalisation-group-improved one-gluon exchange kernel in rainbow-ladder truncation; *EF parametrisation*, entire function parametrisation of solutions to the gap and Bethe-Salpeter equations; and *LF CQM*, light-front constituent-quark model. The results are listed in units of $e/[2m_\rho]$.

$q\gamma q$	$-0.066\,\tilde{d}^e_- - 0.199\,\tilde{d}^e_+$
BSA	$-0.120\,\tilde{d}^e_- + 0.108\,\tilde{d}^e_+$
$S(k)$	$1.538\,\tilde{d}^e_-$
acm ($\times\mu^{\rm acm}$)	$0.775\,\tilde{d}^e_- + 2.396\,\tilde{d}^e_+$
our CEDM	$(1.35 + 0.78\,\mu^{\rm acm})\,\tilde{d}^e_- - (0.09 - 2.40\,\mu^{\rm acm})\,\tilde{d}^e_+$
total	$1.16\,\tilde{d}^e_- - 0.69\,\tilde{d}^e_+$
sum rules [62]	$-0.13\,\tilde{d}^e_-$

Table 1.3. Contributions to the ρ-meson EDM associated with a quark chromoelectric dipole moment, with $\tilde{d}^e_\mp = e(\tilde{d}_u \mp \tilde{d}_d)$. Row 1: quark-photon vertex correction, Sec. 1.4.2.1; Row 2: ρ-meson Bethe-Salpeter amplitude correction, Sec. 1.4.2.2; Row 3: dressed-quark propagator correction, Sec. 1.4.2.3; Row 4: anomalous chromomagnetic moment contributions, Sec. 1.4.3.1; Row 5: sum of preceding four rows; Row 6: Row 5 evaluated with $\mu^{\rm acm} = -1/4$; and Row 7: sum rules result from Ref. [62], evaluated here with a heavy s-quark.

$q\gamma q$	-1.005×10^{-5}
BSA	-9.114×10^{-7}
$S(k)$	0
acm ($\times \mu^{\rm acm}$)	$2.763 \times 10^{-5}\, \mu^{\rm acm}$
our $D = 6$ *total*	$-(1.096 - 2.763\, \mu^{\rm acm}) \times 10^{-5}$

Table 1.4. Contributions to the ρ-meson EDM associated with the dimension-six operator in Eq. (1.2). Each row should be multiplied by $e v_H \mathcal{K}/\Lambda^2$. Row 1: quark-photon vertex correction, Sec. 1.4.1.1; Row 2: ρ-meson Bethe-Salpeter amplitude correction, Sec. 1.4.1.2; Row 3: dressed-quark propagator correction, Sec. 1.4.1.3; Row 4: anomalous chromomagnetic moment contributions, Sec. 1.4.3.1; and Row 5: sum of preceding four rows.

CHAPTER 2

SCALAR AND TENSOR CHARGES OF THE NUCLEON

2.1 Introduction

In recent years a global approach to the description of nucleon structure has emerged, one in which we may express our knowledge of the nucleon in the Wigner distributions of its basic constituents and thereby provide a multidimensional generalisation of the familiar parton distribution functions (PDFs). The Wigner distribution is a quantum mechanics concept analogous to the classical notion of a phase space distribution. Following from such distributions, a natural interpretation of measured observables is provided by construction of quantities known as generalised parton distributions (GPDs) [187, 188, 189, 190, 191, 192, 193, 194] and transverse momentum-dependent distributions (TMDs) [195, 196, 197, 198, 199, 200, 201]: GPDs are linked to a *spatial* tomography of the nucleon; and TMDs allow for its *momentum* tomography. A new generation of experiments aims to provide the empirical information necessary to develop a phenomenology of nucleon Wigner distributions.

At leading-twist there are eight distinct TMDs, only three of which are nonzero in the collinear limit; i.e., in the absence of parton transverse momentum within the target, $k_\perp = 0$: the unpolarized (f_1), helicity (g_{1L}) and transversity (h_{1T}) distribu-

[0]Reprinted article with permission from M. Pitschmann, C. Y. Seng, C. D. Roberts and S. M. Schmidt, Phys. Rev. D **91** (2015) 074004, Copyright (2015) by the American Physical Society. DOI: http://dx.doi.org/10.1103/PhysRevD.91.074004

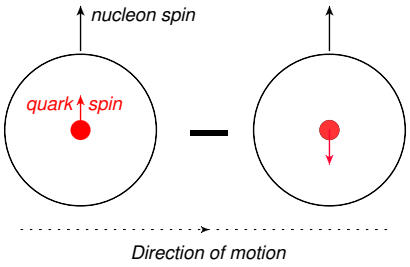

Figure 2.1. The tensor charge, Eq. (2.1), measures the net light-front distribution of transversely polarised quarks inside a transversely polarized proton.

tions. In connection with the last of these, one may define the proton's tensor charges ($q = u, d, \ldots$)

$$\delta_T q = \int_{-1}^{1} dx\, h_{1T}^{q}(x) = \int_{0}^{1} dx\, \left[h_{1T}^{q}(x) - h_{1T}^{\bar{q}}(x)\right] , \tag{2.1}$$

which, as illustrated in Fig. 2.1, measures the light-front number-density of quarks with transverse polarisation parallel to that of the proton minus that of quarks with antiparallel polarisation; viz., it measures any bias in quark transverse polarisation induced by a polarisation of the parent proton. The charges $\delta_T q$ represent a close analogue of the nucleon's flavour-separated axial-charges, which measure the difference between the light-front number-density of quarks with helicity parallel to that of the proton and the density of quarks with helicity antiparallel [202]. In nonrelativistic systems the helicity and transversity distributions are identical because boosts and rotations commute with the Hamiltonian.

The transversity distribution is measurable using Drell-Yan processes in which at least one of the two colliding particles is transversely polarised [203]; but such data is not yet available. Alternatively, the transversity distribution is accessible via semi-inclusive deep-inelastic scattering using transversely polarised targets and also in unpolarised e^+e^- processes, by studying azimuthal correlations between produced hadrons that appear in opposing jets ($e^+e^- \to h_1 h_2 X$). Capitalising on these obser-

vations, the transversity distributions were extracted through an analysis of combined data from the HERMES, COMPASS and Belle collaborations [45]; and those distributions have been used to produce an estimate of the proton's tensor charges, with the following flavour-separated results:

$$\delta_T u = 0.39^{+0.18}_{-0.12}\,, \quad \delta_T d = -0.25^{+0.30}_{-0.10}\,, \tag{2.2}$$

at a renormalisation scale $\zeta_A = 0.9\,\mathrm{GeV}$. Given that the tensor charges are a defining intrinsic property of the nucleon, the magnitude of the errors in Eqs. (2.2) is unsatisfactory. It is therefore critical to better determine $\delta_T u$, $\delta_T d$. Consequently, following upgrades at the Thomas Jefferson National Accelerator Facility (JLab), it is anticipated [204] that experiments [205, 206] in Hall-A (SoLID) and Hall-B (CLAS12) will provide a far more precise determination of the tensor charges.

Naturally, measurement of the transversity distribution and the tensor charges will not reveal much about the strong interaction sector of the Standard Model unless these quantities can be calculated using a framework with a traceable connection to QCD. This point is emphasised with particular force by the circumstances surrounding the pion's valence-quark PDF. As reviewed elsewhere [207], numerous authors suggested that QCD was challenged by a PDF parametrisation based on a precise πN Drell-Yan measurement [208]. However, the appearance of nonperturbative calculations within the framework of continuum QCD [209, 210] forced reanalyses of the cross-section, with the inclusion of next-to-leading-order evolution [211] and soft-gluon resummation [212], so that now those claims are known to be false and the pion's valence-quark PDF may be viewed as a success for QCD [213]. The comparisons between experiment and computations of the pion and kaon parton distribution amplitudes and electromagnetic form factors have reached a similar level of understanding [214, 215].

Herein, therefore, we compute the proton tensor charges using a confining, symmetry-preserving Dyson-Schwinger equation (DSE) treatment of a single quark-quark in-

teraction; namely, a vector $\otimes$ vector contact-interaction. This approach has proved useful in a variety of contexts, which include meson and baryon spectra, and their electroweak elastic and transition form factors [64, 65, 66, 67, 68, 69, 216, 217, 218, 219, 220]. In fact, so long as the momentum of the probe is smaller in magnitude than the dressed-quark mass produced by dynamical chiral symmetry breaking (DCSB), many results obtained in this way are practically indistinguishable from those produced by the most sophisticated interactions that have thus far been employed in DSE studies [221, 70, 71, 222].

It is apposite to remark here that confinement and DCSB are two key features of QCD; and much of the success of the contact-interaction approach owes to its efficacious expression of these emergent phenomena in the Standard Model. They are explained in some detail elsewhere [221, 70, 71, 222] so that here we remark only that confinement may be expressed via dynamically-driven changes in the analytic structure of QCD's propagators and vertices; and DCSB is the origin of more than 98% of the mass of visible material in the Universe. These phenomena are intimately connected; and whereas the nature of confinement is still debated, DCSB is a theoretically established nonperturbative feature of QCD [223], which has widespread, measurable impacts on hadron observables, e.g. Refs. [69, 217, 224, 225, 226, 227, 228, 215, 229], so that its expression in QCD is empirically verifiable.

Apart from the hadron physics imperative, the value of the nucleon tensor charges can be directly related to the visible impact of a dressed-quark electric dipole moment (EDM) on neutron and proton EDMs [109]. Novel beyond-the-Standard-Model (BSM) scalar operators may also conceivably be measurable in precision neutron experiments so that one typically considers both the nucleon scalar and tensor charges when exploring bounds on BSM physics [230]. The sum of the scalar charges of all active quark flavours is simply the nucleon σ-term, which we therefore also compute herein.

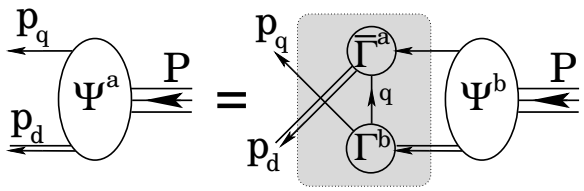

Figure 2.2. Poincaré covariant Faddeev equation. Ψ is the Faddeev amplitude for a nucleon of total momentum $P = p_q + p_d$. The shaded rectangle demarcates the kernel of the Faddeev equation: *single line*, dressed-quark propagator; Γ, diquark correlation (Bethe-Salpeter) amplitude; and *double line*, diquark propagator. (See Apps. A, B for details.)

Relying on material provided in numerous appendices, we provide a brief outline of our computational framework in Sec. 2.2: both the Faddeev equation treatment of the nucleon and the currents which describe the interaction of a probe with a baryon composed from consistently-dressed constituents. This presentation scheme enables us to embark quickly upon the description and analysis of our results for the scalar and tensor charges, Secs. 2.3 and 2.4, respectively. In Sec. 2.5 we use our results for the tensor charges in order to determine the impact of valence-quark EDMs on the neutron and proton EDMs. Section 2.6 is an epilogue.

2.2 Nucleon Faddeev Amplitude and Relevant Interaction Currents

We base our description of the nucleon's dressed-quark-core on solutions of a Faddeev equation, which is illustrated in Fig. 2.2, and formulated and described in Apps. A, B. In order to determine the scalar and tensor charges of the nucleon described by this Faddeev equation, the $Q^2 = 0$ values of three interaction currents are needed: elastic electromagnetic, which determines the canonical normalisation of the nucleon's Faddeev amplitude; scalar; and tensor. The computation of these quantities is detailed in App. C.

2.3 Sigma-Term

The contribution of a given quark flavour ($q = u, d, \ldots$) to a nucleon's σ-term is defined by the matrix element

$$\sigma_q = m_q \, \langle N(p) | \bar{q} \mathbb{I} q | N(p) \rangle \,, \tag{2.3}$$

where $|N(p)\rangle$ is the state vector of a nucleon with four-momentum p. The σ-term is independent of the renormalisation scale used in the computation, even though the individual pieces in the product on the right-hand-side (rhs) are not. As explained in App. E, the scale appropriate to our symmetry-preserving regularisation of the contact interaction is $\zeta_H \approx M$, where M is the dressed-quark mass.

Our computed value of the nucleon's σ-term is reported in Eq. (C.49); viz.,

$$\sigma_N = \sigma_u + \sigma_d = m \, 3.05 = 21 \, \text{MeV}. \tag{2.4}$$

This result is consistent with that obtained using the Feynman-Hellmann theorem in connection with the results from which Ref. [67] was prepared. An interesting way to expose this is to recall Eq. (B.28), which states that our analysis describes a nucleon that is 77% dressed-quark + scalar-diquark and 23% dressed-quark + axial-vector diquark. In the isospin symmetric limit, which we typically employ, it follows that

$$\begin{aligned} \sigma_N &= 0.77 \, [\sigma_Q + \sigma_{qq^0}] + 0.23 \, [\sigma_Q + \sigma_{qq^1}] && (2.5) \\ &= \sigma_Q + 0.77 \, \sigma_{qq^0} + 0.23 \, \sigma_{qq^1}, && (2.6) \end{aligned}$$

where

$$\sigma_Q = m\frac{\partial M}{\partial m} = 9.6\,\mathrm{MeV}, \tag{2.7a}$$

$$\sigma_{qq^0} = m\frac{\partial m_{qq^0}}{\partial m} = 16\,\mathrm{MeV}, \tag{2.7b}$$

$$\sigma_{qq^1} = m\frac{\partial m_{qq^1}}{\partial m} = 10\,\mathrm{MeV}, \tag{2.7c}$$

again computed using material in Ref. [67]. Inserting Eqs. (2.7) into Eq. (2.6), one obtains $\sigma_N = 24\,\mathrm{MeV}$.[1] Apparently, so far as the contribution of explicit chiral symmetry breaking to the mass of the nucleon's dressed-quark core is concerned, the contact-interaction nucleon is a simple system. This analysis also shows that our diagrammatic computational method is sound; and hence Eq. (2.4) is the rainbow-ladder (RL) truncation[2] prediction of a vector $\otimes$ vector contact-interaction treated in the Faddeev equation via the static approximation. (Inclusion of meson-baryon loop effects will increase the result in Eq. (2.4) by approximately 15% [231].)

In addition, the fact that Eqs. (2.4) and (2.6) yield similar results emphasises the important role of diquark correlations because if the nucleon were just a sum of three massive, weakly-interacting dressed-quarks, then one would have

$$\sigma_N^{3M} = 3\,\sigma_Q = 29\,\mathrm{MeV}\,, \tag{2.8}$$

which is 21% too large.

Adopting a different perspective, we note that the value in Eq. (2.4) is roughly one-half that produced by a Faddeev equation kernel that incorporates scalar and axial-vector diquark correlations in addition to propagators and interaction vertices that possess QCD-like momentum dependence [231]. It compares similarly with the

[1] The origin of the 11% mismatch is explained in Sec. C.1.7.

[2] The rainbow-ladder truncation is the leading-order term in the most widely used, global-symmetry-preserving DSE truncation scheme [76, 77].

value inferred in a recent analysis [232] of lattice-QCD results for octet baryon masses in $2+1$-flavour QCD:

$$\sigma_N = 45 \pm 6\,\mathrm{MeV}\,. \tag{2.9}$$

In order to understand the discrepancy, consider Eqs. (2.7). The value of σ_Q matches expectations based on gap equation kernels whose ultraviolet behaviour is consistent with QCD [231, 233]. On the other hand, with such interactions one typically finds $\sigma_{qq^0} \gtrsim \sigma_{qq^1} \gtrsim \sigma_\rho = 25\,\mathrm{MeV}$. We therefore judge that Eq. (2.4) underestimates the physical value of σ_N; and that the mismatch originates primarily in the rigidity of the diquark Bethe-Salpeter amplitudes produced by the contact interaction, which leads to weaker m-dependence of the diquark (and hence nucleon) masses than is obtained with more realistic kernels.[3] Notwithstanding this, Eq. (2.4) is a useful benchmark, providing a sensible result via a transparent method.

Further valuable information may be obtained from the results in App. C.2 if one supposes that the ratio of contact-interaction d- and u-quark contributions is more reliable than the net value of σ_N. In this connection, note that for a proton constituted as a weakly interacting system of three massive dressed-quarks in the isospin symmetric limit

$$\frac{\sigma^{3M}_{N,d}}{\sigma^{3M}_{N,u}} = \frac{1}{2}\,. \tag{2.10}$$

Comparing this with our computed value

$$\frac{\sigma_{N,d}}{\sigma_{N,u}} = 0.65\,, \tag{2.11}$$

one learns that diquark correlations work to accentuate the contribution of the singly-represented valence-quark to the proton σ-term relative to that of doubly-represented valence-quarks: the magnification factor is 1.3.

[3] Consider that if one uses $\sigma_{qq^0} = \sigma_{qq^1} = 30\,\mathrm{MeV}$, then $\sigma_N \approx 40\,\mathrm{MeV}$.

Let's take this another step and assume that $\hat{\sigma}_{N,u}$, $\hat{\sigma}_{N,d}$ in App. C.2 respond weakly to changes in m. This is valid so long as solutions of the dressed-quark gap equation satisfy

$$\left.\frac{dM}{dm}\right|_{(m_u+m_d)/2} \overset{m_u,m_d \ll M}{\approx} \left.\frac{dM}{dm}\right|_{m_u,m_d}, \tag{2.12}$$

which is found to be a good approximation in all available studies (see, e.g., Refs. [234, 235]). One may then estimate the effects of isospin symmetry violation owing to the difference between u- and d-quark current-masses. Taking the value of the mass ratio from Ref. [181], one finds

$$\frac{m_u}{m_d} = 0.48 \pm 0.1 \quad \Rightarrow \quad \frac{m_d\,\hat{\sigma}_{N,d}}{m_u\,\hat{\sigma}_{N,u}} = 1.35^{+0.47}_{-0.30}\,. \tag{2.13}$$

Alternatively, one might use the mass ratio inferred from a survey of numerical simulations of lattice-regularised QCD [236], in which case

$$\frac{m_u}{m_d} = 0.47 \pm 0.04 \quad \Rightarrow \quad \frac{m_d\,\hat{\sigma}_{N,d}}{m_u\,\hat{\sigma}_{N,u}} = 1.38^{+0.17}_{-0.14}\,. \tag{2.14}$$

We predict, therefore, that the d-quark contribution to that part of the proton's mass which arises from explicit chiral symmetry breaking is roughly 37% greater than that from the u-quark. This value is commensurate with a contemporaneous estimate based on lattice-QCD [237]. It is noteworthy that if the proton were a weakly interacting system of three massive dressed-quarks, then Eq. (2.14) would yield $1.06^{+0.13}_{-0.11}$; and hence one finds again that the presence of diquark correlations within the proton enhances the contribution of d-quarks to the proton's σ-term.

2.4 Tensor Charge

The tensor charge associated with a given quark flavour in the proton is defined via the matrix element ($q = u, d, \ldots$)

$$\langle P(p,\sigma)|\bar{q}\sigma_{\mu\nu}q|P(p,\sigma)\rangle = \delta_T q\, \bar{u}(p,\sigma)\sigma_{\mu\nu} u(p,\sigma)\,, \tag{2.15}$$

where $u(p,\sigma)$ is a spinor and $|P(p,\sigma)\rangle$ is a state vector describing a proton with momentum p and spin σ.[4] With $\delta_T u$, $\delta_T d$ in hand, the isoscalar and isovector tensor charges are readily computed:

$$g_T^{(0)} = \delta_T u + \delta_T d\,,\; g_T^{(1)} = \delta_T u - \delta_T d\,. \tag{2.16}$$

Importantly, the tensor charge is a scale-dependent quantity. Its evolution is discussed in App. F.

Our analysis of the proton's tensor charge in a symmetry-preserving RL-truncation treatment of a vector $\otimes$ vector contact-interaction is detailed in App. C.3. At the model scale, ζ_H, which is determined and explained in App. E, we obtain the results in Table C.3, which represent a parameter-free prediction: the current-quark mass and the two parameters that define the interaction were fixed elsewhere [66], in a study of π- and ρ-meson properties.

It is natural to ask for an estimate of the systematic error in the values reported in Table C.3. As we saw in Sec. 2.3, the error might pessimistically be as much as a factor of two. However, that is an extreme case because, as observed in the Introduction, one generally finds that our treatment of the contact interaction produces results for low-momentum-transfer observables that are practically indistinguishable from those produced by RL studies that employ more sophisticated interactions [64, 65, 67, 66, 68, 69, 216, 217, 218, 219, 220]. It is therefore notable that analyses of hadron physics observables using the RL truncation and one-loop QCD renormalisation-group-improved (RGI) kernels for the gap and bound-state equations produce results that are typically within 15% of the experimental value [221]. We

[4] In the isospin symmetric limit: $\delta_T^p u := \delta_T u = \delta_T^n d$, $\delta_T^p d := \delta_T d = \delta_T^n u$.

therefore ascribe a relative error of 15% to the results in Table C.3 so that our predictions are:

$$\begin{array}{r|cccc} & \delta_T u & \delta_T d & g_T^{(0)} & g_T^{(1)} \\ \zeta_H \approx M & 0.69(10) & -0.14(2) & 0.55(8) & 0.83(12) \end{array} . \tag{2.17}$$

One means by which to check our error estimate is to repeat the calculations described herein using a modern RGI kernel [83] in the gap and bound-state equations. That has not yet been done but one may nevertheless infer what it might yield. Consider first Ref. [238], which computes the dressed-quark-tensor vertex using a RL-treatment of a QCD-based kernel: one observes that the dressed-quark's tensor charge is markedly suppressed; namely, with a QCD-based momentum-dependent kernel, a factor of approximately one-half appears on the rhs of Eq. (C.50). This DCSB-induced suppression would tend to reduce the values in Eq. (2.17). On the other hand, the use of a more sophisticated momentum-dependent kernel in the bound-state equations increases the amount of dressed-quark orbital angular momentum in the proton, an effect apparent in the reduction of the fraction of proton helicity carried by dressed u- and d-quarks when one shifts from a contact-interaction framework to a QCD-kindred approach [226, 229]. Hence, the tensor charges are determined by two competing effects, the precise balance amongst which can only be revealed by detailed calculations.

In this context, however, it is worth noting that similar DCSB-induced effects are observed in connection with g_A, the nucleon's axial charge. The axial-charge of a dressed-quark is suppressed [202], owing to DCSB; but that is compensated in the calculation of g_A by dressed-quark orbital angular momentum in the nucleon's Faddeev wave-function, with the computed value of the nucleon's axial-charge being 20% larger than that of a dressed-quark. The net effect is that a computation of g_A

using the framework of Refs. [229] can readily produce a result that is within 15% of the empirical value [221, 202]. This suggests that our error estimate is reasonable.

The predictions in Eq. (2.17) are quoted at the model scale, whose value is explained in App. E. In order to make a sensible comparison with estimates obtained in modern simulations of lattice-regularised QCD, those results must be evolved to $\zeta_2 = 2\,\mathrm{GeV}$. We therefore list here the results obtained under leading-order evolution to $\zeta_2 = 2\,\mathrm{GeV}$, obtained via multiplication by the factor in Eq. (F.4):

$$\begin{array}{c|cccc} & \delta_T u & \delta_T d & g_T^{(0)} & g_T^{(1)} \\ \zeta_2 & 0.55(8) & -0.11(2) & 0.44(7) & 0.66(10) \end{array} . \tag{2.18}$$

The error in Eq. (F.4) does not propagate significantly into these results.

Notably, the dominant contribution to $\delta_T u$ arises from Diagram 1: tensor probe interacting with a dressed u-quark with a scalar diquark as the bystander. The tensor probe interacting with the axial-vector diquark, with a dressed-quark as a spectator, Diagram 4, produces the next largest piece. However, that is largely cancelled by the sum of Diagrams 5 and 6: tensor probe causing a transition between scalar- and axial-vector diquark correlations within the proton whilst the dressed-quark is a bystander. It is a large negative contribution for both $\delta_T u$ and $\delta_T d$: indeed, owing to a significant cancellation between Diagrams 2 and 4 in the d-quark sector, which describe the net result from quark + axial-vector-diquark contributions, the sum of Diagrams 5 and 6 provides almost the entire result for $\delta_T d$.

A particularly important result is the impact of the proton's axial-vector diquark correlation. As determined in App. C.3.6, with a symmetry-preserving treatment of a contact interaction, $\delta_T d$ is only nonzero if axial-vector diquark correlations are present. Significantly, in dynamical calculations the strength of axial-vector diquark correlations relative to scalar diquark correlations is a measure of DCSB [69]. In the absence of axial-vector diquark correlations [Eqs. (C.73), Eq. (F.4)]

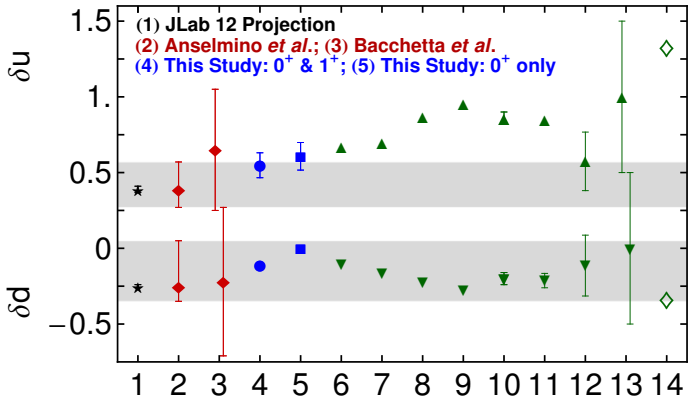

Figure 2.3. Flavour separation of the proton's tensor charge: "1" – illustration of anticipated accuracy in planned JLab experiment [205], with central values based on Eq. (2.2); "2" – results in Eq. (2.2), drawn from Ref. [45]; "3" phenomenological estimate in Ref. [239] "4" – prediction herein, Eq. (2.18); "5" – result obtained herein with omission of axial-vector diquark correlations, Eq. (2.19); "6-13" – estimates from Refs. [109, 240, 241, 242, 243, 244, 245, 246], respectively. By way of context, we note that were the proton a weakly-interacting collection of three massive valence-quarks described by an SU(4)-symmetric spin-flavour wave function, then [246] the quark axial and tensor charges are identical, so that $\delta_T u = 4/3$ and $\delta_T d = -1/3$ at the model scale. These values are located at "14".

$$\begin{array}{c|cccc} & \delta_{T\not{1}} u & \delta_{T\not{1}} d & g^{(0)}_{T\not{1}} & g^{(1)}_{T\not{1}} \\ \zeta_2 & 0.61(9) & 0 & 0.61(9) & 0.61(9) \end{array} ; \tag{2.19}$$

i.e., $\delta_T d$ vanishes altogether and $\delta_T u$ is increased by 11%. We expect that the influence of axial-vector diquark correlations will be qualitatively similar in the treatment of more sophisticated kernels for the gap and bound-state equations. A hint in support of this expectation may be drawn from the favourable comparison, depicted in Fig. 2.3, between the predictions for $\delta_T u$ in Eq. (2.19), "4", and the result of Ref. [109], "5". The latter employed a proton and tensor-current that suppressed but did not entirely eliminate the contribution from axial-vector diquark correlations. This same comparison also supports the verity of our error estimate.

Additionally, it is valuable to note that the magnitude of $\delta_T u$ is a direct probe of the strength of DCSB and hence of the strong interaction at infrared momenta. This

could be anticipated, e.g., from Eqs. (C.55), (C.64), the expressions for Diagrams 1 and 4, which produce the dominant positive contributions to $\delta_T u$: both show a strong numerator dependence on the dressed-quark mass, M; and $M/m \gg 1$ is a definitive signal of DCSB. To quantify the effect, we reduced $\alpha_{\rm IR}$ in the gap and Bethe-Salpeter equations by 20% and recomputed all relevant quantities. This modification reduced the dressed-quark mass by 33%: $M = 0.368 \to M_< = 0.246\,$GeV. Combined with knock-on effects throughout all correlations and bound-states, the 20% reduction in $\alpha_{\rm IR}$ produces [Table C.4 and Eq. (F.4)]

$$\begin{array}{l|cccc} M \to M_< & \delta_T u & \delta_T d & g_T^{(0)} & g_T^{(1)} \\ \zeta_2 & 0.44 & -0.12 & 0.32 & 0.56 \end{array} , \tag{2.20}$$

which expresses a 20% decrease in $\delta_T u$. As we signalled, the greatest impact of the cut in $\alpha_{\rm IR}$ and hence M is a reduction in the size of the contributions from Diagrams 1 and 4: the former describes the tensor probe interacting with a dressed-quark whilst a scalar diquark is a spectator; and the latter involves a tensor probe exploring an axial-vector diquark with a dressed-quark bystander.

As remarked in the Introduction, the tensor charge is a defining intrinsic property of the proton and hence there is great interest in its reliable experimental and theoretical determination. In Fig. 2.3 we therefore compare our predictions with results from other analyses [109, 239, 240, 241, 242, 243, 244, 245, 246]. Evidently, of all available computations, our contact-interaction predictions are in best agreement with the phenomenological estimates in Eq. (2.2).

Another interesting point is highlighted by a comparison between our predictions and the values obtained when the proton is considered to be a weakly-interacting collection of three massive valence-quarks described by an SU(4)-symmetric spin-flavour wave function [246]: $\delta_T^{\rm SU(4)} u = 2 e_u$ and $\delta_T^{\rm SU(4)} d = e_d$ cf. our results, Eq. (2.17), $\delta_T u = 0.52(2 e_u)$, $\delta_T d = 0.42(e_d)$. The presence of diquark correlations in the pro-

ton amplitude significantly suppresses the magnitude of the tensor charge associated with each valence quark whilst simultaneously increasing the ratio $\delta_T d/\delta_T u$ by approximately 20%.

2.5 Electric Dipole Moments

In typical extensions of the Standard Model, quarks acquire an EDM [55, 56]; i.e., an interaction with the photon that proceeds via a current of the form:

$$\tilde{d}_q \, q\gamma_5\sigma_{\mu\nu}q \,, \tag{2.21}$$

where $\tilde{d}_q$ is the quark's EDM and here we consider $q = u, d$. The EDM of a proton containing quarks which interact in this way is defined as follows:

$$\langle P(p,\sigma)|\mathcal{J}^{\rm EDM}_{\mu\nu}|P(p,\sigma)\rangle = \tilde{d}_p \, \bar{u}(p,\sigma)\gamma_5\sigma_{\mu\nu}u(p,\sigma) \,, \tag{2.22}$$

where

$$\mathcal{J}^{\rm EDM}_{\mu\nu}(x) = \tilde{d}_u \, \bar{u}(x)\gamma_5\sigma_{\mu\nu}u(x) + \tilde{d}_d \, \bar{d}(x)\gamma_5\sigma_{\mu\nu}d(x) \,. \tag{2.23}$$

At this point it is useful to recall a simple Dirac-matrix identity:

$$\gamma_5\sigma_{\mu\nu} = \frac{1}{2}\varepsilon_{\mu\nu\alpha\beta}\sigma_{\alpha\beta} \,, \tag{2.24}$$

using which one can write

$$\mathcal{J}^{\rm EDM}_{\mu\nu} = \frac{1}{2}\varepsilon_{\mu\nu\alpha\beta}\left[\tilde{d}_u \, \bar{u}\sigma_{\alpha\beta}u + \tilde{d}_d \, \bar{d}\sigma_{\alpha\beta}d\right] \,. \tag{2.25}$$

It follows that

$$\begin{aligned}
&\langle P(p,\sigma)|\mathcal{J}^{\rm EDM}_{\mu\nu}|P(p,\sigma)\rangle \\
&= \frac{1}{2}\varepsilon_{\mu\nu\alpha\beta}\left[\tilde{d}_u\,\delta_T u\,+\tilde{d}_d\,\delta_T d\right]\bar{u}(p,\sigma)\sigma_{\alpha\beta}u(p,\sigma) \qquad (2.26)\\
&= \left[\tilde{d}_u\,\delta_T u\,+\tilde{d}_d\,\delta_T d\right]\bar{u}(p,\sigma)\gamma_5\sigma_{\mu\nu}u(p,\sigma)\,; \qquad (2.27)
\end{aligned}$$

namely, the quark-EDM contribution to a proton's EDM is completely determined once the proton's tensor charges are known:

$$\tilde{d}_p = \tilde{d}_u\,\delta_T u\,+\tilde{d}_d\,\delta_T d\,. \qquad (2.28)$$

With emerging techniques, it is becoming possible to place competitive upper-limits on the proton's EDM using storage rings in which polarized particles are exposed to an electric field [247].

An analogous result for the neutron is readily inferred. In the limit of isospin symmetry,

$$\begin{aligned}
&\langle N(p,\sigma)|\bar{u}\sigma_{\mu\nu}u|N(p,\sigma)\rangle = \langle P(p,\sigma)|\bar{d}\sigma_{\mu\nu}d|P(p,\sigma)\rangle\,,\\
&\langle N(p,\sigma)|\bar{d}\sigma_{\mu\nu}d|N(p,\sigma)\rangle = \langle P(p,\sigma)|\bar{u}\sigma_{\mu\nu}u|P(p,\sigma)\rangle\,; \qquad (2.29)
\end{aligned}$$

and hence

$$\tilde{d}_n = \tilde{d}_u\,\delta_T d\,+\tilde{d}_d\,\delta_T u\,. \qquad (2.30)$$

Using the results in Eq. (2.17), we therefore have

$$\tilde{d}_n = -0.14\,\tilde{d}_u + 0.69\,\tilde{d}_d\,,\ \tilde{d}_p = 0.69\,\tilde{d}_u - 0.14\,\tilde{d}_d\,. \qquad (2.31)$$

It is worth contrasting Eqs. (2.31) with the results one would obtain by assuming that the nucleon is merely a collection of three massive valence-quarks described by

an SU(4)-symmetric spin-flavour wave function. Then, by analogy with magnetic moment computations, a procedure also made valid by Eq. (2.24):

$$\tilde{d}_n = -\frac{1}{3}\,\tilde{d}_u + \frac{4}{3}\,\tilde{d}_d\,,\ \tilde{d}_p = \frac{4}{3}\,\tilde{d}_u - \frac{1}{3}\,\tilde{d}_d\,, \tag{2.32}$$

values which are roughly twice the size that we obtain.

The impact of our predictions for the scalar and tensor charges on BSM phenomenology may be elucidated, e.g., by following the analysis in Refs. [230, 248].

2.6 Conclusion

We employed a confining, symmetry-preserving, Dyson-Schwinger equation treatment of a vector $\otimes$ vector contact interaction in order to compute the dressed-quark-core contribution to the nucleon σ-term and tensor charges. The latter enabled us to determine the effect of dressed-quark electric dipole moments (EDMs) on the neutron and proton EDMs.

A characteristic feature of DSE treatments of ground-state baryons is the predicted presence of strong scalar and axial-vector diquark correlations within these bound-states. Indeed, in some respects the baryons can be viewed as weakly interacting dressed-quark + diquark composites. The diquark correlations are active participants in all scattering events and therefore serve to modify the contribution to observables of the singly-represented valence-quark relative to that of the doubly-represented quark.

Regarding our analysis of the proton's σ-term, we estimate that with a realistic d-u mass splitting, the singly-represented d-quark contributes 37% more than the doubly-represented u-quark to that part of the proton mass which owes to explicit chiral symmetry breaking [Eqs. (2.13), (2.14)].

Our predictions for the proton's tensor charges, $\delta_T u$, $\delta_T d$, are presented in Eq. (2.18). In this case, compared to results obtained in simple quark models, diquark correlations act to reduce the size of $\delta_T u$, $\delta_T d$ by a factor of two and increase the ratio

$\delta_T d/\delta_T u$ by roughly 20%. Two additional observations are particularly significant. First, the magnitude of $\delta_T u$ is a direct measure of the strength of DCSB in the Standard Model, diminishing rapidly with the difference between the scales of dynamical and explicit chiral symmetry breaking. Second, $\delta_T d$ measures the strength of axial-vector diquark correlations in the proton, vanishing with P_{1^+}/P_{0^+}; i.e., the ratio of axial-vector- and scalar-diquark interaction probabilities, which is also a measure of DCSB.

Our analysis of the Faddeev equation employed a simplifying truncation; viz., a variant of the so-called static approximation. A natural next step is recalculation of the tensor charges after eliminating that truncation. Subsequently or simultaneously, one might also employ the approaches of Refs. [249, 229] in order to obtain DSE predictions with a more direct connection to QCD.

CHAPTER 3

AN INTRODUCTION TO THE CHIRAL PERTURBATION THEORY

In this chapter we provide a brief introduction to the Chiral Perturbation Theory (ChPT) which is a low-energy effective theory of Quantum Chromodynamics (QCD) that describes the strong interaction governing interactions between hadrons. There are many pedagogical articles of this topic and here we mainly follow the logic and notations in Ref. [172].

3.1 The motivation

QCD is long believed to be the appropriate theory for the strong interaction. It is an $SU(3)_c$ non-Abelian gauge theory that can be described by the following Lagrangian:

$$\mathcal{L} = \sum_q \{\bar{q} i \not{D} q - m_q \bar{q} q\} - \frac{1}{4} G^a_{\mu\nu} G^{a\mu\nu} \tag{3.1}$$

where q is the quark field and $iD_\mu \equiv i\partial_\mu - g_s T^a A^a_\mu$ is the $SU(3)_c$ covariant derivative. The free parameters in the theory are the strong coupling constant g_s and the quark masses $\{m_q\}$.

As we have explained in the introduction, QCD is perturbative at high energy and is extremely successful in this regime, examples including the prediction of scaling violation behavior in deep inelastic scattering (DIS). On the other hand, the theory becomes highly non-perturbative when the energy scale is lowered to the mass of light hadrons as the running coupling constant $g_s(\mu)$ diverges in the infrared limit.

Therefore conventional perturbative treatment to QCD is not applicable for the study of the low-energy properties of hadrons.

Lattice QCD (LQCD) is currently the only promising way to tackle this problem from the first principle. It involves numerical evaluations of the QCD path integral in a discretized spacetime using Monte Carlo method. This method is proved to be extremely successful in many areas, for example the precise reproduction of the hadronic spectrum. However it applicability is also severely limited by various technical issues such as the large amount of CPU time. The alternative way to approach is problem is through the application of effective field theories (EFTs) which are theories that try to mimic some, if not all, of the properties of QCD in the infrared limit. These theories are suitably engineered such that calculations in the low energy regime are tractable.

ChPT is the most general effective field theory at low energy that is constructed based on one particular symmetry of QCD, namely the chiral symmetry. Instead of quarks and gluons, the degrees of freedom in ChPT are mesons and baryons. It is particularly successful in describing the residual strong interaction between hadrons that involves exchange of light mesons. In this chapter we shall introduce the basic concepts and ingredients needed for the construction of ChPT Lagrangian without diving into any specific calculation of Feynman diagrams. These basic concepts are very helpful for the understanding of most of the contents in the next two chapters.

3.2 Chiral symmetry and spontaneous symmetry breaking

3.2.1 Chiral transformation

Apart from the color $SU(3)$, the QCD Lagrangian possesses another symmetry known as the chiral symmetry in the limit of massless quarks. To be definite let us consider the QCD with two lightest quark u and d (the discussion below can be straightforwardly generalized to include the strange quark). We can separate

each quark field into its left- and right-handed components and define the following doublets:

$$Q_{L/R} \equiv \begin{pmatrix} u \\ d \end{pmatrix}_{L/R} . \tag{3.2}$$

The two-flavor QCD Lagrangian can then be rewritten as

$$\mathcal{L} = \bar{Q}_L i D_\mu Q_L + \bar{Q}_R i D_\mu Q_R - \bar{Q}_R M Q_L - \bar{Q}_L M^\dagger Q_R - \frac{1}{4} G^a_{\mu\nu} G^{a\mu\nu} \tag{3.3}$$

where $M = \mathrm{diag}(m_u \;\; m_d)$ is the quark mass matrix. It is clear that if we take the quark masses to be zero then the quark doublet fields with different handedness do not mix with each other. In other words, the massless two-flavor QCD Lagrangian is invariant under the following $SU(2)_L \times SU(2)_R$ transformation:

$$\begin{aligned} SU(2)_L : \quad Q_L &\rightarrow U_L Q_L \\ SU(2)_R : \quad Q_R &\rightarrow U_R Q_R \end{aligned} \tag{3.4}$$

where $U_{L/R} \equiv \exp\{i\vec{\theta}_{L/R} \cdot \vec{\tau}/2\}$ are two independent 2×2 special unitary matrices. This symmetry is explicitly broken by the quark mass matrix M, however since current quark masses m_u and m_d are only a few MeV, much lighter than the lightest hadron mass $m_{\pi^0} \approx 135$ MeV, so one naively expects the chiral symmetry to be pretty well respected. It is also extremely useful to realize that the $SU(2)_L \times SU(2)_R$ symmetry is equivalent to an $SU(2)_V \times SU(2)_A$ symmetry defined by the following "vector" and "axial" transformation to the quark doublet:

$$\begin{aligned} SU(2)_V : \quad Q &\rightarrow \exp\{i\vec{\theta}_V \cdot \frac{\vec{\tau}}{2}\} Q \\ SU(2)_A : \quad Q &\rightarrow \exp\{i\vec{\theta}_A \cdot \frac{\vec{\tau}}{2}\gamma_5\} Q. \end{aligned} \tag{3.5}$$

In particular, the $SU(2)_V$ symmetry is known as the isospin symmetry and it is a good symmetry even with non-zero quark masses provided that $m_u = m_d$.

3.2.2 Spontaneous symmetry breaking

Unlike the isospin symmetry which is proven to be a good approximate symmetry, nature does not seem to respect the $SU(2)_A$ symmetry. A clear evidence is the following: one can easily prove that if $SU(2)_A$ is a good symmetry, then it implies that for any hadron (made up of light quarks) there must be a corresponding hadron with the same mass but with the opposite parity. This "parity doubling" effect is however not observed experimentally. For example, let us consider the lightest $J^p = (1/2)^+$ baryon (i.e. proton) which has a mass of 938 MeV. If parity doubling is true, one shall observe a $J^p = (1/2)^-$ baryon with approximately the same mass. Such baryon is however never been observed; the lightest $(1/2)^-$ baryon has a mass around 1535 MeV which can never be interpreted as the parity counterpart of the proton.

The non-existence of the parity doubling could be explained if the QCD vacuum $|0\rangle$ is non-invariant under the axial transformation, i.e.

$$\hat{Q}_A^a |0\rangle \neq 0 \tag{3.6}$$

where $\hat{Q}_A^a \equiv \int d^3x \bar{Q}\gamma^0\gamma_5 \frac{\tau^a}{2} Q$ is the conserved charge of $SU(2)_A$. The non-invariance of the vacuum under a certain symmetry signifies a spontaneous symmetry breaking (SSB). According to the Nambu-Goldstone theorem, a SSB implies existence of massless spin-zero bosons known as Nambu-Goldstone (NG) bosons. Indeed, we find that the lightest pseudo-scalar mesons (i.e. the pion triplet) have masses around 135-140 MeV which are much lighter than all the remaining hadrons. We may then identify them as the NG bosons due to the SSB of the $SU(2)_A$ symmetry. Their non-zero masses are simply due to the existence of small quark masses that explicitly breaks $SU(2)_A$. Finally we should point out that even though the non-observation of parity doubling and the existence of very light pions are significant evidence that SSB indeed happens in QCD, but so far there is no rigorous proof that this is indeed the

case based on first-principle calculation. ChPT is therefore an effective field theory of QCD based on the assumption that SSB takes place at low energy and the pion triplet are the corresponding NG bosons.

3.3 Non-linear realization of NG bosons

In this section we want to introduce the concept of the non-linear representation of NG bosons which is crucial in the construction of the ChPT Lagrangian.

3.3.1 Basic idea

In order to easily understand the idea let us consider the following simple example. Imagine a Lagrangian $\mathcal{L}(\phi)$ which possesses a symmetry group $h_1 \times h_2$, and we know that the symmetry h_1 (say with m generators) is spontaneously broken while h_2 remains a good symmetry. Then, we may parameterize the field $\phi(x)$ as the following:

$$\phi(x) = \mathcal{R}(\xi(x))\rho(x) \tag{3.7}$$

where $\mathcal{R}$ is the transformation matrix of h_1 and $\xi(x) = (\xi_1(x), \xi_2(x), ...\xi_m(x))$ are the "rotational angles" of the symmetry transformation h_1, except that now they are spacetime-dependent fields. Finally, $\rho(x)$ is a field which is invariant under the transformation h_1.

With this parameterization it is clear that the fields $\{\xi_i(x)\}$ are automatically the NG bosons (up to normalization factors) due to the SBB of h_1. The way to see this is very simple: if $\{\xi_i(x)\}$ are spacetime-independent, then we can perform another h_1 transformation on $\phi(x)$:

$$\phi'(x) = \mathcal{R}^{-1}(\xi)\phi(x) = \mathcal{R}^{-1}(\xi)\mathcal{R}(\xi)\rho(x) = \rho(x). \tag{3.8}$$

Now, since $\mathcal{L}$ is invariant under h_1, so we will have $\mathcal{L}(\phi) = \mathcal{L}(\phi') = \mathcal{L}(\rho)$, i.e. the fields $\{\xi_i\}$ will not appear in the Lagrangian. This implies that, if the fields $\{\xi_i\}$ are

to appear in the Lagrangian then they must be spacetime-dependent. The only way for this to happen is that every term in the Lagrangian $\mathcal{L}$ which involve only $\{\xi_i\}$ must also involve derivatives on $\{\xi_i\}$. This immediately excludes any mass term of $\{\xi_i\}$ as it does not involve derivatives. They are therefore massless bosons and can be identified as NG bosons due to the SSB of the symmetry group h_1.

3.3.2 Example of non-linear realization: $SU(2)_L \times SU(2)_R$

To elaborate the general idea above and derive one essential building block for the actual ChPT, let us proceed to the study of non-linear realization of Goldstone bosons in a simple theory with spontaneously-broken $SU(2)_L \times SU(2)_R$ symmetry. The fermionic building blocks can be written as ψ_R and ψ_L which transform as $\psi_R \to U_R\psi_R$ and $\psi_L \to U_L\psi_L$ under $SU(2)_L \times SU(2)_R$. Now, if we want to write down an $SU(2)_L \times SU(2)_R$-invariant theory that involves interaction between ψ_R and ψ_L, then it is essential to introduce a 2×2 matrix $\Sigma(x)$ that transforms as:

$$\Sigma(x) \to U_R \Sigma(x) U_L^\dagger. \tag{3.9}$$

With this matrix, terms like $\bar{\psi}_R \Sigma \psi_L$ will be invariant.

Recall from the previous section that $SU(2)_R \times SU(2)_L$ is also equivalent to $SU(2)_V \times SU(2)_A$. Starting from Eq. (3.9), it is easy to show that $\Sigma(x)$ should transform under $SU(2)_A$ as

$$SU(2)_A: \quad \Sigma(x) \to \exp\{i\vec{\theta}_A \cdot \frac{\vec{\tau}}{2}\} \Sigma(x) \exp\{i\vec{\theta}_A \cdot \frac{\vec{\tau}}{2}\} \tag{3.10}$$

where $\vec{\theta}_A \equiv (\vec{\theta}_R - \vec{\theta}_L)/2$. Now, assuming that $SU(2)_A$ is spontaneously broken, we may follow the spirit of non-linear realization introduced in the previous subsection and reparameterize $\Sigma(x)$ as

$$\Sigma(x) \equiv \sqrt{U(x)}\sigma(x)\sqrt{U(x)} \tag{3.11}$$

where

$$\sqrt{U(x)} \equiv \exp\{i\vec{\xi}(x) \cdot \frac{\vec{\tau}}{2}\} \tag{3.12}$$

and the field $\sigma(x)$ is invariant under $SU(2)_A$. By construction, the triplet field $\vec{\xi}(x)$ plays the role of NG bosons (up to normalization factors). Furthermore, we require that $\vec{\xi}(x)$ transforms as a triplet under the good symmetry $SU(2)_V$ just like what happens to ordinary pions. One may show that this requirement implies the following transformation rule of $\sqrt{U(x)}$ under $SU(2)_V$:

$$SU(2)_V: \quad \sqrt{U(x)} \to \exp\{i\vec{\theta}_V \cdot \frac{\vec{\tau}}{2}\} \sqrt{U(x)} \exp\{-i\vec{\theta}_V \cdot \frac{\vec{\tau}}{2}\} \tag{3.13}$$

($\vec{\theta}_V \equiv (\vec{\theta}_R + \vec{\theta}_L)/2$). Combining Eq. (3.10) and (3.13) we immediately see that $\sigma(x)$ is an invariant under $SU(2)_V \times SU(2)_A$. It is therefore a scalar field instead of a matrix. Finally, the $\Sigma(x)$ matrix can now be written as

$$\Sigma(x) = \sigma(x) U(x) \tag{3.14}$$

where $U(x) = \exp\{i\vec{\tau} \cdot \vec{\xi}(x)\}$ and transforms under $SU(2)_L \times SU(2)_R$ as $U(x) \to U_R U(x) U_L^\dagger$. The scalar field $\sigma(x)$ is a massive excitation and it plays no role in maintaining the symmetry of the Lagrangian, therefore it can be integrated out in the effective theory. On the other hand, the matrix $U(x)$ serves as the non-linear realization of the NG bosons and will be one of the main building blocks of our low-energy effective theory of QCD.

3.4 ChPT for NG bosons

Now we are ready to construct the effective field theory of QCD based on symmetry consideration. As we showed in Sec. 3.2, the two-flavor QCD possesses the following properties:

1. It is invariant under $SU(2)_V \times SU(2)_A$ in the massless quark limit;

2. $SU(2)_A$ is spontaneously broken at low energy and pions are the NG bosons;

3. $SU(2)_A$ is explicitly broken by the insertion of quark mass matrix M.

It is then natural to require our effective theory to obey the properties listed above. In fact, we want to construct the MOST GENERAL Lagrangian that satisfies these three requirements. Obviously there are infinitely many terms with arbitrary mass dimensions that may satisfy these three criteria and we shall include all of them in our Lagrangian. This unavoidably makes ChPT an unrenormalizable theory which is a common feature for most of the effective field theories. Despite its non-renormalizability, ChPT still possesses finite predictive power due to the following reason. Due to the non-linear realization, terms involving pions must contain either derivatives or insertions of quark mass matrix M (and we will see later that $m_\pi^2 \sim m_q$). It therefore exists a "power counting" rule saying that one may arrange terms in ChPT according to an increasing power of p/Λ_χ where p is either the pion mass or a small momentum of pion while $\Lambda_\chi \sim$1 GeV is an energy scale related to the chiral symmetry breaking. Hence, for any given precision level, one only needs to include a finite number of terms in the chiral Lagrangian as the remaining terms are suppressed by more powers of p/Λ_χ. This concept of power counting is essential as it makes calculations in ChPT tractable.

3.4.1 $O(p^2)$: Chiral invariant terms

Let us concentrate on the pure Goldstone terms in ChPT in this section. These terms can be constructed using the matrix $U(x)$ we discussed in the previous section. Following standard notations, we define the normalized pion fields $\vec{\pi}(x)$ through

$$U(x) = \exp\{i\frac{\vec{\pi}(x)\cdot\vec{\tau}}{F_\pi}\} \tag{3.15}$$

and the parameter F_π is known as the pion decay constant. In our convention $F_\pi \approx 93$ MeV but it is also worth knowing that in other conventions F_π may take different

values (the most common example is that $F_\pi \approx 186$ MeV in the $SO(4)$ representation of ChPT).

We start by constructing the leading order chiral-invariant Lagrangian using $U(x)$. As discussed in Sec. 3.3, any chiral-invariant term of pions must involve derivatives. One may easily show that the only chiral-invariant operator in $O(p^2)$ is given by:

$$\mathcal{L}^{(2)}_{\rm inv} = \frac{F_\pi^2}{4}{\rm Tr}[(\partial_\mu U)(\partial^\mu U^\dagger)]. \tag{3.16}$$

The prefactor $F_\pi^2/4$ serves for the normalization of the pion kinetic term. Expansion of this Lagrangian according to power of pion fields gives:

$$\mathcal{L}^{(2)}_{\rm inv} = \frac{1}{2}(\partial_\mu \vec{\pi})^2 + \frac{1}{6F_\pi^2}[(\vec{\pi}\cdot\partial_\mu\vec{\pi})^2 - \vec{\pi}^2(\partial_\mu\vec{\pi})^2] + O(\pi^6) \tag{3.17}$$

which gives the pion kinetic terms as well as interaction terms involving even number of pions. The interaction strengths of different terms are all inter-related due to chiral symmetry.

3.4.2 Spurion and chiral symmetry breaking terms at $O(p^2)$

Eq. (3.16) is not the only available term at $O(p^2)$ because we need also to include chiral symmetry breaking terms at the same order. These terms involve insertions of quark mass matrix M following definite rules. Before we proceed, it is useful to introduce the concept of "spurion" which is crucial in constructions of symmetry-breaking terms in an effective theory. To understand this concept let us consider the quark mass term in QCD. It has the following form:

$$\mathcal{L}^m_{\rm QCD} = -\bar{Q}_R M Q_L + h.c.. \tag{3.18}$$

This term is obviously not chiral invariant, however it "would be" chiral invariant if we imagine that the constant matrix M would transform as $M \to U_R M U_L^\dagger$ under

$SU(2)_L \times SU(2)_R$. The matrix M is an example of spurion which is defined as a constant quantity which would make a given theory invariant under certain transformation if we imagine that it would transform according to some specific rule.

Since ChPT is an effective theory of QCD it should break chiral symmetry explicitly in the exact same ways as QCD does, namely: one should construct operators involving insertions of the constant quark mass matrix M in such as way that, if $M \to U_R M U_L^\dagger$ under chiral rotation then these operators would be chiral invariant. There is only one such operator at leading order, namely:

$$\mathcal{L}_m^{(2)} = \frac{F_\pi^2 B_0}{2} \mathrm{Tr}[MU^\dagger + UM^\dagger]. \tag{3.19}$$

Here B_0 is a free parameter with mass dimension 1. The expansion of $\mathcal{L}_m^{(2)}$ gives:

$$\mathcal{L}_m^{(2)} = F_\pi^2 B_0 (m_u + m_d)(1 - \frac{\vec{\pi}^2}{2! \cdot F_\pi^2} + \frac{(\vec{\pi}^2)^2}{4! \cdot F_\pi^4}) + O(\pi^6). \tag{3.20}$$

We obtain from $\mathcal{L}_m^{(2)}$ a constant term, an isospin-invariant pion mass term and a series of interaction terms with even number of pions. The squared pion mass is then identified as $m_\pi^2 = B_0(m_u + m_d)$. It is interesting to notice that $m_\pi \sim \sqrt{m_q}$, i.e. the pion mass depends non-analytically to the quark masses.

Finally, combining Eq. (3.16) and (3.19) we obtain the full mesonic chiral Lagrangian at $O(p^2)$:

$$\begin{aligned} \mathcal{L}^{(2)} &= \frac{F_\pi^2}{4} \mathrm{Tr}[(\partial_\mu U)(\partial^\mu U^\dagger)] + \frac{F_\pi^2 B_0}{2} \mathrm{Tr}[MU^\dagger + UM^\dagger] \\ &= \text{const} + \frac{1}{2}(\partial_\mu \vec{\pi})^2 - \frac{m_\pi^2}{2}\vec{\pi}^2 + \frac{1}{6F_\pi^2}[(\vec{\pi} \cdot \partial_\mu \vec{\pi})^2 - \vec{\pi}^2 (\partial_\mu \vec{\pi})^2] + \frac{m_\pi^2}{24 F_\pi^2}(\vec{\pi}^2)^2 \\ &\quad + O(\pi^6) \end{aligned} \tag{3.21}$$

3.4.3 Brief discussion of $O(p^4)$ Lagrangian

If we restrict our requirement of precision level to $O(p^2)$, then what we need is the application of Eq. (3.21) at tree-level. However, to increase our precision to $O(p^4)$

one needs to include extra terms in the chiral Lagrangian at this order. If we ignore the coupling with external fields then the relevant terms are:

$$\begin{aligned}\mathcal{L}^{(4)} &= L_1\{\mathrm{Tr}[(\partial_\mu U)(\partial^\mu U^\dagger)]\}^2 + L_2\mathrm{Tr}[(\partial_\mu U)(\partial_\nu U^\dagger)]\mathrm{Tr}[(\partial^\mu U)(\partial^\nu U^\dagger)] \\ &+L_3\mathrm{Tr}[(\partial_\mu U)(\partial^\mu U^\dagger)(\partial_\nu U)(\partial^\nu U^\dagger)] + L_4\mathrm{Tr}[(\partial_\mu U)(\partial^\mu U^\dagger)]\mathrm{Tr}[MU^\dagger + UM^\dagger] \\ &+L_5\mathrm{Tr}[(\partial_\mu U)(\partial^\mu U^\dagger)(MU^\dagger + UM^\dagger)] + L_6\{\mathrm{Tr}[MU^\dagger + UM^\dagger]\}^2 \\ &+L_7\{\mathrm{Tr}[MU^\dagger - UM^\dagger]\}^2 + L_8\mathrm{Tr}[MU^\dagger MU^\dagger + UM^\dagger UM^\dagger]. \qquad (3.22)\end{aligned}$$

The parameter $\{L_i\}$ are low energy constants (LECs) which cannot be determined by any symmetry argument.

To obtain full results up to $O(p^4)$ one needs to apply Eq. (3.21) to one loop as well as Eq. (3.22) at tree level. In general the 1-loop integrals contributed by the $O(p^2)$ Lagrangian contain UV-divergences and these divergences can be canceled by the $O(p^4)$ low energy constants $\{L_i\}$. One may define $L_i = A_i + L_i^r$ where A_i are responsible for the cancelation of the UV-divergences of the loop integrals and $\{L_i^r\}$ are renormalized LECs which are finite numbers. They have to be either determined by experiment or fitted to lattice data.

3.5 Baryons in ChPT

So far we have only included pions in our chiral Lagrangian so the next step is obviously to include baryons. Again we restrict ourselves to a two-flavor QCD so the ground state baryons are just proton and neutron.

3.5.1 Transformation rule of the nucleon field

It is well-known that p and n form an isospin doublet and can be written collectively as a two-component nucleon field $N = (p\ n)^T$. Under $SU(2)_V$ the nucleon field should transform as

$$SU(2)_V \quad : N \to \exp\{i\vec{\theta}_V \cdot \frac{\vec{\tau}}{2}\}N. \tag{3.23}$$

On the other hand, it is not clear how $N(x)$ should transform under the full chiral symmetry $SU(2)_L \times SU(2)_R$. In fact, this transformation can be chosen arbitrarily and the only requirement is that it reduces to Eq. (3.23) when $\vec{\theta}_R = \vec{\theta}_L$. Different choices will all give the same result as far as physical observables are concerned.

The first and probably most obvious choice one could think about is to let $N_{L/R} \to U_{L/R}N_{L/R}$ under $SU(2)_L \times SU(2)_R$. This choice is completely fine, but then one could build chiral-invariant terms such as $\bar{N}_R U N_L$ which do not involve any derivative. For these terms it is not totally obvious whether or not the usual power counting scheme still holds because there seems to be no momentum suppression. To avoid this trouble one may choose a different kind of chiral transformation for N. The most standard choice is defined as the following. First we consider the chiral transformation of $u(x) \equiv \sqrt{U(x)}$. It can be written as:

$$u \to U_R u K^\dagger = K u U_L^\dagger \tag{3.24}$$

where $K = K(\pi(x))$ is a 2×2 unitary matrix which depends on the pion fields. The last equality of the equation above comes the fact that $U = u \cdot u$ transforms as $U \to U_R U U_L^\dagger$. Following Eq. (3.13), it is obvious that $K \to \exp\{i\vec{\theta}_V \cdot \frac{\vec{\tau}}{2}\}$ (which is the isospin transformation matrix) when $\vec{\theta}_R = \vec{\theta}_L$. Now the transformation rule of the nucleon field N under chiral rotation can be chosen as:

$$N \to KN \tag{3.25}$$

which obviously reduces to Eq. (3.23) in the isospin limit.

3.5.2 Nucleon Lagrangian at $O(p^1)$

We still need several other building blocks for the construction of the baryon ChPT Lagrangian. First, consider a naive kinetic term of the nucleon field $\bar{N}i\not{\partial}N$. This term is obviously not chiral invariant because the matrix K is spacetime-dependent. It is therefore essential to construct a chiral covariant derivative $\mathcal{D}_\mu$ which transforms under $SU(2)_L \times SU(2)_R$ as:

$$\mathcal{D}_\mu \to K\mathcal{D}_\mu K^\dagger. \tag{3.26}$$

One could verify that the correct form of the chiral covariant derivative is

$$\mathcal{D}_\mu = \partial_\mu + \frac{1}{2}(u^\dagger\partial_\mu u + u\partial_\mu u^\dagger). \tag{3.27}$$

With this, the term $\bar{N}i\not{\mathcal{D}}N$ is now chiral invariant. Expansion of this term gives the nucleon kinetic term and interaction terms involving nucleon and even number of pions.

It is also possible to construct operators that describe interactions between nucleon and odd number of pions. For that purpose one should introduce another piece of building block:

$$u_\mu \equiv i(u^\dagger\partial_\mu u - u\partial_\mu u^\dagger). \tag{3.28}$$

It is an axial vector as it transforms under parity as $u_\mu \to -u^\mu$. Also, one can straightforwardly show that u_μ transforms under $SU(2)_L \times SU(2)_R$ as $u_\mu \to Ku_\mu K^\dagger$. With the introduction of this axial vector one could construct a new classes of chiral-invariant operators. The only operator at the leading order has the form of $\bar{N}\gamma^\mu\gamma_5 u_\mu N$, where the γ_5 is included to make the whole term parity-even since we know that QCD conserves parity.

Finally, one shall not forget that a simple nucleon mass term $-m_N\bar{N}N$ is also chiral invariant so it has to be included in the chiral Lagrangian. Note that this mass comes from dynamical chiral symmetry breaking and not from quark mass

insertion, hence it remains non-zero even in the chiral limit. Combining all the terms we obtained above, we can now write down the nucleon Lagrangian in ChPT to the order $O(p^1)$:

$$\begin{aligned}\mathcal{L}_N^{(1)} &= \bar{N}(i\not{D} - m_N + \frac{g_A}{2}\gamma^\mu\gamma_5 u_\mu)N \\ &= \bar{N}i\not{\partial}N - m_N\bar{N}N - \frac{g_A}{2F_\pi}\bar{N}\gamma^\mu\gamma_5(\partial_\mu\vec{\pi})\cdot\vec{\tau}N + \frac{1}{4F_\pi^2}\bar{N}\gamma^\mu(\partial_\mu\vec{\pi}\times\vec{\pi})\cdot\vec{\tau}N \\ &\quad + O(\pi^3) \end{aligned} \tag{3.29}$$

It is interesting to notice that the pion-nucleon coupling constant g_A is the same g_A that appears in the neutron beta decay form factor. This is known as the Goldberger-Treiman relation.

3.6 Heavy Baryon Chiral Perturbation Theory

The nucleon Lagrangian in Eq. (3.29) is pathological not due to any symmetry consideration but due to the introduction of a large nucleon mass m_N that breaks the chiral power counting. Recall our discussion in Sec. 3.4 that the success of ChPT as an effective theory relies on the existence of a power counting scheme, where different terms can be arranged according to an increasing power of p/Λ_χ and $p \ll 1$ GeV. The introduction of a massive baryon, however, provides a new scale $p \sim m_N \sim 1$ GeV to the theory and $m_N/\Lambda_\chi \sim 1$ is obviously not a valid expansion parameter. The breakdown of the power counting rule renders the theory useless because there can be infinitely many terms in the Lagrangian which are equally important in the calculation of a given observable and there is no way we can take all these terms into account simultaneously.

The standard way to get around this problem is to introduce a phase shift to the nucleon field N that removes the large nucleon mass m_N in the theory. The redefined nucleon field now acts as a massless excitation with a residual momentum $k \ll 1$

GeV such that $k/\Lambda_\chi \ll 1$ so the chiral power counting is recovered. ChPT with this treatment is known as Heavy Baryon Chiral Perturbation Theory (HBChPT). In this section we shall introduce some basic concepts of HBChPT.

3.6.1 The velocity superselection rule

First let us consider a very heavy particle with mass m. Its initial momentum p can be defined as:

$$p^\mu \equiv mv^\mu + k^\mu \tag{3.30}$$

where v can be interpreted as its "velocity" and k^μ is a residual momentum where $k \ll m$. Now, imagine that it interacts with another light particle with a typical momentum much less than m. The final momentum $p'$of the heavy particle can be written as:

$$p'^\mu \equiv mv'^\mu + k'^\mu. \tag{3.31}$$

The difference between the initial and final momentum is then

$$p'^\mu - p^\mu = m(v'^\mu - v^\mu) + (k'^\mu - k^\mu). \tag{3.32}$$

It is clear now that in the large m limit we must have $v = v'$ in order for the momentum change to be finite, which means the velocity of a heavy particle is conserved during a soft interaction even though its momentum is not. This is known as the "velocity superselection rule". The picture can be visualized easily: when a light ball bounces off a very heavy ball, the heavy ball experiences a finite momentum change due to momentum conservation but its velocity is hardly changed.

Applying this concept to the nucleon in ChPT, we are able to label the nucleon field N with a four-velocity v which is conserved during interactions involving exchange of soft momenta.

3.6.2 Light and heavy components of the nucleon field

Let us make the discussion above more rigorous in terms of mathematical formulation. First, we define an arbitrary constant vector v^μ satisfying the following relations:

$$\begin{aligned} v^2 &= 1 \\ v^0 &\geq 1 \end{aligned} \tag{3.33}$$

and two velocity projection operators

$$P_{v\pm} \equiv \frac{1 \pm \not{v}}{2}. \tag{3.34}$$

One can easily verify the following properties for the projection operators:

$$\begin{aligned} P_{v+} + P_{v-} &= 1 \\ (P_{v\pm})^2 &= P_{v\pm} \\ P_{v\pm} P_{v\mp} &= 0 \\ \not{v} P_{v\pm} &= \pm P_{v\pm}. \end{aligned} \tag{3.35}$$

Next, we shall define the "light" component N_v and the "heavy" component H_v of the nucleon field as the following:

$$\begin{aligned} N_v &\equiv e^{im_N v\cdot x} P_{v+} N \\ H_v &\equiv e^{im_N v\cdot x} P_{v-} N. \end{aligned} \tag{3.36}$$

Obviously, the original nucleon field N is related to these two components by $N(x) = e^{-im_N v\cdot x}(N_v(x) + H_v(x))$. Also, note that this decomposition acts only on the Dirac space of the nucleon field and has nothing to do with the isospin space.

3.6.3 The heavy baryon expansion

With this decomposition we are now ready to formulate the heavy baryon expansion of the ChPT Lagrangian. Our goal is to expand the ChPT Lagrangian in powers of p/m_N where p is an energy scale much less than 1 GeV. With this expansion, the nucleon mass m_N can only appear in denominator and not numerator, hence the power counting of our chiral Lagrangian will be safe. Let us start with the following nucleon Lagrangian:

$$\mathcal{L} = \bar{N}(i\not{D} - m_N + \Gamma)N \tag{3.37}$$

where Γ can take any form. Substitution of the decomposed form of N into the equation above leads to:

$$\mathcal{L} = \bar{N}_v(i\not{D}+\Gamma)N_v + \bar{H}_v(i\not{D}-2m_N+\Gamma)H_v + \bar{N}_v(i\not{D}-2m_N+\Gamma)H_v + \bar{H}_v(i\not{D}+\Gamma)N_v. \tag{3.38}$$

If we concentrate on the first two terms of the equation above, it seems that N_v is a massless excitation while H_v is a massive excitation with mass $2m_N$. One could then integrate out the heavy field H_v in the Lagrangian and obtain and effective theory of the light field N_v only. This procedure creates infinitely many terms that can be arranged by increasing powers of $1/m_N$ and that is exactly the heavy baryon expansion we are looking for.

There is one further step we need to perform to Eq. (3.38) before H_v can be integrated out. One should be aware that after the velocity projection N_v and H_v are effectively two-component spinors although formally they still have four components. Similarly, the Dirac structure of $(i\not{D}-2m_N+\Gamma)$ also contains redundancies that needs to be removed otherwise it will have no inverse. The removal of this redundancy involves sandwiching Dirac matrices between velocity projection operators. Some useful results are summarized below:

$$
\begin{aligned}
P_{v\pm}\not{A}P_{v\pm} &= \pm A\cdot v P_{v\pm} \\
P_{v\pm}\not{A}P_{v\mp} &= \not{A}_\perp P_{v\mp} = P_{v\pm}\not{A}_\perp \\
P_{v\pm}\not{A}\gamma_5 P_{v\pm} &= \not{A}_\perp \gamma_5 P_{v\pm} \\
P_{v\pm}\not{A}\gamma_5 P_{v\mp} &= \pm A\cdot v\gamma_5 P_{v\mp}
\end{aligned} \tag{3.39}
$$

with $A_\perp^\mu \equiv A^\mu - v\cdot A v^\mu$. For notational convenience, we shall also define for any Dirac structure Γ, $\Gamma_{ij} \equiv P_{vi}\Gamma P_{vj}$ (for example, $\Gamma_{+-} = P_{v+}\Gamma P_{v-}$). With this, Eq. (3.38) can be rewritten as

$$
\begin{aligned}
\mathcal{L} &= \bar{N}_v(iv\cdot\mathcal{D} + \Gamma_{++})N_v + \bar{H}_v(-iv\cdot\mathcal{D} - 2m_N + \Gamma_{--})H_v \\
&\quad + \bar{N}_v(i\not{\mathcal{D}}_\perp + \Gamma_{+-})H_v + \bar{H}_v(i\not{\mathcal{D}}_\perp + \Gamma_{-+})N_v.
\end{aligned} \tag{3.40}
$$

The heavy field H_v can now be integrated out from Eq. (3.40) simply by completing the square. The effective Lagrangian we obtain is the following:

$$
\begin{aligned}
\mathcal{L}_{\text{eff}} &= \bar{N}_v(iv\cdot\mathcal{D} + \Gamma_{++})N_v \\
&\quad + \bar{N}_v(i\not{\mathcal{D}}_\perp + \Gamma_{+-})(2m_N + iv\cdot\mathcal{D} - \Gamma_{--})^{-1}(i\not{\mathcal{D}}_\perp + \Gamma_{-+})N_v.
\end{aligned} \tag{3.41}
$$

This effective Lagrangian can be easily expanded in powers of $1/m_N$.

3.6.4 Reduction of Dirac structures

The fermionic degree of freedom in Eq. (3.41) is the light nucleon field N_v which is effectively a two-component spinor. Recall that for a theory with two-component Pauli spinors there are only two independent types of matrices in the spin space, namely 1 and $\vec{\sigma}$. We expect the same to happen here, where all the Dirac structures can be reduced to either 1 or some kind of spin matrix.

It turns out that the appropriate definition of the spin matrix is given by

$$S_v^\alpha \equiv \frac{i}{2}\sigma^{\alpha\beta}\gamma_5 v_\beta. \tag{3.42}$$

Some useful relations involving the spin matrix are summarized below:

$$\begin{aligned} S_v \cdot v &= 0 \\ \{S_v^\mu, S_v^\nu\} &= \frac{1}{2}(v^\mu v^\nu - g^{\mu\nu}) \\ \overline{S_v^\mu} &= S_v^\mu \\ [P_{v+}, S_v^\nu] &= 0 \\ [S_v^\mu, S_v^\nu] &= i\varepsilon^{\mu\nu\alpha\beta} v_\alpha S_\beta^v. \end{aligned} \tag{3.43}$$

Note that the first four equalities hold in arbitrary dimension while the last equality is only true when $d = 4$. One can demonstrate that the S_v^μ defined above indeed possesses well-known properties of spin matrices. For instance, consider a static nucleon where $v^\mu = (1, \vec{0})$. Then the last equality becomes $[S_v^i, S_v^j] = i\varepsilon^{ijk} S_v^k$ which is indeed the correct commutation rule for spin operators.

One may proceed to show that any Dirac matrix sandwiched between N_v and $\bar{N}_v$ will reduce to either 1 or S_v^μ. A complete list of such reductions is given below:

$$\begin{aligned} \bar{N}_v \gamma_5 N_v &= 0 \\ \bar{N}_v \gamma^\mu N_v &= v^\mu \bar{N}_v N_v \\ \bar{N}_v \gamma^\mu \gamma_5 N_v &= 2\bar{N}_v S_v^\mu N_v \\ \bar{N}_v \sigma^{\mu\nu} N_v &= 2\varepsilon^{\mu\nu\alpha\beta} v_\alpha \bar{N}_v S_\beta^v N_v \\ \bar{N}_v \sigma^{\mu\nu}\gamma_5 N_v &= 2i(v^\mu \bar{N}_v S_v^\nu N_v - v^\nu \bar{N}_v S_v^\mu N_v). \end{aligned} \tag{3.44}$$

Again, the first three equalities hold in arbitrary dimension while the last two equalities are true only when $d = 4$.

3.6.5 Leading order HBChPT Lagrangian

Finally we shall apply the heavy baryon formalism to Eq. (3.29). With $\Gamma = (g_A/2)\not{u}\gamma_5$ we have:

$$\bar{N}_v \Gamma_{++} N_v = \frac{g_A}{2}\bar{N}_v \not{u}_\perp \gamma_5 N_v = \frac{g_A}{2}\bar{N}_v(\not{u} - u\cdot v\not{v})\gamma_5 N_v = g_A \bar{N}_v u\cdot S_v N_v. \tag{3.45}$$

Therefore, to the leading order in $1/m_N$ expansion one simply gets:

$$\mathcal{L}_{\text{eff}} = \bar{N}_v(iv\cdot\mathcal{D} + g_A S_v\cdot u)N_v + O(\frac{1}{m_N}). \tag{3.46}$$

The free-particle EOM derived from this Lagrangian is simply $iv\cdot\partial N_v = 0$, which implies the following on-shell condition:

$$v\cdot k = 0 \tag{3.47}$$

where k is the residual momentum carried by the light nucleon field N_v. The Feynman propagator of the light field is given by:

$$iS(k) = \frac{i}{v\cdot k + i\epsilon}. \tag{3.48}$$

These are basically all the ingredients we need in the evaluation of Feynman diagrams using the leading order HBChPT Lagrangian.

CHAPTER 4

NUCLEON ELECTRIC DIPOLE MOMENTS AND THE ISOVECTOR PARITY- AND TIME-REVERSAL-ODD PION-NUCLEON COUPLING

4.1 Introduction

Electric dipole moments (EDMs) of neutral atoms, molecules, and the neutron provide sensitive probes of new sources of time-reversal (T) and parity (P) violation. Current upper limits on the EDMs of the ^{199}Hg atom [147], $d_A(^{199}\mathrm{Hg})$, and neutron [148], d_n, place tight constraints on the QCD vacuum angle within the Standard Model (SM) as well as on possible sources of sources of CP-violation (CPV) arising from physics beyond the SM (BSM)[1]. The existence of BSM CPV is needed in order to explain the cosmic baryon asymmetry (for a recent review, see Ref. [52]). If the asymmetry had been generated at temperatures of order the electroweak (EW) scale, then d_n provides a particularly sensitive probe.

At energies below the scale of BSM interactions Λ but above the EW scale, one may characterize the effects of BSM CPV interactions in terms of an effective theory involving only SM fields:

$$\mathcal{L}_{\rm CPV} = \mathcal{L}_{\rm CKM} + \mathcal{L}_{\bar{\theta}} + \mathcal{L}^{\rm eff}_{\rm BSM} \ , \tag{4.1}$$

where $\mathcal{L}_{\rm CKM}$ and $\mathcal{L}_{\bar{\theta}}$ denote the SM Cabibbo-Kobayashi-Maskawa (CKM) [24] and QCD vacuum angle [34, 265, 264] CPV Lagrangians, respectively, and

[1] In what follows, we assume CPT conservation, so that the signal for a non-vanishing neutron EDM would also indicate the presence of CP-violation.

$$\mathcal{L}^{\rm eff}_{\rm BSM} = \frac{1}{\Lambda^2}\ \sum_i \alpha_i^{(6)}\ \mathcal{O}_i^{(6)} + \cdots\ , \tag{4.2}$$

gives the set of non-renormalizable CPV effective operators at the weak scale $v = 246$ GeV generated by BSM physics at a scale $\Lambda > v$. For brevity, we have indicated only those entering at dimension (d) six, while the $+\cdots$ indicate those of higher dimension[2]. Among the more widely considered $d = 6$ CPV operators are the elementary fermion EDMs, the quark chromo-EDMs, and the Weinberg three-gluon operator.

In this study, we focus on one particular $d = 6$ operator that naturally arises in left-right symmetric model (LRSM) extensions of the SM, that gives rise to EDMs of nucleons, nuclei, and diamagnetic atoms, and that has received considerably less attention than the other operators that arise at this order in the effective theory:

$$\mathcal{O}_{\varphi ud} = i(\tilde{\varphi}^\dagger D_\mu \varphi)\bar{u}_R\gamma^\mu d_R\ , \tag{4.3}$$

where φ is the Higgs doublet, $\tilde{\varphi} = i\tau_2\varphi^*$, D_μ is the $\mathrm{SU}(2)_L{\times}\mathrm{U}(1)_Y$ covariant derivative and u_R (d_R) is the right-handed up-quark (down-quark) field. In LRSMs, the corresponding Wilson coefficient $C_{\varphi ud}$ is generated by mixing between the left- and right-handed W bosons in the presence of either spontaenous CPV and/or explicit CPV in the right-handed quark CKM matrix.

After electroweak symmetry-breaking wherein $\varphi^T \to (0, v/\sqrt{2})$, the exchange of the $W^\pm$ contained in the covariant derivative with a left-handed quark current leads to an effective four quark interaction[3]

$$\mathcal{L}^{\rm eff}_{\rm LR,\,CPV} = -i\frac{\mathrm{Im}\, C_{\varphi ud}}{\Lambda^2}\left[\bar{d}_L\gamma^\mu u_L\,\bar{u}_R\gamma_\mu d_R - \bar{u}_L\gamma^\mu d_L\,\bar{d}_R\gamma_\mu u_R\right]\ . \tag{4.4}$$

---

[2]A complete list of dimension six operators may be found in Refs. [29], while those directly relevant to EDMs are listed in Tables three and four of Ref. [164].

[3]Corrections due to the evolution of the four quark interaction to hadronic scales are minor, see the discussion in Ref. [266].

The interaction in Eq. (4.4) breaks isospin symmetry, thereby giving rise to, among other interactions, the isovector TVPV πNN interaction:

$$\mathcal{L}^{\rm TVPV}_{\pi N,\ I=1} = \bar{g}_\pi^{(1)} \bar{N} \pi^0 N \ , \tag{4.5}$$

where N and π^0 are the nucleon and neutral pion fields, respectively. This interaction leads to long-range contributions to the nuclear Schiff moment that induces $d_A(^{199}\mathrm{Hg})$ as well as long-range contributions to d_n that can be computed in chiral perturbation theory. The present limits on these EDMs, thus, imply constraints on the mass M_{W_R} of the right-handed W-boson and associated CPV phases in the LRSM.

Following this line of reasoning, the authors of Refs. [267, 268] have derived constraints on M_{W_R} and the strength of spontaneous CPV in the LRSM from the limits on d_n and the corresponding implications of CPV in the neutral kaon sector. The results imply that $M_{W_R} > 10$ TeV. In related work, the authors of Ref. [269] observed that $\mathcal{O}_{\varphi ud}$ will also induce a semi-leptonic CPV operator that contributes to neutron decay. Even without specifying to the LRSM, the d_n limits on $C_{\varphi ud}$ then constrain the magnitude of possible effects in T-odd neutron decay correlations. In both cases, the d_n constraints relied on an earlier pion-loop calculation performed by the authors of Ref. [270] using a relativistic meson-nucleon field theory approach. The results indicate that the leading term in d_n resulting from the interaction (4.5) is proportional to the neutron anomalous magnetic moment κ_n and is independent of the pion-to-nucleon mass ratio, m_π/m_N. From the standpoint of effective field theory (EFT), this result is surprising, as the anomalous magnetic moment vertex brings in an inverse power of the nucleon mass while consistent power counting in chiral perturbation theory requires that loops only bring in momenta of order of the pion mass. The absence of any m_π/m_N suppression in the computation of Ref. [270] is not consistent with this expectation.

In what follows, we repeat the pion loop computation associated with (4.5) using heavy baryon chiral perturbation theory (HBChPT) [163] and show that the result proportional to $\bar{g}_\pi^{(1)}\kappa_n$ is suppressed by $(m_\pi/m_N)^2 \sim 0.02$. HBChPT implements the power counting required by an EFT by expanding about both the static nucleon ($m_N \to \infty$) and chiral ($m_\pi \to 0$) limits. Our results imply considerably weaker constraints on $C_{\varphi ud}$ from the long-range contribution to d_n than obtained in the studies of Refs. [267, 268, 269]. Presently uncalculable short-distance contributions associated with loop momenta of order one GeV that reside in the nucleon EDM counterterm may imply stronger constraints as suggested by naïve dimensional analysis (NDA). In this context, one may view the relativistic meson theory computation of Ref. [270] as providing a model estimate of the short-distance contributions. Generally speaking, however, both the sign and magnitude of NDA and/or model estimates for the short distance contributions are subject to uncertainty, so the most conservative implications will be inferred from the calculable long-distance terms.

In this respect, we note that the diamagnetic EDMs provide an in principle more robust benchmark than d_n, as the nuclear Schiff moment arises from tree-level pion exchange between two nucleons and is relatively free from the uncertainties associated with short-distance contributions. In practice, the many-body nuclear theory uncertainty associated with the interaction (4.5) are substantial [164], with the situation for ^{199}Hg being particularly unsettled. Looking to the future, storage-ring searches for EDMs of light nuclei such as the deuteron or ^{3}He nucleus [247] would provide theoretically cleaner probes of $\mathcal{O}_{\varphi ud}$ since the short-distance contributions to such EDMs are relatively minor and since the few-body nuclear theory is well under control [271]. In the immediate term, however, the long-range contribution to d_n appears to be the most trustworthy avenue for accessing $\mathcal{O}_{\varphi ud}$.

In the remainder of this paper, we discuss the details of our calculation. In Section 4.2 we summarize the HBChPT framework as it applies to the computation of TVPV

observables and give the details of our nucleon EDM computation. In Section 4.3 we compare our results with those of Ref. [270]. We discuss the implications and summarize in Section 4.4.

4.2 HBChPT Calculation

Loop computations performed with a relativistic meson-nucleon field theory and dimensional regularization include explicit contributions from loop momenta of order m_N, thereby eliminating the possibility of a consistent power counting[4]. In HBChPT [163], one removes these contributions by first redefining the nucleon degrees of freedom in terms of heavy fields having fixed velocity v

$$N_v = \frac{1+\not{v}}{2} e^{i m_N v\cdot x} N \ , \tag{4.6}$$

where

$$p^\mu = m_N v^\mu + k^\mu \ , \tag{4.7}$$

with k being a residual momentum. We henceforth omit the "v" subscript. Derivatives acting on the heavy fields give the small residual momenta, and the propagator of a heavy-nucleon field no longer contains the nucleon mass. The results of loop integrals involving the N fields then scale with powers of Q/m_N and Q/Λ_χ, where Q is of order m_π or the external momentum (assumed to be well below one GeV), $\Lambda_\chi = 2\pi F_\pi$ is the scale of chiral symmetry breaking, and $F_\pi = 186$ MeV is the pion decay constant[5]. One, thus, obtains a consistent EFT power counting.

---

[4] A relativistic approach can provide a reliable power counting if more complicated regularizations schemes are applied, for a review see Ref. [272].

[5] Note that other work in HBChPT uses $f_\pi = F_\pi/2$.

The HBChPT interactions are constructed from the heavy nucleon and pion fields, the velocity v^μ, and the spin S^μ with $S = (\vec{\sigma}/2, 0)$ in the nucleon rest frame $v = (\vec{0}, 1)$. It is also useful to project vectors in their components parallel and orthogonal to the velocity. We use a subscript $\perp$ to denote the perpendicular components. For example, the perpendicular covariant derivative is

$$\mathcal{D}^\mu_\perp = \mathcal{D}^\mu - v^\mu v \cdot \mathcal{D} \ . \tag{4.8}$$

We note that HBChPT operators are manifestly invariant under rotations and translations. Under boosts, the HBChPT operators are only invariant order by order in the Q/m_N expansion, leading to non-trivial constraints on the interactions in the effective Lagrangian and on their coefficients [163, 273].

The resulting, leading order (LO) P- and T-conserving Lagrangian for f fermion fields is (see Ref. [274] for more details)

$$\mathcal{L}^{(0)} = \frac{1}{2} D_\mu \boldsymbol{\pi} \cdot D^\mu \boldsymbol{\pi} - \frac{m_\pi^2}{2D} \boldsymbol{\pi}^2 + \bar{N} \left(iv \cdot \mathcal{D} - \frac{2 g_A}{F_\pi} S^\mu \boldsymbol{\tau} \cdot D_\mu \boldsymbol{\pi} \right) N \ , \tag{4.9}$$

where $g_A = 1.27$ is the pion-nucleon axial-vector coupling. At LO, electromagnetism can be included by making the derivatives in Eq. (4.9) covariant under $U_{\rm em}(1)$,

$$\begin{aligned} (D_\mu \pi)_i \ &\to \ (D_{\mu,{\rm em}} \pi)_i = \frac{1}{D} \left(\partial_\mu \delta_{ij} + e A_\mu \epsilon_{3ij} \right) \pi_j \ , \\ \mathcal{D}_\mu N \ &\to \ \mathcal{D}_{\mu,{\rm em}} N = \left[\partial_\mu + \frac{i}{F_\pi^2} \boldsymbol{\tau} \cdot (\boldsymbol{\pi} \times D_{\mu,{\rm em}} \boldsymbol{\pi}) + \frac{ie}{2} A_\mu \left(1 + \tau_3 \right) \right] N \ , \end{aligned} \tag{4.10}$$

where e is the proton charge, $e > 0$ and $D = 1 + \boldsymbol{\pi}^2 / F_\pi^2$. For brevity, in the following we omit the label "em".

The anomalous magnetic moment that is of particular interest to this work first appears at next-to-leading order (NLO) in Q/m_N, together with the nucleon kinetic

energy, a recoil correction to the axial pion-nucleon coupling, the nucleon sigma term, and the proton-neutron mass difference

$$\begin{aligned}\mathcal{L}^{(1)} &= -\frac{1}{2m_N}\bar{N}\mathcal{D}_\perp^2 N + \frac{g_A}{F_\pi m_N}\left(iv\cdot D\boldsymbol{\pi}\right)\cdot\bar{N}\boldsymbol{\tau}\, S\cdot\mathcal{D}_- N \\ &\quad + \frac{1}{4m_N}\varepsilon^{\alpha\beta\mu\nu}v_\alpha\bar{N}S_\beta\left[(1+\kappa_0)+(1+\kappa_1)\tau_3\right]NeF_{\mu\nu} \\ &\quad + \Delta m_N\left(1-\frac{2\boldsymbol{\pi}^2}{F_\pi^2 D}\right)\bar{N}N + \frac{\delta m_N}{2}\bar{N}\left(\tau^3-\frac{2\pi_3}{F_\pi^2 D}\boldsymbol{\tau}\cdot\boldsymbol{\pi}\right)N + \ldots \quad (4.11)\end{aligned}$$

Here, κ_1 and κ_0 are the isovector and isoscalar anomalous magnetic moments (AMMs), $\kappa_1 = 3.7$, $\kappa_0 = -0.12$, and Δm_N and δm_N the nucleon sigma term and nucleon mass splitting originating in the quark masses. A lattice calculation found $\delta m_N = 2.26$ MeV [275], while evaluations of Δm_N range between 45 and 60 MeV [276]. The "$+\cdots$" in Eq. (4.11) denote other operators with chiral index $\Delta = 1$, like the pion mass splitting term, which are not relevant for our discussion.

In Eq. (4.11), the nucleon AMM couples to the magnetic field, and this interaction does not contribute directly to the nucleon EDM. However, the AMM does couple to the electric field at next-to-next-to-leading order (NNLO) through the spin-orbit interaction that appears in $\Delta = 2$ Lagrangian:

$$\begin{aligned}\mathcal{L}^{(2)} &= \frac{g_A}{4m_N^2 F_\pi}D_\mu\boldsymbol{\pi}\cdot\left(\bar{N}\boldsymbol{\tau}S^\mu\mathcal{D}^2_{\perp,-}N - \bar{N}\boldsymbol{\tau}\mathcal{D}^\mu_{\perp,-}S\cdot\mathcal{D}_{\perp,-}N\right) \\ &\quad - \frac{i}{16m_N^2}\varepsilon^{\alpha\beta\mu\nu}\bar{N}S_\alpha\left[(1+2\kappa_0)+(1+2\kappa_1)\tau_3\right]\mathcal{D}_{\beta,\perp,-}]N\, eF_{\mu\nu} + \ldots \quad (4.12)\end{aligned}$$

The first term in Eq. (4.12) is a relativistic correction to g_A, while the second term is the spin-orbit nucleon-photon coupling. Reparametrization invariance fixes the coupling constant of the interactions in Eq. (4.12) in terms of the couplings in Eqs. (4.9) and (4.11) [163, 273].

Next we list the TVPV interactions originating in the four-quark operator in Eq. (4.4). The construction of these interactions has been discussed in detail in Ref.

[277], and here we only summarize the results. As already mentioned, the isovector TVPV pion-nucleon interaction in Eq. (4.5) with coupling $\bar{g}_\pi^{(1)}$ is induced at leading order. Additionally, the quantum numbers of the neutral pion allow the existence of a pion tadpole term. This tadpole can be removed from the Lagrangian via a field redefinition of the pion and nucleon fields [278]. These field redefinitions induce an additional LO contribution to the isovector TVPV pion-nucleon that can be absorbed into $\bar{g}_\pi^{(1)}$. The tadpole removal also induces a contribution to the isoscalar TVPV pion-nucleon interaction

$$\mathcal{L}_{\pi N,\ I=0}^{\rm TVPV} = \bar{g}_\pi^{(0)} \bar{N} \boldsymbol{\tau} \cdot \boldsymbol{\pi} N \ . \tag{4.13}$$

Though formally LO, this contribution vanishes in the isospin limit $m_u = m_d$ and is suppressed by the ratio $\bar{g}_\pi^{(0)}/\bar{g}_\pi^{(1)} = \delta m_N/(2\Delta m_N) \simeq 0.02$.

We find that there exist no NLO corrections proportional to $\bar{g}_\pi^{(1)}$ and $\bar{g}_\pi^{(0)}$, because they depend on structures like $(1 \pm \not{v})(1 \mp \not{v})$ that vanish. The first non-vanishing corrections proportional to $\bar{g}_\pi^{(1)}$ appear at NNLO and are given by

$$\mathcal{L}_{\pi N,\, I=1}^{\rm TVPV(NNLO)} = -\frac{\bar{g}_\pi^{(1)}}{4m_N^2}(D_\nu \pi_3)\bar{N}[S^\mu, S^\nu]\mathcal{D}_{\mu,-}N - \frac{\bar{g}_\pi^{(1)}}{8m_N^2}\pi_3 \bar{N}\mathcal{D}_{\perp,-}^2 N \ . \tag{4.14}$$

For brevity, we do not list the remaining NLO and NNLO TVPV interactions [277] that are not relevant for the present discussion.

Finally, the combination of Eq. (4.4) and electromagnetic interactions gives rise to the EDM interaction

$$\mathcal{L}_{\rm em}^{\rm TVPV} = -2\bar{N}(\bar{d}_0 + \bar{d}_1\tau^3) S^\mu N\, v^\nu F_{\mu\nu} + \dots \ , \tag{4.15}$$

where $\bar{d}_0$ and $\bar{d}_1$ are, respectively, the isoscalar and isovector short-range contributions to the nucleon EDM and the "$+\cdots$" stand for terms with one or more pions or relativistic corrections not relevant for the discussion here.

We now compute the contributions to the nucleon EDM generated by the interactions in Eqs. (4.5,4.9,4.11-4.15). In the HBChPT framework, the EDM enters as a TVPV contribution to the nucleon EM current:

$$J^{\mu}_{\rm TVPV}(q) \;\; = \;\; 2i\,(d_0 + d_1\tau_3)\,(S\cdot q v^{\mu} - S^{\mu} v\cdot q + \ldots) \;\; , \tag{4.16}$$

where q^{μ} is the four-momentum of the outgoing photon and

$$\mathcal{L}^{\rm TVPV}_{\gamma N} = -J^{\mu}_{\rm TVPV} A_{\mu} \; . \tag{4.17}$$

The dots in Eq. (4.16) denote relativistic corrections to the leading order current. The neutron (proton) EDM is given by $d_0 - d_1$ $(d_0 + d_1)$. For virtual photons, the nucleon EDMs become the electric dipole form factors (see, *e.g.*, Refs. [279, 280, 281]). For purposes of our calculation, however, we focus on the static limits.

Contributions to the nucleon EDM arise from tree-level diagrams involving the short-range interactions in Eq. (4.15) and from one-loop diagrams involving the TVPV pion-nucleon vertices. The largest one-loop diagrams involve the P- and T-conserving vertices from Eq. (4.9) only, while corrections appear due to insertions of vertices from Eq. (4.11) or (4.12).

The contributions to $d_{0,1}$ proportional to $\bar{g}_{\pi}^{(1)}$ and $\bar{g}_{\pi}^{(0)}$ up to order $\mathcal{O}(Q/m_N)$ have been computed previously in Refs. [281, 282], and they are independent of $\kappa_{0,1}$. The reason being that $\mathcal{O}(Q/m_N)$ electromagnetic interactions given in Eq. (4.11) do not contribute to the nucleon EDM since the interaction with the external field is purely magnetic in the rest frame of the nucleon. The contributions proportional to the AMMs therefore enter at $\mathcal{O}(Q/m_N)^2$ and are generated by the vertex correction diagrams in Fig. 4.1 along with the corresponding wave function renormalization graphs in Fig. 4.2. Because $\bar{g}_{\pi}^{(0)}/\bar{g}_{\pi}^{(1)}$ is small, at this order we focus on diagrams involving $\bar{g}_{\pi}^{(1)}$ only. The number of open circles indicates the order in the (Q/m_N)

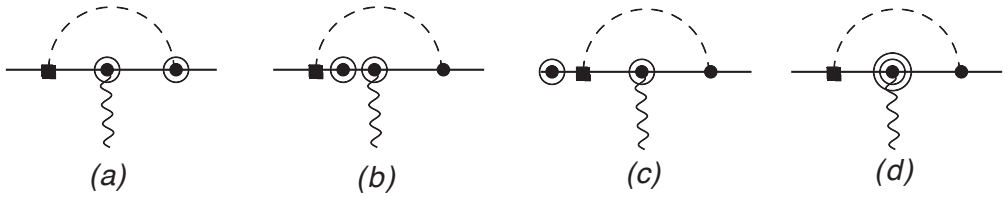

Figure 4.1. One-loop diagrams contributing to the nucleon EDMs at next-to-next-to-leading order. Solid, dashed and wavy lines represent the propagation of nucleons, pions and photons, respectively. A square marks the isovector TVPV interaction from Eq. (4.5), other vertices representing the T- and P-conserving interactions. Each circle on the vertex represents a suppression factor proportional to $1/m_N$. For simplicity only one possible ordering is shown.

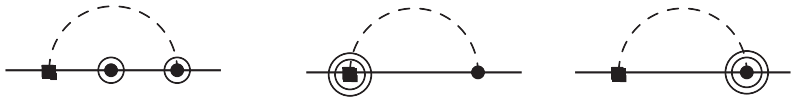

Figure 4.2. One-loop diagrams contributing to wave function renormalization. The notation is as in Fig. 4.1.

expansion. Again, because the $\mathcal{O}(Q/m_N)$ electromagnetic interactions are purely magnetic, the contributions from the topologies of Figs. 4.1(a-c) vanish individually. We also find that the sum of contributions proportional to $\bar{g}_\pi^{(1)}$ that arise from the $\mathcal{O}(Q/m_N)^2$ wave function renormalization vanish. The only surviving, non-vanishing contribution is generated by the topology of Fig. 4.1(d).

At $\mathcal{O}(Q/m_N)^2$, an additional set of contributions to the proton EDM proportional to $\bar{g}_\pi^{(1)}$ are generated by the graphs in Fig. 4.3. The latter contain only the coupling to the nucleon charge and various combinations of (a) $\mathcal{O}(Q/m_N)$ corrections to the πNN interactions and nucleon propagator as well as (b) $\mathcal{O}(Q/m_N)^2$ corrections to one of the couplings or propagator and LO interactions for the remaining components of the diagram. Finally, at this order in principle contributions appear due to two-loop diagrams involving $\bar{g}_\pi^{(1)}$ and LO P- and T-conserving vertices. However, the sum of these diagrams vanishes.

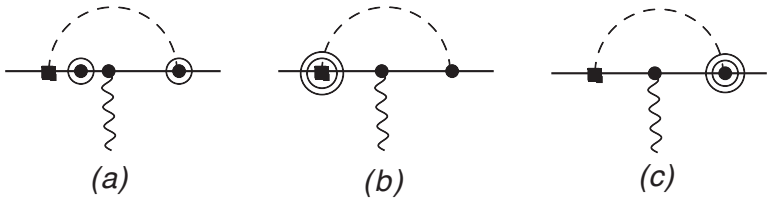

Figure 4.3. Representative one-loop diagrams contributing at order $(m_\pi/m_N)^2$ to the proton EDM proportional to $\bar{g}_\pi^{(1)}$ and independent of the anomalous magnetic moment coupling. The notation is as in Fig. 4.1.

Before giving our result, we first quote the LO and NLO results, including the contributions involving both $\bar{g}_\pi^{(1)}$ and $\bar{g}_\pi^{(0)}$. It should be noted that the results involving $\bar{g}_\pi^{(0)}$ are actually suppressed by the smallness of $\bar{g}_\pi^{(0)}/\bar{g}_\pi^{(1)}$ for the CPV source in Eq. (4.4). The LO contribution proportional to $\bar{g}_\pi^{(0)}$ has been first calculated in Ref. [282], while the NLO corrections have been calculated in Refs. [281]. Together they give

$$\begin{aligned} d_0^{\rm LO+NLO} &= \bar{d}_0 - \frac{e g_A}{4\pi^2 F_\pi}\,\frac{\pi m_\pi}{4 m_N}\left(3\bar{g}_\pi^{(0)} + \bar{g}_\pi^{(1)}\right) \,, \\ d_1^{\rm LO+NLO} &= \bar{d}_1 - \frac{e g_A}{4\pi^2 F_\pi}\left[\bar{g}_\pi^{(0)}\left(L - \ln\frac{m_\pi^2}{\mu^2} + \frac{5\pi}{4}\frac{m_\pi}{m_N}\right) + \frac{\pi}{4}\frac{m_\pi}{m_N}\bar{g}_\pi^{(1)}\right] \,. \end{aligned} \tag{4.18}$$

The contribution of $\bar{g}_\pi^{(0)}$ to the isovector EDM is UV divergent, with divergence encoded in the factor

$$L \equiv \frac{2}{4-d} - \gamma_E + \ln 4\pi \,, \tag{4.19}$$

in terms of number of space-time dimensions d and the Euler-Mascheroni constant γ_E. The divergence is absorbed by the low-energy constant $\bar{d}_1$, which also contains an *a priori* unknown non-vanishing finite contribution. It is conventional to absorb L entirely into $\bar{d}_1$, thereby isolating the terms non-analytic in quark mass that are unique to the loops. Notice that, at this order, the $\bar{g}_\pi^{(1)}$ terms do not contribute to

the neutron EDM. For the interaction $C_{\varphi ud}$ in Eq. (4.4), this implies that the largest non-analytic contributions only affect the proton EDM because $\bar{g}_\pi^{(0)}$ is suppressed.

At NNLO, $\bar{g}_\pi^{(1)}$ contributes to the nucleon EDM via the diagrams in Figs. 4.1 and 4.3. At this order in the Q/m_N expansion, we neglect small $\bar{g}_\pi^{(0)} m_\pi^2/m_N^2$ corrections, and only give terms proportional to $\bar{g}_\pi^{(1)}$. We find that the contributions are divergent:

$$\begin{aligned} d_0^{\rm NNLO} &= \frac{e g_A \bar{g}_\pi^{(1)}}{64\pi^2 F_\pi} \frac{m_\pi^2}{m_N^2} \left[(5+4\kappa_1) \left(L - \log \frac{m_\pi^2}{\mu^2} \right) + 1 \right] , \\ d_1^{\rm NNLO} &= \frac{e g_A \bar{g}_\pi^{(1)}}{64\pi^2 F_\pi} \frac{m_\pi^2}{m_N^2} \left[(5+4\kappa_0) \left(L - \log \frac{m_\pi^2}{\mu^2} \right) + 1 \right] . \end{aligned} \tag{4.20}$$

Again, we can absorb L and other finite pieces analytic in the quark mass into the LECs $\bar{d}_{0,1}$. It is also instructive to express results through $\mathcal{O}(Q/m_N)^2$ for the neutron and proton EDM's separately:

$$d_n = \bar{d}_n - \frac{e g_A}{4\pi^2 F_\pi} \left\{ \bar{g}_\pi^{(0)} \left(\ln \frac{m_\pi^2}{m_N^2} - \frac{\pi m_\pi}{2 m_N} \right) + \frac{\bar{g}_\pi^{(1)}}{4} (\kappa_1 - \kappa_0) \frac{m_\pi^2}{m_N^2} \ln \frac{m_\pi^2}{m_N^2} \right\} \tag{4.21}$$

$$\begin{aligned} d_p = \bar{d}_p + \frac{e g_A}{4\pi^2 F_\pi} \Bigg\{ & \bar{g}_\pi^{(0)} \left(\ln \frac{m_\pi^2}{m_N^2} - \frac{2\pi m_\pi}{m_N} \right) \\ & - \frac{\bar{g}_\pi^{(1)}}{4} \left[\frac{2\pi m_\pi}{m_N} + \left(\frac{5}{2} + \kappa_0 + \kappa_1 \right) \frac{m_\pi^2}{m_N^2} \ln \frac{m_\pi^2}{m_N^2} \right] \Bigg\} , \end{aligned} \tag{4.22}$$

where we have also absorbed analytic terms into $\bar{d}_p = \bar{d}_0 + \bar{d}_1$ ($\bar{d}_n = \bar{d}_0 - \bar{d}_1$) and evaluated the result at a renormalization scale $\mu = m_N$. We observe again that unlike d_p, d_n contains no terms proportional to $\bar{g}_\pi^{(1)}$ linear in m_π and that its non-analytic quark mass dependence first appears at NNLO. Thus, compared to the estimates based on Ref. [270], the d_n contributions proportional to $\kappa_{0,1}$ are suppressed by two powers of m_π/m_N, leading to a factor of ~ 50 suppression.

In principle, the magnitude of the finite parts of the $\bar{d}_{0,1}$, corresponding to "short range" dynamics, may be larger than those arising from the loops. In practice, the relative importance of the short-range and loop contributions depends on the properties of the four-quark operator in consideration. To illustrate, we consider the

interaction of Eq. (4.4). Using general chiral symmetry arguments and NDA [283], we expect [277, 164]

$$\bar{g}_\pi^{(1)} \sim \frac{\Lambda_\chi^3}{F_\pi \Lambda^2} \frac{\mathrm{Im} C_{\varphi ud}}{(4\pi)^2} , \tag{4.23}$$

$$\bar{d}_{0,1} \sim \frac{e\Lambda_\chi}{\Lambda^2} \frac{\mathrm{Im} C_{\varphi ud}}{(4\pi)^2} , \tag{4.24}$$

where $\Lambda_\chi = 2\pi F_\pi \sim m_N$. Substituting the estimate (4.23) into Eqs. (4.18) we have that

$$\bar{d}_{0,1}^{\mathrm{NLO,\,loop}} \sim \frac{e}{(2\pi F_\pi)^2} \frac{\pi m_\pi}{4 m_N} \frac{\Lambda_\chi^3}{\Lambda^2} \frac{\mathrm{Im} C_{\varphi ud}}{(4\pi)^2} \sim \frac{e\Lambda_\chi}{\Lambda^2} \frac{\pi m_\pi}{4 m_N} \frac{\mathrm{Im} C_{\varphi ud}}{(4\pi)^2} . \tag{4.25}$$

The result in Eq. (4.25) is suppressed by one power of m_π/m_N with respect to the NDA estimate (4.24).

The non-analytic NNLO loop contributions are suppressed by an additional factor of m_π/m_N with respect to NLO contributions to $d_{0,1}$, and of m_π^2/m_N^2 with respect to the short-distance low-energy constants $\bar{d}_{0,1}$. For the isoscalar EDM, the suppression is somewhat mitigated by the enhancement due to the large value of κ_1.

To obtain a sense of the relative importance of various terms in Eqs. (4.21) and (4.22), we assume $\bar{g}_\pi^{(0)}/\bar{g}_\pi^{(1)} = 0.02$ as one expects for the source in Eq. (4.4). In this case, the formally LO contribution to d_n, proportional to $\bar{g}_\pi^{(0)}$, and the $O(m_\pi^2/m_N^2)$ correction proportional to $\bar{g}_\pi^{(1)} \times \kappa_n$ are numerically comparable. For the proton EDM, the NLO contribution proportional to $\bar{g}_\pi^{(1)} m_\pi/m_N$ is about twice as large as the NNLO term. The two contribution enter with opposite sign, and partially cancel, so that net contributions of the two couplings $\bar{g}_\pi^{(0)}$ and $\bar{g}_\pi^{(1)}$ to d_p are also of similar magnitude. The comparison with the short-range contributions is more uncertain. If we use the NDA estimates of $\bar{d}_n$, $\bar{d}_p$, and $\bar{g}_\pi^{(1)}$ in Eqs. (4.23) and (4.24) we find that the pion loops enter at the 10% to 20% level with respect to the short-range terms. However, deviations from the NDA expectations can affect this conclusion. More robust estimates require a first principles determination of $\bar{d}_n$, $\bar{d}_p$, $\bar{g}_\pi^{(0)}$ and $\bar{g}_\pi^{(1)}$ in

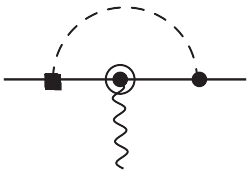

Figure 4.4. One-loop diagram contributing to the nucleon EDM in relativistic chiral perturbation theory. A square marks a TVPV interaction, other vertices representing the T- and P-conserving interactions in Eqs. (4.27) and (4.28).

terms of the coefficient $C_{\varphi ud}$, which, at the moment, is not available (model estimates are summarized in Ref. [164]).

Finally our result for d_n in Eq. (4.21) can be used to obtain a limit on $\bar{g}_\pi^{(1)}$. Using the experimental upper bound $|d_n| < 2.9 \cdot 10^{-26}\, e\,\mathrm{cm}$ [148] and assuming no cancellations with other contributions, we obtain

$$|\bar{g}_\pi^{(1)}| \lesssim 1.1 \times 10^{-10} \ . \tag{4.26}$$

4.3 Comparison with Earlier Work

It is instructive to compare the HBChPT results with those of Ref. [270]. The latter compute the contribution from Fig. 4.4 using the TVPV interactions in Eqs. (4.5) and (4.13), together with the T- and P-conserving pseudoscalar pion-nucleon coupling

$$\mathcal{L}_p = \frac{2m_N g_A}{F_\pi} \bar{N} i\gamma^5 \boldsymbol{\tau} \cdot \boldsymbol{\pi} N \ , \tag{4.27}$$

the relativistic version of the nucleon propagator, and the nucleon magnetic moment Lagrangian

$$\mathcal{L} = -\frac{e}{8m_N} \bar{N} \sigma^{\mu\nu} F_{\mu\nu} \left[\kappa_0 + \kappa_1 \tau_3\right] N \ . \tag{4.28}$$

We have repeated the calculation using these ingredients and obtain

$$
\begin{aligned}
d_0 &= e(3\bar{g}_\pi^{(0)}\kappa_0 + \bar{g}_\pi^{(1)}\kappa_1)\,\frac{g_A}{16\pi^2 F_\pi} F_P\left(\frac{m_\pi^2}{m_N^2}\right)\,, \\
d_1 &= e(-\bar{g}_\pi^{(0)}\kappa_1 + \bar{g}_\pi^{(1)}\kappa_0)\,\frac{g_A}{16\pi^2 F_\pi} F_P\left(\frac{m_\pi^2}{m_N^2}\right)\,,
\end{aligned}
\tag{4.29}
$$

where, when expanded for small x,

$$
F_P(x) = \frac{3}{2}\left[\frac{4}{3} - \frac{2}{3}\pi\sqrt{x} - x\log x + O(x^{3/2})\right]\,. \tag{4.30}
$$

The result obtained in Ref. [270] is similar apart from the first term in Eq. (4.30) that is 1 in their work instead of 4/3 as we find. The discrepancy can be traced back to a term containing the product of Dirac matrices $\gamma_\alpha\sigma^{\mu\nu}\gamma^\alpha$. This combination is proportional to $d-4$, but comes in front of a divergent integral. In the limit $d \to 4$, the $1/(d-4)$ from the loop integral cancels the $d-4$ in the product of Dirac matrices, leaving a constant piece.

Comparing with the HBChPT results in Eq. (4.20), we see that the relativistic calculation with pseudoscalar coupling yields contributions proportional to $\bar{g}_\pi^{(1)}\kappa_{0,1}$ that arise at lower order in m_π/m_N. The zeroth order term in Eq. (4.29) clearly conflicts with the power counting expected in a well-behaved EFT since there appears no m_π/m_N suppression. Using Eq. (4.23) in Eq. (4.29) would conflict with the chiral/NDA expectations in Eq. (4.25), overestimating the latter by a factor of $m_N/m_\pi \sim 10$.

The term non-analytic in the quark mass ($m_\pi \sim \sqrt{m_{u,d}}$) proportional to $(m_\pi/m_N)\kappa_{0,1}$ in Eq. (4.29) respects, in principle, the chiral/NDA estimate, but in the HBChPT calculation this term is absent. We can trace this discrepancy back to the use of the pseudoscalar coupling in Eq. (4.27) which breaks chiral symmetry. Repeating the calculation with the relativistic axial-vector pion-nucleon coupling that conserves chiral symmetry, we find that the $(m_\pi/m_N)\kappa_{0,1}$ term does not appear. The first non-analytic terms that appear are then proportional to $(m_\pi^2/m_N^2)\kappa_{0,1}$, as they should

be. We refrain from giving all details, but have confirmed that by using appropriate matching conditions the non-analytic terms appearing in the HBChPT and relativistic calculation (with axial-vector pion-nucleon coupling) are the same[6]. Of course, in the relativistic calculation with pseudovector coupling there still appear analytic terms that are lower order in m_π/m_N that may overestimate the dependence of the nucleon EDM on $\bar{g}_\pi^{(0)}$ and $\bar{g}_\pi^{(1)}$.

4.4 Implications and Conclusions

From the foregoing discussion, it is evident that any phenomenological constraints obtained from experimental limits on d_n and the results in Eq. (4.29) are likely to be at least an order of magnitude too stringent. In HBChPT, the loop contributions proportional to $\kappa_{0,1}$ arise at NNLO in the Q/m_N expansion, while κ-independent contributions start off at NLO. For the isoscalar EDM, the NNLO contribution is numerically comparable to the NLO term due to the large magnitude of κ_1, whereas for the neutron the NLO contribution is absent and the NNLO suppression is more severe. In terms of the "left-right symmetric" four-quark interaction (4.4), the NLO loop contributions and the chiral/NDA estimates for the short distance LEC are numerically comparable although the loops can be expected to be somewhat smaller due to to a m_π/m_N suppression. Consequently, we see no reasonable way around the m_π/m_N suppression that should be applied to the analysis of the LRSM. For other scenarios that lead to a different subset of the $d = 6$ CPV operators, such as the Weinberg operator or chiral invariant four-quark operators, the loop contributions associated with $\bar{g}_\pi^{(1)}$ will be further suppressed compared to the short distance contri-

[6]The chiral symmetry-breaking impact of the pseudoscalar coupling enters through the tree-level, parity-conserving, pion-photon production sub-graphs of the one-loop TVPV diagrams. Matching onto the HBChPT Lagrangian requires introduction of an explicit chiral symmetry-breaking operator. No such operator is required when matching with the relativistic, pseudovector calculation.

butions. On the other hand, a scenario in which the isovector quark chromo-EDM is the dominant $d = 6$ CPV source will have a similar phenomenology as the LRSM[7].

For the LRSM with spontaneous CPV, the relaxed constraints may allow for consistency between EDMs, the kaon CPV parameter ϵ, and a right-handed W-boson (W_R) with mass of a few TeV rather than the lower bound of 10 TeV quoted in Ref. [267] (see the right panel of Fig. 8 for an illustration of the impact of relaxed EDM constraints). In this case, discovery of the W_R at the Large Hadron Collider would still be possible, though it would likely imply that a second neutral CP-even Higgs boson would be too heavy to be observed.

Similar conclusions apply to the analysis of Ref. [269] that considered the implications of d_n limits for the P-conserving, T-violating neutron decay correlation $\vec{J} \cdot \vec{p}_e \times \vec{p}_\nu$ with a coefficient denoted by D. Separating out the final state interactions (D_f) that can mimic *bona fide* T-violation (D_t), the authors of Ref. [269] use the work of Ref. [268] that, in turn, relied one the relativistic meson theory calculation of Ref. [270], to conclude that $|D_t/\kappa| < 10^{-7}$, where κ denotes the combination of Fermi and Gamow-Teller matrix elements, g_A, and the vector coupling g_V that enters the correlation. This bound lies well below the computed final state interaction contribution $|D_f\kappa| \sim 10^{-5}$ with an uncertainty at the 10^{-7} level. In this case, it would not be possible to disentangle final state contributions from possible LRSM contributions for experiment performed with 10^{-7} level sensitivity. However, applying the relaxed EDM constraint we obtain here would lead to $|D_t/\kappa| < 10^{-6}$, opening a window for a future D-correlation experiment to observe a non-vanishing LRSM effect.

[7]Deviations from these expectations might appear in the EDMs of multi-nucleon systems [277].

CHAPTER 5

REEXAMINATION OF THE STANDARD MODEL NUCLEON ELECTRIC DIPOLE MOMENT

The search for permanent electric dipole moment (EDM) of elementary and composite particles is motivated by its CP-violating nature. We live in a universe in which the amount of baryons and antibaryons are unequal. In order to explain this asymmetry CP-violating interactions are needed to fulfill one of the three Sakharov criteria [38]. EDMs of elementary and composite particles are, in most cases, direct consequences of these interactions which can be probed in low-energy experiments. Since the first upper limit on the neutron EDM obtained by Smith, Purcell and Ramsey in 1957 [33], numerous experiments have been performed to improve the sensitivity of EDM measurements in different particle systems. Currently, the most stringent bounds on EDMs are set for the electron ($8.7 \times 10^{-29} e\,\text{cm}$, 90% C.L.)[146] and the mercury atom ($3.1 \times 10^{-29} e\,\text{cm}$, 95% C.L.)[147], while the current upper limit on neutron and proton EDMs are $2.9 \times 10^{-26} e\,\text{cm}$ (90% C.L.)[148] and $7.9 \times 10^{-25} e\,\text{cm}$ (95% C.L.) respectively (the latter is deduced from the bound on the mercury EDM). Future experiments are designed (or have been considered) to push these bounds even further down. For the neutron EDM, this includes the experiment at Paul Scherrer Institut (PSI)[149], the CryoEDM and PNPI/ILL experiment at Institut Laue-Langevin (ILL)[150], the SNS neutron EDM experiment at Oak Ridge, the TRIUMF experiment in Canada and the Munich experiment at Germany. These experiments

---

[0]Reprinted article with permission from C. Y. Seng, Phys. Rev. C **91** (2015) no.2, 025502. DOI: http://dx.doi.org/10.1103/PhysRevC.91.025502

are designed to reach a $10^{-28}e\,\mathrm{cm}$ precision level for the neutron EDM [151]. Also, both COSY[152] and BNL[153] have proposed storage ring experiments designed to measure the proton EDM to a level of $10^{-29}e\,\mathrm{cm}$ precision.

Although numerous Beyond Standard Model (BSM) scenarios have been proposed that give rise to measurable EDMs within current experimental precision level, so far no definitive signal of such physics has been observed [1]. Therefore, the CP-violating phase of the Cabibbo-Kobayashi-Maskawa (CKM) matrix in the Standard Model (SM) remains the only source for intrinsic EDMs. Questions have been raised concerning the expected size of EDMs coming from purely SM physics[154]. A simple dimensional analysis using constituent quark masses may suggest that the SM-induced neutron EDM could be as large as $10^{-29}e\,\mathrm{cm}$, approaching the level of sensitivity for future EDM experiments. It is therefore important to have a better estimate for the SM contribution to the nucleon EDM. To leading order, the quark EDM induced by the CKM matrix starts at three-loops [155]. A detailed calculation showed that the valence-quark contribution to the neutron EDM is of order $10^{-34}e\,\mathrm{cm}$ [156]. It was also shown that long-distance contributions, namely contributions with baryons and mesons as effective degrees of freedom (DOFs), could generate a much larger hadronic EDM. For instance, the pion-loop contribution to the neutron EDM was first studied in a paper by Barton and White [157] which produced log-divergent results in the chiral limit indicating that the long-range contribution may dominate. On the other hand, in a series of papers, Gavela et.al. studied the pole-diagram contribution with the CP-violating phase generated by $|\Delta S| = 1$ electroweak [158] and gluonic penguin diagrams [159]. They claimed that the latter is dominant and derived a SM neutron EDM of order $10^{-31}e\,\mathrm{cm}$. The possibility of a long-range contribution to the neutron

[1] There are indeed some hopeful candidates, for example the muon $g-2$ anomaly; but no conclusive statement can be made before one could further improve the experimental precision and reduce the theoretical uncertainty of the SM prediction.

EDM from the CKM matrix was first pointed out by Khriplovich and Zhitnitsky[160]. He et.al [161] did a thorough chiral-loop calculation and re-analyzed the pole-diagram contribution in [158, 159] and argued that the two are of the same order of magnitude. Their estimate for the neutron EDM is $1.6 \times 10^{-31} e\,\mathrm{cm} - 1.4 \times 10^{-33} e\,\mathrm{cm}$, which is currently the most widely accepted estimate for the SM neutron EDM. In recent years, the charm contribution to nucleon EDMs is also considered and it is roughly $10^{-31} e$ cm [162].

The purpose of this paper is to revisit the previous study of both chiral-loop and the pole contributions to the nucleon EDM in order to sharpen our SM benchmark value. On the theoretical side, one could improve earlier work in several ways. For instance, the chiral loop calculation in [161] adopted an older meson theory utilizing a pseudoscalar strong baryon-meson coupling that should be replaced by the standard axial-vector coupling. Also, their work that utilized an effective hadronic Lagrangian in computing chiral-loop diagrams faced another well-known problem in the loss of power counting similar to that happening in the relativistic Chiral Perturbation Theory (ChPT). ChPT is a non-renormalizable theory that involves infinitely many interaction terms. Its predictive power therefore relies on the fact that higher order terms are suppressed by powers of p/Λ_χ where p is the typical mass or momentum scales of hadronic DOFs and $\Lambda_\chi \sim 1$GeV. This expansion however becomes ambiguous when baryons are included because a typical baryon mass is $M_B \sim 1$GeV. Therefore, M_B/Λ_χ is no longer a small expansion parameter. Heavy Baryon Chiral Perturbation Theory (HBchPT) [163] provides a convincing way to get around this issue by performing a field redefinition in the baryon field to scale out its mass-dependence. By doing this, one can split the baryon field into "light" and "heavy" components, where the former depends only on its residual momentum which is well below 1 GeV. After integrating out the heavy component of the baryon field, the effective Lagrangian can be written as a series expansion of $1/m_N$. This eliminates the possibility of a

factor m_N appearing in the numerator and thus restores the power counting. Many works have appeared recently calculating the nucleon EDM induced by different BSM physics using HBchPT (see [164] for a general overview). Although the convergence of the SU(3) HBchPT is not as good as its SU(2) counterpart because m_K/m_N is not very small [165, 166, 167, 168, 169], it is still theoretically beneficial as it provides a formal classification of different contributions into leading and sub-leading orders. In this work, the chiral-loop contribution to the nucleon EDM are recalculated up to the leading-order (LO) in the heavy baryon (HB)-expansion.

Additionally, previous numerical results of loop and pole contributions face large uncertainties due to poorly-known values of physical constants in the weak sector at that time. For example, the CP-violating phase δ of the CKM matrix quoted in Ref. [161] had an uncertainty that spans one order of magnitude. The fitting of certain low energy constants (LECs) such as weak baryon-meson interaction strengths, has been updated since. Also, their theoretical estimation of various CP-phases in the effective weak Lagrangian was based on older work [170, 171] which had been improved by others. Furthermore, for previous work on pole contributions, their estimation on effective CP-phases was based only on a single gluonic penguin operator without considering the full analysis of operator mixing and renormalization group running. Moreover, the approximate form of their analytic expressions was based on the out-of-date assumption that $m_t \ll m_W$. In this work, I do a more careful determination of weak LECs, taking all these issues into account. Combining my calculation and an estimate of higher-order effects, I predict a range of the long-distance SM contribution to the nucleon EDM to be around $(1-6)\times 10^{-32} e\,\text{cm}$. I identify the main sources of uncertainty and discuss possible steps one could take to improve upon that. At the same time, I use dimensional analysis to estimate the size of possible short-distance counterterms. I find that they could be as large as $4\times 10^{-32} e\,\text{cm}$.

This work is arranged as follows: in Section II I will briefly outline the main ingredients of the SU(3) HBchPT and introduce the weak Lagrangian responsible for the generation of the nucleon EDM. In Section III I will determine the LECs. In Section IV and V Iderive the analytic expressions for loop and pole contributions to the nucleon EDM respectively and calculate their numerical values. In Section VI I will provide some further discussions and draw my conclusions.

5.1 HBchPT: Strong and Electroweak Interactions

In this section, I review some basic concepts of ChPT with the primary aim of establishing conventions and notation. ChPT is a low-energy effective field theory (EFT) of quantum chromodynamics (QCD) with hadrons as low energy DOFs. QCD exhibits a global chiral symmetry in the limit of massless quarks. However this symmetry is spontaneously broken in the ground state and leads to the emergence of Goldstone bosons which are identified as pseudoscalar mesons. The corresponding EFT obeys the same symmetry. An infinite tower of operators respecting the symmetry with increasing mass dimensions is organized in the Lagrangian. However, only a finite number of operators are retained since the the dropped higher-dimensional operators make contributions that are suppressed by powers of p/Λ_χ.

I use the standard non-linear representation of chiral fields [172, 174, 173], in which the pseudoscalar meson octet is incorporated in the exponential function $U = \exp\{i\phi/F_\pi\}$, where

$$\phi = \sum_{a=1}^{8} \phi_a \lambda_a = \begin{pmatrix} \pi^0 + \frac{1}{\sqrt{3}}\eta_8 & \sqrt{2}\pi^+ & \sqrt{2}K^+ \\ \sqrt{2}\pi^- & -\pi^0 + \frac{1}{\sqrt{3}}\eta_8 & \sqrt{2}K^0 \\ \sqrt{2}K^- & \sqrt{2}\bar{K}^0 & -\frac{2}{3}\eta_8 \end{pmatrix} \tag{5.1}$$

with $F_\pi \approx 93$MeV. The matrix U transforms under the chiral rotation as: $U \to LUR^\dagger$, where L and R are elements of $SU(3)_L$ and $SU(3)_R$ respectively. The mass term of

the meson octet is introduced using spurion analysis: the QCD Lagrangian would exhibit chiral invariance if the quark mass matrix $M = \mathrm{diag}\{m_u, m_d, m_s\}$ transforms as $M \to LMR^\dagger$. Therefore, its low energy effective theory written in terms of the spurion field M should also exhibit a similar invariance. The lowest-order operator that is invariant is $\mathrm{Tr}[MU^\dagger + UM^\dagger]$. This operator gives rise to non-zero meson masses which are isospin-symmetric.

The ground state $J^P = (1/2)^+$ baryon octet is assembled into the matrix:

$$B = \begin{pmatrix} \frac{\Sigma^0}{\sqrt{2}} + \frac{\Lambda}{\sqrt{6}} & \Sigma^+ & p \\ \Sigma^- & -\frac{\Sigma^0}{\sqrt{2}} + \frac{\Lambda}{\sqrt{6}} & n \\ \Xi^- & \Xi^0 & -\frac{2\Lambda}{\sqrt{6}} \end{pmatrix}. \tag{5.2}$$

It transforms as: $B \to KBK^\dagger$ with $K = K(L, R, U)$ being a unitary matrix. In order to couple baryons with the pseudoscalar octet, we define $\xi = \sqrt{U}$ which transforms as $\xi \to L\xi K^\dagger = K\xi R^\dagger$ and introduce the Hermitian axial vector:

$$\mathcal{A}_\mu = \frac{i}{2}[\xi\partial_\mu\xi^\dagger - \xi^\dagger\partial_\mu\xi] \tag{5.3}$$

which transforms as $\mathcal{A}_\mu \to K\mathcal{A}_\mu K^\dagger$ under the chiral rotation (we have neglected its coupling with external fields because it is not needed in this work).

I now proceed with with the formulation of HBchPT. In order to scale out the heavy mass-dependence, I rewrite its momentum as

$$p_\mu = m_N v_\mu + k_\mu, \tag{5.4}$$

where m_N is the nucleon mass, v_μ is the velocity of the baryon (which is conserved in the $m_N \to \infty$ limit) and k_μ is the residual momentum of the baryon which is well

below 1 GeV. I therefore rescale the baryon field and retain its "light" component [2]:

$$B_v(x) = e^{im_N v\cdot x}\frac{1+\not{v}}{2}B(x) \tag{5.5}$$

The subscript v will be dropped from now on. OI integrate out the remaining component which is "heavy". The baryon propagator thus becomes:

$$iS_B(k) = \frac{i}{v\cdot k - \delta_B + i\epsilon} \tag{5.6}$$

where $\delta_B = m_B - m_N$ is the baryon mass splitting. This procedure also reduces Dirac structures to either 1 or S^μ with the latter being the spin-matrix of the baryon satisfying $S\cdot v = 0$. In this work I concentrate only on terms that are leading order in the HB-expansion (with the exception of the baryon electromagnetic dipole transition operator that appears in pole diagrams as I will explain below).

The lowest-order strong Lagrangian involving only the $(1/2)^+$ baryons, Goldstone bosons and electromagnetic fields relevant to our work is given by:

$$\begin{aligned}\mathcal{L} \;=\; & \frac{F_\pi^2}{4}\mathrm{Tr}[\mathcal{D}_\mu U \mathcal{D}^\mu U^\dagger] + \frac{F_\pi^2}{4}\mathrm{Tr}[\chi_+] + \mathrm{Tr}[\bar{B} iv\cdot\mathcal{D} B] + 2D\mathrm{Tr}[\bar{B}S^\mu\{\mathcal{A}_\mu, B\}] \\ & + 2F\mathrm{Tr}[\bar{B}S^\mu[\mathcal{A}_\mu, B]] + \frac{b_D}{2B_0}\mathrm{Tr}[\bar{B}\{\chi_+, B\}] + \frac{b_F}{2B_0}\mathrm{Tr}[\bar{B}[\chi_+, B]] \\ & + \frac{b_0}{2B_0}\mathrm{Tr}[\bar{B}B]\mathrm{Tr}[\chi_+]\end{aligned} \tag{5.7}$$

where $D = 0.80$, $F = 0.50$ [172] and $\mathcal{D}_\mu U = \partial_\mu U + ieA_\mu[Q, U]$. Here

$$Q = \mathrm{diag}\{2/3, -1/3, -1/3\} \tag{5.8}$$

is the quark charge matrix while B_0 is a parameter characterizing the chiral quark condensate and $\chi_+ = 2B_0(\xi^\dagger M\xi^\dagger + \xi M\xi)$ introduces the quark-mass dependence.

[2] in the sense that it only depends on the residual momentum

The last three terms in Eq. (5.7) are responsible for the mass splitting within the baryon octet [175]. Since I have scaled out the nucleon mass from the baryon field B the proton and neutron will appear as massless excitations and the other baryons will have an excitation energy given by the "residual" mass δ_B. This is important later during the computation of pole diagrams.

For the purpose of pole diagram contributions I need also to include the $(1/2)^-$ baryon octet. The importance of these resonances can be traced back to the observation of the unexpectedly large violation of Hara's theorem [176] which states that the parity-violating radiative $B \to B'\gamma$ transition amplitude should vanish in the exact SU(3) limit. The authors of Ref. [177] (and later improved by [178]) pointed out that this apparent puzzle could be resolved by including baryon resonances that give rise to pole diagrams which enhance the violation of Hara's theorem. Therefore, one should naturally expect that the same kind of diagrams will also play an important role in the determination of the nucleon EDM. The resonance $(1/2)^-$ octet is denoted as $\mathcal{R}$:

$$\mathcal{R} = \begin{pmatrix} \frac{\Sigma^{0*}}{\sqrt{2}} + \frac{\Lambda^*}{\sqrt{6}} & \Sigma^{+*} & p^* \\ \Sigma^{-*} & -\frac{\Sigma^{0*}}{\sqrt{2}} + \frac{\Lambda^*}{\sqrt{6}} & n^* \\ \Xi^{-*} & \Xi^{0*} & -\frac{2\Lambda^*}{\sqrt{6}} \end{pmatrix}. \tag{5.9}$$

It transforms in the same way as B except that it has a negative intrinsic parity.

The part of strong and electromagnetic chiral Lagrangian involving $\mathcal{R}$ which is relevant to our work is given by:

$$\begin{aligned} \mathcal{L}_{\mathcal{R}} &= \mathrm{Tr}[\bar{\mathcal{R}} iv\cdot\mathcal{D}\mathcal{R}] - \bar{\delta}_{\mathcal{R}}\mathrm{Tr}[\bar{\mathcal{R}}\mathcal{R}] + \frac{\tilde{b}_D}{2B_0}\mathrm{Tr}[\bar{\mathcal{R}}\{\chi_+,\mathcal{R}\}] + \frac{\tilde{b}_F}{2B_0}\mathrm{Tr}[\bar{\mathcal{R}}[\chi_+,\mathcal{R}]] \\ &+ \frac{\tilde{b}_0}{2B_0}\mathrm{Tr}[\bar{\mathcal{R}}\mathcal{R}]\mathrm{Tr}[\chi_+] \\ &- 2r_D(\mathrm{Tr}[\bar{\mathcal{R}}(v_\mu S_\nu - v_\nu S_\mu)\{f_+^{\mu\nu}, B\}] + \mathrm{Tr}[\bar{B}(v_\mu S_\nu - v_\nu S_\mu)\{f_+^{\mu\nu}, R\}]) \\ &- 2r_F(\mathrm{Tr}[\bar{\mathcal{R}}(v_\mu S_\nu - v_\nu S_\mu)[f_+^{\mu\nu}, B]] + \mathrm{Tr}[\bar{B}(v_\mu S_\nu - v_\nu S_\mu)[f_+^{\mu\nu}, \mathcal{R}]]). \end{aligned} \tag{5.10}$$

The second to fifth terms of $\mathcal{L}_{\mathcal{R}}$ give the average residual mass and mass-splitting among the $(1/2)^-$ baryon octet. Constants r_D and r_F are electromagnetic coupling strengths between B and $\mathcal{R}$ and $f_+^{\mu\nu}$ is the chiral field strength tensor of the electromagnetic field that, in the SU(3) version of ChPT, is given by [172]:

$$f_+^{\mu\nu} = -e[\xi^\dagger Q\xi + \xi Q\xi^\dagger]F^{\mu\nu} \tag{5.11}$$

with $e > 0$. The reason we include r_D and r_F terms even though they are formally $1/m_N$-suppressed is that they will then be compensated by small denominator δ_B factors in pole diagrams.

Next I introduce the relevant weak Lagrangian that gives rise to the nucleon EDM. As the only CP-violating effect in the SM is the complex phase in the CKM matrix, the strange quark must be included. The CP-phase is attached to various $|\Delta S| = 1$ four-quark operators that are responsible for kaon decay and nonleptonic hyperon decays. It is well-known that the product of two charged weak currents could transform as $(8_L, 1_R)$ or $(27_L, 1_R)$ under the SU(3) chiral rotation. Extra $|\Delta S| = 1$ operators could be induced via gluonic or electroweak penguin diagrams. The former transforms as $(8_L, 1_R)$ while the latter may introduce a $(8_L, 8_R)$ component that is however suppressed by the smallness of the fine structure constant. Furthermore, since $(8_L, 1_R)$ operators have isospin $I = 1/2$ while $(27_L, 1_R)$ operators can have both $I = 1/2$ and $I = 3/2$ components we would naturally expect the latter to be subdominant as compared to the $(8_L, 1_R)$ operators. Otherwise the $I = 3/2$ channel would be as important as the $I = 1/2$ channel in non-leptonic decay processes, violating the experimentally observed $|\Delta I| = 1/2$ dominance in these processes. Hence, effective operators I introduce later should also transform as $(8_L, 1_R)$.

The pure mesonic Lagrangian that triggers the $|\Delta I| = 1/2$ kaon decay channel is given by [174]:

$$\mathcal{L}_8 = g_8 e^{i\varphi}\mathrm{Tr}[\lambda_+ D_\mu U D^\mu U^\dagger] + h.c \tag{5.12}$$

where $\lambda_+ = (\lambda_6 + i\lambda_7)/2$. The non-zero value of φ introduces the CP-violating effect. Meanwhile, the corresponding baryonic operator that triggers the nonleptonic hyperon decay is given by [179]:

$$\mathcal{L}_w^{(s)} = h_D e^{i\varphi_D} \mathrm{Tr}[\bar{B}\{\xi^\dagger \lambda_+ \xi, B\}] + h_F e^{i\varphi_F} \mathrm{Tr}[\bar{B}[\xi^\dagger \lambda_+ \xi, B]] + h.c. \tag{5.13}$$

Here the superscript (s) indicates that these operators mediate S-wave decays. In principle there is a counterpart operator with the Dirac structure γ_5, which is time-reversal odd and is proportional to the complex phase in the CKM matrix. I do not need this extra operator because it vanishes at leading order in the HB-expansion upon the non-relativistic reduction of the Dirac structure. Also, our definitions of h_D and h_F here are slightly different from [179] as we take h_D, h_F to be real, with the complex phases explicitly factored out.

Finally, for the purpose of including pole-diagram contributions, I need the weak Lagrangian that triggers the $B - \mathcal{R}$ transition. The lowest order Lagrangian is given by [180]:

$$\mathcal{L}_w^{B\mathcal{R}} = i w_D e^{i\tilde{\varphi}_D} \mathrm{Tr}[\bar{\mathcal{R}}\{h_+, B\}] + i w_F e^{i\tilde{\varphi}_F} \mathrm{Tr}[\bar{\mathcal{R}}[h_+, B]] + h.c \tag{5.14}$$

where $h_+ \equiv \xi^\dagger \lambda_+ \xi + \xi^\dagger \lambda_- \xi$. The counterpart with a γ_5 structure similarly vanishes at leading order in the HB-expansion.

5.2 Determination of the LECs

There are altogether 12 LECs that enter into the estimate for the nucleon EDM: seven interaction strengths $\{r_D, r_F, g_8, h_D, h_F, w_D, w_F\}$ and five CP-violating phases

$\{\varphi, \varphi_D, \varphi_F, \tilde{\varphi}_D, \tilde{\varphi}_F\}$. They are either extracted from experiments or obtained by theoretical modeling [3].

Pure electromagnetic $B - \mathcal{R}$ transition coupling strengths r_D and r_F are fitted to electromagnetic decays of $(1/2)^-$ resonances. The authors of Ref. [178] obtain:

$$er_D = 0.033\text{GeV}^{-1}, er_F = -0.046\text{GeV}^{-1}. \tag{5.15}$$

The constant g_8 is fitted to the $K_s^0 \to \pi^+\pi^-$ decay rate, ignoring the small CP-violating effect [181], giving

$$g_8 = 6.84 \times 10^{-10}\text{GeV}^2. \tag{5.16}$$

The CP-phase φ is, up to a negative sign, the phase of the $K^0 \to \pi\pi(I = 0)$ decay amplitude:

$$\varphi = -\xi_0 = -\frac{\text{Im}A_0}{\text{Re}A_0} \tag{5.17}$$

In principle one could extract ξ_0 from the measurement of the CP-violating parameter ϵ' in the kaon decay. However, ϵ' is a linear combination of ξ_0 and another CP-violating phase, ξ_2, of the $I = 3/2$ channel. Simple estimation [174] suggests that ξ_2 is of the same order as ξ_0 making ξ_0 hard to extract directly from the experiment. I therefore refer to theoretical estimation based on the large-N_c approach [182] which gives:

$$\varphi = -\xi_0 \approx -\sqrt{2}|\epsilon| \times (-6 \times 10^{-2}) \approx 1.89 \times 10^{-4} \approx 6.4J, \tag{5.18}$$

where $J = (2.96^{+0.20}_{-0.16}) \times 10^{-5}$ [181] is the Jarlskog invariant[183]. It is worthwhile to mention that, in Ref. [161] the uncertainty of J spans an order of magnitude leading

[3]Unfortunately, none of these LECs in the literature come with error bars, so I cannot estimate the error introduced by the fitting of LECs.

to the main source of the error in the estimate of the neutron EDM during that time. Today, J is determined with much higher precision so the associated uncertainty is sub-leading compared to uncertainties due to higher-order effects in the HB-expansion and unknown short-distance counterterms, which we will discuss later.

The four remaining interaction strengths h_D, h_F, w_D, w_F were determined in [180] by simultaneously fitting them to the s and p-wave amplitudes of nonleptonic hyperon decays:

$$\begin{aligned} h_D &\approx 0.44 \times 10^{-7}\text{GeV} \\ h_F &\approx -0.50 \times 10^{-7}\text{GeV} \\ w_D &\approx -1.8 \times 10^{-7}\text{GeV} \\ w_F &\approx 2.3 \times 10^{-7}\text{GeV}. \end{aligned} \tag{5.19}$$

The last two constants were determined by setting $m_{\mathcal{R}} \approx 1535\text{MeV}$.

Finally, I need to know the four remaining CP-phases $\{\varphi_D, \varphi_F, \tilde{\varphi}_D, \tilde{\varphi}_F\}$. These phases have been considered in ref [158], but their treatments are less satisfactory due to the neglect of the operator mixing effect and a certain outdated approximation of the small top quark mass assumption. In order to improve upon that, I review a more recent work done in Ref. [179] that determined $\{\varphi_D, \varphi_F\}$ and apply scaling arguments to provide an estimate of $\{\tilde{\varphi}_D, \tilde{\varphi}_F\}$. Ref. [179] pointed out that after considering operator mixing and renormalization group running, the dominant operator that gives rise to the CP-violating phase in the $|\Delta S| = 1$, $|\Delta I| = 1/2$ sector is given by:

$$\hat{Q}_6 = -2 \sum_q \bar{d}(1+\gamma_5) q \bar{q} (1-\gamma_5) s. \tag{5.20}$$

Ref [179] then computed the factorizable and non-factorizable contributions to φ_D, φ_F induced by $\hat{Q}_6$. Here "factorizable" means to regard $\hat{Q}_6$ as a product of two chiral

quark densities and match it to chiral operators. The matching is done by realizing that $\bar{q}_R q_L \sim \partial\mathcal{L}_{QCD}/\partial m_q = \partial\mathcal{L}_{\rm chiral}/\partial m_q$. On the other hand, the "non-factorizable" contribution is obtained simply by taking the hadronic matrix element of $\hat{Q}_6$ using the quark model. These two contributions are distinct because the factorizable piece contains a factor of chiral quark condensate $F_\pi^2 B_0$ through:

$$\langle 0|\,\bar{q}_L^i q_R^j \bar{q}_R^k q_L^l\,|B\bar{B}'\rangle \sim \langle 0|\,\bar{q}_L^i q_R^j\,|0\rangle\,\langle 0|\,\bar{q}_R^k q_L^l\,|B\bar{B}'\rangle = -\frac{1}{2}F_\pi^2 B_0\delta_{ij}\,\langle 0|\,\bar{q}_R^k q_L^l\,|B\bar{B}'\rangle \tag{5.21}$$

while the same quantity never appears in a quark model calculation. Combining the two, they found $\mathrm{Im}(h_D \exp i\varphi_D) \approx -2.2$, $\mathrm{Im}(h_F \exp i\varphi_F) \approx 6.1$, both in units of $\sqrt{2}F_\pi G_F m_{\pi^+}^2 J$. This leads to:

$$\varphi_D \approx -1.5J, \varphi_F \approx -3.6J. \tag{5.22}$$

It is straightforward to see that $\tilde{\varphi}_D$ and $\tilde{\varphi}_F$ receive no factorizable contribution. This is because it would require terms like $\bar{\mathcal{R}} m_q B$ to appear in the strong chiral Lagrangian. Such terms would violate parity and therefore cannot exist. For the non-factorizable part, my strategy is the following: first I compute the matrix elements $\langle\mathcal{R}|\,\hat{Q}_6\,|B\rangle$ and $\langle B'|\,\hat{Q}_6\,|B\rangle$ using the quark model to find their ratio. Then, I use this ratio to infer the value of the non-factorizable part of $\tilde{\varphi}_D$, $\tilde{\varphi}_F$ by appropriately scaling the non-factorizable part of φ_D, φ_F given in Ref. [179].

To obtain an estimate of hadronic matrix elements I adopt the harmonic oscillator model [177]. The structure of the spin-flavor wavefunction of the baryon octet leads to the following ratio:

$$\langle n^*|\,\hat{Q}_6\,|\Sigma^0\rangle : \langle n^*|\,\hat{Q}_6\,|\Lambda\rangle : \langle p^*|\,\hat{Q}_6\,|\Sigma^+\rangle = 1 : \sqrt{3} : -\sqrt{2} \tag{5.23}$$

which requires that $w_F\tilde{\varphi}_F = (1/3)w_D\tilde{\varphi}_D$ in our chiral Lagrangian. I also obtain the ratio between $B - B'$ and $B - \mathcal{R}$ matrix elements:

$$\frac{\langle p^*|\,\hat{Q}_6\,|\Sigma^+\rangle}{\langle p|\,\hat{Q}_6\,|\Sigma^+\rangle} = -\sqrt{\frac{2}{3\pi}}\frac{1}{mR_0}. \tag{5.24}$$

where $m \approx 0.34\text{GeV}, R_0 \approx 2.7\text{GeV}^{-1}$ are harmonic oscillator parameters. With this ratio and the non-factorizable contribution to φ_D, φ_F given in [179], I obtain the non-factorizable contribution to $\tilde{\varphi}_D, \tilde{\varphi}_F$:

$$\tilde{\varphi}_D \approx 0.04J, \tilde{\varphi}_F \approx -0.01J \tag{5.25}$$

These phases are about two orders of magnitude smaller than the three other CP-phases because they are not enhanced by the chiral quark condensate. Therefore, I disregard them in the rest of our calculation.

To end this section, I point out that there is an important sign issue in the determination of LECs. Since LECs are fitted to experiments that only involve squared amplitudes, an overall undetermined sign is left ambiguous. Therefore, if two sets of LECs are fitted separately to two unrelated experiments (for example, $\{r_D, r_F\}$ are to fit to baryon electromagnetic transitions and $\{h_D, h_F, w_D, w_F\}$ are to fit to non-leptonic hyperon decays), there is no unique way to determine the relative sign between these two sets of LECs. This introduces an extra uncertainty because a change of a relative sign can turn a constructive interference to destructive and vice versa. I will discuss the impact of this uncertainty in the last section.

5.3 One loop contribution

In this section I present analytic and numerical results of the one-1oop contribution to the proton and neutron EDM using HBchPT. The nucleon EDM d_N is defined by the term linear in the incoming photon momentum q of the P and T-violating $NN\gamma$ amplitude

$$iM \equiv -2d_N v\cdot\varepsilon\bar{u}_N S\cdot q u_N. \tag{5.26}$$

Here ε^μ is the photon polarization vector. Note that the equation has been simplified by applying the on-shell condition to the nucleon: $v\cdot q = -q^2/2m_N \to 0$.

Since each weak interaction vertex has $|\Delta S| = 1$, I need at least two insertions of weak interaction vertices to obtain an EDM that is flavor diagonal. Most one-loop integrals are UV-divergent and are regularized using the $\overline{\text{MS}}$ scheme in which the combination

$$L \equiv \frac{2}{4-d} - \gamma + \ln(4\pi) \tag{5.27}$$

is subtracted. Also, since all CP-violating phases $\{\varphi_i\}$ are small, I use the small angle approximation $\sin\varphi_i \approx \varphi_i$. Finally, following the usual spirit of ChPT, during the calculation of loops we assume that the heavy DOFs could be integrated out and their effects show up in the LECs of the effective operators consist of lighter DOFs [4]. Hence what enter the loops are the lightest DOFs, which in our case are the pseudoscalar meson octet and the ground-state $(1/2)^+$ baryon octet.

There are four distinct types of 1-loop diagrams (see Fig.5.1) that give non-zero contribution to the nucleon EDM (diagrams of other kinds are all vanishing at leading order in the HB-expansion. See the Appendix for the argument). Fig. 1(a)-(c) (plus reflections) in Fig.5.1 contribute to both neutron and proton EDM. For the neutron, it reads:

---

[4]The reader should anyway be alerted that this may not always be the case. For example, Ref. [186] pointed out that one needs to include the baryon decuplet in order to reconcile with the result of the large N_c-expansion

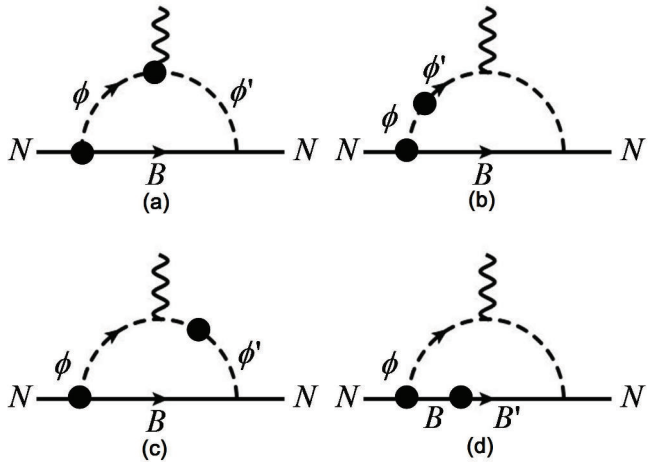

Figure 5.1. One-1oop contributions to the nucleon EDM. Each round dot denotes a $|\Delta S| = 1$ weak insertion. Fig. 1(a)-(c) (and reflections) contribute to both neutron and proton EDM; while Fig. 1(d) (and reflection) contributes only to proton EDM.

$$\begin{aligned} d_n^{\rm 1-loop} &= -\frac{eg_8(Dh_D\{\varphi-\varphi_D\}+Fh_F\{\varphi-\varphi_F\})}{4\pi^2F_\pi^4(m_\pi^2-m_K^2)}(m_\pi^2\ln\frac{m_\pi^2}{\mu^2}-\{\pi\leftrightarrow K\}) \\ &\quad -\frac{\delta_\Sigma eg_8(D-F)(h_D\{\varphi-\varphi_D\}+h_F\{\varphi_F-\varphi\})}{4\pi^2F_\pi^2(m_\pi^2-m_K^2)}(m_\pi^2\frac{\arctan\frac{\sqrt{m_\pi^2-\delta_\Sigma^2}}{\delta_\Sigma}}{\sqrt{m_\pi^2-\delta_\Sigma^2}} \\ &\quad -\{\pi\leftrightarrow K\}) \end{aligned} \tag{5.28}$$

I found that all terms analytic in quark masses cancel each other. Also notice that there is no extra singularity in the limit $m_K \to m_\pi$ or $\delta_B \to 0$. Numerical estimation with $\mu = m_N$ gives

$$|d_n^{\rm 1-loop}| = 1.5\times10^{-32} e\,{\rm cm}. \tag{5.29}$$

Similar calculations are done for the proton EDM. Figs. 1(a)-(c) give

$$
\begin{aligned}
d_p^{1-\mathrm{loop},1} &= \frac{eg_8(D\{h_D[\varphi-\varphi_D]+3h_F[\varphi-\varphi_F]\}+3F\{h_D[\varphi-\varphi_D]+h_F[\varphi_F-\varphi]\})}{24\pi^2F_\pi^4(m_\pi^2-m_K^2)} \\
&\times(m_\pi^2\ln\frac{m_\pi^2}{\mu^2}-\{\pi\leftrightarrow K\}) \\
&-\frac{\delta_\Sigma eg_8(D-F)(h_D\{\varphi-\varphi_D\}+h_F\{\varphi_F-\varphi\})}{8\pi^2F_\pi^4(m_\pi^2-m_K^2)}(m_\pi^2\frac{\arctan\frac{\sqrt{m_\pi^2-\delta_\Sigma^2}}{\delta_\Sigma}}{\sqrt{m_\pi^2-\delta_\Sigma^2}} \\
&-\{\pi\leftrightarrow K\}) \\
&-\frac{\delta_\Lambda eg_8(D+3F)(h_D\{\varphi-\varphi_D\}+3h_F\{\varphi-\varphi_F\})}{24\pi^2F_\pi^4(m_\pi^2-m_K^2)}(m_\pi^2\frac{\arctan\frac{\sqrt{m_\pi^2-\delta_\Lambda^2}}{\delta_\Lambda}}{\sqrt{m_\pi^2-\delta_\Lambda^2}} \\
&-\{\pi\leftrightarrow K\}) \qquad (5.30)
\end{aligned}
$$

There is one extra type of diagrams contributing to the proton EDM corresponding to two insertions of h_i vertices (Fig. 1(d)). The corresponding diagrams do not generate the neutron EDM simply because there is no appropriate non-vanishing combination of B, B', ϕ. This diagram for the proton EDM gives

$$
\begin{aligned}
d_p^{1-\mathrm{loop},2} &= -\frac{eh_Dh_F(D-F)(\varphi_D-\varphi_F)(\pi-2\arctan\frac{\delta_\Sigma}{\sqrt{m_K^2-\delta_\Sigma^2}})}{16\pi^2F_\pi^2\sqrt{m_K^2-\delta_\Sigma^2}} \\
&-\frac{eh_Dh_F(D+3F)(\varphi_D-\varphi_F)(\pi-2\arctan\frac{\delta_\Lambda}{\sqrt{m_K^2-\delta_\Lambda^2}})}{48\pi^2F_\pi^2\sqrt{m_K^2-\delta_\Lambda^2}}. \qquad (5.31)
\end{aligned}
$$

This contribution is interesting since it is UV-finite. It depends non-analytically on quark masses and hence uniquely characterizes long-distance physics [5]. Numerically, these give

$$
\begin{aligned}
|d_p^{1-\mathrm{loop},1}| &= 6.1\times10^{-33}e\,\mathrm{cm} \\
|d_p^{1-\mathrm{loop},2}| &= 1.1\times10^{-32}e\,\mathrm{cm}. \qquad (5.32)
\end{aligned}
$$

[5] One can show that Eq. (5.31) remains real even when $\delta_K, \delta_\Lambda > m_K$ by using the identity $\arctan z = \frac{1}{2i}\log\frac{1+iz}{1-iz}$.

I choose to present numerical results of $d^{1-\text{loop},1}$ and $d^{1-\text{loop},2}$ separately because the former is proportional to $g_8 h_i$ while the latter is proportional to $h_i h_j$. Since the relative sign between g_8 and h_i is experimentally undetermined, these two terms can either add or subtract each other.

As a short conclusion, I stress once again that within the HBchPT formalism, my analytic results of 1-loop diagrams, Eq. (5.28), (5.30) and (5.31) fully respect power counting as no powers of m_B appear in the numerator upon carrying out loop integrals. This is in contrast with the relativistic calculation done in Ref. [161], in which the authors include diagrams involving MDM-like coupling that should have an explicit $1/m_B$ suppression according to the power counting, but is canceled by a factor of m_B appearing in the numerator coming from the loop integral.

Finally let me discuss the effect of counterterms. Since $d_n^{1-\text{loop}}$ and $d_p^{1-\text{loop},1}$ are UV-divergent, I need to introduce corresponding counterterms d_n^0, d_p^0 to absorb the infinities. These counterterms are generated by short-distance physics. Therefore their precise values cannot be calculated. To estimate the size of these counterterms we perform a naive dimensional analysis (NDA). Following [184], there are ten $\Delta S = 1$ four-quark operators that mix under renormalization. The effective Hamiltonian can be written as:

$$H_{\text{eff}}^{\Delta S=1} = \frac{G_F}{\sqrt{2}} V_{\text{ud}} V_{\text{us}}^* \sum_{i=1}^{10} C_i(\mu) \hat{Q}_i(\mu) + h.c. \tag{5.33}$$

Under conditions that $\Lambda_{\text{QCD}} \approx 0.2\text{GeV}$, $\mu = 1\text{GeV}$ and the top-quark mass $m_t = 174\text{GeV}$, the largest flavor-diagonal CP-violating effect comes from the product of $\hat{Q}_2$ and $\hat{Q}_6$ with Wilson coefficients $C_2 = 1.31 - 0.044\tau$ and $C_6 = -0.011 - 0.080\tau$ where $\tau = -V_{\text{td}} V_{\text{ts}}^* / V_{\text{ud}} V_{\text{us}}^*$. This gives:

$$d_p^0, d_n^0 \sim \frac{1}{16\pi^2} \frac{G_F^2}{2} |V_{\text{ud}} V_{\text{us}}^*|^2 \text{Im}(C_2 C_6^*) \Lambda_\chi^3 \approx 4 \times 10^{-32} e\,\text{cm}. \tag{5.34}$$

Here $1/16\pi^2$ is a necessary loop factor while the factor Λ_χ^3 is included to achieve the correct mass dimension. I choose $\Lambda_\chi \sim 1\text{GeV}$ instead of some other scale like

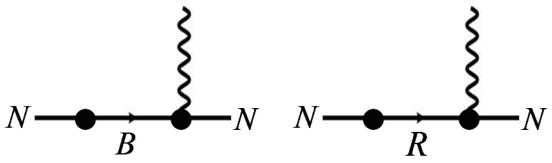

Figure 5.2. (with reflections) Class I pole diagrams.

$\Lambda_{\rm QCD} \sim 200$MeV to provide a conservative upper limit for d_p^0 and d_N^0. This analysis shows that the short-distance contribution to the nucleon EDM could be as large as the long-distance contribution[6]. However the NDA estimation is rarely trustable and it may happen that some accidental cancelations could suppress the actual value of d_n^0, d_p^0 from what is expected in Eq. (5.34). In this sense, a detailed study of the long-distance contribution is worthwhile because it sets a solid bound below which any measurable nucleon EDM could be safely regarded as being consistent with the SM prediction.

5.4 Pole Contribution

Next I estimate the contribution of pole diagrams to the nucleon EDM. For baryon intermediate states, I include the flavor octet part of the $(56, 0^+)$ and $(70, 1^-)$ baryon supermultiplets. Here I adopt the standard spin-flavor $SU(6)$ notation $(\mathcal{D}, L^p)$ where $\mathcal{D}$ is the dimension of the $SU(6)$ representation, L is the orbital angular momentum and p is the parity. For generality, we first write down all possible pole configurations that can contribute and divide it into two classes: Class I are those in which the photon vertex involves a weak insertion and Class II are those in which the photon vertex is purely electromagnetic (see Fig 5.2 and 5.3).

[6] A follow-up work from the author to compute these short-distance contributions within certain nucleon model framework is currently in progress.

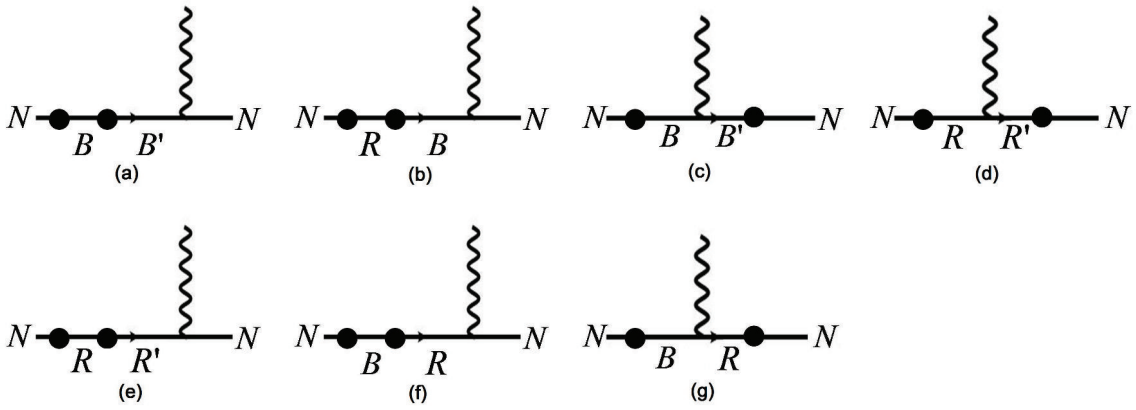

Figure 5.3. (with reflections) Class II pole diagrams.

I want to single out the leading pole diagrams. First, one would expect that Class I contributions are much smaller than Class II for two reasons: (1) the weak photon vertex in Class I diagrams is due to the transition quark magnetic dipole moment (MDM) that contains a $m_s + m_d$ suppression factor or the transition quark EDM that is suppressed by $m_s - m_d$ (the latter, which vanishes if $m_s \to m_d$, is an explicit demonstration of Hara's theorem [176]); (2) Class II diagrams have one more pole in the denominator. With these observations I may safely discard Class I diagrams since they are sub-leading.

Within Class II, Fig. 3(a)-(d) can be shown to have an extra $1/m_N$ suppression [185]. These four diagrams involve MDM-like baryon radiative transition vertices that have the structure of $(1/m_B)\epsilon^{\mu\nu\alpha\beta}v_\nu q_\alpha S_\beta$ at leading order. This structure is orthogonal to the EDM structure $v^\mu S \cdot q$ so it cannot generate an EDM. Therefore in order to obtain an EDM one needs to go to the next order in the HB-expansion leading to an extra $1/m_N$ suppression, so I can discard these four diagrams. Finally, Fig. 3(e) is smaller than Fig. 3(f)-(g) due to an extra propagator of a heavy excited state R. After all these considerations, I only need to evaluate Fig. 3(f)-(g). Using Feynman rules obtained from the Lagrangian in Section II, I obtain

Nucleon\EDM	$\lvert d_N^{1-\mathrm{loop},1}\rvert$	$\lvert d_N^{1-\mathrm{loop},2}\rvert$	$\lvert d_N^{\mathrm{pole}}\rvert$
neutron	1.5×10^{-32}	0	1.4×10^{-32}
proton	6.1×10^{-33}	1.1×10^{-32}	1.4×10^{-32}

Table 5.1. Different contributions to the SM neutron and proton EDM in units of $e\,$cm, assuming the sign of LECs are those given in Section III.

$$
\begin{aligned}
d_n^{\mathrm{pole}} &= \frac{4er_D}{9\delta_\Lambda\delta_{\Lambda^*}\delta_{N^*}\delta_{\Sigma^*}\delta_\Sigma}(h_D\varphi_D\{3w_F[2\delta_{\Lambda^*}\delta_{\Sigma^*}(\delta_\Lambda-\delta_\Sigma)+\delta_{N^*}\{\delta_{\Lambda^*}(\delta_\Lambda+\delta_\Sigma)\\
&\quad +\delta_{\Sigma^*}(\delta_\Sigma-3\delta_\Lambda)\}]-w_D[2\delta_{\Lambda^*}\delta_{\Sigma^*}(3\delta_\Lambda+\delta_\Sigma)+\delta_{N^*}\{3\delta_{\Lambda^*}(\delta_\Lambda+\delta_\Sigma)\\
&\quad +\delta_{\Sigma^*}(3\delta_\Lambda-\delta_\Sigma)\}]\}+3h_F\varphi_F\{w_D[2\delta_{\Lambda^*}\delta_{\Sigma^*}(\delta_\Lambda-\delta_\Sigma)+\delta_{N^*}\{\delta_{\Lambda^*}(\delta_\Lambda-3\delta_\Sigma)\\
&\quad +\delta_{\Sigma^*}(\delta_\Lambda+\delta_\Sigma)\}]+w_F[\delta_{N^*}\{3\delta_{\Sigma^*}(\delta_\Lambda+\delta_\Sigma)-\delta_{\Lambda^*}(\delta_\Lambda-3\delta_\Sigma)\}\\
&\quad -2\delta_{\Lambda^*}\delta_{\Sigma^*}(\delta_\Lambda+3\delta_\Sigma)]\})\\
d_p^{\mathrm{pole}} &= -\frac{8e(\delta_{N^*}-\delta_{\Sigma^*})(r_D+3r_F)(w_D-w_F)(h_D\varphi_D-h_F\varphi_F)}{3\delta_{N^*}\delta_{\Sigma^*}\delta_\Sigma}.
\end{aligned}
\tag{5.35}
$$

In the expression above I have neglected the two small phases $\tilde{\varphi}_D$ and $\tilde{\varphi}_F$. Note that Eq. (5.35) diverges in the $\delta\to0$ limit. This simply indicates that non-degenerate perturbation theory fails in this limit and one needs to switch to degenerate perturbation theory. Numerically, Eq. (5.35) gives:

$$
|d_n^{\mathrm{pole}}|\approx|d_p^{\mathrm{pole}}|\approx1.4\times10^{-32}e\,\mathrm{cm}. \tag{5.36}
$$

Numerical results are summarized in Table 5.1. I caution the readers that all these numbers are only indicative of the size, because I have not yet addressed the sign ambiguities plaguing the determination of certain LECs as emphasized at the end of section III. This will be done in the next section.

5.5 Discussion and Summary

Now I consider the uncertainty due to the undetermined relative sign between different groups of LECs. Since r_D and r_F are fitted simultaneously to the electromag-

netic decay of $(1/2)^-$ resonance they should be multiplied by a common undetermined sign factor $\delta_r = \pm 1$. The constant g_8 is fitted to the kaon decay rate, so it should carry a separate sign factor δ_g. Its phase φ however is determined theoretically so it does not have a sign ambiguity. The four remaining interaction strengths $\{h_D, h_F, w_D, w_F\}$ are fitted simultaneously to s and p-wave amplitudes of the hyperon non-leptonic decay, so they should carry a common undetermined sign factor δ_{hw}. Their corresponding phases are determined by first calculating $\mathrm{Im}\{h_i \exp i\varphi_i\}$ and $\mathrm{Im}\{w_i \exp i\tilde{\varphi}_i\}$ theoretically and then by dividing them by the experimentally-determined $\{h_i, w_i\}$ so the four remaining phases $\{\varphi_D, \varphi_F, \tilde{\varphi}_D, \tilde{\varphi}_F\}$ should also carry the same sign factor δ_{hw}. Summing up loop and pole diagram contributions and allowing $\{\delta_r, \delta_g, \delta_{hw}\}$ to freely change between 1 and -1, I obtain a range of possible d_n and d_p:

$$\begin{aligned} 8.7 \times 10^{-34} e\,\mathrm{cm} < |d_n| < 2.8 \times 10^{-32} e\,\mathrm{cm} \\ 3.3 \times 10^{-33} e\,\mathrm{cm} < |d_p| < 3.3 \times 10^{-32} e\,\mathrm{cm} \end{aligned} \tag{5.37}$$

The surprisingly small lower bounds of $|d_n|, |d_p|$ are due to an accidental cancelation between loop and pole-diagram contributions for a very specific set of $\{\delta_i\}$. There is no reason to believe that this cancellation persists at higher order. To estimate the size of higher-order contributions, I recall that the HB-expansion parameter is of order $m_K/m_N \sim 0.5$. Therefore to be conservative, I could assign a 100% error due to the next-to-leading-order (NLO) effects in the HB-expansion. Also, by looking at Table 5.1 one can see that both loop and pole diagrams are of order $10^{-32} e\,\mathrm{cm}$. So if I assume no fine cancellation between these two parts after adding the NLO contributions from the HB-expansion, then I should expect the long-distance contribution to the nucleon EDM to lie within the range:

$$1 \times 10^{-32} e\,\mathrm{cm} < \{|d_n|, |d_p|\} < 6 \times 10^{-32} e\,\mathrm{cm}. \tag{5.38}$$

My estimated upper bound for d_n is about half the corresponding value predicted in [161]. Eq. (5.38) is three (four) orders of magnitude smaller than the proposed precision level of the future proton (neutron) EDM experiments.

To summarize, even though it is well-known that the nucleon EDM induced by the Standard Model CKM matrix is well below the limit of our current experimental precision, it is still worth a thorough study as it is currently the only source of intrinsic EDMs in nature whose existence is certain. I re-analyze previous works on chiral loop and pole diagram contributions to the nucleon EDM using HBchPT at the leading order in HB-expansion, with an up-to-date determination of relevant LECs that enter our calculation. Combined with the uncertainty due to unknown relative signs of LECs and an estimate of higher-order contributions, I obtain the range for the long-distance contribution to the nucleon EDM in Eq. (5.38). Although an incalculable short-distance physics which appears as counterterms in our work could be as large as the long-distance contribution, the study of the long-distance contribution is still worthwhile as it provides a safe borderline below which any nucleon EDM is consistent with the SM prediction. Finally, there are several ways to improve upon the estimate carried out in this work. For instance, a combined analysis of lattice simulations and better experimental measurements of various hadronic decay processes is expected to provide a better control of both the magnitudes and signs of the required LECs. If the LECs could be determined more precisely, then a complete analysis of NLO-effects in the HB-expansion would be much desired to further restrict the allowed range of d_n and d_p.

CHAPTER 6

HIGHER-TWIST CORRECTION TO PVDIS AND ITS RELATION TO THE PARTON ANGULAR MOMENTUM

6.1 Introduction

As a complement to the studies at high-energy frontier, measurements at the intensity frontier (or precision frontier) provide powerful tools in the search for physics Beyond the Standard Model (BSM). Observables such as the muon anomalous magnetic moment are measured to very high precision, and experimental results are then compared with theoretical predictions. To the extent that the latter are sufficiently reliable, any possible deviation would point to BSM physics. Alternately, these experiments can provide new insights into the dynamics of the Standard Model.

Electron-deuteron parity violating deep inelastic scattering (eD PVDIS) is an excellent example of this class of studies. Historically, it provided the first experimental measurement of weak mixing angle θ_W [19]. Nowadays, with the prospect of the Jefferson Laboratory 12-GeV upgrade and the use of a new spectrometer called SoLID, the left-right asymmetry of PVDIS can be measured with 0.5% precision over the kinematic range $0.3 < x_B < 0.7$ [46]. With this level of precision, one will be able to probe or constrain an interesting set of BSM scenarios, such as a leptophobic Z' boson[116, 117] and supersymmetry[118], as well as to study hadronic physics effects which are yet to be fully understood, such as charge symmetry violation (CVC) and higher-twist (HT).

---

[0]Reprinted article with permission from C. Y. Seng and M. J. Ramsey-Musolf, Phys. Rev. C **88** (2013) no.1, 015202. Copyright (2013) by the American Physical Society. DOI: http://dx.doi.org/10.1103/PhysRevC.88.015202

The effect of HT [119] is a potentially important Standard Model correction that originates from the interaction between partons. This correction in general scales as $(Q^2)^{-(\tau-2)/2}$, with the twist $\tau > 2$, so its effect is enhanced at low Q^2. In the framework of the operator product expansion (OPE), the higher-twist correction can be expressed as a convolution of a high-energy and low-energy piece; the former (embodied in the Wilson coefficients) can be calculated using perturbative methods, whereas the latter involves hadronic matrix elements that require understanding of non-perturbative QCD. Studying the higher-twist correction may help us in probing correlations between the confined quarks and gluons inside the nucleon, so it is interesting to explore HT matrix elements within various model approaches. One advantage of eD PVDIS process is that the HT contribution to the leading term in the PV asymmetry (defined below) arises from a single operator matrix element and can, in principle, be separated kinematically from the subleading terms that have a more complicated HT structure. With this motivation in mind, several previous works [120, 47, 48, 121] have been carried out to study the twist-four (i.e. $\tau = 4$) correction to the left-right asymmetry of eD PVDIS. In what follows, we report on a study that follows-up these earlier works.

The study of HT may also shed light on another important issue, namely, the spin structure of the nucleon. Nearly twenty-five years ago, the EMC collaboration [128] performed a DIS experiment with longitudinally-polarized muons on a target of longitudinally-polarized protons, obtaining a value for the structure function $g_1(x_B)$ over the range $0.01 < x_B < 0.7$. After extrapolating to the low- and high-x_B region, the collaboration obtained a value for the leading moment of $g_1(x_B)$ that contradicted the Ellis-Jaffe sum rule [129] and implied that that the spin of proton is not built up entirely from the quark spin. The result has been confirmed by a variety of subsequent studies. A key question in nuclear physics research has, thus, become explaining in detail the source of nucleon spin in terms of QCD degrees of freedom.

From a theoretical perspective, arriving at a decomposition of the nucleon spin in terms of gauge-invariant matrix elements of local operators that afford a straightforward partonic interpretation has been a vexing problem, and different approaches have been pursued over the years[123, 124, 125, 126, 127]. In each case, reference is usually made to the interpretation in the light-cone – gauge dependence notwithstanding – given its historical importance for thinking about parton dynamics. However, while the meaning of the quark helicity is gauge invariant, the relative importance of other aspects of partonic angular momentum (gluon helicity and quark and gluon orbital angular momentum) in general vary with the choice of gauge and even definition. Nonetheless, it is interesting to ask how different observables may probe different aspects of partonic angular momentum and to do so in a way that is both gauge-invariant and as insensitive as possible to a particular angular momentum decomposition.

In this respect, we will study HT in the context of light-cone quantization. In early work within this framework, it has been shown that one particular component of parton angular momentum – identified as quark orbital angular momentum (OAM) under light-cone quantization using light-cone gauge – is responsible for the non-zero value of Sivers function and Boer-Mulders function [130, 131] in semi-inclusive deep inelastic scattering (SIDIS) [132]. In light of these results, it is also interesting to study how the inclusion of the same component of parton angular momentum modifies the current model predictions for HT corrections to eD PVDIS. Indeed, in all the previous studies of eD PVDIS, only the Fock component of the nucleon wavefunction with zero parton OAM has been included.

After including quark OAM in the light-cone amplitudes, we observe a rather non-intuitive phenomenon: although the absolute magnitude of individual non-zero quark OAM contributions can be significant, they largely cancel against each other. We will argue that this cancelation is largely independent of the detailed model for

the relevant light-cone amplitudes. As a result, the twist-four correction to PVDIS is almost transparent to the inclusion of quark OAM. In contrast, other hadronic quantities, such as the parton distribution functions (PDF), Sivers function, and Boer-Mulders function, manifest non-negligible dependence on quark OAM. Generalizing from the particular choice of light-cone quantization and light-cone gauge, we thus conclude that whatever features of parton angular momentum are responsible for the observed behavior of the PDFs, Sivers, and Boer-Mulders functions, they should have a relatively minor impact on the HT correction to eD PVDIS of interest here. Moreover, any deviation from the light-cone predictions obtained here and in previous works[120, 47, 48] – should they be observed expermentally – would signal the importance of other aspects of parton angular momentum and/or higher Fock space components of the nucleon wavefunction.

The discussion of the computation leading to these observations is arranged in the following order: in Section II we summarize the relevant results of the general formulation of the twist-four correction to eD PVDIS; in Section III we introduce the light-cone wavefunction with quark OAM-dependence; in Section IV we present the analytic expressions of the hadronic matrix elements needed for the twist-4 correction, and demonstrate the generic cancelation between non-zero quark OAM components; in Section V we present the numerical results using one specific choice of nucleon wavefunction, and discuss their physical significance. Detailed formulae appear in the Appendix.

6.2 Higher-twist in PVDIS: general formulation

Here, we review the well-known results for the twist-four correction in eD PVDIS. We will simply quote the central equations that are relevant to our study without any derivation and refer the reader to Refs. [47, 48] for the details.

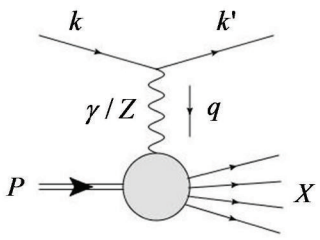

Figure 6.1. Kinematics of e-D PVDIS: a deuteron of momentum P interacts with an incoming electron of momentum k via an exchange of a single photon or Z-boson, and breaks into hadrons which are denoted collectively as X

In eD PVDIS, longitudinally-polarized electron beams are incident on unpolarized deuteron targets. One measures the PV right-left asymmetry

$$A_{RL} = \frac{d\sigma_R - d\sigma_L}{d\sigma_R + d\sigma_L} \tag{6.1}$$

where $d\sigma_{R/L}$ is the differential cross-section for the scattering of the right/left-handed electrons. At the one-boson exchange (OBE) level, the leading parity-violating piece comes from the interference between photon and Z-boson exchange diagrams (see Fig 6.1). The low-energy Z-boson exchange interaction can be described by the following effective 4-fermion interaction:

$$\mathcal{L}_{PV} = \frac{G_F}{\sqrt{2}}[\bar{e}\gamma^\mu\gamma_5 e(C_{1u}\bar{u}\gamma_\mu u + C_{1d}\bar{d}\gamma_\mu d) + \bar{e}\gamma^\mu e(C_{2u}\bar{u}\gamma_\mu\gamma_5 u + C_{2d}\bar{d}\gamma_\mu\gamma_5 d)] \tag{6.2}$$

where, at tree level, we have:

$$C_{1u} = -\frac{1}{2} + \frac{4}{3}\sin^2\theta_W \tag{6.3}$$

$$C_{1d} = \frac{1}{2} - \frac{2}{3}\sin^2\theta_W \tag{6.4}$$

$$C_{2u} = -\frac{1}{2} + 2\sin^2\theta_W \tag{6.5}$$

$$C_{2d} = \frac{1}{2} - 2\sin^2\theta_W \tag{6.6}$$

Neglecting contributions from sea quarks, assuming charge symmetry ($u_V^p = d_V^n$, *etc.* with q_V^N being the valence quark PDF of nucleon N), the leading-twist SM prediction is given by the Cahn-Gilman formula[122]:

$$A_{RL} = \frac{G_F Q^2}{2\sqrt{2}\pi\alpha}\frac{3}{5}[(2C_{1u} - C_{1d}) + (2C_{2u} - C_{2d})\frac{1-(1-y)^2}{1+(1-y)^2}] \tag{6.7}$$

where $Q^2 = -q^2$ and $y = P \cdot q / P \cdot k$.

To include corrections from possible BSM and as well as other SM pieces, we can reparametrize the Cahn-Gilman formula [47]:

$$A_{RL} = -\frac{G_F Q^2}{2\sqrt{2}\pi\alpha}\frac{3}{5}[\tilde{a}_1 + \tilde{a}_2\frac{1-(1-y)^2}{1+(1-y)^2}] \tag{6.8}$$

with $\tilde{a}_i = -(2C_{iu} - C_{id})(1 + R_i)$. Here, R_i describes any deviation of the C_i from the expressions in Eqs. (6.3) to (6.6), including both SM and BSM corrections. In this paper we concentrate on R_1^{HT}, namely the higher-twist correction to $\tilde{a}_1$.

Bjorken and Wolfenstein [133, 134] showed that, if one assumes isospin symmetry and neglects sea quark contributions, then there is only one matrix element that contributes to R_1^{HT} (for a detailed review of these arguments in a more modern context, see Ref. [47]). This observation significantly simplifies the theoretical interpretation of the asymmetry, allowing us to concentrate on one particular matrix element without needing to to disentangle the contributions from many different sources. In brief, the Bjorken and Wolfenstein argument works as follows: A_{RL} arises from the interference between the electromagnetic and weak neutral currents. First, one can decompose both currents into an isoscalar S and an isovector V term. The matrix elements of the $S \times V$ cross-term vanishes because deuteron is an isosinglet. Furthermore, at leading twist, we have $\langle SS \rangle = \langle VV \rangle$. Therefore, the difference between $\langle SS \rangle$ and $\langle VV \rangle$ that enters hadronic tensor $W_{\mu\nu}$

$$W^{\mu\nu}_{ud}(P,q) = \frac{1}{8\pi M_D}\int d^4z e^{iq\cdot z}\,\langle D(P)|\,\bar{u}(z)\gamma^\mu u(z)\bar{d}(0)\gamma^\nu d(0) + (u\leftrightarrow d)\,|D(P)\rangle \quad (6.9)$$

with M_D being the mass of deuteron, is the only matrix element giving a HT correction to R_1.

Below, we will compute the matrix element (6.9) using an expansion of string operators [135] in order to extract the twist-four piece; the latter is expressed in terms of the deuteron twist-four distribution function $\tilde{Q}_D(x_B)$, which will be computed in Section IV.

6.3 The light-cone amplitudes

The main challenge in proceeding from (6.9) is our ignorance of the details of the nucleon wavefunctions. As QCD is non-perturbative at the hadronic scale, analytical expressions for the wavefunctions are unknown. At present, lattice QCD can provide only HT contributions to structure function moments and not the x_B-dependence of the R_1^{HT} that is of interest to the SoLID experiment. Consequently, one must turn to various models that seek to incorporate non-perturbative dynamics. Previous works on R_1^{HT} include the use of MIT bag model [47] and isotropic light-cone wavefunctions that contain both quark and gluon Fock components [48]; their results yield similar shapes for the x_B-dependence but differ somewhat in magnitude, with a maximum R_1^{HT} of $0.003 \sim 0.005$ at $0.2 < x_B < 0.7$ for $Q^2 = 4\text{GeV}^2$, which is a little bit lower than the achievable precision level in the SoLID experiment.

In this work we study how the inclusion of additional parton angular momentum might modify the R_1^{HT} prediction. For this purpose, we adopt the formalism developed in Ref. [136], starting from a light-cone formulation of quark states which is equivalent to the well-known "infinite momentum frame" point of view that gives the PDF its intuitive meaning as a parton momentum probability distribution [119]. We then perform a light-cone expansion of the nucleon state, retaining only the portion of

Fock space containing three valence quarks with all possible quark OAM. To illustrate, we consider a spin-up proton. Its three valence quarks can form a total helicity of $\pm 1/2, \pm 3/2$; therefore in order to keep the total proton spin in z-direction to be $1/2$ we need to assign different z-component quark OAM (i.e. l_z) for different combinations.

A spin-up proton state, then, can be parametrized as the follows:

$$|P\uparrow\rangle = |P\uparrow\rangle^{l_z=0} + |P\uparrow\rangle^{l_z=1} + |P\uparrow\rangle^{l_z=-1} + |P\uparrow\rangle^{l_z=2} \tag{6.10}$$

with

$$\begin{aligned} |P\uparrow\rangle^{l_z=0} &= \frac{\epsilon^{abc}}{\sqrt{6}}\int [DX_3](\psi^{(1)}(1,2,3) + i(k_1^x k_2^y - k_1^y k_2^x)\psi^{(2)}(1,2,3)) \times \\ &\quad u^\dagger_{a\uparrow}(1)\{u^\dagger_{b\downarrow}(2)d^\dagger_{c\uparrow}(3) - d^\dagger_{b\downarrow}(2)u^\dagger_{c\uparrow}(3)\}\,|0\rangle \end{aligned} \tag{6.11}$$

$$\begin{aligned} |P\uparrow\rangle^{l_z=1} &= \frac{\epsilon^{abc}}{\sqrt{6}}\int [DX_3](k^+_{1\perp}\psi^{(3)}(1,2,3) + k^+_{2\perp}\psi^{(4)}(1,2,3)) \times \\ &\quad (u^\dagger_{a\uparrow}(1)u^\dagger_{b\downarrow}(2)d^\dagger_{c\downarrow}(3) - d^\dagger_{a\uparrow}(1)u^\dagger_{b\downarrow}(2)u^\dagger_{c\downarrow}(3))\,|0\rangle \end{aligned} \tag{6.12}$$

$$\begin{aligned} |P,\uparrow\rangle^{l_z=-1} &= \frac{\epsilon^{abc}}{\sqrt{6}}\int [DX_3](-k^-_{2\perp}\psi^{(5)}(1,2,3))(u^\dagger_{a\uparrow}(1)u^\dagger_{b\uparrow}(2)d^\dagger_{c\uparrow}(3) \\ &\quad -u^\dagger_{a\uparrow}(1)d^\dagger_{b\uparrow}(2)u^\dagger_{c\uparrow}(3))\,|0\rangle \end{aligned} \tag{6.13}$$

$$\begin{aligned} |P\uparrow\rangle^{l_z=2} &= \frac{\epsilon^{abc}}{\sqrt{6}}\int [DX_3]k^+_{1\perp}k^+_{3\perp}\psi^{(6)}(1,2,3)(u^\dagger_{a\downarrow}(1)d^\dagger_{b\downarrow}(2)u^\dagger_{c\downarrow}(3) \\ &\quad -u^\dagger_{a\downarrow}(1)u^\dagger_{b\downarrow}(2)d^\dagger_{c\downarrow}(3))\,|0\rangle \end{aligned} \tag{6.14}$$

where $k^\pm_{i\perp} = k^x_i \pm ik^y_i$, while $u^\dagger_{ai}(1)$ means the creation operator of an up-quark (same for down-quark) with color a, spin i and momentum k_1 etc, satisfying the light-cone anti-commutation relation:

$$\{u_{ai}(p), u^\dagger_{bj}(p')\} = 2p^+(2\pi)^3\delta_{ab}\delta_{ij}\delta(p^+ - p'^+)\delta^{(2)}(\vec{p}_\perp - \vec{p}'_\perp) \tag{6.15}$$

The integration measure is [1]:

$$\int [DX_3] = \sqrt{2}\frac{dx_1 dx_2 dx_3}{\sqrt{2x_1 2x_2 2x_3}}\frac{d^2\vec{k}_{1\perp} d^2\vec{k}_{2\perp} d^2\vec{k}_{3\perp}}{(2\pi)^9} 2\pi\delta(1-x_1-x_2-x_3)\times (2\pi)^2\delta^{(2)}(\vec{k}_{1\perp}+\vec{k}_{2\perp}+\vec{k}_{3\perp}) \quad (6.16)$$

The proton wavefunction amplitudes $\{\psi^{(1)}...\psi^{(6)}\}$ are generally unknown functions. Although the expansion (6.11)$\sim$(6.14) is generic, the explicit form of $\psi^{(i)}$ is model-dependent. In this work, we chose the form of $\psi^{(i)}$ derived in Ref. [130] by starting from the static solution of a constituent quark model [137] (which works well in predicting many electroweak properties of the baryons) and applying a Melosh rotation to the solution to obtain non-zero l_z components [138]. This choice of proton wavefunction is used to predict the first moment of Sivers function, and turns out to agree fairly well with the experimental measurements from HERMES and COMPASS [139][2].

6.4 Matrix elements between nucleon states

Following [135], in order to obtain the twist-four distribution function $\tilde{Q}_D(x)$ we need to evaluate the matrix elements between state $|D(P)\rangle$ of the following operators:

$$\begin{aligned} Q_A(b,z) &\equiv : \bar{u}(b_1 z)t^a \not{z}\gamma_5 u(b_2 z)\bar{d}(b_3 z)t^a \not{z}\gamma_5 d(b_4 z) : \\ Q_V(b,z) &\equiv : \bar{u}(b_1 z)t^a \not{z} u(b_2 z)\bar{d}(b_3 z)t^a \not{z} d(b_4 z) : \end{aligned} \quad (6.17)$$

where z is a coordinate on light cone, and the parameters $b \equiv \{b_1, b_2, b_3, b_4\}$ characterize the light-cone separation between quark field operators.

---

[1] There might be difference in constant factors in the definition of integration measure by different authors, which only affects the overall normalization.

[2] Ref. [130] and Ref. [139] defined their first moment of Sivers function with a sign difference.

When computing the matrix elements of $Q_{V,A}$ in Eq. (6.17) we assume an incoherent impulse approximation in which the incoming photon strikes only one of the two nucleons (see, *e.g.* Ref. [145] for further discussions regarding the impulse approximation); hence, matrix elements of the operators (6.17) can be related to the same matrix elements taken between proton states (or equivalently between neutron states, given isospin symmetry). Also, since the quantities we compute do not depend on the proton spin, we can take it to be $+1/2$ along the z-direction without loss of generality.

Now, starting from the operators (6.17), we define two distribution functions $Q_{\pm}(x_\xi)$ via

$$\begin{aligned} & \langle P(p)\uparrow| \left\{ Q_V(b,z) \pm Q_A(b,z) \right\} |P(p)\uparrow\rangle \\ \equiv \;& (p\cdot z)^2 \int \prod_{k=1}^{4} dx_{\xi_k} \delta(\sum_i x_{\xi_i}) e^{-i(p\cdot z)\sum_k b_k x_{\xi_k}} Q_{\pm}(x_\xi) \end{aligned} \tag{6.18}$$

with x_ξ collectively representing $\{x_{\xi_1}, x_{\xi_2}, x_{\xi_3}, x_{\xi_4}\}$, the light-cone momentum fractions: $\xi_i^+ = x_{\xi_i} p^+$. Meanwhile $|P(p)\uparrow\rangle$ is the spin-up proton state with momentum p. Substituting (6.11)$\sim$(6.14) into (6.18) we are able to express $Q_{\pm}(x_\xi)$ in terms of the proton wavefunction amplitudes. It is easy to observe that only diagonal terms, (*i.e.* terms with the same l_z in initial and final states), could give non-vanishing contributions. After a rather lengthy derivation with the aid of Eq. (H.2), we obtain:

$$\begin{aligned} Q_{\pm}(x_\xi) \;=\; & -\frac{32\pi^3}{3} \int \frac{d^2\vec{\xi}_{1\perp}}{(2\pi)^3} \cdots \frac{d^2\vec{\xi}_{4\perp}}{(2\pi)^3} \theta(-x_{\xi_1})\theta(x_{\xi_2})\theta(-x_{\xi_3})\theta(x_{\xi_4})\theta(1-x_{\xi_2}-x_{\xi_4}) \times \\ & \delta^2(\vec{\xi}_{1\perp}+\vec{\xi}_{2\perp}+\vec{\xi}_{3\perp}+\vec{\xi}_{4\perp}) \sum_{l_z} \psi^{\pm}_{l_z}(-\xi_1, -\xi_3, \xi_2, \xi_4) \end{aligned} \tag{6.19}$$

where the explicit formulas of $\psi^{\pm}_{l_z}$ are given in Appendix I.

The proton twist-four distribution function can now be expressed in terms of the $Q_{\pm}$ (refer to Eq. (42) of Ref. [48] after some rearrangement):

$$\tilde{Q}_p(x_B) \equiv 2\mathrm{Re}\int_{-1}^{1}\frac{\prod_{k=1}^{4}dx_{\xi_k}}{x_{\xi_2}x_{\xi_3}(x_{\xi_2}+x_{\xi_3})}\delta(\sum_k x_{\xi_k})\{(x_{\xi_2}+x_{\xi_3})\delta(x_B+x_{\xi_1}+x_{\xi_2}) - x_{\xi_3}\delta(x_B+x_{\xi_1}) - x_{\xi_2}\delta(x_{\xi_4}-x_B)\}[(1+P_{14}P_{23})Q_+(x_\xi) - (P_{12}+P_{34})Q_-(x_\xi)] \quad (6.20)$$

Here P_{ij} is the permutation operator, e.g.

$$P_{12}Q_+(x_{\xi_1},x_{\xi_2},x_{\xi_3},x_{\xi_4}) = Q_+(x_{\xi_2},x_{\xi_1},x_{\xi_3},x_{\xi_4}). \quad (6.21)$$

The deuteron twist-four distribution function $\tilde{Q}_D(x_B)$ can be expressed in terms of $\tilde{Q}_p(x_B)$ through an incoherent impulse approximation [140], which says that a general deuteron hadronic tensor can be related to the corresponding hadronic tensors of proton and neutron by:

$$M_D W_D^{\mu\nu}(p,q) \approx M_N W_p^{\mu\nu}(\frac{p}{2},q) + M_N W_n^{\mu\nu}(\frac{p}{2},q) \quad (6.22)$$

where M_N is the mass of nucleon. In the equation above each hadronic tensor is multiplied by the particle's mass, because following Eq. (6.9) the hadronic tensor we defined has dimension -1. Now we can express both sides of Eq. (6.22) in terms of dimensionless structure functions $\{F_i(x_B)\}$. Using isospin symmetry and the fact that $\tilde{Q}(x_B)$ is proportional to $x_B^{-1}F_1^{ud}(x_B)$ (see Eq. (34) of Ref. [48]), we obtain [3]:

$$\frac{1}{2}\tilde{Q}_D(x_B/2) \approx \tilde{Q}_p(x_B) + \tilde{Q}_n(x_B) \approx 2\tilde{Q}_p(x_B) \quad (6.23)$$

Finally, following the logic of Ref. [48], one can the derive the twist-four contribution to R_1:

[3] In Ref. [48], the authors did not multiply their hadronic tensors by particle mass in the impulse approximation formula, therefore the corresponding relation they obtained is off by a factor 1/2; same for the relation of quark distribution functions.

$$R_1^{HT}(x_B, Q^2) = \frac{1}{Q^2}\frac{\alpha_s \pi}{5(1-\frac{20}{9}\sin^2\theta_W)}\frac{x_B \tilde{Q}_D(x_B)}{u_D(x_B)+d_D(x_B)} \tag{6.24}$$

with $q_D(x_B)$ being the parton distribution function for quark of flavor q in the deuteron

$$\langle D(P)|\,\bar{q}(z)\not{z}q(-z)\,|D(P)\rangle = 2(P\cdot z)\int_{-1}^{1} dx e^{2i(P\cdot z)x} q_D(x) \tag{6.25}$$

Note that we neglect the logarithmic Q^2-dependence of the structure functions in this analysis. We can express q_D in terms of PDF of the proton and neutron again by the impulse approximation (6.22), but now comparing the structure function $F_2(x_B)$ on both sides, which is proportional to $x_B^{-1}q(x_B)$. The result is:

$$q_D(x_B/2) \approx q_p(x_B) + q_n(x_B) \tag{6.26}$$

where $q_p(x)$ and $q_n(x)$ are defined as in Eq. (6.25) but for proton/neutron states. Furthermore, neglecting CSV effects we have:

$$u_n(x_B) = d_p(x_B), d_n(x_B) = u_p(x_B) \tag{6.27}$$

Therefore, it is sufficient to just calculate $u_p(x_B)$ and $d_p(x_B)$ using the proton light-cone wavefunction (6.11)$\sim$(6.14). Using (H.3) and (H.4) , we can compute the quark PDFs of the (spin-up) nucleons by calculating the matrix element on LHS of Eq. (6.25) with nucleon states, and compare it with the form on RHS to extract the PDFs. Same with the twist-four distribution functions, only terms diagonal to l_z survive, so we can separate the result into components of different l_z as the following:

$$\begin{aligned} u_p(x_B) + d_p(x_B) &= d_n(x_B) + u_n(x_B) \\ &= \frac{1}{(2\pi)^6}\int_0^1 dx_1 \int d^2\vec{k}_{1\perp} d^2\vec{q}_\perp \Theta(1-x_B-x_1)\sum_{l_z} A^{l_z}(q,1,2) \end{aligned} \tag{6.28}$$

where the functions $A^{l_z}(q,1,2)$ are given in Appendix I.

We now proceed to show that a partial cancelation occurs between contributions of $l_z = +1$ and $l_z = -1$. For this purpose, we combine (6.19) and (6.20), together with the fact that $\psi^{\pm}_{l_z}(q,l,q',l')^* = \psi^{\pm}_{l_z}(q',l',q,l)$, to simplify the expression of $\tilde{Q}_p(x_B)$ as:

$$\tilde{Q}_p(x_B) = \tilde{Q}^+_p(x_B) + \tilde{Q}^-_p(x_B) \tag{6.29}$$

where

$$\begin{aligned}
\tilde{Q}^+_p(x_B) &= \frac{64\pi^3}{3}\int_0^1 \prod_{i=1}^4 dx_{\xi_i}\delta(x_{\xi_1}-x_{\xi_2}+x_{\xi_3}-x_{\xi_4})\theta(1-x_{\xi_2}-x_{\xi_4})\times \\
&\{\frac{\delta(x_B-x_{\xi_1}+x_{\xi_2})}{x_{\xi_2}x_{\xi_3}}+\frac{\delta(x_B-x_{\xi_1})}{x_{\xi_2}(x_{\xi_2}-x_{\xi_3})}-\frac{\delta(x_B-x_{\xi_4})}{x_{\xi_3}(x_{\xi_2}-x_{\xi_3})} \\
&+\frac{\delta(x_B+x_{\xi_3}-x_{\xi_4})}{x_{\xi_1}x_{\xi_4}}\}\int\prod_{i=1}^4\frac{d^2\vec{\xi}_{i\perp}}{(2\pi)^3}\delta^2(\vec{\xi}_{\perp 1}-\vec{\xi}_{\perp 2}+\vec{\xi}_{\perp 3}-\vec{\xi}_{\perp 4})\times \\
&\sum_{l_z}\mathrm{Re}\psi^+_{l_z}(\xi_1,\xi_3,\xi_2,\xi_4)
\end{aligned} \tag{6.30}$$

$$\begin{aligned}
\tilde{Q}^-_p(x_B) &= \frac{64\pi^3}{3}\int_0^1 \prod_{i=1}^4 dx_{\xi_i}\delta(x_{\xi_1}-x_{\xi_2}-x_{\xi_3}+x_{\xi_4})\theta(1-x_{\xi_2}-x_{\xi_3})\times \\
&\{\frac{\delta(x_B+x_{\xi_1}-x_{\xi_2})}{x_{\xi_2}x_{\xi_3}}-\frac{\delta(x_B-x_{\xi_4})}{x_{\xi_3}(x_{\xi_2}+x_{\xi_3})}-\frac{\delta(x_B-x_{\xi_1})}{x_{\xi_2}(x_{\xi_2}+x_{\xi_3})} \\
&+\frac{\delta(x_B-x_{\xi_1}+x_{\xi_2})}{x_{\xi_2}x_{\xi_3}}\}\int\prod_{i=1}^4\frac{d^2\vec{\xi}_{i\perp}}{(2\pi)^3}\delta^2(\vec{\xi}_{\perp 1}-\vec{\xi}_{\perp 2}-\vec{\xi}_{\perp 3}+\vec{\xi}_{\perp 4})\times \\
&\sum_{l_z}\mathrm{Re}\psi^-_{l_z}(\xi_2,\xi_3,\xi_1,\xi_4)
\end{aligned} \tag{6.31}$$

First we qualitatively analyze the contribution from each l_z-component to $\tilde{Q}^{\pm}_p(x_B)$. This can be done by simply referring to Eqs. (I.1)$\sim$(I.8) of the Appendix B. The result is summarized in Table 6.1. We observe that the $l_z = +1$ (-1) piece contributes mainly to $\tilde{Q}^-_p$ ($\tilde{Q}^+_p$). Also notice that we do not include the $l_z = 2$ component as its effect is tiny.

l_z	Contribution to $\tilde{Q}_p^+(x_B)$	Contribution to $\tilde{Q}_p^-(x_B)$
0	subdominant	dominant
+1	subdominant	dominant
-1	all	zero

Table 6.1. The contributions from different l_z-components to $\tilde{Q}_p^{\pm}(x_B)$. The l_z=0,+1 components contribute mostly to $\tilde{Q}_p^-$ ("dominant") and less so to $\tilde{Q}_p^+$ ("subdominant"), while the l_z=-1 component contributes only to $\tilde{Q}_p^+$.

Next we study the behavior of different contributions to $\tilde{Q}_p^{\pm}(x_B)$ with respect to x_B, showing that those associated with the $l_z \pm 1$ components largely cancel. The individual contributions from the latter are shown in the top two panels of Fig. 6.2. We observe that the $l_z = -1$ contribution, which contributes only to $\tilde{Q}_p^+(x_B)$ changes sign at $x_B \approx 0.4$, whereas the $l_z = +1$ contribution does not. Consequently, the two contributions will cancel against each other for $x_B \gtrsim 0.4$. While the cancellation is not exact, it becomes more effective at larger values of x_B, a region that is weighted most strongly in R_1^{HT} by the factor of x_B in the numerator of Eq. (6.24) and the corresponding presence of $u_D(x_B) + d_D(x_B)$ in the denominator.

We also note that this sign change and cancellation appears to be rather generic. To see why, let us naively take:

$$\int \prod_{i=1}^{4} \frac{d^2\vec{\xi}_{i\perp}}{(2\pi)^3} \delta^2(...) \mathrm{Re}\psi_{l_z}^{\pm} \approx \text{constant} \equiv C \tag{6.32}$$

assuming the function above is well-behaved with respect to $\{x_{\xi_i}\}$. This approximation simply means that we do not care about the details of the proton wavefunction amplitudes. Under this approximation, the numerical integration (6.30) and (6.31) can be performed quite trivially, and the result is shown in the lower two panels of Fig 6.2. In this case, we show $\tilde{Q}_p^{\pm}(x_B)$ as the $l_z = \pm 1$ components contribute primarily to one or the other of these two quantities (see Table 6.1). Although the the assumption in Eq. (6.32) breaks down at large and small x_B, one can see that a sign change of

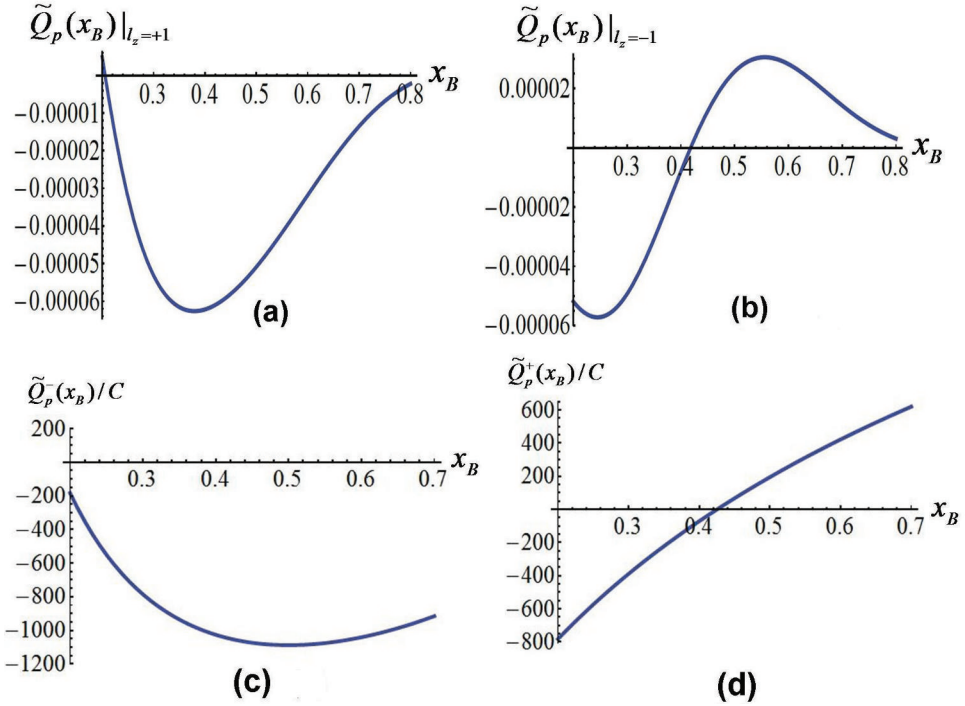

Figure 6.2. (Color online) Top panels: full results for $l_z \pm 1$ contributions to $\tilde{Q}_p(x_B)$. Bottom panels: behavior of $\tilde{Q}_p^{\mp}(x_B)$ ignoring the details of nucleon wavefunction amplitudes. The constant C is defined in Eq. (6.32).

$\tilde{Q}_p^+(x_B)$ from negative to positive occurs near $x_B = 0.4$, implying that $\tilde{Q}_p^+(x_B)$ and $\tilde{Q}_p^-(x_B)$ will have different signs for $x_B \gtrsim 0.4$. Therefore, according to Table 6.1, the contribution to $\tilde{Q}_p(x_B)$ from $l_z = 1$ and $l_z = -1$ should partially cancel other for $x_B \gtrsim 0.4$. Furthermore, since the argument above does not depend on the details of the nucleon wavefunction (as long as it is well-behaved), this feature of partial cancelation should be generic.

6.5 Numerical results and discussion

Eqs. (6.30) and (6.31) are our starting point for the numerical evaluation of $\tilde{Q}_p(x_B)$, which involves an eight-fold integration. To perform this integration, we adopt the Monte Carlo numerical integration called Divonne contained in the CUBA Library, which is an algorithm package designed for multi-dimensional numerical in-

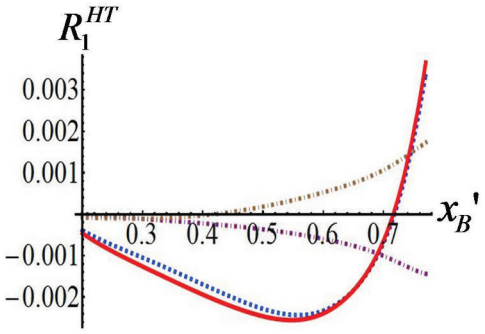

Figure 6.3. (Color online)The Twist-4 correction to R_1 at $Q^2 = 4\text{GeV}^2$. The blue dashed curve shows the $l_z = 0$ contribution; purple dot-dashed curve shows the $l_z = 1$ contribution; brown dot-dashed curve shows the $l_z = -1$ contribution; the red solid curve is the sum of all. $l_z = 2$ contribution is negligible and therefore not included.

tegration [141]. For each l_z component, we evaluate the value of $\tilde{Q}_p(x_B)$ at a series of discrete $\{x_{B,i}\}$, and then link them together using a best-fit line. Also, we take $\alpha_s = 0.5$ at 1GeV following the renormalization group (RG) prediction of the running coupling constant at 4-loop order together with a 3-loop threshold matching, with the quark thresholds taken to be $M_c = 1.5$ GeV and $M_b = 4.7$ GeV respectively [142].

Our main result is shown in Fig. 6.3, which gives R_1^{HT} versus $x'_B \equiv 2x_B$ at $Q^2 = 4\text{GeV}^2$. First, let us compare this outcome with that of Refs. [47] and [48]. It turns out that all three calculations predict similar curve shape for R_1^{HT}, only with slightly different positions of peak and zero-point. Concerning the magnitude, our work predicts a maximum absolute value $|R_1^{HT}| \approx 2.6 \times 10^{-3}$ between $0.2 < x'_B < 0.7$, which is smallest in magnitude among all the three predictions, and is about a half of the size to that of Ref. [48]. This is understandable because the authors include a 3-quark+1-gluon Fock-space component whose contribution is comparable in magnitude to that of the pure 3-quark state. Nonetheless, all three calculations suggest that $|R_1^{HT}|$ lies below that of the expected SoLID precision.

Next we study the OAM-dependence in detail. To that end, we first introduce some nomenclature: in the following, we will use the notation $(|l_z| \otimes |l_{z'}|)$, which denotes a generic matrix element taking between two hadronic states, of which one of

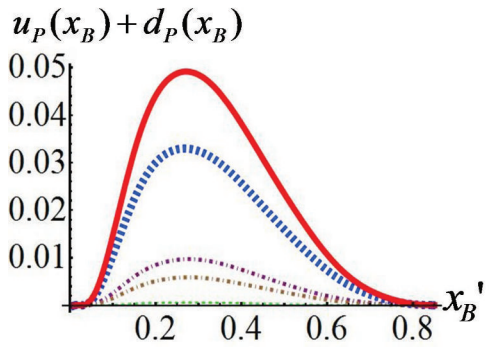

Figure 6.4. (color online)The unnormalized QDF of spin-up proton, splitted into contributions from different l_z components. Blue thick-dashed curve shows contribution from $l_z = 0$ component; purple dot-dashed curve shows contribution from $l_z = 1$ component; brown dot-dashed curve shows contribution from $l_z = -1$ component; green thin-dashed curve shows contribution from $l_z = 2$ component; red solid curve is the sum of all contributions.

them has absolute value of quark OAM in z-direction being $|l_z|$ and the other being $|l_{z'}|$.

From our arguments at the end of Section 6.4, we expect that although $l_z = \pm 1$ individually contribute a significant amount to $\tilde{Q}_p(x_B)$, they should largely cancel against each other for $x_B > 0.4$, making the total $(1 \otimes 1)$ contribution rather small, and therefore leaving the $(0 \otimes 0)$ contribution as the dominant piece. This expectation is born out by the curves in Fig. 6.3. The purple dot-dashed curve and brown dot-dashed curve curves give the individual $(l_z = 1) \otimes (l_z = 1)$ and $(l_z = -1) \otimes (l_z = -1)$ contributions, respectively , which exhibit the expected cancellation for $x'_B > 0.4$. The blue dashed curve and red solid curve give the $(0 \otimes 0)$ and total contributions, respectively. It is clear that the former dominates the total. This $(0 \otimes 0)$ dominance is a rather unique feature of the particular twist-four contribution of interest here, and one that is not shared by other diagonal matrix elements. For example, if one calculate proton quark PDFs (leading twist) using the same set of wavefunctions, the $(0 \otimes 0)$ and $(1 \otimes 1)$ contributions are comparable; moreover, since they have the same sign, the two $|l_z| = 1$ pieces do not cancel each other (see Fig.6.4).

On the other hand, we also note that there are hadronic matrix elements that depend crucially on the existence of non-zero quark OAM in light cone quantization. In particular, in Ref. [130], the authors studied the Sivers function [196] and Boer-Mulders function [143], which are examples of transverse momentum dependent parton distribution functions (TMDs), appearing in semi-inclusive deep inelastic scattering. Importantly, both distribution functions depend on off-diagonal matrix elements of l_z: the Sivers function is sensitive to $(0 \otimes 1)$ while Boer-Mulders function is sensitive to both $(0 \otimes 1)$ and $(1 \otimes 2)$. Simply speaking, the existence of non-zeo quark OAM is responsible for the non-vanishing values of the Sivers and Boer-Mulders functions. Combining this observation with our analysis of the HT matrix element, we conclude that the twist-four correction to eD PVDIS is essentially transparent to the parton angular momentum dynamics that generate the Sivers and Boer-Mulders functions.

It is also interesting to study the impact of sea-parton dynamics on the behavior of the HT matrix element. To that end, we performed a qualitative analysis of the contribution made by the Fock space component containing 3 quarks + 1 gluon, using the general form suggested in Ref. [144] that includes non-zero gluon OAM. The authors of Ref. [48] computed the contribution of the 3q+1g state with $l_z = 0$, which turns out to have a similar shape to that of the $l_z = 0$ 3q-state contribution. To our knowledge, however, there exist no explicit functional forms for the 3q+1g nucleon wavefunction with non-zero parton OAM. Consequently, our analysis is purely analytic at this point. We observe that, in contrast to the 3q state contribution, the matrix element of 3q+1g state for a fixed l_z can contribute significantly to both $\tilde{Q}_p^{\pm}(x_B)$ simultaneously; therefore there is no obvious correlation between l_z and $\tilde{Q}_p^{\pm}(x_B)$ and hence no obvious pattern of partial cancelation. In Table 6.2 we summarize the importance of different $(|l_z| \otimes |l'_z|)$ contributions to various distribution functions, considering only the contributions of 3q states.

Distribution Functions	Dominant	Subdominant
Quark Distribution Functions	(0×0), (1⊗1)	(2⊗2)
PVDIS Twist-Four Correction	(0⊗0)	(1⊗1), (2⊗2)
Sivers Function	(0⊗1)	(1⊗2)
Boer-Mulders Function	(0⊗1), (1⊗2)	—

Table 6.2. The dependence on different quark light-cone OAM components of various distribution functions.

Combining observations, we may draw the following conclusion: if a future eD PVDIS measurement yields a sufficiently precise determination of R_1^{HT} as a function of x'_B, one can compare the experimental curve with our current theoretical prediction. A significant deviation from the predicted curve (*e.g.*, the peak and zero-point are shifted by a considerable amount), could signal the importance of parton angular momentum dynamics beyond those responsible for the Sivers, Boer-Mulders, and spin-independent parton distribution functions.

6.6 Summary

The next generation of parity-violating electron scattering experiments are poised to probe both possible BSM physics as well as novel features of hadron and nuclear structure. In this work, we have studied one particular hadronic effect, namely, the twist-four contribution to $\tilde{a}_1$, the y-independent term in the PV asymmetry. Using a set of proton light-cone wavefunctions with non-zero quark orbital angular momentum, we evaluated the twist-four contribution as a function of x_B, identifying the contributions from different OAM-components. Our total for the correction R_1^{HT} is similar in both shape and magnitude to those obtained in previous works, indicating that higher-precision than expected with the SoLID experiment would be needed to discern this HT effect. An effort to achieve such precision may be worthwhile, because R_1^{HT} appears to be rather unique, in the sense that it is not significantly affected by the parton angular momentum physics responsible for the existence of some other

DIS observables such as the Sivers and Boer-Mulders functions. Thus, by combining the results of a more precise measurement of the asymmetry with measurements of other distribution functions, it is possible to probe complementary aspects of parton angular momentum and, perhaps, shed new light on the role of angular momentum in the structure of the nucleon.

CHAPTER 7

CONCLUSION

There are many open questions in both the SM and BSM physics remained to be answered. In particular, this thesis focuses mainly on: (1) the understanding of QCD at low energy and its application in hadrons and nuclear systems, and (2) the description of effects of new physics through effective field theory and probes of BSM physics in various low energy experiments, including tests of fundamental symmetries in hadrons and nuclei. These two areas of research merge naturally as the development of various effective approaches to the low energy QCD does not only offers a better understanding of the original theory itself in the non-perturbative regime but also provides inputs, such as various QCD matrix elements, that are needed to interpret searches for BSM physics via low energy precision experiments. Throughout this thesis, I try to address the following questions with several case studies:

1. What are the currently-available effective approaches to hadron physics and how well can they reproduce behaviors of QCD at low energy,

2. How precisely can we evaluate the relevant QCD matrix elements with our currently knowledge and computational technique in hadron physics,

3. What are the limitations and deficiencies of each effective approach, and

4. What can we do to improve our current knowledge and computational techniques in the two areas listed above.

In the first two chapters involving the application of Dyson-Schwinger Equation, the main motivation is to search for a unified formalism that can be used to study

the low energy effects of all effective operators in the same footing with a manageable amount of theoretical calculation. We show that DSE with an extremely simple contact interaction approximation is capable to reproduce many known static properties of hadrons as good as other more sophisticated methods. With this simple approximation we calculated both the EDM of a ρ-meson induced by several effective operators up to dimension 6 and various static charges of nucleon.

Upon comparing our result with existing calculations we find that the degree of agreement with other calculations depends operator-by-operator. This raises a general question of how one could possibly estimate the degree of accuracy within each model calculations. Currently there exists no commonly-agreed algorithm for this purpose. As far as practical usage is concerned, the standard way adopted by the community is simply to take the spread of calculations performed using different models as the theoretical error of the calculated quantity. This is obviously not promising enough because any additional theoretical effort in the future will only increase the amount of spread and not decrease it. Therefore, we believe that an essential step in the future is to develop a universal formalism that allows us to quantify the theoretical calculation within any given model.

In the next three chapters I switch my attention to Chiral Perturbation Theory. I demonstrate how an effective theory can be built based on very general arguments of symmetry. This kind of effective theory is sensitive to the IR behavior of QCD. One of the many unique features of ChPT is the prediction of non-analytical dependence on quark masses in scattering amplitudes. Besides, the importance of a valid power counting scheme in non-renormalizable field theories is also stressed in these chapter. In fact, both the works on $\bar{g}_\pi^{(i)}$ and SM EDM are basically improvements of existing literatures using the heavy baryon formalism that respects chiral power counting. In particular, it is shown in the $\bar{g}_\pi^{(i)}$ calculation that the loss of valid power counting in

ChPT may lead to an overestimation of $O(m_N/m_\pi)$ $\sim$10 times in the calculation of low energy observables.

Some obvious deficiencies of ChPT-like effective theories are also clearly revealed in these two works. The key point is that effective theories constructed merely from the symmetry considerations contains too many degrees of freedom (in parameters) compared to the original theory. A direct consequence is that the constructed EFT then contains infinitely many free parameters undetermined by the theory itself. For example, UV-divergences in chiral loop integrals must be canceled by counterterms which appear as higher-order LECs. These counterterms are not *a priori* known and what we can do at most without referring to inputs from lattice or other model calculations is to estimate their order of magnitudes using dimensional analysis. For the observables studied in Chapter 4 and 5 we find that the size of these counterterms can be as large as the loop correction so the ignorance of the numerical values of counterterms renders our theory prediction less useful. Currently the only promising way to determine these pieces is through fittings in lattice simulation. I believe that one of the interesting future directions will be to explore alternative methods in the determination of counterterms involving applications of chiral-improved models.

In Chapter 6 I present an alternative viewpoint to the interplay between low energy QCD and searches of BSM physics. In this chapter, the key message is not just that better QCD calculation is needed for the interpretation of experiment, but the opposite is also true. In this particular example, the twist-four matrix element which is a relevant SM background in BSM searches through PVDIS could actually be measured experimentally and it turns out to also teach us interesting features of QCD, in this case the role of parton angular momentum in the nucleon spin. Combining with other parton distribution functions measurable in SIDIS, it provides a possibility for us to perform a systematic study on different components of parton angular momentum in nucleon separately.

As a conclusion, we are still very far away from having a satisfactory effective description of hadrons that is universal, theoretically clean and computationally economical. With particular working examples, I give a flavor of how much one can do using current available effective approaches in terms of calculations of relevant QCD matrix elements that play key roles in the low-energy tests of fundamental symmetries in systems of hadrons and point out several possible directions one may improve from. It will be a true excitement if any of us here can live long enough to witness a fundamental breakthrough either in the understanding of QCD at hadronic scale or the search of BSM physics as either of them could easily be listed as one of the greatest triumphs of mankind since the born of modern physics.

APPENDIX A

CONTACT INTERACTION

In this appendix we include some detail of the contact interaction approximation we used to describe the low-energy interaction between quarks in our DSE formalism. Our treatment of the contact interaction begins with the gap equation

$$S(p)^{-1} = i\gamma \cdot p + m + \int \frac{d^4q}{(2\pi)^4} g^2 D_{\mu\nu}(p-q) \frac{\lambda^a}{2} \gamma_\mu S(q) \frac{\lambda^a}{2} \Gamma_\nu(q,p), \tag{A.1}$$

wherein m is the Lagrangian current-quark mass, $D_{\mu\nu}$ is the vector-boson propagator and Γ_ν is the quark–vector-boson vertex. We work with the choice

$$g^2 D_{\mu\nu}(p-q) = \delta_{\mu\nu} \frac{4\pi\alpha_{\rm IR}}{m_G^2}\,, \tag{A.2}$$

where $m_G = 0.8\,\text{GeV}$ is a gluon mass-scale typical of the one-loop renormalisation-group-improved interaction introduced in Ref. [83], and the fitted parameter $\alpha_{\rm IR}/\pi = 0.93$ is commensurate with contemporary estimates of the zero-momentum value of a running-coupling in QCD [93, 94]. Equation (A.2) is embedded in a rainbow-ladder (RL) truncation of the DSEs, which is the leading-order in the most widely used, global-symmetry-preserving truncation scheme [76, 77]. This means

$$\Gamma_\nu(p,q) = \gamma_\nu \tag{A.3}$$

in Eq. (A.1) and in the subsequent construction of the Bethe-Salpeter kernels.

One may view the interaction in Eq. (A.2) as being inspired by models of the Nambu–Jona-Lasinio type [95]. However, our treatment is atypical. Moreover, as noted in the Introduction, one normally finds Eqs. (A.2), (A.3) produce results for low-momentum-transfer observables that are practically indistinguishable from those produced by more sophisticated interactions [64, 65, 67, 66, 68, 69, 216, 217, 218, 219, 220]. Using Eqs. (A.2), (A.3), the gap equation becomes

$$S^{-1}(p) = i\gamma\cdot p + m + \frac{16\pi}{3}\frac{\alpha_{\rm IR}}{m_G^2}\int\frac{d^4q}{(2\pi)^4}\,\gamma_\mu\,S(q)\,\gamma_\mu\,, \tag{A.4}$$

an equation in which the integral possesses a quadratic divergence. When the divergence is regularised in a Poincaré covariant manner, the solution is

$$S(p)^{-1} = i\gamma\cdot p + M\,, \tag{A.5}$$

where M is momentum-independent and determined by

$$M = m + M\frac{4\alpha_{\rm IR}}{3\pi m_G^2}\int_0^\infty ds\,s\,\frac{1}{s+M^2}\,. \tag{A.6}$$

We define Eq. (A.4) by writing [96]

$$\begin{aligned}\frac{1}{s+M^2} &= \int_0^\infty d\tau\,{\rm e}^{-\tau(s+M^2)} \\ &\to \int_{\tau_{\rm uv}^2}^{\tau_{\rm ir}^2} d\tau\,{\rm e}^{-\tau(s+M^2)} \qquad\qquad (A.7)\\ &= \frac{{\rm e}^{-(s+M^2)\tau_{\rm uv}^2} - e^{-(s+M^2)\tau_{\rm ir}^2}}{s+M^2}\,, \qquad\qquad (A.8)\end{aligned}$$

where $\tau_{\rm ir,uv}$ are, respectively, infrared and ultraviolet regulators. It is apparent from Eq. (A.8) that a finite value of $\tau_{\rm ir} =: 1/\Lambda_{\rm ir}$ implements confinement by ensuring the absence of quark production thresholds [97]. Since Eq. (A.2) does not define a renormalisable theory, then $\Lambda_{\rm uv} := 1/\tau_{\rm uv}$ cannot be removed but instead plays a dynamical

role, setting the scale of all dimensioned quantities. Using Eq. (A.7), the gap equation becomes

$$M = m + M\frac{4\alpha_{\rm IR}}{3\pi m_G^2}\,\mathcal{C}^{\rm iu}(M^2)\,, \tag{A.9}$$

where,

$$\mathcal{C}^{\rm iu}(\omega) = \omega\left[\Gamma(-1,\omega\tau_{\rm uv}^2) - \Gamma(-1,\omega\tau_{\rm ir}^2)\right], \tag{A.10}$$

with $\Gamma(\alpha, y)$ being the incomplete gamma-function.

At this point we also list expressions for the other regularised integrals that we employ herein:

$$\mathcal{C}_n^{\rm iu}(\omega) = (-1)^n\frac{\omega^n}{n!}\frac{d^n}{d\omega^n}\,\mathcal{C}^{\rm iu}(\omega)\,, \tag{A.11}$$

$$\begin{aligned}\mathcal{D}^{\rm iu}(\omega) &= \int_R ds\,\frac{s^2}{s+M^2}\\ &= 2\omega^2\left[\Gamma(-2,\omega\tau_{\rm uv}^2) - \Gamma(-2,\omega\tau_{\rm ir}^2)\right],\end{aligned} \tag{A.12}$$

$$\begin{aligned}\mathcal{E}^{\rm iu}(\omega) &= \int_R ds\,\frac{s^3}{s+M^2}\\ &= 6\omega^3\left[\Gamma(-3,\omega\tau_{\rm uv}^2) - \Gamma(-3,\omega\tau_{\rm ir}^2)\right],\end{aligned} \tag{A.13}$$

$$\check{\mathcal{G}}_1^{\rm iu}(\omega) = \int_R ds\,\frac{s}{(s+\omega)^3} = \frac{1}{2}\frac{d^2}{d\omega^2}\,\mathcal{C}^{\rm iu}(\omega)\,, \tag{A.14}$$

$$\begin{aligned}\check{\mathcal{G}}_2^{\rm iu}(\omega) &= \int_R ds\,\frac{s^2}{(s+\omega)^3}\\ &= \bar{\mathcal{C}}_1^{\rm iu}(\omega) - \frac{\omega}{2}\frac{d^2}{d\omega^2}\,\mathcal{C}^{\rm iu}(\omega)\,,\end{aligned} \tag{A.15}$$

$$\begin{aligned}\check{\mathcal{G}}_3^{\rm iu}(\omega) &= \int_R ds\,\frac{s^3}{(s+\omega)^3}\\ &= \mathcal{C}^{\rm iu}(\omega) - 2\,\mathcal{C}_1^{\rm iu}(\omega) + \mathcal{C}_2^{\rm iu}(\omega)\,,\end{aligned} \tag{A.16}$$

$$\begin{aligned}\check{\mathcal{G}}_4^{\rm iu}(\omega) &= \int_R ds\,\frac{s^4}{(s+\omega)^3} = \mathcal{D}^{\rm iu}(\omega)\\ &\quad - 2\omega\,\mathcal{C}^{\rm iu}(\omega) + 3\omega\,\mathcal{C}_1^{\rm iu}(\omega) - \omega\,\mathcal{C}_2^{\rm iu}(\omega)\,,\end{aligned} \tag{A.17}$$

$$\check{\mathcal{G}}_5^{\rm iu}(\omega) = \int_R ds\,\frac{s^5}{(s+\omega)^3} = \mathcal{E}^{\rm iu}(\omega) - 2\omega\,\mathcal{D}^{\rm iu}(\omega)$$

$$+ 3\omega^2\, \mathcal{C}^{\rm iu}(\omega) - 4\omega^2\, \mathcal{C}_1^{\rm iu}(\omega) + \omega^2\, \mathcal{C}_2^{\rm iu}(\omega)\,, \tag{A.18}$$

where $\{\mathcal{G}_i = \check{\mathcal{G}}_i/(16\pi^2),\, i = 1, \ldots, 5\}$.

The parameters that specify our treatment of the contact interaction were determined in a study of π- and ρ-meson properties [66]; viz., $\alpha_{\rm IR}/\pi = 0.93$ and (in GeV)

$$m = 0.007\,,\ \Lambda_{\rm ir} = 0.240\ \ \Lambda_{\rm uv} = 0.905\,, \tag{A.19}$$

using which, Eq. (A.9) yields

$$M = 0.368\,{\rm GeV}. \tag{A.20}$$

With the aim of exploring the impact of DCSB on our results, herein we also consider results obtained with $\alpha_{\rm IR}/\pi = 0.74$, in which case

$$M \to M_< = 0.246\,{\rm GeV}. \tag{A.21}$$

APPENDIX B

FADDEEV EQUATION

We describe the dressed-quark-cores of the nucleon via solutions of a Poincaré-covariant Faddeev equation [250]. The equation is derived following upon the observation that an interaction which describes mesons also generates quark-quark (diquark) correlations in the colour-$\bar{3}$ channel [251]. The fidelity of the diquark approximation to the quark-quark scattering kernel has been verified [91].

In RL truncation, the colour-antitriplet diquark correlations are described by an homogeneous Bethe-Salpeter equation that is readily inferred from the analogous meson equation; viz., following Ref. [251] and expressing the diquark amplitude as

$$\Gamma^c_{qq}(k;P) = \Gamma_{qq}(k;P) C^\dagger H^c, \tag{B.1}$$

with

$$\{H^1 = i\lambda^7, H^2 = -i\lambda^5, H^3 = i\lambda^2\}\,, \epsilon_{c_1c_2c_3} = (H^{c_3})_{c_1c_2}\,, \tag{B.2}$$

where $\{\lambda^{2,5,7}\}$ are Gell-Mann matrices, then

$$\Gamma_{qq}(k;P) = -\frac{8\pi}{3}\frac{\alpha_{\rm IR}}{m_G^2}\int\frac{d^4q}{(2\pi)^4}\,\gamma_\mu \chi_{qq}(q;P)\gamma_\mu\,, \tag{B.3}$$

where $\chi_{qq}(q;P) = S(q)\Gamma_{qq}(P)S(q-P)$ and Γ_{qq} is the diquark Bethe-Salpeter amplitude, which is independent of the relative momentum when using a contact interaction [66].

Scalar and axial-vector quark-quark correlations are dominant in studies of the nucleon:

$$\Gamma^{0^+}_{qq}(P) = i\gamma_5 E_{qq0}(P) + \frac{1}{M}\gamma_5\gamma\cdot P F_{qq0}(P)\,, \tag{B.4}$$

$$i\Gamma^{1^+}_{qq\,\mu}(P) = i\gamma^T_\mu E_{qq1}(P), \tag{B.5}$$

where $P_\mu\gamma^T_\mu = 0$. These amplitudes are canonically normalised:

$$P_\mu = 2\mathrm{tr}\int \frac{d^4q}{(2\pi)^4}\Gamma^{0^+}_{qq}(-P)\frac{\partial}{\partial P_\mu}S(q+P)\Gamma^{0^+}_{qq}(P)S(q); \tag{B.6}$$

and

$$P_\mu = \frac{2}{3}\mathrm{tr}\int \frac{d^4q}{(2\pi)^4}\Gamma^{1^+}_{qq\,\alpha}(-P)\frac{\partial}{\partial P_\mu}S(q+P)\Gamma^{1^+}_{qq\,\alpha}(P)S(q). \tag{B.7}$$

A $J = \frac{1}{2}$ baryon is represented by a Faddeev amplitude

$$\Psi = \Psi_1 + \Psi_2 + \Psi_3\,, \tag{B.8}$$

where the subscript identifies the bystander quark and, e.g., $\Psi_{1,2}$ are obtained from Ψ_3 by a cyclic permutation of all the quark labels. We employ a simple but realistic representation of Ψ. The spin- and isospin-$\frac{1}{2}$ nucleon is a sum of scalar and axial-vector diquark correlations:

$$\Psi_3(p_i,\alpha_i,\tau_i) = \mathcal{N}^{0^+}_3 + \mathcal{N}^{1^+}_3\,, \tag{B.9}$$

with (p_i,α_i,τ_i) the momentum, spin and isospin labels of the quarks constituting the bound state, and $P = p_1 + p_2 + p_3$ the system's total momentum.

The scalar diquark piece in Eq. (B.9) is

$$\mathcal{N}_3^{0^+}(p_i,\alpha_i,\tau_i) = [\Gamma^{0^+}(\frac{1}{2}p_{[12]};K)]^{\tau_1\tau_2}_{\alpha_1\alpha_2}\Delta^{0^+}(K)\,[\mathcal{S}(\ell;P)u(P)]^{\tau_3}_{\alpha_3}, \tag{B.10}$$

where: the spinor satisfies Eq. (G.4), with M the mass obtained by solving the Faddeev equation, and it is also a spinor in isospin space with $\varphi_+ = \mathrm{col}(1,0)$ for the charge-one state and $\varphi_- = \mathrm{col}(0,1)$ for the neutral state; $K = p_1 + p_2 =: p_{\{12\}}$, $p_{[12]} = p_1 - p_2$, $\ell := (-p_{\{12\}} + 2p_3)/3$;

$$\Delta^{0^+}(K) = \frac{1}{K^2 + m^2_{qq_{0^+}}} \tag{B.11}$$

is a propagator for the scalar diquark formed from quarks 1 and 2, with $m_{qq_{0^+}}$ the mass-scale associated with this correlation, and Γ^{0^+} is the canonically-normalised Bethe-Salpeter amplitude described above; and $\mathcal{S}$, a 4×4 Dirac matrix, describes the relative quark-diquark momentum correlation.

The axial-vector component in Eq. (B.9) is

$$\mathcal{N}^{1^+}(p_i,\alpha_i,\tau_i) = [\mathtt{t}^i\,\Gamma^{1^+}_\mu(\frac{1}{2}p_{[12]};K)]^{\tau_1\tau_2}_{\alpha_1\alpha_2}\Delta^{1^+}_{\mu\nu}(K)\,[\mathcal{A}^i_\nu(\ell;P)u(P)]^{\tau_3}_{\alpha_3}\,, \tag{B.12}$$

where the symmetric isospin-triplet matrices are

$$\mathtt{t}^+ = \frac{1}{\sqrt{2}}(\tau^0+\tau^3)\,,\ \mathtt{t}^0 = \tau^1\,,\ \mathtt{t}^- = \frac{1}{\sqrt{2}}(\tau^0-\tau^3)\,, \tag{B.13}$$

and the other elements in Eq. (B.12) are straightforward generalisations of those in Eq. (B.10) with, e.g.,

$$\Delta^{1^+}_{\mu\nu}(K) = \frac{1}{K^2 + m^2_{qq_{1^+}}}\left(\delta_{\mu\nu} + \frac{K_\mu K_\nu}{m^2_{qq_{1^+}}}\right). \tag{B.14}$$

One can now write the Faddeev equation for Ψ_3:

$$\begin{bmatrix} \mathcal{S}(k;P)\,u(P) \\ \mathcal{A}^i_\mu(k;P)\,u(P) \end{bmatrix} = -4\int \frac{d^4\ell}{(2\pi)^4}\,\mathcal{M}(k,\ell;P) \begin{bmatrix} \mathcal{S}(\ell;P)\,u(P) \\ \mathcal{A}^j_\nu(\ell;P)\,u(P) \end{bmatrix}. \tag{B.15}$$

The kernel in Eq. (B.15) is

$$\mathcal{M}(k,\ell;P) = \begin{bmatrix} \mathcal{M}_{00} & (\mathcal{M}_{01})^j_\nu \\ (\mathcal{M}_{10})^i_\mu & (\mathcal{M}_{11})^{ij}_{\mu\nu} \end{bmatrix}, \tag{B.16}$$

with

$$\begin{aligned} \mathcal{M}_{00} &= \Gamma^{0^+}(k_q - \ell_{qq}/2;\ell_{qq})\,S^{\rm T}(\ell_{qq}-k_q) \\ &\quad \times \bar{\Gamma}^{0^+}(\ell_q - k_{qq}/2;-k_{qq})\,S(\ell_q)\,\Delta^{0^+}(\ell_{qq})\,, \end{aligned} \tag{B.17}$$

where: $\ell_q = \ell$, $k_q = k$, $\ell_{qq} = -\ell + P$, $k_{qq} = -k + P$, the superscript "T" denotes matrix transpose, $\bar{\Gamma}$ is defined in Eq. (G.9); and

$$\begin{aligned} (\mathcal{M}_{01})^j_\nu &= \mathtt{t}^j\,\Gamma^{1^+}_\mu(k_q - \ell_{qq}/2;\ell_{qq}) S^{\rm T}(\ell_{qq}-k_q) \\ &\quad \times \bar{\Gamma}^{0^+}(\ell_q - k_{qq}/2;-k_{qq})\,S(\ell_q)\,\Delta^{1^+}_{\mu\nu}(\ell_{qq}), \end{aligned} \tag{B.18}$$

$$\begin{aligned} (\mathcal{M}_{10})^i_\mu &= \Gamma^{0^+}(k_q - \ell_{qq}/2;\ell_{qq})\,S^{\rm T}(\ell_{qq}-k_q)\,\mathtt{t}^i \\ &\quad \times \bar{\Gamma}^{1^+}_\mu(\ell_q - k_{qq}/2;-k_{qq})\,S(\ell_q)\,\Delta^{0^+}(\ell_{qq}), \end{aligned} \tag{B.19}$$

$$\begin{aligned} (\mathcal{M}_{11})^{ij}_{\mu\nu} &= \mathtt{t}^j\,\Gamma^{1^+}_\rho(k_q - \ell_{qq}/2;\ell_{qq})\,S^{\rm T}(\ell_{qq}-k_q)\,\mathtt{t}^i \\ &\quad \times \bar{\Gamma}^{1^+}_\mu(\ell_q - k_{qq}/2;-k_{qq})\,S(\ell_q)\,\Delta^{1^+}_{\rho\nu}(\ell_{qq}). \end{aligned} \tag{B.20}$$

The dressed-quark propagator is described in Sec. A and the diquark propagators are given in Eqs. (B.11), (B.14), so the Faddeev equation is complete once the diquark

Bethe-Salpeter amplitudes are computed from Eqs. (B.3) – (B.7). However, we follow Ref. [67] and employ a simplification of the kernel; viz., in the Faddeev equation, the quark exchanged between the diquarks is represented as

$$S^{\rm T}(k) \to \frac{g_N^2}{M}\,, \tag{B.21}$$

where $g_N = 1.18$. This is a variant of the so-called "static approximation," which itself was introduced in Ref. [252] and has subsequently been used in studying a range of nucleon properties [253]. In combination with diquark correlations generated by Eq. (A.2), whose Bethe-Salpeter amplitudes are momentum-independent, Eq. (B.21) generates Faddeev equation kernels which themselves are momentum-independent. The dramatic simplifications which this produces are the merit of Eq. (B.21). Nevertheless, we are currently exploring the veracity of this truncation.

The general forms of the matrices $\mathcal{S}(\ell;P)$ and $\mathcal{A}^i_\nu(\ell;P)$, which describe the momentum-space correlation between the quark and diquark in the nucleon, are described in Refs. [254, 255]. However, with the interaction described in Sec. A augmented by Eq. (B.21), they simplify greatly; viz.,

$$\mathcal{S}(P) = s(P)\,\mathbb{I}\,, \tag{B.22a}$$

$$i\mathcal{A}^j_\mu(P) = a^j_1(P)\gamma_\mu\gamma_5 + i a^j_2(P)\gamma_5\hat{P}_\mu\,, j = +,0\,, \tag{B.22b}$$

with the scalars s, $a^i_{1,2}$ independent of the relative quark-diquark momentum and $\hat{P}^2 = -1$.

The mass of the ground-state nucleon is then determined by a 5×5 matrix Faddeev equation; viz., $\Psi = K\Psi$, with the eigenvector defined via

$$\Psi(P)^{\rm T} = \left[s(P)\; a^+_1(P)\; a^0_1(P)\; a^+_2(P)\; a^0_2(P)\right], \tag{B.23}$$

and the kernel ($\not{k}_\pm = \pm\sqrt{2}$)

$$K(P) = \begin{bmatrix} K^{00}_{ss} & \not{k}_- K^{01}_{sa_1} & K^{01}_{sa_1} & \not{k}_- K^{01}_{sa_2} & K^{01}_{sa_2} \\ \not{k}_- K^{10}_{a_1 s} & 0 & \not{k}_+ K^{11}_{a_1 a_1} & 0 & \not{k}_+ K^{11}_{a_1 a_2} \\ K^{10}_{a_1 s} & \not{k}_+ K^{11}_{a_1 a_1} & K^{11}_{a_1 a_1} & \not{k}_+ K^{11}_{a_1 a_2} & K^{11}_{a_1 a_2} \\ \not{k}_- K^{10}_{a_2 s} & 0 & \not{k}_+ K^{11}_{a_2 a_1} & 0 & \not{k}_+ K^{11}_{a_2 a_2} \\ K^{10}_{a_2 s} & \not{k}_+ K^{11}_{a_2 a_1} & K^{11}_{a_2 a_1} & \not{k}_+ K^{11}_{a_2 a_2} & K^{11}_{a_2 a_2} \end{bmatrix}, \tag{B.24}$$

whose entries are given explicitly in Eqs. (B20), (B21) of Ref. [68]. Given the structure of the kernel, the eigenvectors exhibit the pattern:

$$a_i^+ = -\sqrt{2} a_i^0, \; i = 1, 2. \tag{B.25}$$

Using the parameters and results described in and connection with Eqs. (A.19), (A.20), the diquark Bethe-Salpeter equations produce the following diquark masses (in GeV)

$$m_{qq0^+} = 0.78\,, \; m_{qq1^+} = 1.06\,, \tag{B.26}$$

and canonically normalised amplitudes:

$$E_{qq0^+} = 2.742\,, \; F_{qq0^+} = 0.314\,, \; E_{qq1^+} = 1.302\,. \tag{B.27}$$

With this input to the Faddeev equation, one obtains [67, 68, 69] $m_N = 1.14\,\mathrm{GeV}$ and the following unit-normalised eigenvector[1]

[1] E_{qq0^+}, F_{qq0^+} listed in Table I(A) of Ref. [68] are incorrect. The values listed in Eq. (B.27) were actually used therein.

$$\begin{array}{ccccc} s(P) & a_1^+(P) & a_1^0(P) & a_2^+(P) & a_2^0(P) \\ 0.88 & -0.38 & 0.27 & -0.065 & 0.046 \end{array} . \tag{B.28}$$

As explained elsewhere [67, 68, 69], the mass is greater than that determined empirically because our Faddeev equation kernel omits resonant contributions; i.e., does not contain effects that may phenomenologically be associated with a meson cloud. It is for this reason that our Faddeev equation describes the nucleon's dressed-quark core. Notably, meson cloud effects typically work to reduce a hadron's mass [256].

Using the reduced coupling value described in connection with Eq. (A.21), the diquark Bethe-Salpeter equations produce the following diquark masses (in GeV)

$$m_{qq0^+} = 0.70\,,\ m_{qq1^+} = 0.98\,, \tag{B.29}$$

and canonically normalised amplitudes:

$$E_{qq0^+} = 2.165\,,\ F_{qq0^+} = 0.139\,,\ E_{qq1^+} = 1.093\,. \tag{B.30}$$

With this input to the Faddeev equation, one obtains $m_N = 1.02\,\mathrm{GeV}$ and the following unit-normalised eigenvector

$$\begin{array}{ccccc} s(P) & a_1^+(P) & a_1^0(P) & a_2^+(P) & a_2^0(P) \\ 0.88 & -0.38 & 0.27 & -0.065 & 0.046 \end{array} . \tag{B.31}$$

Plainly, a 20% cut in the infrared value of the coupling diminishes the strength of DCSB by 33%. This feeds into reductions of the diquark Bethe-Salpeter amplitudes and a 10% cut in the nucleon mass. On the other hand, the nucleon's Faddeev amplitude, which describes its internal structure, is almost unchanged. The same pattern is seen in studies of the temperature dependence of nucleon properties [218].

APPENDIX C

INTERACTION CURRENTS

In this appendix we explain the interaction currents involved in the calculation of nucleon static charges using the Fadeev equation. In order to translate the diagrams drawn in this appendix into formulae, it is helpful to bear the following points in mind.

(1) In front of a closed fermion trace; i.e., a vertex, one should, as usual, include a factor of (-1).

(2a) States entering a diagram are described by the amplitudes

$$\Gamma^{0^+}_{qq}(P) = \gamma_5 \left(iE_{qq0^+} + \frac{1}{M} \gamma \cdot P \, F_{qq0^+} \right), \tag{C.1a}$$

$$\Gamma^{1^+}_{qq\mu}(P) = iE_{qq1^+} \gamma^T_\mu \,, \tag{C.1b}$$

$$\mathcal{S}(P) \; = s \, \mathbb{I} \,, \tag{C.1c}$$

$$\mathcal{A}^j_\mu(P) = a^j_1 \gamma_\mu \gamma_5 + i a^j_2 \gamma_5 \hat{P}_\mu \,. \tag{C.1d}$$

(N.B. In this Appendix we have absorbed the "i" of Eqs. (B.5), (B.22) into the labels $\Gamma^{1^+}_{qq\mu}(P)$ and $\mathcal{A}^j_\mu$.)

(2b) States leaving a diagram are described by the amplitudes

$$\Gamma^{0^+}_{qq}(-P) = \gamma_5 \left(iE_{qq0^+} - \frac{1}{M} \gamma \cdot P \, F_{qq0^+} \right), \tag{C.2a}$$

$$\Gamma^{1^+}_{qq\mu}(-P) = iE_{qq1^+} \gamma^T_\mu \,, \tag{C.2b}$$

$$\mathcal{S}(-P) \; = s \, \mathbb{I} =: \bar{\mathcal{S}} \,, \tag{C.2c}$$

$$\mathscr{A}_\mu^j(-P) = a_1^j \gamma_5 \gamma_\mu + i a_2^j \gamma_5 \hat{P}_\mu \,. \tag{C.2d}$$

In these equations,

$$\gamma_\mu^T = \gamma_\nu \mathbb{P}_{\mu\nu}(P)\,, \quad \mathbb{P}_{\mu\nu}(P) = \delta_{\mu\nu} + \frac{P_\mu P_\nu}{m_{qq1^+}^2}\,. \tag{C.3}$$

(3) In the traces arising from a closed fermion loop, we have: $\bar{e}_j \bar{N}$ for charge form factors, where $\bar{e}_0 = \frac{1}{3}e$, $\bar{e}_+ = \frac{4}{3}e$, where e is the positron charge; and $2\bar{N}$ for scalar and tensor form factors. Note that $\bar{N} = 2$ for diquark initial and final states.

C.1 Electromagnetic Current

In computing the charge form factor of any hadron, one must employ the dressed-quark-photon vertex [257, 258]. That vertex may be obtained by solving an inhomogeneous Bethe-Salpeter equation whose unrenormalised form is determined by the inhomogeneous term γ_μ. The complete solution for the contact-interaction's vector vertex in RL truncation can be found in Refs. [65, 216]; but that result is not necessary herein because we only require the result at $Q^2 = 0$, which is fixed by the Ward identity. With the contact interaction, that means

$$\mathscr{V}_\mu^q(Q) \stackrel{Q^2=0}{=} e_q \gamma_\mu \,, \tag{C.4}$$

where e_q is the quark's electric charge.

The $Q^2 = 0$ value of the elastic electromagnetic proton current determines the canonical normalisation of the nucleon's Faddeev amplitude [259]. Given the Faddeev equation in Fig. 2.2, the complete result is obtained by summing the six one-loop

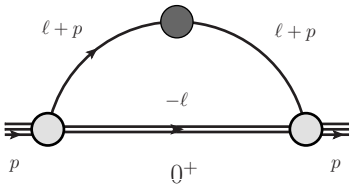

Figure C.1. Diagram 1: The probe interacts with a quark within the proton and the 0^+ diquark is a bystander.

diagrams that we now describe. There would be more diagrams if the interaction were momentum dependent [259].

C.1.1 Diagram 1 – em

The first contribution is depicted in Fig. C.1, which translates into the following expression

$$
\begin{aligned}
e\,Q_{p,1}\,\Lambda^+(p)\gamma_\mu\Lambda^+(p) &= \mathcal{N}\,\Lambda^+(p)\,\bar{\mathcal{S}}\int\frac{d^4\ell}{(2\pi)^4} \\
&\quad \times S(\ell+p)e_u\gamma_\mu S(\ell+p)\Delta^{0^+}(-\ell)\,\mathcal{S}\,\Lambda^+(p) \qquad \text{(C.5)} \\
&= 2\,\mathcal{N}\,\Lambda^+(p)\,s^2\int_0^1 dx\,(1-x)\int\frac{d^4\ell}{(2\pi)^4} \\
&\quad \frac{\{i\gamma\cdot(\ell+xp)-M\}\,e_u\gamma_\mu\,\{i\gamma\cdot(\ell+xp)-M\}}{[\ell^2-x(1-x)m_N^2+(1-x)M^2+xm_{qq_0}^2]^3}\,\Lambda^+(p)\,, \qquad \text{(C.6)}
\end{aligned}
$$

where here and hereafter we (often) suppress the parity-+ superscript on the diquark label, $\mathcal{S}$ is the scalar-diquark piece of the Faddeev amplitude and $\mathcal{N}$ is the (as yet undetermined) canonical normalisation constant for the Faddeev amplitude that ensures that the proton charge is unity; i.e., $Q_p = 1$.

Applying the projection operator

$$
\mathcal{P}_\mu = \frac{1}{2}\,\gamma_\mu\,, \qquad \text{(C.7)}
$$

and performing the trace, one obtains

$$
\begin{aligned}
e\,Q_{p,1} = e_u\,\mathcal{N}\,s^2 \int_0^1 dx\,(1-x) \int \frac{d^4\ell}{(2\pi)^4} \\
\frac{\ell^2 + 2(M+xm_N)^2}{[\ell^2 - x(1-x)m_N^2 + (1-x)M^2 + xm_{qq_0}^2]^3} \qquad \text{(C.8)} \\
\to \quad e_u\,\mathcal{N}\,s^2 \int_0^1 dx\,(1-x) \Big\{ \mathcal{G}_2^{\rm iu}\Big(x(x-1)m_N^2 \\
+(1-x)M^2 + xm_{qq_0}^2\Big) + 2(M+xm_N)^2 \\
\times \mathcal{G}_1^{\rm iu}\Big(x(x-1)m_N^2 + (1-x)M^2 + xm_{qq_0}^2\Big)\Big\}\,, \qquad \text{(C.9)}
\end{aligned}
$$

where $\mathcal{G}_1^{\rm iu}(\omega)$, $\mathcal{G}_2^{\rm iu}(\omega)$ are defined in Eqs. (A.14), (A.15), respectively, and $e_u = \frac{2}{3}e$. This expression evaluates to

$$
\begin{aligned}
eQ_{p,1} &= D_1\,e_u\,\mathcal{N} \\
&= 0.0182622\,e_u\,\mathcal{N} = 0.0121748\,e\,\mathcal{N}\,. \qquad \text{(C.10)}
\end{aligned}
$$

C.1.2 Diagram 2 – em

The second contribution is almost identical to that depicted in Fig. C.1: the only change being that in this instance a 1^+ diquark is the bystander. However, owing to isospin symmetry, which we assume herein, and Eq. (B.25), this term yields

$$
\begin{aligned}
eQ_{p,2} &= (2\,e_d + \,e_u)\,D_2^0\,\mathcal{N} \\
&= (2\,e_d + \,e_u)\,0.00195845\,\mathcal{N} = 0\,, \qquad \text{(C.11)}
\end{aligned}
$$

where D_2^0 is the contribution obtained with a $\{ud\}$-diquark spectator.

C.1.3 Diagram 3 – em

The third contribution is depicted in Fig. C.2, which represents the following expression

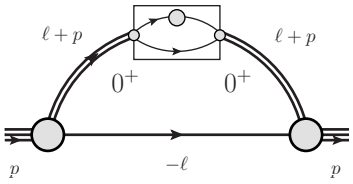

Figure C.2. Diagram 3: The probe interacts with the 0^+ diquark within the proton and the dressed-quark is a bystander.

$$
\begin{aligned}
& eQ_{p,3}\,\Lambda^+(p)\gamma_\mu\Lambda^+(p) \\
& = \mathcal{N}\,\Lambda^+(p)\;\bar{\mathcal{S}}\int\frac{d^4\ell}{(2\pi)^4}\,\Delta^{0^+}(\ell+p) \\
& \quad\times\mathcal{V}^0_\mu(\ell+p)\Delta^{0^+}(\ell+p)S(-\ell)\,\mathcal{S}\,\Lambda^+(p) \qquad \text{(C.12)} \\
& = -2\,\mathcal{N}\,\Lambda^+(p)\,s^2\int_0^1 dx\,(1-x)\int\frac{d^4\ell}{(2\pi)^4} \\
& \quad\times\frac{i\gamma\cdot(-\ell+(1-x)p)-M}{[\ell^2-x(1-x)m_N^2+(1-x)m_{qq_0}^2+xM^2]^3} \\
& \quad\times\mathcal{V}^0_\mu(\ell+xp)\,\Lambda^+(p)\,. \qquad \text{(C.13)}
\end{aligned}
$$

The vertex is given by ($\bar{N}=2$)

$$
\begin{aligned}
\mathcal{V}^0_\mu(P) &= -\bar{e}_0\bar{N}\int\frac{d^4q}{(2\pi)^4}\,\mathrm{tr}\Big\{S(q+P/2)\gamma_\mu S(q+P/2) \\
&\quad\times\Gamma^{0^+}_{qq}(P)S(q-P/2)\bar{\Gamma}^{0^+}_{qq}(-P)\Big\} \qquad \text{(C.14)} \\
&= 2\bar{e}_0\bar{N}\int_0^1 dx\,(1-x)\int\frac{d^4q}{(2\pi)^4} \\
&\quad\times\mathrm{tr}\Big\{[i\gamma\cdot(q+xP)-M]\,\gamma_\mu\,[i\gamma\cdot(q+xP)-M] \\
&\quad\times\gamma_5\Big(iE_{qq_0}+\frac{1}{M}\,\gamma\cdot P\,F_{qq_0}\Big) \\
&\quad\times[i\gamma\cdot(q+(x-1)P)-M] \\
&\quad\times\gamma_5\Big(iE_{qq_0}-\frac{1}{M}\,\gamma\cdot P\,F_{qq_0}\Big)\Big\} \\
&\quad\times\Big(q^2-x(1-x)m_{qq_0}^2+M^2\Big)^{-3}, \qquad \text{(C.15)}
\end{aligned}
$$

where, again, $\bar{e}_0 = \frac{1}{3}e$; and P is the incoming as well as the outgoing momentum of the 0^+ diquark, owing to our need to only consider vanishing momentum transfer $Q \to 0$, and we choose P to be an on-shell momentum. Applying the projector in Eq. (C.7) and evaluating the trace, one obtains

$$\begin{aligned} eQ_{p,3} &= D_3\,\bar{e}_0\,\mathcal{N} \\ &= 0.008733364\,\bar{e}_0\,\mathcal{N} = 0.00291112\,e\,\mathcal{N}\,. \end{aligned} \tag{C.16}$$

C.1.4 Diagram 4 – em

The fourth contribution is almost identical to that depicted in Fig. C.2: the only change being that in this instance the 1^+ diquark is probed, so that one has

$$\begin{aligned} & eQ_{p,4}\,\Lambda^+(p)\gamma_\mu\Lambda^+(p) \\ & = \mathcal{N}\sum_{j\in 0,+}\Lambda^+(p)\,\mathcal{A}^j_\alpha(-p)\int\frac{d^4\ell}{(2\pi)^4}\,\Delta^{1^+}_{\alpha\alpha'}(\ell+p) \\ & \quad \times V^j_{\alpha'\mu\beta'}(\ell+p)\Delta^{1^+}_{\beta'\beta}(\ell+p)S(-\ell)\,\mathcal{A}^j_\beta(p)\,\Lambda^+(p) \qquad \text{(C.17)} \\ & = -2\,\mathcal{N}\sum_{j\in 0,+}\Lambda^+(p)\,\gamma_5\Big(a_1^j\gamma_\alpha + ia_2^j\hat{p}_\alpha\Big)\int_0^1 dx\,(1-x) \\ & \quad \times\int\frac{d^4\ell}{(2\pi)^4}\frac{i\gamma\cdot(-\ell+(1-x)p)-M}{[\ell^2-x(1-x)m_N^2+(1-x)m_{qq_1}^2+xM^2]^3} \\ & \quad \times\mathbb{P}_{\alpha\alpha'}(\ell+xp)\,\mathcal{V}^j_{\alpha'\mu\beta'}(\ell+xp)\,\mathbb{P}_{\beta'\beta}(\ell+xp) \\ & \quad \times\Big(a_1^j\gamma_\beta + ia_2^j\hat{p}_\beta\Big)\gamma_5\,\Lambda^+(p)\,. \qquad \text{(C.18)} \end{aligned}$$

The vertex is ($\bar{N}=2$)

$$\begin{aligned} \mathcal{V}^j_{\alpha\mu\beta}(P) = -\bar{e}_j\bar{N}\int\frac{d^4q}{(2\pi)^4}\,\mathrm{tr}\Big\{ & S(q+P/2)\gamma_\mu S(q+P/2) \\ & \times\Gamma^{1^+}_{qq\beta}(P)S(q-P/2)\bar{\Gamma}^{1^+}_{qq\alpha}(-P)\Big\} \end{aligned} \tag{C.19}$$

$$
\begin{aligned}
&= -2\bar{e}_j \bar{N} E_{qq_1}^2 \int_0^1 dx\,(1-x) \int \frac{d^4q}{(2\pi)^4} \\
&\quad \times \mathrm{tr}\{[i\gamma\cdot(q+xP)-M]\,\gamma_\mu\,[i\gamma\cdot(q+xP)-M] \\
&\quad \times \gamma_\beta^T(P)\,[i\gamma\cdot(q+(x-1)P)-M]\,\gamma_\alpha^T(P)\} \\
&\quad \times [q^2 - x(1-x)m_{qq_1}^2 + M^2]^{-3}\,, \qquad \text{(C.20)}
\end{aligned}
$$

where, as noted above, $\bar{e}_0 = \frac{1}{3}e$ and $\bar{e}_+ = \frac{4}{3}e$, and P is the incoming as well as outgoing momentum of the 1^+ diquark. Applying the projector in Eq. (C.7) and evaluating the trace, one obtains

$$
\begin{aligned}
eQ_{p,4} &= (2\,\bar{e}_+ + \bar{e}_0)\,D_4^0\,\mathcal{N} \\
&= (2\,\bar{e}_+ + \bar{e}_0)\,0.00090133\,\mathcal{N} = 0.002704\,e\,\mathcal{N}\,, \qquad \text{(C.21)}
\end{aligned}
$$

where D_4^0 is the contribution from the $\{ud\}$-diquark.

C.1.5 Diagram 5 – em

This contribution is depicted in Fig. C.3. In this case

$$
Q_{p,5} e\,\Lambda^+(p)\gamma_\mu\Lambda^+(p) = 0\,, \qquad \text{(C.22)}
$$

because the vertex vanishes at zero momentum transfer; i.e.,

$$
\mathcal{V}_{\mu\alpha} = 0\,. \qquad \text{(C.23)}
$$

Consequently

$$
Q_{p,5} = 0\,. \qquad \text{(C.24)}
$$

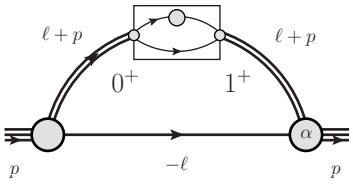

Figure C.3. Diagram 5: The probe is absorbed by a 0^+-diquark, which is thereby transformed into a 1^+ diquark.

C.1.6 Diagram 6 – em

This is the conjugate contribution to that depicted in Fig. C.3; namely, a 1^+ diquark absorbs the probe and is thereby transformed into a 0^+ diquark. In a symmetry preserving treatment of any reasonable interaction, this contribution is identical to that produced by Diagram 5.

C.1.7 Current Conservation

If a truly Poincaré invariant regularisation is employed, then one has Ward identities relating the charges in Eqs. (C.10), (C.21) and (C.11), (C.16)

$$D_1 = D_3\,,\; D_2^0 = D_4^0\,, \tag{C.25}$$

which ensure: simple additivity of the quark and diquark electric charges, and thereby guarantee a unit-charge isospin=$(+1/2)$ baryon through a single rescaling factor [259]; and a neutral isospin=$(-1/2)$ baryon without fine tuning. Owing to the cutoffs we have introduced, however, these identities are violated: Eq. (C.10) cf. (C.16), Eq. (C.11) cf. (C.21). Following Ref. [68], we ameliorate this flaw by enforcing the Ward identities:

$$D_{1,3} \to D_{\overline{13}} = (D_1 + D_3)/2 = 0.01350\,, \tag{C.26a}$$

$$D_{2,4} \to D_{\overline{24}} = 3(D_2^0 + D_4^0)/2 = 0.00429\,. \tag{C.26b}$$

	$Q_{p,i}/\mathcal{N}$	$Q^{\kappa}_{p,i}/\mathcal{N}$
Diagram 1	0.01217	0.0090
Diagram 2	0	0
Diagram 3	0.00291	0.00450
Diagram 4	0.00270	0.00426
Diagram 5	0	
Diagram 6	0	
Sum	0.0178	0.0178

Table C.1. Column 1: Summary of the results computed from all diagrams considered in connection with the proton's charge. Column 2: Results scaled as described in Sec. C.1.7.

This corresponds to introducing a rescaling factor for each of the diagrams involved: $D_i \to \kappa_i D_i$, $\kappa_{1,3} = D_{\overline{13}}/D_{1,3}$, $\kappa_{2,4} = D_{\overline{24}}/D_{2,4}$. Diagrams 5 and 6 are unaffected because they are equal and do not contribute to a baryon's charge.

C.1.8 Canonical Normalisation

The results computed from all diagrams considered in connection with the proton's charge are collected in Table C.1. As noted above, the canonical normalisation is fixed by requiring

$$Q_p = \sum_{i=1}^{6} Q_{p,i} = 1\,, \tag{C.27}$$

from which it follows that

$$\mathcal{N} = \frac{1}{0.01777} = 56.27\,. \tag{C.28}$$

C.2 Scalar Current

When computing the scalar charge of any hadron, one must employ the dressed-quark-scalar vertex. That vertex, too, is obtained by solving an inhomogeneous Bethe-Salpeter equation: in this case, the unrenormalised form is determined by

the inhomogeneous term $\mathbb{I}$. The complete solution for the contact-interaction's scalar vertex in RL truncation can be found in Refs. [216], and at $Q^2 = 0$ this yields:

$$\mathcal{V}^q_{\mathbb{I}} = \frac{1}{1 + \frac{4\alpha_{\rm IR}}{3\pi m_G^2}\Big(2\,\mathcal{C}^{\rm iu}_1(M^2) - \mathcal{C}^{\rm iu}(M^2)\Big)}\,\mathbb{I} = 1.37\,\mathbb{I}\,, \tag{C.29}$$

where M is the dressed-quark mass in Eq. (A.20).

As a check on this result, we note again that since the vertex is only required at $Q^2 = 0$, one can appeal to a Ward identity [260], which takes the form

$$\mathcal{V}_{\mathbb{I}}(Q) \stackrel{Q^2=0}{=} \mathbb{I}\,\frac{\partial M}{\partial m} \tag{C.30}$$

when the contact interaction is used. Employing the results from which Ref. [67] was prepared, this expression, too, yields the numerical value in Eq. (C.29).

The nucleon's scalar charge is also known as the nucleon σ-term; and using our implementation of the contact interaction, one need consider only relevant analogues of the six diagrams described explicitly in App. C.1. In this case, Diagrams 1–4 provide a nonzero contribution and the complete result is obtained from the sum.

C.2.1 Diagram 1 – scalar

This is the contribution produced by the scalar probe interacting with a the dressed-quark whilst the 0^+ $[ud]$-diquark is a spectator:

$$\begin{aligned}\hat{\sigma}_{q,1}\,\Lambda^+(p)\mathbb{I}\Lambda^+(p) &= \mathcal{N}^\kappa_1\,\Lambda^+(p)\,\bar{\mathcal{S}}\int\frac{d^4\ell}{(2\pi)^4}\,S(\ell+p)\\ &\quad\times\mathcal{V}^q_{\mathbb{I}}\,S(\ell+p)\Delta^{0^+}(-\ell)\,\mathcal{S}\,\Lambda^+(p) \qquad\text{(C.31)}\\ &= 2\,\mathcal{N}^\kappa_1\,\Lambda^+(p)\,s^2\int_0^1 dx\,(1-x)\int\frac{d^4\ell}{(2\pi)^4}\\ &\quad\times\frac{\{i\gamma\cdot(\ell+xp)-M\}\,\mathcal{V}^q_{\mathbb{I}}\,\{i\gamma\cdot(\ell+xp)-M\}}{[\ell^2-x(1-x)m_N^2+(1-x)M^2+xm^2_{qq_0}]^3}\,\Lambda^+(p)\,, \qquad\text{(C.32)}\end{aligned}$$

where $\mathcal{N}_1^\kappa = \kappa_1 \mathcal{N}$, with κ_1 defined in connection with Eqs. (C.26), $\mathcal{N}$ given in Eq. (C.28). Applying the projector

$$\mathcal{P} = \frac{1}{2}\,\mathbb{I}\,, \tag{C.33}$$

and evaluating the trace, one obtains

$$\hat{\sigma}_{u,1} = \hat{\sigma}_{q,1} = 0.309\,,\ \hat{\sigma}_{d,1} = 0\,. \tag{C.34}$$

It was plain from the outset that this diagram would only produce a contribution to $\hat{\sigma}_{u,1}$ because the d-quark is sequestered inside the scalar diquark.

C.2.2 Diagram 2 – scalar

In this case we have the scalar probe interacting with the dressed-quark and the 1^+ diquarks being spectators:

$$\begin{aligned}
&\hat{\sigma}_{q_{j,2}}\,\Lambda^+(p)\mathbb{I}\Lambda^+(p) \\
&= \mathcal{N}_2^\kappa\,\Lambda^+(p)\,\mathcal{A}_\alpha^j(-p)\int \frac{d^4\ell}{(2\pi)^4}\,S(\ell+p)\mathcal{V}_\mathbb{I}^q \\
&\quad\times S(\ell+p)\Delta^{1^+}_{\alpha\beta}(-\ell)\,\mathcal{A}_\beta^j(p)\,\Lambda^+(p) \qquad\qquad (C.35)\\
&= 2\,\mathcal{N}_2^\kappa\,\Lambda^+(p)\,\gamma_5\Big(a_1^j\gamma_\alpha + i a_2^j \hat{p}_\alpha\Big)\int_0^1 dx\,(1-x)\int\frac{d^4\ell}{(2\pi)^4} \\
&\quad\times \frac{\{i\gamma\cdot(\ell+xp)-M\}\,\mathcal{V}_\mathbb{I}^q\,\{i\gamma\cdot(\ell+xp)-M\}}{[\ell^2 - x(1-x)m_N^2 + (1-x)M^2 + x m_{qq^1}^2]^3} \\
&\quad\times \mathbb{P}_{\alpha\beta}(\ell-(1-x)p)\Big(a_1^j\gamma_\beta + i a_2^j\hat{p}_\beta\Big)\gamma_5\,\Lambda^+(p). \qquad\qquad (C.36)
\end{aligned}$$

Applying the projector in Eq. (C.33) and evaluating the trace, one finds, owing to Eq. (B.25),

$$\hat{\sigma}_{u,2} = \hat{\sigma}_{q_{0,2}} = 0.0318\,,\ \hat{\sigma}_{d,2} = \hat{\sigma}_{q_{+,2}} = 0.0636 = 2\hat{\sigma}_{u,2}\,. \tag{C.37}$$

C.2.3 Diagram 3 – scalar

The third diagram describes the scalar probe interacting with the 0^+ $[ud]$-diquark and the dressed-quark acting merely as an onlooker:

$$\begin{aligned}\hat{\sigma}_{q,3}\,\Lambda^+(p)\mathbb{I}\Lambda^+(p) &= \mathcal{N}_3^\kappa\,\Lambda^+(p)\,\bar{\mathcal{S}}\int\frac{d^4\ell}{(2\pi)^4}\,\Delta^{0^+}(\ell+p)\\ &\times\mathcal{V}_{\mathbb{I}}^0(\ell+p)\Delta^{0^+}(\ell+p)S(-\ell)\,\mathcal{S}\,\Lambda^+(p) \qquad \text{(C.38)}\\ &= -2\,\mathcal{N}_3^\kappa\,s^2\int_0^1 dx\,(1-x)\int\frac{d^4\ell}{(2\pi)^4}\Lambda^+(p)\\ &\times\frac{[i\gamma\cdot(-\ell+(1-x)p)-M]\,\mathcal{V}_{\mathbb{I}}^0(\ell+xp)\,\Lambda^+(p)}{[\ell^2-x(1-x)m_N^2+(1-x)m_{qq^0}^2+xM^2]^3}\,. \qquad \text{(C.39)}\end{aligned}$$

The vertex is given by ($\bar{N}=2$)

$$\begin{aligned}\mathcal{V}_{\mathbb{I}}^0(P) &= -2\bar{N}\int\frac{d^4q}{(2\pi)^4}\,\mathrm{tr}\Big\{S(q+P/2)\mathcal{V}_{\mathbb{I}}^q S(q+P/2)\\ &\times\Gamma_{qq}^{0^+}(P)S(q-P/2)\bar{\Gamma}_{qq}^{0^+}(-P)\Big\} \qquad \text{(C.40)}\\ &= 4\bar{N}\int_0^1 dx\,(1-x)\int\frac{d^4q}{(2\pi)^4}\,\mathrm{tr}\Big\{[i\gamma\cdot(q+xP)-M]\\ &\times\mathcal{V}_{\mathbb{I}}^q\,[i\gamma\cdot(q+xP)-M]\,\gamma_5\Big(iE_{qq_0}+\frac{1}{M}\,\gamma\cdot P\,F_{qq_0}\Big)\\ &\times[i\gamma\cdot(q+(x-1)P)-M]\,\gamma_5\Big(iE_{qq_0}\\ &-\frac{1}{M}\,\gamma\cdot P\,F_{qq_0}\Big)\Big\}\Big(q^2-x(1-x)m_{qq_0}^2+M^2\Big)^{-3}. \qquad \text{(C.41)}\end{aligned}$$

Applying the projector in Eq. (C.33) and evaluating the trace, one obtains

$$\hat{\sigma}_{u,3}=\frac{\hat{\sigma}_{q,3}}{2}=1.0419=\hat{\sigma}_{d,3}\,. \qquad \text{(C.42)}$$

C.2.4 Diagram 4 – scalar

The fourth diagram describes the scalar probe interacting with a 1^+ $\{uu\}$- or $\{ud\}$-diquark where the dressed-quark acts merely as an onlooker:

$$
\begin{aligned}
&\hat{\sigma}_{q_{j,4}}\,\Lambda^+(p)\mathbb{I}\Lambda^+(p)\\
&=\mathcal{N}_4^\kappa\,\Lambda^+(p)\,\mathcal{A}_\alpha^j(-p)\int\frac{d^4\ell}{(2\pi)^4}\,\Delta^{1^+}_{\alpha\alpha'}(\ell+p)\,\mathcal{V}^{\mathbb{I}}_{\alpha'\beta'}(\ell+p)\\
&\quad\times\Delta^{1^+}_{\beta'\beta}(\ell+p)S(-\ell)\,\mathcal{A}^j_\beta(p)\,\Lambda^+(p) \qquad \text{(C.43)}\\
&=-2\,\mathcal{N}_4^\kappa\,\Lambda^+(p)\,\gamma_5\Big(a_1^j\gamma_\alpha+ia_2^j\hat{p}_\alpha\Big)\int_0^1 dx\,(1-x)\\
&\quad\times\int\frac{d^4\ell}{(2\pi)^4}\frac{i\gamma\cdot(-\ell+(1-x)p)-M}{[\ell^2-x(1-x)m_N^2+(1-x)m_{qq_1}^2+xM^2]^3}\\
&\quad\times\mathbb{P}_{\alpha\alpha'}(\ell+xp)\,\mathcal{V}^{\mathbb{I}}_{\alpha'\beta'}(\ell+xp)\,\mathbb{P}_{\beta'\beta}(\ell+xp)\\
&\quad\times\Big(a_1^j\gamma_\beta+ia_2^j\hat{p}_\beta\Big)\gamma_5\,\Lambda^+(p)\,. \qquad \text{(C.44)}
\end{aligned}
$$

The vertex is given by ($\bar{N}=2$)

$$
\begin{aligned}
&\mathcal{V}^{\mathbb{I}}_{\alpha\beta}(P)=-2\bar{N}\int\frac{d^4q}{(2\pi)^4}\,\mathrm{tr}\Big\{S(q+P/2)\mathcal{V}^q_{\mathbb{I}}S(q+P/2)\\
&\quad\times\Gamma^{1^+}_{qq\beta}(P)S(q-P/2)\bar{\Gamma}^{1^+}_{qq\alpha}(-P)\Big\} \qquad \text{(C.45)}\\
&=-4\bar{N}E_{qq_1}^2\int_0^1 dx\,(1-x)\int\frac{d^4q}{(2\pi)^4}\,\mathrm{tr}\{[i\gamma\cdot(q+xP)\\
&\quad-M]\,\mathcal{V}^q_{\mathbb{I}}\,[i\gamma\cdot(q+xP)-M]\,\gamma_\beta^T\,[i\gamma\cdot(q+(x-1)P)\\
&\quad-M]\,\gamma_\alpha^T\}[q^2-x(1-x)m_{qq_1}^2+M^2]^{-3} \qquad \text{(C.46)}\\
&\to 16M\bar{N}E_{qq_1}^2\,\mathcal{V}^q_{\mathbb{I}}\mathbb{P}_{\alpha\beta}(P)\int_0^1 dx\,(1-x)\\
&\quad\times\Big(M^2-x(x-2)m_{qq_1}^2\Big)\,\mathcal{G}_1^{\mathrm{iu}}\Big(x(x-1)m_{qq_1}^2+M^2\Big)\,, \qquad \text{(C.47)}
\end{aligned}
$$

where P is again both the incoming and outgoing momentum of the 1^+ diquark.

Applying the projector in Eq. (C.33) and evaluating the trace, one finds

$$
\hat{\sigma}_{u,4}=\frac{\hat{\sigma}_{q_{0,4}}}{2}+\hat{\sigma}_{q_{+,4}}=0.465\,,\ \hat{\sigma}_{d,4}=\frac{\hat{\sigma}_{q_{0,4}}}{2}=0.0938\,. \qquad \text{(C.48)}
$$

	$\hat{\sigma}_u$	$\hat{\sigma}_d$	σ [MeV]
Diagram 1	0.309	0	2.163
Diagram 2	0.032	0.063	0.666
Diagram 3	1.042	1.042	14.587
Diagram 4	0.465	0.094	3.914
Diagram 5	0	0	0
Diagram 6	0	0	0
Total Result	1.85	1.20	21.33

Table C.2. Summary of the results computed from all diagrams considered in connection with the proton's scalar charge.

C.2.5 Proton σ-term

The results obtained from all diagrams considered in connection with the proton's scalar charge are collected in Table C.2. The proton σ-term is

$$\sigma_N = m \sum_{i=1}^{6} [\hat{\sigma}_{u,i} + \hat{\sigma}_{d,i}] = 21.33\,\text{MeV}. \tag{C.49}$$

In the isospin symmetric limit, the neutron σ-term is identical.

C.3 Tensor Current

When computing the tensor charge of any hadron, one must employ the dressed-quark-tensor vertex. However, as explained elsewhere [67], any dressing of the tensor vertex must depend linearly on the relative momentum [261] and such dependence is impossible using a symmetry-preserving regularisation of a vector $\otimes$ vector contact interaction. Hence, in our case, the quark-tensor vertex is unmodified from its bare form; viz.,

$$\mathcal{V}^q_{\mu\nu} = \sigma_{\mu\nu}\,. \tag{C.50}$$

Naturally, when computing the proton's tensor charge using our implementation of the contact interaction, one need only consider relevant analogues of the six diagrams described explicitly in App. C.1. In this case, Diagrams 1,2,4,5,6 provide nonzero

contributions. Diagram 3 yields zero because Poincaré invariance entails that a scalar diquark cannot possess a tensor charge.

C.3.1 Diagram 1 – tensor

As usual, we first consider the case of the tensor probe interacting with the dressed-quark and the 0^+ $[ud]$-diquark being a spectator:

$$\begin{aligned}\delta_1 q\,\Lambda^+(p)\sigma_{\mu\nu}\Lambda^+(p) &= \mathcal{N}_1^\kappa\,\Lambda^+(p)\,\bar{\mathcal{S}}\int\frac{d^4\ell}{(2\pi)^4}\,S(\ell+p)\sigma_{\mu\nu}\\ &\quad\times S(\ell+p)\Delta^{0^+}(-\ell)\,\mathcal{S}\,\Lambda^+(p) \qquad\text{(C.51)}\\ &= 2\,\mathcal{N}\,s^2\int_0^1 dx\,(1-x)\int\frac{d^4\ell}{(2\pi)^4}\Lambda^+(p)\,\{i\gamma\cdot(\ell+xp)\\ &\quad - M\}\,\sigma_{\mu\nu}\,\{i\gamma\cdot(\ell+xp)-M\}\Lambda^+(p)\\ &\quad\times[\ell^2 - x(1-x)m_N^2 + (1-x)M^2 + xm_{qq_0}^2]^{-3}\,. \qquad\text{(C.52)}\end{aligned}$$

Applying the projector

$$\mathcal{P}_{\mu\nu} = \frac{1}{12}\,\sigma_{\mu\nu}\,, \qquad\text{(C.53)}$$

and evaluating the trace, one obtains

$$\begin{aligned}\delta_1 q &= 2\,\mathcal{N}_1\,s^2\int_0^1 dx\,(1-x)\int\frac{d^4\ell}{(2\pi)^4}\\ &\quad\times\frac{(M+xm_N)^2}{[\ell^2 - x(1-x)m_N^2 + (1-x)M^2 + xm_{qq_0}^2]^3} \qquad\text{(C.54)}\\ &\to 2\,\mathcal{N}\,s^2\int_0^1 dx\,(1-x)(M+xm_N)^2\\ &\quad\times\mathcal{G}_1^{\rm iu}\Big(x(x-1)m_N^2 + (1-x)M^2 + xm_{qq_0}^2\Big)\,, \qquad\text{(C.55)}\end{aligned}$$

where $\mathcal{G}_1^{\rm iu}(\omega)$ is defined in Eq. (A.14). As a result we find

$$\delta_{T1}u = \delta_1 q = 0.581\,, \quad \delta_{T1}d = 0\,. \qquad\text{(C.56)}$$

C.3.2 Diagram 2 – tensor

When the tensor probe interacts with the dressed-quark and the 1^+ diquarks are spectators, one has

$$\begin{aligned}
&\delta_2 q_j\, \Lambda^+(p)\sigma_{\mu\nu}\Lambda^+(p) \\
&= \mathcal{N}_2^\kappa\, \Lambda^+(p)\, \mathcal{A}_\alpha^j(-p) \int \frac{d^4\ell}{(2\pi)^4}\, S(\ell+p)\sigma_{\mu\nu} \\
&\quad \times S(\ell+p)\, \Delta^{1^+}_{\alpha\beta}(-\ell)\, \mathcal{A}_\beta^j(p)\, \Lambda^+(p) \qquad \text{(C.57)} \\
&= 2\,\mathcal{N}_2^\kappa\, \Lambda^+(p)\, \gamma_5 \Big(a_1^j \gamma_\alpha + i a_2^j \hat{p}_\alpha\Big) \int_0^1 dx\, (1-x) \int \frac{d^4\ell}{(2\pi)^4} \\
&\quad \times \frac{\{i\gamma\cdot(\ell+xp)-M\}\,\sigma_{\mu\nu}\,\{i\gamma\cdot(\ell+xp)-M\}}{[\ell^2 - x(1-x)m_N^2 + (1-x)M^2 + x m_{qq_1}^2]^3} \\
&\quad \times \mathbb{P}_{\alpha\beta}(\ell-(1-x)p)\Big(a_1^j\gamma_\beta + i a_2^j \hat{p}_\beta\Big)\gamma_5\Lambda^+(p). \qquad \text{(C.58)}
\end{aligned}$$

Applying the projector in Eq. (C.53) and evaluating the resulting trace, one finds, owing to Eq. (B.25):

$$\delta_{T2} d = \delta_2 q_+ = 2\delta_2 q_0 = -0.0359 = 2\delta_{T2} u\,. \qquad \text{(C.59)}$$

C.3.3 Diagram 4 – tensor

The next nonzero contribution arises from the tensor probe interacting with a 1^+ $\{uu\}$- or $\{ud\}$-diquark where the dressed-quark acts merely as an onlooker:

$$\begin{aligned}
&\delta_4 q_j\, \Lambda^+(p)\sigma_{\mu\nu}\Lambda^+(p) \\
&= \mathcal{N}_4^\kappa\, \Lambda^+(p)\, \mathcal{A}_\alpha^j(-p) \int \frac{d^4\ell}{(2\pi)^4}\, \Delta^{1^+}_{\alpha\alpha'}(\ell+p)\mathcal{V}^2_{\alpha'\mu\nu\beta'}(\ell+p) \\
&\quad \times \Delta^{1^+}_{\beta'\beta}(\ell+p) S(-\ell)\, \mathcal{A}_\beta^j(p)\, \Lambda^+(p) \qquad \text{(C.60)} \\
&= -2\,\mathcal{N}_4^\kappa\, \Lambda^+(p)\, \gamma_5 \Big(a_1^j \gamma_\alpha + i a_2^j \hat{p}_\alpha\Big) \int_0^1 dx\, (1-x) \int \frac{d^4\ell}{(2\pi)^4} \\
&\quad \times \frac{i\gamma\cdot(-\ell+(1-x)p)-M}{[\ell^2 - x(1-x)m_N^2 + (1-x)m_{qq_1}^2 + xM^2]^3}
\end{aligned}$$

$$\times \mathbb{P}_{\alpha\alpha'}(\ell + xp)\, \mathcal{V}^2_{\alpha'\mu\nu\beta'}(\ell + xp)$$
$$\times \mathbb{P}_{\beta'\beta}(\ell + xp)\Big(a_1^j \gamma_\beta + i a_2^j \hat{p}_\beta\Big)\gamma_5\, \Lambda^+(p)\,. \tag{C.61}$$

The vertex is ($\bar{N} = 2$)

$$\mathcal{V}^2_{\alpha\mu\nu\beta}(P) = -2\bar{N}\int \frac{d^4q}{(2\pi)^4}\,\mathrm{tr}\Big\{S(q + P/2)\sigma_{\mu\nu}S(q + P/2)$$
$$\times \Gamma^{1^+}_{qq\beta}(P)S(q - P/2)\bar{\Gamma}^{1^+}_{qq\alpha}(-P)\Big\} \tag{C.62}$$
$$= -4\bar{N}E^2_{qq_1}\int_0^1 dx\,(1-x)\int \frac{d^4q}{(2\pi)^4}\,\mathrm{tr}\Big[[i\gamma\cdot(q + xP)$$
$$- M]\,\sigma_{\mu\nu}\,[i\gamma\cdot(q + xP) - M]\,\gamma_\beta^T$$
$$\times [i\gamma\cdot(q + (x-1)P) - M]\,\gamma_\alpha^T\Big]$$
$$\times [q^2 - x(1-x)m^2_{qq_1} + M^2]^{-3} \tag{C.63}$$
$$\to 16iM\bar{N}E^2_{qq_1}\Big(\mathbb{P}_{\alpha\mu}(P)\mathbb{P}_{\beta\nu}(P) - \mathbb{P}_{\alpha\nu}(P)\mathbb{P}_{\beta\mu}(P)\Big)$$
$$\times \int_0^1 dx\,(1-x)\Big\{\Big(M^2 - x(x-2)m^2_{qq_1}\Big)\,\mathcal{G}_1^{\mathrm{iu}}(\omega)$$
$$+ \mathcal{G}_2^{\mathrm{iu}}\Big(x(x-1)m^2_{qq_1} + M^2\Big)\Big\} \tag{C.64}$$

where P is the incoming and outgoing momentum of the 1^+ diquark, and $\mathcal{G}_1^{\mathrm{iu}}(\omega)$, $\mathcal{G}_2^{\mathrm{iu}}(\omega)$ are defined in Eqs. (A.14), (A.15). Applying the projector in Eq. (C.53) and evaluating the resulting trace, one finds

$$\delta_{T4}u = \frac{\delta_4 q_0}{2} + \delta_4 q_+ = 0.292\,,\ \delta_{T4}d = \frac{\delta_4 q_0}{2} = 0.0589\,. \tag{C.65}$$

C.3.4 Diagram 5 – tensor

This is the contribution to the tensor charge arising when a scalar diquark absorbs the tensor probe and is thereby transformed into a 1^+ diquark. Naturally, in a

symmetry preserving treatment of any reasonable interaction, this contribution is identical to that produced by Diagram 6. Concretely, one has:

$$
\begin{aligned}
&\delta_5 q\,\Lambda^+(p)\sigma_{\mu\nu}\Lambda^+(p) \\
&= \mathcal{N}_5^\kappa\,\Lambda^+(p)\,\mathcal{A}_\alpha^0(-p)\int\frac{d^4\ell}{(2\pi)^4}\,\Delta^{1^+}_{\alpha\beta}(\ell+p)\,\mathcal{V}^{10}_{\beta\mu\nu}(\ell+p) \\
&\quad\times\Delta^{0^+}(\ell+p)S(-\ell)\,\mathcal{S}\,\Lambda^+(p) \qquad\qquad (C.66)\\
&= -2\,\mathcal{N}_5^\kappa\,\Lambda^+(p)\,\gamma_5\Big(a_1^0\gamma_\alpha + i a_2^0\hat{p}_\alpha\Big)\int_0^1 dx\int_0^1 dy\,y\int\frac{d^4\ell}{(2\pi)^4} \\
&\quad\times[i\gamma\cdot(-\ell+yp)-M]\,\mathcal{V}^{10}_{\beta\mu\nu}(\ell+(1-y)p) \\
&\quad\times\mathbb{P}_{\alpha\beta}(\ell+(1-y)p)\,s\,\Lambda^+(p)[\ell^2+y(y-1)m_N^2 \\
&\quad+xym_{qq_1}^2+(1-x)ym_{qq_0}^2+(1-y)M^2]^{-3}\,. \qquad\qquad (C.67)
\end{aligned}
$$

The transition vertex is $\mathcal{V}^{10}_{\beta\mu\nu}(P,P)$ where ($\bar{N}=2$)

$$
\begin{aligned}
&\mathcal{V}^{10}_{\beta\mu\nu}(P,P') = -2\bar{N}\int\frac{d^4q}{(2\pi)^4}\,\mathrm{tr}\Big\{S(q+P')\sigma_{\mu\nu}S(q+P) \\
&\quad\times\Gamma^{0^+}_{qq}(P)S(q)\bar{\Gamma}^{1^+}_{qq\beta}(-P')\Big\} \qquad\qquad (C.68)\\
&= 4i\bar{N}E_{qq_1}\int_0^1 dx\int_0^1 dy\,y\int\frac{d^4q}{(2\pi)^4} \\
&\quad\times\mathrm{tr}\Big\{[i\gamma\cdot(q+yP'-xyP)-M]\,\sigma_{\mu\nu} \\
&\quad\times[i\gamma\cdot(q-(1-y)P'+(1-xy)P)-M] \\
&\quad\times\gamma_5\Big(iE_{qq_0}+\frac{1}{M}\,\gamma\cdot P\,F_{qq_0}\Big) \\
&\quad\times[i\gamma\cdot(q-(1-y)P'-xyP)-M]\,\gamma_\beta^T(P')\Big\} \\
&\quad\times\Big(q^2-(1-x)y(1-y)m_{qq_1}^2 \\
&\qquad-x(1-x)y^2m_{qq_0}^2+M^2\Big)^{-3}, \qquad\qquad (C.69)
\end{aligned}
$$

where P and P' are the incoming and outgoing momenta of the diquarks, respectively. (Some details about the on-shell procedure can be found in App. D.) Applying the

	$\delta_T u$	$\delta_T d$	$g_T^{(0)}$	$g_T^{(1)}$
Diagram 1	0.581	0	0.581	0.581
Diagram 2	−0.018	−0.036	−0.054	0.018
Diagram 3	0	0	0	0
Diagram 4	0.292	0.059	0.351	0.233
Diagram 5+6	−0.164	−0.164	−0.329	0
Total Result	0.691	−0.141	0.550	0.832

Table C.3. Summary of results computed from all diagrams considered in connection with the proton's tensor charge. They represent values at the model scale, $\zeta_H \approx M$, described in App. E.

projector in Eq. (C.53), evaluating the resulting trace and combining the result with that from Diagram 6, one finds

$$\delta_{T,5+6} u = \delta_{T,5+6} d = \delta q_5 = -0.164\,. \tag{C.70}$$

C.3.5 Proton tensor charge

The results obtained from all diagrams considered in connection with the proton's tensor charges are collected in Table C.3. Notably, the values of the tensor charges depend on the renormalisation scale associated with the tensor vertex. This is discussed in App. F.

C.3.6 Proton tensor charge – scalar diquark only

It is interesting to consider the impact of the axial-vector diquark on the tensor charges. This may be exposed by comparing the results in Table C.3 with those obtained when the axial-vector diquark is eliminated from the nucleon. We implement that suppression by using the following nucleon Faddeev amplitude:

$$\begin{array}{ccccc} s(P) & a_1^+(P) & a_1^0(P) & a_2^+(P) & a_2^0(P) \\ 1.0 & 0 & 0 & 0 & 0 \end{array}\,, \tag{C.71}$$

and then repeating the computations in Apps. C.1, C.3. Naturally, in this case only Diagrams 1 and 3 can possibly yield nonzero contributions to any quantity.

Recomputing the canonical normalisation, we obtain

$$\mathcal{N}_{\not I} = \frac{1}{0.0174} = 57.50\,, \tag{C.72}$$

which is 2% larger than the complete result in Eq. (C.28).

Regarding the tensor charges, Diagram 3 also vanishes in this instance so that the net result is simply that produced by Diagram 1:

$$\begin{array}{cccc} \delta_{T\not I} u & \delta_{T\not I} d & g^{(0)}_{T\not I} & g^{(1)}_{T\not I} \\ 0.765 & 0 & 0.765 & 0.765 \end{array} . \tag{C.73}$$

Comparison with Table C.3 shows that with a symmetry-preserving treatment of a vector $\otimes$ vector contact interaction, the d-quark contribution to the proton's tensor charge is only nonzero in the presence of axial-vector diquark correlations and these correlations reduce the u-quark contribution by 10%.

C.3.7 Proton tensor charge – Reduced DCSB

In order to expose the effect of DCSB on the tensor charges, we repeated all relevant calculations above beginning with the value of $\alpha_{\rm IR}$ used to produce Eq. (A.21) and thereby obtained the results listed in Table C.4.

	$\delta_T u$	$\delta_T d$	$g_T^{(0)}$	$g_T^{(1)}$
Diagram 1	0.495	0	0.495	0.495
Diagram 2	−0.020	−0.039	−0.059	0.020
Diagram 3	0	0	0	0
Diagram 4	0.236	0.047	0.283	0.189
Diagram 5+6	−0.160	−0.160	−0.319	0
Total Result	0.551	−0.151	0.400	0.703

Table C.4. Summary of results computed from all diagrams considered in connection with the proton's tensor charge using input based on $\alpha_{\rm IR}/\pi = 0.74$, quoted at the model scale, $\zeta_H \approx M$, described in App. E.

APPENDIX D

ON-SHELL CONSIDERATIONS FOR THE TRANSITION DIAGRAMS

For the practitioner it will likely be helpful here to describe our treatment of the denominator that arises when using a Feynman parametrisation to compute the transition diagrams. Namely, one has

$$\begin{aligned}
&\frac{1}{(q+P')^2+M^2}\frac{1}{(q+P)^2+M^2}\frac{1}{q^2+M^2} \\
&= 2\int_0^1 dx \int_0^1 dy\, y\{(q+(1-y)P'+xyP)^2 \\
&\quad + (1-y)yP'^2 + xy(1-xy)P^2 \\
&\quad - 2(1-y)xyP'\cdot P + M^2\}^{-3}\,.
\end{aligned} \tag{D.1}$$

At this point, a shift of the integration variable $q \to q-(1-y)P'-xyP$ yields

$$\begin{aligned}
&2\int_0^1 dx \int_0^1 dy\, y\{q^2 + (1-y)yP'^2 + xy(1-xy)P^2 \\
&\quad - 2(1-y)xyP'\cdot P + M^2\}^{-3}\,.
\end{aligned} \tag{D.2}$$

Next, we employ on-shell relations, which for Diagram 5 are given by

$$P'^2 = -m_{qq_1}^2\,,\ P^2 = -m_{qq_0}^2\,. \tag{D.3}$$

Then, since $Q^2 \equiv (P'-P)^2 = P'^2 + P^2 - 2P'\cdot P = 0$:

$$P'\cdot P = -\frac{m_{qq_0}^2 + m_{qq_1}^2}{2}\,. \tag{D.4}$$

Hence, the Feynman integral associated with Diagram 5 is

$$2\int_0^1 dx \int_0^1 dy\, y\{q^2 - (1-x)y(1-y)m_{qq_1}^2 - x(1-x)y^2 m_{qq_0}^2 + M^2\}^{-3}\,. \tag{D.5}$$

Diagram 6 is obtained via $m_{qq_0} \leftrightarrow m_{qq_1}$.

APPENDIX E

MODEL SCALE

In modern studies of QCD's gap equation, which use DCSB-improved kernels and interactions that preserve the one-loop renormalisation group behaviour of QCD, the dressed-quark mass is renormalisation point invariant. As in QCD, however, the current-quark mass is not. Therefore, in quoting a current-quark mass in Eq. (A.19), a question immediately arises: to which scale, ζ_H, does this current-quark mass correspond?

As noted in App. A, the contact-interaction does not define a renormalisable theory and the scale ζ_H should therefore be part of the definition of the interaction. We define ζ_H so as to establish contact between the current-quark mass in Eq. (A.19) and QCD.

Current-quark masses in QCD are typically quoted at a scale of $\zeta_2 = 2\,\mathrm{GeV}$. A survey of available estimates indicates [181]

$$m(\zeta_2) = \frac{m_u(\zeta_2) + m_d(\zeta_2)}{2} = 3.5^{+0.7}_{-0.2}\,; \tag{E.1}$$

and this value compares well with that determined from a compilation of estimates using numerical simulations of lattice-regularised QCD [236]:

$$m(\zeta_2) = \frac{m_u(\zeta_2) + m_d(\zeta_2)}{2} = 3.4 \pm 0.2\,. \tag{E.2}$$

On the other hand, we have determined an average value of the u- and d-quark masses appropriate to our interaction that is $m(\zeta_H) := m = 7\,\mathrm{MeV}$.

The scale dependence of current-quark masses in QCD is expressed via

$$\frac{m(\zeta')}{m(\zeta)} = \left[\frac{\alpha_s(\zeta')}{\alpha_s(\zeta)}\right]^{\gamma_m} , \tag{E.3}$$

where $\alpha_s(\zeta)$ is the running coupling and $\gamma_m = 12/(33 - 2n_f)$, with n_f the number of active fermion flavours, is the mass anomalous dimension. Plainly, the running current-quark mass increases as the scale is decreased.

Using the one-loop running coupling, with $n_f = 4$ and $\Lambda_{\rm QCD} = 0.234\,{\rm GeV}$ [83], then

$$m(\zeta_H) \approx 2m(\zeta_2) \quad \text{for} \quad \zeta_H = 0.39 \pm 0.02\,{\rm GeV}\,; \tag{E.4}$$

and thus we have determined the model-scale. Given the arguments in Refs. [207, 262, 213], the outcome $\zeta_H \approx M$ is both internally consistent and reasonable. (We use the one-loop expression owing to the simplicity of our framework. Employing next-to-leading-order (NLO) evolution leads simply to a 25% increase in $\zeta_{\rm H}$ with no material phenomenological differences.)

APPENDIX F

SCALE DEPENDENCE OF THE TENSOR CHARGE

Whilst the values of the tensor charges are gauge- and Poincaré-invariant, they depend on the renormalisation scale, ζ, employed to compute the dressed inhomogeneous tensor vertex

$$\Gamma_{\mu\nu}(k;Q;\zeta) = S_1(k;Q;\zeta)\sigma_{\mu\nu} + \dots \,, \tag{F.1}$$

at zero total momentum, $Q = 0$. (k is the relative momentum.) The renormalisation constant $Z_T(\zeta,\Lambda)$ is the factor required as a multiplier for the Bethe-Salpeter equation inhomogeneity, $\sigma_{\mu\nu}$, in order to achieve $S_1(k^2 = \zeta^2; Q = 0; \zeta) = 1$.

At one-loop order in QCD [263]:

$$\Gamma_{\mu\nu}(k;Q;\zeta) \overset{\zeta^2 \gg \Lambda_{\rm QCD}^2}{=} \left[\frac{\alpha_S(\zeta_0^2)}{\alpha_S(\zeta^2)}\right]^{\eta_T} \Gamma_{\mu\nu}(k;Q;\zeta_0)\,, \tag{F.2}$$

where $\eta_T = (-1/3)\gamma_m$. The pointwise behaviour of $\Gamma_{\mu\nu}(k;Q=0;\zeta)$ is illustrated in Ref. [238].

Equation (F.2) entails

$$\delta q(\zeta) \overset{\zeta^2 \gg \Lambda_{\rm QCD}^2}{=} \left[\frac{\alpha_S(\zeta_0^2)}{\alpha_S(\zeta^2)}\right]^{\eta_T} \delta q(\zeta_0)\,, \tag{F.3}$$

and hence that δq decreases as ζ increases. It follows, for example and in connection with our analysis, that

$$\frac{\delta q(\zeta_2)}{\delta q(\zeta_H)} = 0.794 \pm 0.015\,, \tag{F.4}$$

with ζ_H drawn from Eq. (E.4).

APPENDIX G

EUCLIDEAN CONVENTIONS

The standard DSE treatment usually deals with Euclidean spacetime so it will be worthwhile to explain the conventions here. In our Euclidean formulation:

$$p \cdot q = \sum_{i=1}^{4} p_i q_i \,; \tag{G.1}$$

$$\{\gamma_\mu, \gamma_\nu\} = 2\,\delta_{\mu\nu}\,;\ \gamma_\mu^\dagger = \gamma_\mu\,;\ \sigma_{\mu\nu} = \frac{i}{2}[\gamma_\mu, \gamma_\nu]\,; \tag{G.2}$$

$$\mathrm{tr}\,[\gamma_5\gamma_\mu\gamma_\nu\gamma_\rho\gamma_\sigma] = -4\,\epsilon_{\mu\nu\rho\sigma}\,, \epsilon_{1234} = 1\,. \tag{G.3}$$

A positive energy spinor satisfies

$$\bar{u}(P,s)\,(i\gamma\cdot P + M) = 0 = (i\gamma\cdot P + M)\,u(P,s)\,, \tag{G.4}$$

where $s = \pm\frac{1}{2}$ is the spin label. The spinor is normalised:

$$\bar{u}(P,s)\,u(P,s) = 2M\,, \tag{G.5}$$

and may be expressed explicitly:

$$u(P,s) = \sqrt{M - i\mathcal{E}}\begin{pmatrix} \chi_s \\ \dfrac{\vec{\sigma}\cdot\vec{P}}{M - i\mathcal{E}}\chi_s \end{pmatrix}\,, \tag{G.6}$$

with $\mathcal{E} = i\sqrt{\vec{P}^2 + M^2}$,

$$\chi_+ = \begin{pmatrix} 1 \\ 0 \end{pmatrix} \,,\; \chi_- = \begin{pmatrix} 0 \\ 1 \end{pmatrix} \,. \tag{G.7}$$

For the free-particle spinor, $\bar{u}(P,s) = u(P,s)^\dagger \gamma_4$.

The spinor can be used to construct a positive energy projection operator:

$$\Lambda_+(P) := \frac{1}{2M} \sum_{s=\pm} u(P,s)\, \bar{u}(P,s) = \frac{1}{2M} \left(-i\gamma \cdot P + M\right). \tag{G.8}$$

A charge-conjugated Bethe-Salpeter amplitude is obtained via

$$\bar{\Gamma}(k;P) = C^\dagger\, \Gamma(-k;P)^{\mathrm{T}}\, C \,, \tag{G.9}$$

where "T" denotes a transposing of all matrix indices and $C = \gamma_2\gamma_4$ is the charge conjugation matrix, $C^\dagger = -C$. We note that

$$C^\dagger \gamma_\mu^{\mathrm{T}}\, C = -\gamma_\mu \,,\; [C, \gamma_5] = 0 \,. \tag{G.10}$$

APPENDIX H

MATRIX ELEMENTS OF TWO AND FOUR-FERMION OPERATORS

In this section we present matrix elements of two-fermion operators ($u^\dagger u$ and $d^\dagger d$) and four-fermion operators ($u^\dagger u d^\dagger d$) between nucleon states that are involved in the calculation of the PVDIS distribution functions. For this purpose let us consider two arbitrary components of proton light-cone wavefunction defined as the following:

$$\begin{aligned} |\psi_\alpha\rangle &\equiv \frac{\epsilon^{abc}}{\sqrt{6}}\int [DX_3]\psi_\alpha(1,2,3)u^\dagger_{a\lambda_1}(1)u^\dagger_{b\lambda_2}(2)d^\dagger_{c\lambda_3}(3)\,|0\rangle \\ |\psi_\beta\rangle &\equiv \frac{\epsilon^{abc}}{\sqrt{6}}\int [DX_3]\psi_\beta(1,2,3)u^\dagger_{a\lambda'_1}(1)u^\dagger_{b\lambda'_2}(2)d^\dagger_{c\lambda'_3}(3)\,|0\rangle \end{aligned} \tag{H.1}$$

It is straightforward to work out the matrix elements of the four-fermion operator between these two states (the symbol "1" denotes the four momentum $k_1 = (x_1 p^+, \vec{k}_{1\perp})$ which is given by $x_1 = 1 - x_q - x_l = 1 - x'_q - x'_l$ and $\vec{k}_{1\perp} = -\vec{q}_\perp - \vec{l}_\perp = -\vec{q}'_\perp - \vec{l}'_\perp$.):

$$\begin{aligned} &\langle\psi_\alpha|\, u^\dagger_{i\rho}(q)u_{i'\rho'}(q')d^\dagger_{j\lambda}(l)d_{j'\lambda'}(l')\,|\psi_\beta\rangle = \frac{32\pi^3}{3}(\delta_{ii'}\delta_{jj'} - \delta_{ij'}\delta_{i'j})\delta_{\lambda_3\lambda}\delta_{\lambda'_3\lambda'}\sqrt{x_q x_l x'_q x'_l} \\ &\delta(x_q + x_l - x'_q - x'_l)\delta^2(\vec{q}_\perp + \vec{l}_\perp - \vec{q'}_\perp - \vec{l'}_\perp)\int dx_1 d^2\vec{k}_{1\perp}\delta(1 - x_1 - x_q - x_l)\times \\ &\delta^2(\vec{k_1}_\perp + \vec{q}_\perp + \vec{l}_\perp)\times \\ &(\delta_{\lambda_1\rho}\delta_{\lambda_2\lambda'_2}\delta_{\rho'\lambda'_1}\psi^*_\alpha(q,1,l)\psi_\beta(q',1,l') + \delta_{\lambda_1\lambda'_2}\delta_{\lambda_2\rho}\delta_{\rho'\lambda'_1}\psi^*_\alpha(1,q,l)\psi_\beta(q',1,l') \\ &+\delta_{\lambda_1\rho}\delta_{\lambda_2\lambda'_1}\delta_{\rho'\lambda'_2}\psi^*_\alpha(q,1,l)\psi_\beta(1,q',l') + \delta_{\lambda\lambda'_1}\delta_{\lambda_2\rho}\delta_{\rho'\lambda'_2}\psi^*_\alpha(1,q,l)\psi_\beta(1,q',l')) \end{aligned} \tag{H.2}$$

and those for two-fermion operators:

$$\begin{aligned}\langle\psi_\alpha|\, d^\dagger_{j\lambda}(l)d_{j'\lambda'}(l')\,|\psi_\beta\rangle &= \frac{4}{3}x_l\delta(x_l-x'_l)\delta^2(\vec{l}_\perp-\vec{l}'_\perp)\delta_{\lambda_3\lambda}\delta_{\lambda'_3\lambda'}\delta_{jj'}\int dx_1dx_2d^2\vec{k}_{1\perp}d^2\vec{k}_{2\perp}\\ &\quad \delta(1-x_1-x_2-x_l)\delta^2(\vec{k}_{1\perp}+\vec{k}_{2\perp}+\vec{l}_\perp)(\delta_{\lambda_1\lambda'_1}\delta_{\lambda_2\lambda'_2}\psi_\beta(1,2,l)\\ &\quad +\delta_{\lambda_1\lambda'_2}\delta_{\lambda_2\lambda'_1}\psi_\beta(2,1,l))\psi^*_\alpha(1,2,l) \qquad \text{(H.3)}\end{aligned}$$

$$\begin{aligned}\langle\psi_\alpha|\, u^\dagger_{j\lambda}(l)u_{j'\lambda'}(l')\,|\psi_\beta\rangle &= \frac{4}{3}x_l\delta(x_l-x'_l)\delta^2(\vec{l}_\perp-\vec{l}'_\perp)\delta_{\lambda_3\lambda'_3}\delta_{jj'}\int dx_1dx_2d^2\vec{k}_{1\perp}d^2\vec{k}_{2\perp}\\ &\quad \delta(1-x_1-x_2-x_l)\delta^2(\vec{k}_{1\perp}+\vec{k}_{2\perp}+\vec{l}_\perp)\times\\ &\quad (\delta_{\lambda_1\lambda}\delta_{\lambda_2\lambda'_2}\delta_{\lambda'\lambda'_1}\psi^*_\alpha(l,1,2)\psi_\beta(l,1,2)\\ &\quad +\delta_{\lambda_1\lambda'_2}\delta_{\lambda_2\lambda}\delta_{\lambda'\lambda'_1}\psi^*_\alpha(1,l,2)\psi_\beta(l,1,2)\\ &\quad +\delta_{\lambda_1\lambda}\delta_{\lambda_2\lambda'_1}\delta_{\lambda'\lambda'_2}\psi^*_\alpha(l,1,2)\psi_\beta(1,l,2)\\ &\quad +\delta_{\lambda_1\lambda'_1}\delta_{\lambda_2\lambda}\delta_{\lambda'\lambda'_2}\psi^*_\alpha(1,l,2)\psi_\beta(1,l,2)) \qquad \text{(H.4)}\end{aligned}$$

APPENDIX I

COMPLETE FORMULAE FOR VARIOUS QUARK DISTRIBUTION FUNCTIONS IN TERMS OF PROTON WAVEFUNCTION AMPLITUDES

In this section we present explicit expressions needed to compute the quark PDFs and the twist-four distribution function.

The distribution functions $\tilde{Q}_p^{\pm}(x_B)$ in Eqs. (6.30) and (6.31) are expressed in terms of $\psi_{l_z}^{\pm}(q, l, q', l')$, which have the following expressions:

$$
\begin{aligned}
\psi^{+}_{l_z=0}(q,l,q',l') &= 2\psi^{(1,2)*}(q,1,l)\psi^{(1,2)}(q',1,l') && \text{(I.1)}\\
\psi^{-}_{l_z=0}(q,l,q',l') &= 2\{\psi^{(1,2)*}(1,q,l)\psi^{(1,2)}(1,q',l') + \psi^{(1,2)*}(q,l,1)\psi^{(1,2)}(q',l',1)\\
&\quad +\psi^{(1,2)*}(1,l,q)\psi^{(1,2)}(q',l',1) + \psi^{(1,2)*}(q,l,1)\psi^{(1,2)}(1,l',q')\\
&\quad +\psi^{(1,2)*}(1,l,q)\psi^{(1,2)}(1,l',q')\} && \text{(I.2)}\\
\psi^{+}_{l_z=1}(q,l,q',l') &= 2\psi^{(3,4)*}(1,q,l)\psi^{(3,4)}(1,q',l') && \text{(I.3)}\\
\psi^{-}_{l_z=1}(q,l,q',l') &= 2\{\psi^{(3,4)*}(q,1,l)\psi^{(3,4)}(q',1,l') + \psi^{(3,4)*}(l,q,1)\psi^{(3,4)}(l',q',1)\\
&\quad +\psi^{(3,4)*}(l,1,q)\psi^{(3,4)}(l',q',1) + \psi^{(3,4)*}(l,q,1)\psi^{(3,4)}(l',1,q')\\
&\quad +\psi^{(3,4)*}(l,1,q)\psi^{(3,4)}(l',1,q')\} && \text{(I.4)}\\
\psi^{+}_{l_z=-1}(q,l,q',l') &= 2\{\psi^{(5,5)*}(q,1,l)\psi^{(5,5)}(q',1,l') + \psi^{(5,5)*}(1,q,l)\psi^{(5,5)}(q',1,l')\\
&\quad +\psi^{(5,5)*}(q,1,l)\psi^{(5,5)}(1,q',l')\\
&\quad +\psi^{(5,5)*}(1,q,l)\psi^{(5,5)}(1,q',l')\} && \text{(I.5)}\\
\psi^{-}_{l_z=-1}(q,l,q',l') &= 0 && \text{(I.6)}\\
\psi^{+}_{l_z=2}(q,l,q',l') &= 2\{\psi^{(6,6)*}(q,1,l)\psi^{(6,6)}(q',1,l') + \psi^{(6,6)*}(1,q,l)\psi^{(6,6)}(q',1,l')\\
&\quad +\psi^{(6,6)*}(q,1,l)\psi^{(6,6)}(1,q',l')\\
&\quad +\psi^{(6,6)*}(1,q,l)\psi^{(6,6)}(1,q',l')\} && \text{(I.7)}\\
\psi^{-}_{l_z=2}(q,l,q',l') &= 0 && \text{(I.8)}
\end{aligned}
$$

The definitions of $\psi^{(i,j)}$ are the following:

$$
\begin{aligned}
\psi^{(1,2)}(1,2,3) &= \psi^{(1)}(1,2,3) + i(k_1^x k_2^y - k_1^y k_2^x)\psi^{(2)}(1,2,3)\\
\psi^{(3,4)}(1,2,3) &= k^{+}_{1\perp}\psi^{(3)}(1,2,3) + k^{+}_{2\perp}\psi^{(4)}(1,2,3)\\
\psi^{(5,5)}(1,2,3) &= -k^{-}_{2\perp}\psi^{(5)}(1,2,3) + k^{-}_{3\perp}\psi^{(5)}(1,3,2)\\
\psi^{(6,6)}(1,2,3) &= k^{+}_{1\perp}(k^{+}_{2\perp}\psi^{(6)}(1,3,2) - k^{+}_{3\perp}\psi^{(6)}(1,2,3)) && \text{(I.9)}
\end{aligned}
$$

On the other hand, the quark distribution functions in (6.28) are given in terms of $A^{l_z}(q,1,2)$, which look like the following:

$$\begin{aligned} A^{l_z=0}(q,1,2) &= \psi^{(1,2)*}(q,1,2)\psi^{(1,2)}(q,1,2) + 2\psi^{(1,2)*}(1,q,2)\psi^{(1,2)}(1,q,2) \\ &+\psi^{(1,2)*}(q,2,1)\psi^{(1,2)}(q,2,1) + \psi^{(1,2)*}(1,2,q)\psi^{(1,2)}(q,2,1) \\ &+\psi^{(1,2)*}(q,2,1)\psi^{(1,2)}(1,2,q) + 2\psi^{(1,2)*}(1,2,q)\psi^{(1,2)}(1,2,q) \\ &+\psi^{(1,2)*}(1,q,2)\psi^{(1,2)}(2,q,1) \end{aligned} \tag{I.10}$$

$$\begin{aligned} A^{l_z=1}(q,1,2) &= 2\psi^{(3,4)*}(q,1,2)\psi^{(3,4)}(q,1,2) + \psi^{(3,4)*}(1,q,2)\psi^{(3,4)}(1,q,2) \\ &+\psi^{(3,4)*}(2,q,1)\psi^{(3,4)}(2,q,1) + \psi^{(3,4)*}(2,1,q)\psi^{(3,4)}(2,q,1) \\ &+\psi^{(3,4)*}(2,q,1)\psi^{(3,4)}(2,1,q) + \psi^{(3,4)*}(2,1,q)\psi^{(3,4)}(2,1,q) \\ &+\psi^{(3,4)*}(1,2,q)\psi^{(3,4)}(1,2,q) \\ &+\psi^{(3,4)*}(q,1,2)\psi^{(3,4)}(q,2,1) \end{aligned} \tag{I.11}$$

$$\begin{aligned} A^{l_z=-1}(q,1,2) &= \psi^{(5,5)*}(q,1,2)\psi^{(5,5)}(q,1,2) + \psi^{(5,5)*}(1,q,2)\psi^{(5,5)}(q,1,2) \\ &+\psi^{(5,5)*}(q,1,2)\psi^{(5,5)}(1,q,2) + \psi^{(5,5)*}(1,q,2)\psi^{(5,5)}(1,q,2) \\ &+\psi^{(5,5)*}(1,2,q)\psi^{(5,5)}(1,2,q) \\ &+\psi^{(5,5)*}(1,2,q)\psi^{(5,5)}(2,1,q) \end{aligned} \tag{I.12}$$

$$\begin{aligned} A^{l_z=2}(q,1,2) &= \psi^{(6,6)*}(q,1,2)\psi^{(6,6)}(q,1,2) + \psi^{(6,6)*}(1,q,2)\psi^{(6,6)}(q,1,2) \\ &+\psi^{(6,6)*}(q,1,2)\psi^{(6,6)}(1,q,2) + \psi^{(6,6)*}(1,q,2)\psi^{(6,6)}(1,q,2) \\ &+\psi^{(6,6)*}(1,2,q)\psi^{(6,6)}(1,2,q) \\ &+\psi^{(6,6)*}(1,2,q)\psi^{(6,6)}(2,1,q) \end{aligned} \tag{I.13}$$

with $q = (x_B p^+, \vec{q}_\perp)$, $x_2 = 1 - x_B - x_1$ and $\vec{k}_{2\perp} = -\vec{q}_\perp - \vec{k}_{1\perp}$.

APPENDIX J

VANISHING ONE-LOOP DIAGRAMS IN THE CALCULATIONS OF SM NUCLEON EDM

Here I will show that all 1-loop diagrams, other than those in Fig. 5.1, do not give rise to the CKM-induced SM nucleon EDM, at least at leading order in the HB-expansion.

All other possible 1-loop diagrams beside those I have calculated are summarized in Fig. J.1. Since the weak Lagrangian used in my work does not involve covariant derivatives of baryon fields, any baryon-photon coupling term has to arise from the ordinary P and T-conserving Lagrangian.

For Fig. 4(a), the photon vertex must arise from Dirac coupling since an MDM coupling is suppressed by $(1/m_N)^2$ as pointed out in [185]. Since the Dirac coupling is independent of the photon momentum q, one can define loop momenta in a way such that the dependence of q only appears in the baryon propagator. However, using the on-shell condition $v \cdot q = 0$, the baryon propagator is actually q-independent and therefore so is the whole diagram. As a result, Fig. 4(a) cannot generate an EDM that is linear in q.

For Fig. 4(b), at leading order in the HB-expansion the $BB'\phi\gamma$ vertex is proportional to S^μ, so it cannot generate an EDM because the latter is proportional to v^μ which is perpendicular to S^μ.

For Fig. 4(c), first I note that the $BB'\phi\phi'$ vertex cannot come from the D or F-term of the ordinary chiral Lagrangian because that would violate parity. Therefore it can only come from $\mathcal{L}_w^{(s)}$. In this case, it can only be parity-conserving and

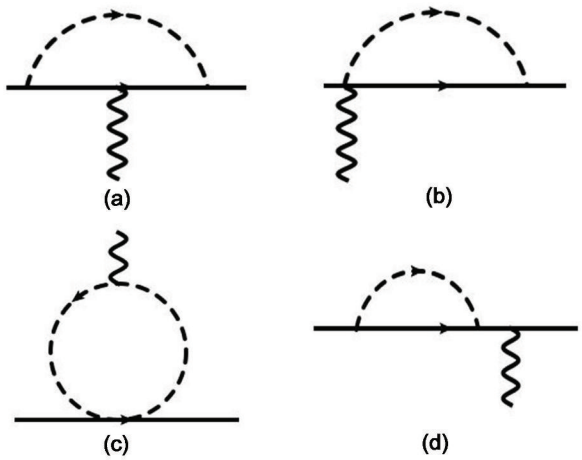

Figure J.1. 1-loop diagrams that vanish at LO HBchPT. The weak vertices could be placed at any allowed position and therefore are not explicitly shown.

time reversal-conserving (PCTC), or parity-conserving and time reversal-violating (PCTV). So in order to get an EDM which is PVTV, one needs to place another PVTC or PVTV vertex in some other part of the diagram. This cannot be done because all $\phi\phi'$ and $\phi\phi'\gamma$ operators I have are parity-conserving.

For Fig. 4(d), one could generate an EDM by coupling the resulting complex mass term of the baryon to its MDM. But again this contribution is suppressed by $(1/m_N)^2$ and should be discarded at leading order in the HB-expansion.

BIBLIOGRAPHY

[1] G. Arnison *et al.* [UA1 Collaboration], Phys. Lett. B **122** (1983) 103.

[2] M. Banner *et al.* [UA2 Collaboration], Phys. Lett. B **122** (1983) 476.

[3] J. E. Augustin *et al.* [SLAC-SP-017 Collaboration], Phys. Rev. Lett. **33** (1974) 1406 [Adv. Exp. Phys. **5** (1976) 141].

[4] J. J. Aubert *et al.* [E598 Collaboration], Phys. Rev. Lett. **33** (1974) 1404.

[5] S. W. Herb, D. C. Hom, L. M. Lederman, J. C. Sens, H. D. Snyder, J. K. Yoh, J. A. Appel and B. C. Brown *et al.*, Phys. Rev. Lett. **39** (1977) 252.

[6] F. Abe *et al.* [CDF Collaboration], Phys. Rev. Lett. **74** (1995) 2626 [hep-ex/9503002].

[7] S. Abachi *et al.* [D0 Collaboration], Phys. Rev. Lett. **74** (1995) 2422 [hep-ex/9411001].

[8] G. Aad *et al.* [ATLAS Collaboration], Phys. Lett. B **716** (2012) 1 [arXiv:1207.7214 [hep-ex]].

[9] S. Chatrchyan *et al.* [CMS Collaboration], Phys. Lett. B **716** (2012) 30 [arXiv:1207.7235 [hep-ex]].

[10] R. Davis, Jr., D. S. Harmer and K. C. Hoffman, Phys. Rev. Lett. **20** (1968) 1205.

[11] Q. R. Ahmad *et al.* [SNO Collaboration], Phys. Rev. Lett. **87** (2001) 071301 [nucl-ex/0106015].

[12] V. C. Rubin and W. K. Ford, Jr., Astrophys. J. **159** (1970) 379.

[13] V. C. Rubin, N. Thonnard and W. K. Ford, Jr., Astrophys. J. **238** (1980) 471.

[14] D. Clowe, M. Bradac, A. H. Gonzalez, M. Markevitch, S. W. Randall, C. Jones and D. Zaritsky, Astrophys. J. **648** (2006) L109 [astro-ph/0608407].

[15] E. Komatsu *et al.* [WMAP Collaboration], Astrophys. J. Suppl. **192** (2011) 18 [arXiv:1001.4538 [astro-ph.CO]].

[16] P. A. R. Ade *et al.* [Planck Collaboration], Astron. Astrophys. **571** (2014) A16 [arXiv:1303.5076 [astro-ph.CO]].

[17] D. Hanneke, S. F. Hoogerheide and G. Gabrielse, Phys. Rev. A **83** (2011) 052122 [arXiv:1009.4831 [physics.atom-ph]].

[18] T. Aoyama, M. Hayakawa, T. Kinoshita and M. Nio, Phys. Rev. Lett. **109** (2012) 111807 [arXiv:1205.5368 [hep-ph]].

[19] C. Y. Prescott, W. B. Atwood, R. L. Cottrell, H. C. DeStaebler, E. L. Garwin, A. Gonidec, R. H. Miller and L. S. Rochester *et al.*, Phys. Lett. B **77** (1978) 347.

[20] S. Schael *et al.* [ALEPH and DELPHI and L3 and OPAL and SLD and LEP Electroweak Working Group and SLD Electroweak Group and SLD Heavy Flavour Group Collaborations], Phys. Rept. **427** (2006) 257 [hep-ex/0509008].

[21] F. Jegerlehner and A. Nyffeler, Phys. Rept. **477** (2009) 1 [arXiv:0902.3360 [hep-ph]].

[22] C. S. Wu, E. Ambler, R. W. Hayward, D. D. Hoppes and R. P. Hudson, Phys. Rev. **105** (1957) 1413.

[23] J. H. Christenson, J. W. Cronin, V. L. Fitch and R. Turlay, Phys. Rev. Lett. **13** (1964) 138.

[24] M. Kobayashi and T. Maskawa, Prog. Theor. Phys. **49** (1973) 652.

[25] Y. Fukuda *et al.* [Super-Kamiokande Collaboration], Phys. Rev. Lett. **81** (1998) 1562 [hep-ex/9807003].

[26] F. P. An *et al.* [Daya Bay Collaboration], Phys. Rev. Lett. **108** (2012) 171803 [arXiv:1203.1669 [hep-ex]].

[27] J. K. Ahn *et al.* [RENO Collaboration], Phys. Rev. Lett. **108** (2012) 191802 [arXiv:1204.0626 [hep-ex]].

[28] S. Weinberg, "The quantum theory of fields. Vol. 2: Modern applications, Cambridge, UK: Univ. Pr. (1996) 489 p

[29] B. Grzadkowski, M. Iskrzynski, M. Misiak and J. Rosiek, JHEP **1010** (2010) 085 [arXiv:1008.4884 [hep-ph]].

[30] D. J. Gross and F. Wilczek, Phys. Rev. Lett. **30** (1973) 1343.

[31] H. D. Politzer, Phys. Rev. Lett. **30** (1973) 1346.

[32] K. G. Wilson, Phys. Rev. D **10** (1974) 2445.

[33] J. H. Smith, E. M. Purcell and N. F. Ramsey, Phys. Rev. **108** (1957) 120.

[34] G. 't Hooft, Phys. Rev. Lett. **37** (1976) 8.

[35] R. D. Peccei and H. R. Quinn, Phys. Rev. Lett. **38** (1977) 1440.

[36] A. E. Nelson, Phys. Lett. B **136** (1984) 387.

[37] S. M. Barr, Phys. Rev. Lett. **53** (1984) 329.

[38] A. D. Sakharov, Pisma Zh. Eksp. Teor. Fiz. **5** (1967) 32 [JETP Lett. **5** (1967) 24] [Sov. Phys. Usp. **34** (1991) 392] [Usp. Fiz. Nauk **161** (1991) 61].

[39] M. B. Gavela, P. Hernandez, J. Orloff and O. Pene, Mod. Phys. Lett. A **9** (1994) 795 [hep-ph/9312215, hep-ph/9312215].

[40] P. Huet and E. Sather, Phys. Rev. D **51** (1995) 379 [hep-ph/9404302].

[41] see e.g. M. Gonzlez-Alonso and J. Martin Camalich, Phys. Rev. Lett. **112** (2014) 4, 042501 [arXiv:1309.4434 [hep-ph]] and the references therein.

[42] P. Langacker, "Precision tests of the standard electroweak model," Singapore, Singapore: World Scientific (1995) 1008 p. (Advanced series on directions in high energy physics: 14)

[43] J. D. Jackson, S. B. Treiman and H. W. Wyld, Phys. Rev. **106** (1957) 517.

[44] H. P. Mumm, T. E. Chupp, R. L. Cooper, K. P. Coulter, S. J. Freedman, B. K. Fujikawa, A. Garcia and G. L. Jones *et al.*, Phys. Rev. Lett. **107** (2011) 102301 [arXiv:1104.2778 [nucl-ex]].

[45] M. Anselmino, M. Boglione, U. D'Alesio, S. Melis, F. Murgia and A. Prokudin, Phys. Rev. D **87** (2013) 094019 [arXiv:1303.3822 [hep-ph]].

[46] P. Bosted et al., Jefferson-Lab proposal PR-09-012, *Precision Measurement of Parity-violation in Deep Inelastic Scattering Over a Broad Kinematic Range*, http://hallaweb.jlab.org/collab/PAC/PAC34/PR-09-012-pvdis.pdf (unpublished).

[47] S. Mantry, M. J. Ramsey-Musolf and G. F. Sacco, Phys. Rev. C **82** (2010) 065205 [arXiv:1004.3307 [hep-ph]].

[48] A. V. Belitsky, A. Manashov and A. Schafer, Phys. Rev. D **84** (2011) 014010 [arXiv:1104.0511 [hep-ph]].

[49] E. M. Purcell and N. F. Ramsey, Phys. Rev. **78** (1950) 807. doi:10.1103/PhysRev.78.807

[50] A. G. Cohen, D. B. Kaplan and A. E. Nelson, Ann. Rev. Nucl. Part. Sci. **43** (1993) 27 doi:10.1146/annurev.ns.43.120193.000331 [hep-ph/9302210].

[51] M. Trodden, Rev. Mod. Phys. **71** (1999) 1463 doi:10.1103/RevModPhys.71.1463 [hep-ph/9803479].

[52] D. E. Morrissey and M. J. Ramsey-Musolf, New J. Phys. **14**, 125003 (2012).

[53] P. G. Harris *et al.*, Phys. Rev. Lett. **82** (1999) 904. doi:10.1103/PhysRevLett.82.904

[54] S. K. Lamoreaux and R. Golub, J. Phys. G **36** (2009) 104002. doi:10.1088/0954-3899/36/10/104002

[55] M. Pospelov and A. Ritz, Annals Phys. **318**, 119 (2005).

[56] M. Ramsey-Musolf and S. Su, Phys. Rept. **456**, 1 (2008).

[57] V. Cirigliano, Y. Li, S. Profumo and M. J. Ramsey-Musolf, JHEP **1001** (2010) 002 doi:10.1007/JHEP01(2010)002 [arXiv:0910.4589 [hep-ph]].

[58] Y. Li, S. Profumo and M. Ramsey-Musolf, JHEP **1008** (2010) 062 doi:10.1007/JHEP08(2010)062 [arXiv:1006.1440 [hep-ph]].

[59] J. Kozaczuk, S. Profumo, M. J. Ramsey-Musolf and C. L. Wainwright, Phys. Rev. D **86** (2012) 096001 doi:10.1103/PhysRevD.86.096001 [arXiv:1206.4100 [hep-ph]].

[60] M. B. Hecht and B. H. J. McKellar, Phys. Rev. C **57** (1998) 2638 doi:10.1103/PhysRevC.57.2638 [hep-ph/9704326].

[61] M. B. Hecht and B. H. J. McKellar, Phys. Rev. C **60** (1999) 065202 doi:10.1103/PhysRevC.60.065202 [hep-ph/9906246].

[62] M. Pospelov and A. Ritz, Phys. Lett. B **471** (2000) 388 doi:10.1016/S0370-2693(99)01343-X [hep-ph/9910273].

[63] S. Weinberg, Phys. Rev. Lett. **63** (1989) 2333. doi:10.1103/PhysRevLett.63.2333

[64] L. X. Gutiérrez-Guerrero, A. Bashir, I. C. Cloët and C. D. Roberts, Phys. Rev. C **81**, 065202 (2010).

[65] H. L. L. Roberts, C. D. Roberts, A. Bashir, L. X. Gutiérrez-Guerrero and P. C. Tandy, Phys. Rev. C **82**, 065202 (2010).

[66] H. L. L. Roberts, A. Bashir, L. X. Gutiérrez-Guerrero, C. D. Roberts and D. J. Wilson, Phys. Rev. C **83**, 065206 (2011).

[67] H. L. L. Roberts, L. Chang, I. C. Cloët and C. D. Roberts, Few Body Syst. **51**, 1 (2011).

[68] D. J. Wilson, I. C. Cloët, L. Chang and C. D. Roberts, Phys. Rev. C **85**, 025205 (2012).

[69] C. Chen, L. Chang, C. D. Roberts, S.-L. Wan and D. J. Wilson, Few Body Syst. **53**, 293 (2012).

[70] L. Chang, C. D. Roberts and P. C. Tandy, Chin. J. Phys. **49**, 955 (2011).

[71] A. Bashir *et al.*, Commun. Theor. Phys. **58**, 79 (2012).

[72] C. D. Roberts, arXiv:1203.5341 [nucl-th].

[73] P. Jain and H. J. Munczek, Phys. Rev. D **48** (1993) 5403 doi:10.1103/PhysRevD.48.5403 [hep-ph/9307221].

[74] P. Maris and C. D. Roberts, Phys. Rev. C **56** (1997) 3369 doi:10.1103/PhysRevC.56.3369 [nucl-th/9708029].

[75] P. Maris and C. D. Roberts, Int. J. Mod. Phys. E **12** (2003) 297 doi:10.1142/S0218301303001326 [nucl-th/0301049].

[76] H. J. Munczek, Phys. Rev. D **52**, 4736 (1995).

[77] A. Bender, C. D. Roberts and L. von Smekal, Phys. Lett. B **380**, 7 (1996).

[78] P. Maris, A. Raya, C. D. Roberts and S. M. Schmidt, Eur. Phys. J. A **18** (2003) 231 doi:10.1140/epja/i2002-10206-6 [nucl-th/0208071].

[79] G. Eichmann, R. Alkofer, I. C. Cloet, A. Krassnigg and C. D. Roberts, Phys. Rev. C **77** (2008) 042202 doi:10.1103/PhysRevC.77.042202 [arXiv:0802.1948 [nucl-th]].

[80] P. Maris and P. C. Tandy, Phys. Rev. C **60** (1999) 055214 doi:10.1103/PhysRevC.60.055214 [nucl-th/9905056].

[81] M. S. Bhagwat and P. Maris, Phys. Rev. C **77** (2008) 025203 doi:10.1103/PhysRevC.77.025203 [nucl-th/0612069].

[82] S. x. Qin, L. Chang, Y. x. Liu, C. D. Roberts and D. J. Wilson, Phys. Rev. C **85** (2012) 035202 doi:10.1103/PhysRevC.85.035202 [arXiv:1109.3459 [nucl-th]].

[83] S.-X. Qin, L. Chang, Y.-X. Liu, C. D. Roberts and D. J. Wilson, Phys. Rev. C **84**, 042202(R) (2011).

[84] P. Maris and C. D. Roberts, Phys. Rev. C **58** (1998) 3659 doi:10.1103/PhysRevC.58.3659 [nucl-th/9804062].

[85] P. Maris and P. C. Tandy, Phys. Rev. C **62** (2000) 055204 doi:10.1103/PhysRevC.62.055204 [nucl-th/0005015].

[86] P. Maris and P. C. Tandy, Phys. Rev. C **65** (2002) 045211 doi:10.1103/PhysRevC.65.045211 [nucl-th/0201017].

[87] M. S. Bhagwat, L. Chang, Y. X. Liu, C. D. Roberts and P. C. Tandy, Phys. Rev. C **76** (2007) 045203 doi:10.1103/PhysRevC.76.045203 [arXiv:0708.1118 [nucl-th]].

[88] G. Eichmann, I. C. Cloet, R. Alkofer, A. Krassnigg and C. D. Roberts, Phys. Rev. C **79** (2009) 012202 doi:10.1103/PhysRevC.79.012202 [arXiv:0810.1222 [nucl-th]].

[89] G. Eichmann, PoS QCD **-TNT-II** (2011) 017 [arXiv:1112.4888 [hep-ph]].

[90] G. Eichmann and C. S. Fischer, Eur. Phys. J. A **48** (2012) 9 doi:10.1140/epja/i2012-12009-6 [arXiv:1111.2614 [hep-ph]].

[91] G. Eichmann, Phys. Rev. D **84**, 014014 (2011).

[92] M. S. Bhagwat, A. Krassnigg, P. Maris and C. D. Roberts, Eur. Phys. J. A **31** (2007) 630 doi:10.1140/epja/i2006-10271-9 [nucl-th/0612027].

[93] A. C. Aguilar, D. Binosi and J. Papavassiliou, JHEP **07**, 002 (2010).

[94] P. Boucaud *et al.*, Phys. Rev. D **82**, 054007 (2010).

[95] Y. Nambu and G. Jona-Lasinio, Phys. Rev. **122**, 345 (1961).

[96] D. Ebert, T. Feldmann and H. Reinhardt, Phys. Lett. B **388**, 154 (1996).

[97] C. D. Roberts, A. G. Williams and G. Krein, Int. J. Mod. Phys. A **7**, 5607 (1992).

[98] S. J. Brodsky, C. D. Roberts, R. Shrock and P. C. Tandy, Phys. Rev. C **82** (2010) 022201 doi:10.1103/PhysRevC.82.022201 [arXiv:1005.4610 [nucl-th]].

[99] L. Chang, C. D. Roberts and P. C. Tandy, Phys. Rev. C **85** (2012) 012201 doi:10.1103/PhysRevC.85.012201 [arXiv:1109.2903 [nucl-th]].

[100] S. J. Brodsky, C. D. Roberts, R. Shrock and P. C. Tandy, Phys. Rev. C **85** (2012) 065202 doi:10.1103/PhysRevC.85.065202 [arXiv:1202.2376 [nucl-th]].

[101] K. Nakamura *et al.* [Particle Data Group Collaboration], J. Phys. G **37** (2010) 075021. doi:10.1088/0954-3899/37/7A/075021

[102] L. Chang, Y. X. Liu and C. D. Roberts, Phys. Rev. Lett. **106** (2011) 072001 doi:10.1103/PhysRevLett.106.072001 [arXiv:1009.3458 [nucl-th]].

[103] M. S. Bhagwat, M. A. Pichowsky, C. D. Roberts and P. C. Tandy, Phys. Rev. C **68** (2003) 015203 doi:10.1103/PhysRevC.68.015203 [nucl-th/0304003].

[104] P. O. Bowman, U. M. Heller, D. B. Leinweber, M. B. Parappilly, A. G. Williams and J. b. Zhang, Phys. Rev. D **71** (2005) 054507 doi:10.1103/PhysRevD.71.054507 [hep-lat/0501019].

[105] M. S. Bhagwat and P. C. Tandy, AIP Conf. Proc. **842** (2006) 225 doi:10.1063/1.2220232 [nucl-th/0601020].

[106] M. S. Bhagwat, I. C. Cloet and C. D. Roberts, arXiv:0710.2059 [nucl-th].

[107] L. Chang and C. D. Roberts, Phys. Rev. C **85** (2012) 052201 doi:10.1103/PhysRevC.85.052201 [arXiv:1104.4821 [nucl-th]].

[108] S. Weinberg, Phys. Rev. Lett. **37** (1976) 657. doi:10.1103/PhysRevLett.37.657

[109] M. B. Hecht, C. D. Roberts and S. M. Schmidt, Phys. Rev. **C64**, 025204 (2001).

[110] P. K. Pallaghy. CP violation, PhD thesis, University of Melbourne, 1996.

[111] F. T. Hawes and M. A. Pichowsky, Phys. Rev. C **59** (1999) 1743 doi:10.1103/PhysRevC.59.1743 [nucl-th/9806025].

[112] J. P. B. C. de Melo and T. Frederico, Phys. Rev. C **55** (1997) 2043 doi:10.1103/PhysRevC.55.2043 [nucl-th/9706032].

[113] H. M. Choi and C. R. Ji, Phys. Rev. D **70** (2004) 053015 doi:10.1103/PhysRevD.70.053015 [hep-ph/0402114].

[114] A. Samsonov, JHEP **0312** (2003) 061 doi:10.1088/1126-6708/2003/12/061 [hep-ph/0308065].

[115] J. E. Kim, AIP Conf. Proc. **1200** (2010) 83 doi:10.1063/1.3327743 [arXiv:0909.3908 [hep-ph]].

[116] M. R. Buckley and M. J. Ramsey-Musolf, Phys. Lett. B **712**, 261 (2012) [arXiv:1203.1102 [hep-ph]].

[117] M. Gonzlez-Alonso and M. J. Ramsey-Musolf, Phys. Rev. D **87** (2013) 5, 055013 doi:10.1103/PhysRevD.87.055013 [arXiv:1211.4581 [hep-ph]].

[118] A. Kurylov, M. J. Ramsey-Musolf and S. Su, Phys. Lett. B **582**, 222 (2004) [hep-ph/0307270].

[119] see, e.g. R.L. Jaffe in *Lectures on QCD: Applications*, (Springer, Germany, 1997).

[120] P. Castorina and P. J. Mulders, Phys. Rev. D **31**, 2760 (1985).

[121] T. Hobbs and W. Melnitchouk, Phys. Rev. D **77** (2008) 114023 doi:10.1103/PhysRevD.77.114023 [arXiv:0801.4791 [hep-ph]].

[122] R. N. Cahn and F. J. Gilman, Phys. Rev. D **17**, 1313 (1978).

[123] M. Burkardt and H. BC, Phys. Rev. D **79** (2009) 071501 doi:10.1103/PhysRevD.79.071501 [arXiv:0812.1605 [hep-ph]].

[124] S. Bashinsky and R. L. Jaffe, Nucl. Phys. B **536** (1998) 303 doi:10.1016/S0550-3213(98)00559-8 [hep-ph/9804397].

[125] X. Ji, X. Xiong and F. Yuan, Phys. Rev. D **88** (2013) 1, 014041 doi:10.1103/PhysRevD.88.014041 [arXiv:1207.5221 [hep-ph]].

[126] X. D. Ji, Phys. Rev. Lett. **78** (1997) 610 doi:10.1103/PhysRevLett.78.610 [hep-ph/9603249].

[127] X. Ji, X. Xiong and F. Yuan, Phys. Rev. Lett. **109** (2012) 152005 doi:10.1103/PhysRevLett.109.152005 [arXiv:1202.2843 [hep-ph]].

[128] J. Ashman *et al.* [European Muon Collaboration], Nucl. Phys. B **328** (1989) 1. doi:10.1016/0550-3213(89)90089-8

[129] J. R. Ellis and R. L. Jaffe, Phys. Rev. D **9** (1974) 1444 [Phys. Rev. D **10** (1974) 1669]. doi:10.1103/PhysRevD.10.1669.2, 10.1103/PhysRevD.9.1444

[130] B. Pasquini and F. Yuan, Phys. Rev. D **81** (2010) 114013 doi:10.1103/PhysRevD.81.114013 [arXiv:1001.5398 [hep-ph]].

[131] B. Pasquini, S. Cazzaniga and S. Boffi, Phys. Rev. D **78** (2008) 034025 doi:10.1103/PhysRevD.78.034025 [arXiv:0806.2298 [hep-ph]].

[132] M. Anselmino, M. Boglione, U. D'Alesio, S. Melis, F. Murgia, E. R. Nocera and A. Prokudin, Phys. Rev. D **83** (2011) 114019 doi:10.1103/PhysRevD.83.114019 [arXiv:1101.1011 [hep-ph]].

[133] J. D. Bjorken, Phys. Rev. D **18** (1978) 3239. doi:10.1103/PhysRevD.18.3239

[134] L. Wolfenstein, Nucl. Phys. B **146** (1978) 477. doi:10.1016/0550-3213(78)90080-9

[135] I. I. Balitsky and V. M. Braun, Nucl. Phys. B **311** (1989) 541. doi:10.1016/0550-3213(89)90168-5

[136] X. d. Ji, J. P. Ma and F. Yuan, Nucl. Phys. B **652** (2003) 383 doi:10.1016/S0550-3213(03)00010-5 [hep-ph/0210430].

[137] F. Schlumpf, Phys. Rev. D **47** (1993) 4114 [Phys. Rev. D **49** (1994) 6246] doi:10.1103/PhysRevD.49.6246, 10.1103/PhysRevD.47.4114 [hep-ph/9212250].

[138] S. Boffi, B. Pasquini and M. Traini, Nucl. Phys. B **649** (2003) 243 doi:10.1016/S0550-3213(02)01016-7 [hep-ph/0207340].

[139] M. Anselmino, M. Boglione, U. D'Alesio, S. Melis, F. Murgia and A. Prokudin, arXiv:1107.4446 [hep-ph].

[140] W. B. Atwood and G. B. West, Phys. Rev. D **7** (1973) 773. doi:10.1103/PhysRevD.7.773

[141] T. Hahn, Comput. Phys. Commun. **168** (2005) 78 doi:10.1016/j.cpc.2005.01.010 [hep-ph/0404043].

[142] S. Bethke, Eur. Phys. J. C **64** (2009) 689 doi:10.1140/epjc/s10052-009-1173-1 [arXiv:0908.1135 [hep-ph]].

[143] D. Boer and P. J. Mulders, Phys. Rev. D **57** (1998) 5780 doi:10.1103/PhysRevD.57.5780 [hep-ph/9711485].

[144] X. d. Ji, J. P. Ma and F. Yuan, Eur. Phys. J. C **33** (2004) 75 doi:10.1140/epjc/s2003-01563-y [hep-ph/0304107].

[145] A. Accardi, M. E. Christy, C. E. Keppel, P. Monaghan, W. Melnitchouk, J. G. Morfin and J. F. Owens, Phys. Rev. D **81** (2010) 034016 doi:10.1103/PhysRevD.81.034016 [arXiv:0911.2254 [hep-ph]].

[146] J. Baron *et al.* [ACME Collaboration], Science **343** (2014) 6168, 269 [arXiv:1310.7534 [physics.atom-ph]].

[147] W. C. Griffith, M. D. Swallows, T. H. Loftus, M. V. Romalis, B. R. Heckel and E. N. Fortson, Phys. Rev. Lett. **102** (2009) 101601.

[148] C. A. Baker, D. D. Doyle, P. Geltenbort, K. Green, M. G. D. van der Grinten, P. G. Harris, P. Iaydjiev and S. N. Ivanov *et al.*, Phys. Rev. Lett. **97** (2006) 131801 [hep-ex/0602020].

[149] I. Altarev, G. Ban, G. Bison, K. Bodek, M. Burghoff, M. Cvijovic, M. Daum and P. Fierlinger *et al.*, Nucl. Instrum. Meth. A **611** (2009) 133.

[150] A. P. Serebrov et al.. 2009. Nucl.Instrum.Meth.,A611,263-266

[151] K. Kumar, Z. -T. Lu and M. J. Ramsey-Musolf, arXiv:1312.5416 [hep-ph].

[152] A. Lehrach, B. Lorentz, W. Morse, N. Nikolaev and F. Rathmann, arXiv:1201.5773 [hep-ex].

[153] Y. K. Semertzidis [Storage Ring EDM Collaboration], arXiv:1110.3378 [physics.acc-ph].

[154] M. Pospelov, talk given at the Winter Workshop on Electric Dipole Moment (EDMs13), February 13-15, 2013, Fermilab (unpublished).

[155] E. P. Shabalin, Sov. J. Nucl. Phys. **32** (1980) 228 [Yad. Fiz. **32** (1980) 443].

[156] A. Czarnecki and B. Krause, Phys. Rev. Lett. **78** (1997) 4339 [hep-ph/9704355].

[157] G. Barton and E. D. White, Phys. Rev. **184** (1969) 1660.

[158] M. B. Gavela, A. Le Yaouanc, L. Oliver, O. Pene, J. C. Raynal and T. N. Pham, Phys. Lett. B **109** (1982) 215.

[159] M. B. Gavela, A. Le Yaouanc, L. Oliver, O. Pene, J. C. Raynal and T. N. Pham, Phys. Lett. B **109** (1982) 83.

[160] I. B. Khriplovich and A. R. Zhitnitsky, Phys. Lett. B **109** (1982) 490.

[161] X. -G. He, B. H. J. McKellar and S. Pakvasa, Int. J. Mod. Phys. A **4** (1989) 5011 [Erratum-ibid. A **6** (1991) 1063].

[162] T. Mannel and N. Uraltsev, Phys. Rev. D **85** (2012) 096002 [arXiv:1202.6270 [hep-ph]].

[163] E. E. Jenkins and A. V. Manohar, Phys. Lett. B **255** (1991) 558.

[164] J. Engel, M. J. Ramsey-Musolf and U. van Kolck, Prog. Part. Nucl. Phys. **71** (2013) 21 [arXiv:1303.2371 [nucl-th]].

[165] E. E. Jenkins, M. E. Luke, A. V. Manohar and M. J. Savage, Phys. Lett. B **302** (1993) 482 [Erratum-ibid. B **388** (1996) 866] [hep-ph/9212226].

[166] U. G. Meissner and S. Steininger, Nucl. Phys. B **499** (1997) 349 [hep-ph/9701260].

[167] L. Durand and P. Ha, Phys. Rev. D **58** (1998) 013010 [hep-ph/9712492].

[168] S. J. Puglia and M. J. Ramsey-Musolf, Phys. Rev. D **62** (2000) 034010 [hep-ph/9911542].

[169] S. J. Puglia, M. J. Ramsey-Musolf and S. L. Zhu, Phys. Rev. D **63** (2001) 034014 [hep-ph/0008140].

[170] B. Guberina and R. D. Peccei, Nucl. Phys. B **163** (1980) 289.

[171] J. F. Donoghue, X. -G. He and S. Pakvasa, Phys. Rev. D **34** (1986) 833.

[172] S. Scherer, Adv. Nucl. Phys. **27** (2003) 277 [hep-ph/0210398].

[173] H. Georgi, *Weak Interactions and Modern Particle Theory*, Menlo Park, Usa: Benjamin/cummings (1984) 165p

[174] J. F. Donoghue, E. Golowich and B. R. Holstein, *Dynamics of the standard model*, Camb. Monogr. Part. Phys. Nucl. Phys. Cosmol. **2** (1992) 1.

[175] N. Kaiser, P. B. Siegel and W. Weise, Nucl. Phys. A **594** (1995) 325 [nucl-th/9505043].

[176] Y. Hara, Phys. Rev. Lett. **12** (1964) 378.

[177] A. Le Yaouanc, O. Pene, J. C. Raynal and L. Oliver, Nucl. Phys. B **149** (1979) 321.

[178] B. Borasoy and B. R. Holstein, Phys. Rev. D **59** (1999) 054019 [hep-ph/9902431].

[179] J. Tandean and G. Valencia, Phys. Rev. D **67** (2003) 056001 [hep-ph/0211165].

[180] B. Borasoy and B. R. Holstein, Phys. Rev. D **59** (1999) 094025 [hep-ph/9902351].

[181] J. Beringer *et al.* [Particle Data Group Collaboration], Phys. Rev. D **86** (2012) 010001.

[182] A. J. Buras and D. Guadagnoli, Phys. Rev. D **78** (2008) 033005 [arXiv:0805.3887 [hep-ph]].

[183] C. Jarlskog, Phys. Rev. Lett. **55** (1985) 1039.

[184] G. Buchalla, A. J. Buras and M. K. Harlander, Nucl. Phys. B **337** (1990) 313.

[185] C. Y. Seng, J. de Vries, E. Mereghetti, H. H. Patel and M. Ramsey-Musolf, Phys. Lett. B **736** (2014) 147 [arXiv:1401.5366 [nucl-th]].

[186] R. F. Dashen, E. E. Jenkins and A. V. Manohar, Phys. Rev. D **49** (1994) 4713 [Erratum-ibid. D **51** (1995) 2489] [hep-ph/9310379].

[187] F. M. Dittes, D. Müller, D. Robaschik, B. Geyer and J. Hořejši, Phys. Lett. B **209**, 325 (1988).

[188] X.-D. Ji, Phys. Rev. D **55**, 7114 (1997).

[189] A. Radyushkin, Phys. Lett. B **380**, 417 (1996).

[190] D. Mueller, D. Robaschik, B. Geyer, F. M. Dittes and J. Hořejši, Fortschr. Phys. **42**, 101 (1994).

[191] K. Goeke, M. V. Polyakov and M. Vanderhaeghen, Prog. Part. Nucl. Phys. **47**, 401 (2001).

[192] M. Diehl, Phys. Rept. **388**, 41 (2003).

[193] A. Belitsky and A. Radyushkin, Phys. Rept. **418**, 1 (2005).

[194] S. Boffi and B. Pasquini, Riv. Nuovo Cim. **30**, 387 (2007).

[195] J. P. Ralston and D. E. Soper, Nucl. Phys. B **152**, 109 (1979).

[196] D. W. Sivers, Phys. Rev. D **41**, 83 (1990).

[197] A. Kotzinian, Nucl. Phys. B **441**, 234 (1995).

[198] P. Mulders and R. Tangerman, Nucl.Phys. **B461**, 197 (1996).

[199] J. C. Collins, Acta Phys. Polon. B **34**, 3103 (2003).

[200] A. V. Belitsky, X.-d. Ji and F. Yuan, Phys. Rev. D **69**, 074014 (2004).

[201] A. Bacchetta *et al.*, JHEP **0702**, 093 (2007).

[202] L. Chang, C. D. Roberts and S. M. Schmidt, Phys. Rev. C **87**, 015203 (2013).

[203] V. Barone, A. Drago and P. G. Ratcliffe, Phys. Rept. **359**, 1 (2002).

[204] J. Dudek *et al.*, Eur. Phys. J. A **48**, 187 (2012).

[205] H. Gao *et al.*, Eur. Phys. J. Plus **126**, 2 (2011).

[206] H. Avakian, EPJ Web Conf. **66**, 01001 (2014).

[207] R. J. Holt and C. D. Roberts, Rev. Mod. Phys. **82**, 2991 (2010).

[208] J. S. Conway *et al.*, Phys. Rev. D **39**, 92 (1989).

[209] M. B. Hecht, C. D. Roberts and S. M. Schmidt, Phys. Rev. C **63**, 025213 (2001).

[210] T. Nguyen, A. Bashir, C. D. Roberts and P. C. Tandy, Phys. Rev. C **83**, 062201(R) (2011).

[211] K. Wijesooriya, P. E. Reimer and R. J. Holt, Phys. Rev. C **72**, 065203 (2005).

[212] M. Aicher, A. Schäfer and W. Vogelsang, Phys. Rev. Lett. **105**, 252003 (2010).

[213] L. Chang *et al.*, Phys. Lett. B **737**, 2329 (2014).

[214] L. Chang, I. C. Cloët, C. D. Roberts, S. M. Schmidt and P. C. Tandy, Phys. Rev. Lett. **111**, 141802 (2013).

[215] C. Shi *et al.*, Phys. Lett. B **738**, 512 (2014).

[216] C. Chen *et al.*, Phys. Rev. C **87**, 045207 (2013).

[217] M. Pitschmann *et al.*, Phys. Rev. C **87**, 015205 (2013).

[218] K.-L. Wang, Y.-X. Liu, L. Chang, C. D. Roberts and S. M. Schmidt, Phys. Rev. D **87**, 074038 (2013).

[219] J. Segovia, C. Chen, C. D. Roberts and S. Wan, Phys. Rev. C **88**, 032201(R) (2013).

[220] J. Segovia *et al.*, Few Body Syst. **55**, 1 (2014).

[221] C. D. Roberts, M. S. Bhagwat, A. Höll and S. V. Wright, Eur. Phys. J. ST **140**, 53 (2007).

[222] I. C. Cloët and C. D. Roberts, Prog. Part. Nucl. Phys. **77**, 1 (2014).

[223] The Committee on the Assessment of and Outlook for Nuclear Physics; Board on Physics and Astronomy; Division on Engineering and Physical Sciences; National Research Council, *Nuclear Physics: Exploring the Heart of Matter* (National Academies Press, 2012).

[224] L. Chang *et al.*, Phys. Rev. Lett. **110**, 132001 (2013).

[225] I. C. Cloët, C. D. Roberts and A. W. Thomas, Phys. Rev. Lett. **111**, 101803 (2013).

[226] C. D. Roberts, R. J. Holt and S. M. Schmidt, Phys. Lett. B **727**, 249 (2013).

[227] L. Chang, C. D. Roberts and S. M. Schmidt, Phys. Lett. B **727**, 255 (2013).

[228] F. Gao, L. Chang, Y.-X. Liu, C. D. Roberts and S. M. Schmidt, Phys. Rev. D **90**, 014011 (2014).

[229] J. Segovia, I. C. Cloet, C. D. Roberts and S. M. Schmidt, Few Body Syst., *in press* (2104), *Nucleon and* Δ *elastic and transition form factors*.

[230] T. Bhattacharya *et al.*, Phys. Rev. D **85**, 054512 (2012).

[231] V. V. Flambaum *et al.*, Few Body Syst. **38**, 31 (2006).

[232] P. E. Shanahan, A. W. Thomas and R. D. Young, Phys. Rev. D **87**, 074503 (2013).

[233] P. Maris and P. C. Tandy, Phys. Rev. C **61**, 045202 (2000).

[234] A. Höll, P. Maris, C. D. Roberts and S. V. Wright, Nucl. Phys. Proc. Suppl. **161**, 87 (2006).

[235] M. Pennington, AIP Conf. Proc. **1343**, 63 (2011).

[236] G. Colangelo *et al.*, Eur. Phys. J. **C71**, 1695 (2011).

[237] F. Erben, P. Shanahan, A. Thomas and R. Young, (arXiv:1408.6628 [nucl-th]), *Dispersive estimate of the electromagnetic charge symmetry violation in the octet baryon masses*.

[238] N. Yamanaka, T. M. Doi, S. Imai and H. Suganuma, Phys. Rev. D **88**, 074036 (2013).

[239] A. Bacchetta, A. Courtoy and M. Radici, JHEP **1303**, 119 (2013).

[240] I. C. Cloët, W. Bentz and A. W. Thomas, Phys. Lett. B **659**, 214 (2008).

[241] B. Pasquini, M. Pincetti and S. Boffi, Phys. Rev. D **76**, 034020 (2007).

[242] M. Wakamatsu, Phys. Lett. B **653**, 398 (2007).

[243] C. Alexandrou *et al.*, PoS **LAT2014**, 326 (2014).

[244] M. Gockeler *et al.*, Phys. Lett. B **627**, 113 (2005).

[245] L. P. Gamberg and G. R. Goldstein, Phys. Rev. Lett. **87**, 242001 (2001).

[246] H.-x. He and X.-D. Ji, Phys. Rev. **52**, 2960 (1995).

[247] J. Pretz, Hyperfine Interact. **214**, 111 (2013).

[248] W. Dekens *et al.*, JHEP **1407**, 069 (2014).

[249] G. Eichmann, J. Phys. Conf. Ser. **426**, 012014 (2013).

[250] R. T. Cahill, C. D. Roberts and J. Praschifka, Austral. J. Phys. **42**, 129 (1989).

[251] R. T. Cahill, C. D. Roberts and J. Praschifka, Phys. Rev. D **36**, 2804 (1987).

[252] A. Buck, R. Alkofer and H. Reinhardt, Phys. Lett. B **286**, 29 (1992).

[253] W. Bentz, I. C. Cloët, T. Ito, A. W. Thomas and K. Yazaki, Prog. Part. Nucl. Phys. **61**, 238 (2008).

[254] M. Oettel, G. Hellstern, R. Alkofer and H. Reinhardt, Phys. Rev. C **58**, 2459 (1998).

[255] I. C. Cloët, A. Krassnigg and C. D. Roberts, (arXiv:0710.5746 [nucl-th]), In *Proceedings of 11th International Conference on* Meson-Nucleon Physics and *the Structure of the Nucleon (MENU 2007)*, Jülich, Germany, 10-14 Sep 2007, eds. H. Machner and S. Krewald, paper 125.

[256] M. B. Hecht *et al.*, Phys. Rev. C **65**, 055204 (2002).

[257] C. D. Roberts, Nucl. Phys. A **605**, 475 (1996).

[258] S.-X. Qin, L. Chang, Y.-X. Liu, C. D. Roberts and S. M. Schmidt, Phys. Lett. B **722**, 384 (2013).

[259] M. Oettel, M. Pichowsky and L. von Smekal, Eur. Phys. J. A **8**, 251 (2000).

[260] L. Chang *et al.*, Phys. Rev. C **79**, 035209 (2009).

[261] C. H. Llewellyn-Smith, Annals Phys. **53**, 521 (1969).

[262] L. Chang, C. D. Roberts and D. J. Wilson, PoS **QCD-TNT-II**, 039 (2012).

[263] V. Barone, Phys. Lett. B **409**, 499 (1997).

[264] C. G. Callan, Jr., R. F. Dashen and D. J. Gross, Phys. Lett. B **63** (1976) 334. doi:10.1016/0370-2693(76)90277-X

[265] R. Jackiw and C. Rebbi, Phys. Rev. Lett. **37** (1976) 172. doi:10.1103/PhysRevLett.37.172

[266] W. Dekens and J. de Vries, JHEP **1305**, 149 (2013).

[267] Y. Zhang, H. An, X. Ji, and R. N. Mohapatra, Nucl. Phys. B **802**, 247 (2008).

[268] H. An, X. Ji, and F. Xu, JHEP **1002**, 043 (2010); F. Xu, H. An and X. Ji, JHEP **1003**, 088 (2010).

[269] J. Ng and S. Tulin, Phys. Rev. D **85**, 033001 (2012).

[270] X. -G. He and B. McKellar, Phys. Rev. D **47**, 4055 (1993).

[271] J. de Vries, R. Higa, C. -P. Liu, E. Mereghetti, I. Stetcu, R. G. E. Timmermans, and U. van Kolck, Phys. Rev. C **84**, 065501 (2011); J. Bsaisou, C. Hanhart, S. Liebig, U.-G. Meißner, A. Nogga, and A. Wirzba, Eur. Phys. J. A **31**, 49 (2013); Y. -H. Song, R. Lazauskas and V. Gudkov, Phys. Rev. C **87**, 015501 (2013).

[272] V. Bernard, Prog. Part. Nucl. Phys. **60** (2008) 82 doi:10.1016/j.ppnp.2007.07.001 [arXiv:0706.0312 [hep-ph]].

[273] M. E. Luke and A. V. Manohar, Phys. Lett. B **286**, 348 (1992); W. Kilian and T. Ohl, Phys. Rev. D **50**, 4649 (1994); R. Sundrum, Phys. Rev. D **57** 331 (1998).

[274] S. Weinberg, *The Quantum Theory of Fields*, Vol. 2 (Cambridge University Press, Cambridge, 1996); V. Bernard, N. Kaiser, and U.-G. Meißner, Int. J. Mod. Phys. E **4**, 193 (1995).

[275] S. R. Beane, K. Orginos and M. J. Savage, Nucl. Phys. B **768** (2007) 38 doi:10.1016/j.nuclphysb.2006.12.023 [hep-lat/0605014].

[276] J. Gasser, H. Leutwyler, and M. E. Sainio, Phys. Lett. B **253**, 252 (1991); J. M. Alarcon, J. Martin Camalich, and J. A. Oller, Phys. Rev. D **85**, 051503 (2012); G. S. Bali *et al.* Nucl. Phys. B **866**, 1 (2013).

[277] J. de Vries, E. Mereghetti, R. G. E. Timmermans and U. van Kolck, Annals Phys. **338** (2013) 50 doi:10.1016/j.aop.2013.05.022 [arXiv:1212.0990 [hep-ph]].

[278] E. Mereghetti, W. H. Hockings and U. van Kolck, Annals Phys. **325** (2010) 2363 doi:10.1016/j.aop.2010.03.005 [arXiv:1002.2391 [hep-ph]].

[279] W. H. Hockings and U. van Kolck, Phys. Lett. B **605** (2005) 273 doi:10.1016/j.physletb.2004.11.043 [nucl-th/0508012].

[280] J. de Vries, R. G. E. Timmermans, E. Mereghetti and U. van Kolck, Phys. Lett. B **695** (2011) 268 doi:10.1016/j.physletb.2010.11.042 [arXiv:1006.2304 [hep-ph]].

[281] S. Narison, Phys. Lett. B **666**, 455 (2008); K. Ottnad, B. Kubis, U.-G. Meißner, and F. -K. Guo, Phys. Lett. B **687**, 42 (2010); E. Mereghetti, J. de Vries, W.H. Hockings, C.M. Maekawa, and U. van Kolck, Phys. Lett. B **696**, 97 (2011); F.-K. Guo and U.-G. Meißner, JHEP **1212**, 097 (2012).

[282] R. J. Crewther, P. Di Vecchia, G. Veneziano, and E. Witten, Phys. Lett. B **88**, 123 (1979); **91**, 487(E) (1980).

[283] A. V. Manohar and H. Georgi, Nucl. Phys. **B234**, 189 (1984); S. Weinberg, Phys. Rev. Lett. **63**, 2333 (1989).